University of Denver
Digital Commons @ DU

Electronic Theses and Dissertations | Graduate Studies

1-1-2016

Metabolomics of Mammalian and Cellular Models of Aging

Nathan Gonzales Duval
University of Denver

Follow this and additional works at: https://digitalcommons.du.edu/etd

 Part of the Biology Commons

Recommended Citation

Duval, Nathan Gonzales, "Metabolomics of Mammalian and Cellular Models of Aging" (2016). *Electronic Theses and Dissertations*. 1139.
https://digitalcommons.du.edu/etd/1139

This Dissertation is brought to you for free and open access by the Graduate Studies at Digital Commons @ DU. It has been accepted for inclusion in Electronic Theses and Dissertations by an authorized administrator of Digital Commons @ DU. For more information, please contact jennifer.cox@du.edu,dig-commons@du.edu.

Metabolomics of Mammalian and Cellular Models of Aging

A Dissertation

Presented to

The Faculty of Natural Sciences and Mathematics

University of Denver

In Partial Fulfillment

of the Requirements for the Degree

Doctor of Philosophy

---

by

Nathan Duval

June 2016

Advisor: Dr. David Patterson

© Copyright by Nathan Duval 2016

All Rights Reserved

Author: Nathan Duval
Title: Metabolomics of Mammalian and Cellular Models of Aging
Advisor: Dr. David Patterson
Degree Date: June 2016

Abstract

Aging is often associated with impaired cognition and a progressive loss of organ function over time accompanied by an increased susceptibility for many disorders, including Alzheimer's disease (AD), Parkinson's disease (PD), heart disease, osteoporosis, type II diabetes, and many forms of cancer. With a rapidly aging population, the negative impacts of aging and age-related disorders is a major cause of increased human suffering both for affected individuals and for families and caregivers. Metabolic changes are also apparent in normal aging, but may increase in magnitude or nature with accompanying disease states or with accelerated aging. Thus, studying aging in a disease state, or in a disorder characterized by accelerated aging, will facilitate identification of these changes. Trisomy of chromosome 21 (HSA21), or Down syndrome (DS), is an intellectual disability characterized by premature aging. We hypothesize that trisomy causes disruption of the metabolome leading to an accelerated aging phenotype. In the Ts65Dn mouse model of DS, a premature aging phenotype is also observed along with other common comorbidities associated with human DS. Here, we report changes in the both global and targeted metabolomics (the study of small molecules) in the brains of the Ts65Dn mouse. We also report that long-term treatment with microencapsulated dietary rapamycin changes the metabolomic profiles in a manner consistent with increases in healthspan.

Purines are molecules essential for many cell processes, including RNA and DNA synthesis, regulation of enzyme activity, protein synthesis and function, energy metabolism and transfer, essential coenzyme function, and cell signaling. Purines are produced via the *de novo* purine biosynthesis pathway. Mutations in purine biosynthetic genes can lead to developmental anomalies in lower vertebrates. Alterations in PAICS (phosphoribosyl-aminoimidazole carboxylase/phosphoribosylaminoimidazole succinocarboxamide synthetase) expression in humans have been associated with various types of cancer. Mutations in adenylosuccinate lyase (ADSL, E.C. 4.3.2.2) or 5-aminoimidazole-4-carboxamide ribonucleotide formyl-transferase/IMP cyclohydrolase (ATIC, E.C. 2.1.2.3/E.C. 3.5.4.10) lead to inborn errors of metabolism with a range of clinical symptoms, including developmental delay, severe neurological symptoms, renal stones, combined immunodeficiency, and autistic features. The pathogenetic mechanism is unknown for any of these conditions, and no effective treatments exist. The study of cells carrying mutations in the various *de novo* purine biosynthesis pathway genes provides one approach to analysis of purine disorders. Here we report the characterization of AdeD Chinese hamster ovary (CHO) cells, which carry genetic mutations encoding p.E177K and p.W363* variants of PAICS. Both mutations impact PAICS structure and completely abolish its biosynthesis. Additionally, we describe a sensitive and rapid analytical method for detection of purine *de novo* biosynthesis intermediates based on high performance liquid chromatography with electrochemical detection. Using this technique, we detected accumulation of 5-Aminoimidazole riboside (AIR) in AdeD cells. In AdeI cells, mutant for the ADSL gene, we detected accumulation of Succinylaminoimidazole carboxamide riboside (SAICAR) and adenylosuccinate (SAMP) and, somewhat unexpectedly,

accumulation of AIR. The use of HPLC coupled electrochemical detection in combination with cellular assay methods have great potential for metabolite profiling of *de novo* purine biosynthesis pathway mutants, identification of novel genetic defects of purine metabolism in humans, and elucidating the regulation of this critical metabolic pathway.

Acknowledgements

To Dr. Patterson…for guiding me towards success.

To grandma and grandpa…para una vida de amor y dedicación.

To Josh... for teaching me that the world isn't so big after all.

To Stacey…for being the love of my life.

To Mom… for scratching gold out of this hard life.

Patterson Lab: David Patterson, Guido N. Vacano, Terry Wilkinson II, Stephen P. Ray, Randall Mazzarino. Linseman Lab: Daniel Linseman, Heather Wilkins, Trisha Stankiewicz, Erika Ross, Aimee Winter, Matthew Bartley. Lorenzon Lab: Nancy Lorenzon, George Talbott. Wayne Matson, Samantha Matson.

Funding sources: University of Denver, Itkin Family Foundation, Lowe Fund of the Denver Foundation.

Table of Contents

List of Tables

List of Figures

List of Abbreviations

DS	*Down syndrome*
AD	*Alzheimer's disease*
IIS	*Insulin and insulin like growth factor signaling*
DNA	*Deoxyribonucleic acid*
RNA	*Ribonucleic acid*
ROS	*Reactive oxygen species*
HPLC	*High pressure (performance) liquid chromatography*
IGF-1	*Insulin-like growth factor 1*
mTOR	*Mechanistic (mammalian) target of rapamycin*
DR	*Dietary restriction*
CR	*Caloric restriction*
AMPK	*AMP activated protein kinase*
AMP	*Adenosine monophosphate*
HSA21	*Homo sapiens chromosome 21*
Mmu16	*Mus musculus chromosome 16*
Mmu17	*Mus musculus chromosome 17*
Mmu10	*Mus musculus chromosome 10*
APP	*Amyloid precursor protein*
PD	*Parkinson's disease*
MS	*Multiple sclerosis*
LMC	*Littermate control*
Ts65Dn	*Trisomic mouse model*
HMDB	*Human metabolome database*
CSF	*Cerebrospinal fluid*
ECD	*Electrochemical detection*
MS	*Mass spectroscopy*
NMR	*Nuclear magnetic resonance*
CEAS	*Coulometric electrode array system*
HEFM	*High energy focused microwave*
DIGE	*Difference gel electrophoresis*
CD	*Cervical dislocation*
DNPS	*De novo purine synthesis*
AICAR	*5-Aminoimidazole-4-carboxamide ribonucleotide*
SAICAR	*Succinylaminoimidazole carboxamide riboside*
ADSL	*Adenylosuccinate lyase*
ATIC	*5-Aminoimidazole-4-Carboxamide Ribonucleotide Formyltransferase/IMP Cyclohydrolase*
PAICS	*phosphoribosylaminoimidazole carboxylase/phosphoribosylaminoimidazole succinocarboxamide synthetase*
AIR	*5-Aminoimidazole riboside*
CAIR	*5-amino-4-carboxyimidazole ribotide*
ANOVA	*Analysis of variance*
HVA	*Homovanillic acid*
4-HBA	*4-hydroxybenzoic acid*
NE	*Norepinephrine*

Chapter One:

Introduction to Aging, Down syndrome and metabolomics

1.1 What is Aging?

Aging may arguably be the most intimate and familiar aspect of human biology. From a young age we witness the aging process in others and we experience the effects of aging first hand. Chronologically, we experience aging, however, the rate at which we age is different for each organism. Biologically, aging is defined as the progressive decline in functioning organ systems with a loss of fertility and an increase in mortality. The progressive impairment in functioning organ systems makes us more susceptible to changes in environment, genetic disturbances, and other processes that lead to disease and eventually death.

According to the United States Census Bureau, the population in the US is changing rapidly. By 2050, the population of the US is estimated to be 400 million, a 27% increase from 2012 estimates of 314 million (Bureau 2014). It is estimated that by 2050 the population over the age of 65 is projected to be 83.7 million, an increase of 94% from the estimated population of 43.1 million in 2012 (Bureau 2014). The size and composition of the population over the age of 65 will be influenced by mortality rates and by survivorship, with regard to age-related disease. The elderly tend to have a higher incidence of costly

chronic diseases; aging is the most common risk factor for age-related diseases and the risk increases in frequency and severity as the population ages. Typically, the mechanisms and causes of these pathologies are researched and subsequently treated individually. This focus on specific diseases has had a profound effect on human health and in many instances has led to an extension of lifespan. However, we have been largely unsuccessful at eliminating, ameliorating, or postponing age-related disease. This has led to a decrease in mortality; however, often elderly people are suffering from multiple diseases or age-related complications (Figure 1). Understanding the basic biology of aging and treating aging as the common symptom of age-related disease, the consequences of advanced age can be hypothetically minimized or eliminated.

1.1 Healthspan and Lifespan

Much of the research on aging is attempting to understand mechanisms, pathways, or genes that prolong lifespan or longevity. Lifespan is understood as the time an organism survives. This does not describe the physiological or pathological state of the organism, rather whether or not it is surviving. It is important to note that extension of lifespan without the extension of healthspan, which is the time an organism spends in a disease free state, may be considered cruel. Through the extension of healthspan mortality will decrease, leading to an extension of lifespan, although a maximum lifespan more than likely exists (Figure 2).

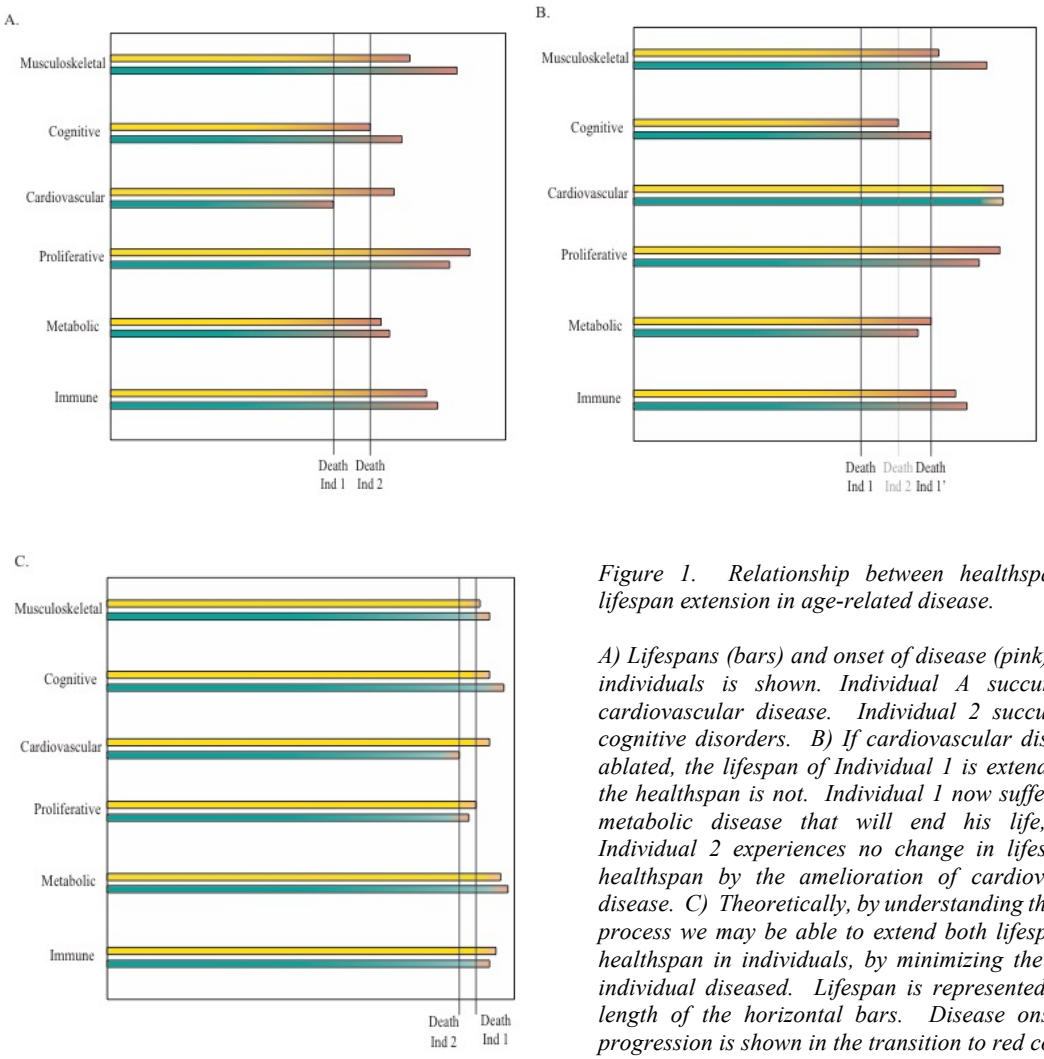

Figure 1. Relationship between healthspan and lifespan extension in age-related disease.

A) Lifespans (bars) and onset of disease (pink) in two individuals is shown. Individual A succumbs to cardiovascular disease. Individual 2 succumbs to cognitive disorders. B) If cardiovascular disease is ablated, the lifespan of Individual 1 is extended, but the healthspan is not. Individual 1 now suffers from metabolic disease that will end his life, while Individual 2 experiences no change in lifespan or healthspan by the amelioration of cardiovascular disease. C) Theoretically, by understanding the aging process we may be able to extend both lifespan and healthspan in individuals, by minimizing the risk of individual diseased. Lifespan is represented as the length of the horizontal bars. Disease onset and progression is shown in the transition to red color.

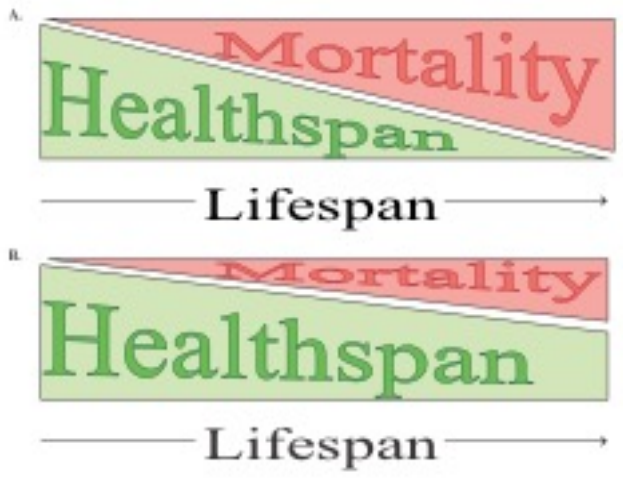

Figure 2. Relationship between healthspan, lifespan and mortality. The extension of lifespan does not describe the health status, or healthspan of an organism, nor does it describe the time spent in a healthy state. A) Shows the lifespan and the hypothetical time spent in a health state (healthspan) or in a state where the probability of mortality increases over time. B) Shows the expansion of healthspan and the subsequent reduction in probability of mortality. Healthspan does not generally assume an extension in lifespan.

1.2 Theories of aging

1.2.1 Discussion of ultimate theories of aging

There is a tendency to regard the aging process as programmed, or pre-determined. This is a common misconception due to its convenience and ability to be easily comprehended. It hypothesizes that aging as a program evolved because it benefits the species by preventing overcrowding and reducing competition for valuable resources. This idea was brought to favor by Weismann (1889) who posited that old "worn out" individuals have no value and are actually harmful by taking the place (resources) for the young (Weismann 1889). This ignores data that show individuals in the wild rarely reach senescent age, or the age when deterioration begins (Lack 1954; Finch et al. 1990;

Medawar 1952). The most common contributors to mortality in wild populations are predation, disease, and accidents. Old age is not a major component of mortality in wild populations; therefore, younger individuals primarily contribute to the next generation so "old" genes (genes that would promote an aging phenotype) should rarely evolve. Additionally, the idea of aging as a program, if true, should provide evidence such as a mechanisms or genes that when manipulated could bypass the aging program.

1.2.2 Antagonistic pleiotropy and mutation accumulation

It is well known that manipulation of certain genes, such as insulin and insulin-like growth factor signaling (IIS) genes, can extend or shorten lifespan in many different evolutionarily divergent species (Barzilai et al. 2012). How did these genes evolve and what is the mechanism that they might be committing an organism to death by age, if they are able to avoid extrinsic mortality? The theory proposed by Medawar (1952) understood that death by extrinsic (environmental) factors was strong evidence that an aging program would not evolve in a natural setting. The theory proposes that late acting mutations in the germline of an organism could provide a slight detriment to an organism's fitness, even if they hindered survival or reproduction. However, over successive generations these mutations would accumulate in the genome. If an organism with these mutated alleles was able to avoid extrinsic mortality, they would experience these late acting mutations as aging (Medawar 1952).

An extension of Medawar's mutation accumulation theory was proposed by George Williams (Williams 2001) postulating the occurrence of special genes that were beneficial

in development and early age, but antagonistic to health at later stages in life. The theory, called "Antagonistic Pleiotropy", attempts to explain the aging phenomenon as driven by genes that are critical to early life when the selective pressures on an organism are strong, but these genes become less beneficial, even harmful late in life when selective pressures are much weaker (Williams 2001).

Together these theories have accounted for most of the thinking in evolutionary genetics of aging research. Although they drive most of the current thinking, little evidence exists to support these theories, in particular the mutation accumulation theory (Shaw et al. 1999). A growing number of genes have been found that do affect aging when they are modulated late in life and have detrimental effects when mutated earlier in life (Jenkins et al. 2004) Many of these genes fall into different categories of proximate aging that is discussed below.

1.2.3 Disposable soma

A different approach to understanding the mechanisms of aging arises from understanding "trade-offs" or allocation of resources of an organism (Kirkwood 1977). The Disposable Soma Theory proposes that energy is scarce and an organism allocates energy resources early in life to maintain good physiological status when it has a higher chance of survival (Kirkwood 1977). This allocation of resources comes at the expense of repair and maintenance mechanisms that promote lifespan (antioxidant pathways, DNA repair). The disposable soma theory makes a few predictions about the aging process: 1) aging is the result of unrepaired cellular and molecular damage through the loss or

dysfunction of mechanisms responsible for cellular maintenance, 2) genes that regulate the levels of repair and maintenance pathways can control the levels of damage through life and therefore longevity, 3) the mechanisms that drive aging are expected to be stochastic in nature and polygenic. Some of these mechanisms that can be considered examples of the disposable soma theory will be discussed briefly below.

1.3 Discussion of important proximate theories of aging

Because aging is a progressive decline in the functioning of many different organ systems and can be modulated through different genes and genetic pathways (polygenic) it is natural for many theories explaining aging to take root. There are many different theories of aging which explain changes that occur during the aging process, which are not mutually exclusive. Many of these explain the existence of an aged phenotype, but fall short of being solely responsible. The overwhelming number of proximate theories of aging segregate into categories based on their origin; genomic instability, mitochondrial dysfunction, proteostasis dysfunction, nutrient sensing, senescence, among others.

Recent advances in aging research have provided an opportunity to classify the molecular and cellular hallmarks of the aging process. Much of the earlier research in aging identified many processes and many features of the aging phenotype. The categorization of these proximate theories aims to unify them in a coherent manner based on 3 criteria proposed by Lopez-Otin *et. al.*: 1) should occur during normal aging, 2) disturbances should accelerate aging, 3) ablation should extend lifespan (López-Otín et al. 2013). Here I will discuss the most popular proximate theories of aging.

1.3.1 Genomic Instability

The accumulation of genomic damage throughout life is a critical component of aging. Organisms have evolved many different DNA repair mechanisms that attempt to repair this damage. As we age, these repair mechanisms can lose effectiveness and these disruptions can have serious effects on lifespan and healthspan. Often, different aspects of aging, such as reactive oxygen species (ROS) can exacerbate DNA damage accumulation by being both a cause of DNA damage and a product of DNA damage. This is particularly true of mitochondrial DNA. It is also important to note that DNA damage is a hallmark of many cancers (Hoeijmakers 2009).

Damage to DNA can come from both exogenous and endogenous sources and affect both nuclear and mitochondrial DNA (Park & Larsson 2011; Payne et al. 2011) Moskalev et al. 2013). These insults to DNA and DNA repair mechanisms can cause disruptions to the transcriptional network and expression of essential genes causing loss of cellular homeostasis. Loss of DNA repair mechanisms have shown to decrease lifespan in different models (Gregg et al. 2012; Hoeijmakers 2009). Damage to mitochondrial DNA is often attributed to the high volume of reactive oxygen species (ROS) due to the energetic nature of mitochondria. The DNA in mitochondria are more susceptible to these insults because their repair mechanisms are less efficient than nuclear DNA (Linnane et al. 1989). However, genome wide analysis of mitochondrial genes finds that most mutations are due to replication errors rather than ROS insults (Ameur et al. 2011).

1.3.2 Telomere Attrition

Also considered a form of DNA damage, telomere erosion or shortening, is an unavoidable consequence of normal cell function. Telomeres are the protective caps at the end of chromosomes. Unfortunately, the replication machinery (DNA polymerases) cannot replicate to the terminal ends of the DNA resulting in a loss with each replication cycle. A particular polymerase, telomerase, is responsible for the addition of repeating sequences to the chromosome ends compensating for the loss during replication (Blackburn et al. 2006). Telomerase is not found in all cell types, or in equal measure between cells, and the action is limiting and is used to explain the loss of replicative capacity of cells (Hayflick & Moorhead 1961). Lengthening the effectiveness of telomerase has been shown to extend lifespan and leads to immortality in cellular models (Bodnar et al. 1998).

Telomere shortening is a function of normal aging (Blasco 2007), and therefore has been considered a biological clock for determining age. Shortening of the telomeres or eliminating telomerase activity has shown to decrease lifespan and reduce healthspan, often leading to disease (Armanios et al. 2009; Herrera et al. 1999). Conversely, increasing the length of telomeres or upregulating the telomerase activity has been shown to extend lifespan and healthspan in a variety of mouse models (Tomás-Loba et al. 2008; Bernardes de Jesus et al. 2012). Telomere biology and aging has been recently reviewed by Blackburn *et. al.* (Blackburn et al. 2015). Evidence that individuals with DS have shortened telomeres suggests that this may contribute to their premature aging phenotype (Gruszecka et al. 2015).

1.3.3 Proteostasis

In addition to repair and homeostatic mechanisms for preserving the genome, cells also contain mechansisms that help to maintain the stability of their proteome. These can be critical mechanisms to maintaining the functionality of the proteome by mechanisms that help fold proteins (heat shock), and pathways involved in the clearance of misfolded proteins. These processes are most important in non-dividing neuronal cells and some cardiac cells. Many diseases, most age-related in nature (e.g. Alzheimer's disease, Parkinson's disease), have well-documented disruption in the proteome resulting in aggregated or misfolded proteins (reviewed in Powers et al. 2009). The stability and function of the proteome has also been demonstrated to be altered with age, including heat shock proteins (Koga et al. 2011; Calderwood et al. 2009). Different evolutionarily divergent species also show changes in the chaperone mediated protein folding and stability associated with aging (Morrow et al. 2004; Swindell et al. 2009). Another important mechanism involved in proteomic stability is the autophagy system. Autophagy is important for the removal of misfolded proteins, as well as normal protein turnover. In non-dividing cells, autophagy plays an important role in the health of the cell through many different mechanisms. For a comprehensive review on the importance of autophagy and aging please see (Rubinsztein et al. 2011).

Interestingly, the inhibition of the mTOR pathway through treatment with rapamycin has been shown to extend lifespan in mice (Harrison et al. 2009; Wilkinson et al. 2012). In yeast, *C. elegans*, and *D. melanogaster* the lifespan extending effects of rapamycin treatment appear to be primarily through autophagy ((Bjedov et al. 2010;

Rubinsztein et al. 2011). Although it remains to be fully studied, autophagy will undoubtedly play a role in mammalian aging as well.

1.3.4 Mitochondrial dysregulation (and reactive oxygen species)

Mitochondria play an essential role in cellular energy production. An unfortunate side effect of these energy producing reactions is the production of ROS. Denham Harman proposed that the accumulation of ROS results in biological aging (Harman 1955; Harman 1992; Harman 2001). Furthermore, manipulation of both ROS levels and ROS scavenging antioxidant proteins does not modulate lifespan (Pérez et al. 2009; Van Remmen et al. 2003). However, genetically impairing mitochondria function without increasing ROS diminish lifespan (Edgar et al. 2009) Trifunovic et al. 2004). As an organism ages, levels of ROS increase, but not in a manner that is consistent with with dysfunction, but rather survival (Hekimi et al. 2011). This may suggest a homeostatic mechanism of ROS, but after reaching a certain threshold become detrimental to cellular function and damage may start to accumulate (Hekimi et al. 2011). Independent of ROS, the mitochondria can influence aging. Genomic instabilities of mitochondrial DNA may result in altered aging (discussed above). Mouse studies have shown diminished lifespan when deficient for DNA polymerase-γ, the polymerase responsible for mtDNA replication (Edgar et al. 2009). Additional pathways involving defective mitochondria and disrupted apoptosis signaling may contribute to altered lifespan.

1.3.5 Nutrient signaling pathways

The most evolutionarily conserved pathway that also happens to modulate aging is the insulin and the insulin-like growth factor 1 (IGF-1) signaling (IIS) pathway. The IGF-1 pathway involves activation by growth hormone and affects the same downstream pathways as those elicited by insulin. These downstream pathways such as FOXO transcription factors and the mTOR pathway have been shown to extend lifespan as well when modulated (Barzilai et al. 2012; Fontana et al. 2010). Additionally, these pathways are also affected during dietary restriction (DR), which is the most effective non-genetic intervention to increase lifespan in evolutionarily divergent species (Kaeberlein et al. 2005; Smith 2005; Anderson & Weindruch 2010; Colman et al. 2009).

Genetic manipulation of different aspects of the IIS pathway show lifespan extension and also shows that these components of IIS signaling are affected by DR (Fontana et al. 2010). Consistent with the disposable soma theory of aging, a reduction in IIS pathways, either by genetic manipulation or DR, will lead to reductions in cell growth and metabolism resulting in reduced cellular damage.

In addition to the IIS pathway, there are other important pathways involved in cellular metabolism and growth, such as the mTOR (mechanistic target of rapamycin) and AMPK (AMP activated protein kinase) pathways. These protein kinases act as nutrient sensing molecules that integrate many upstream signals such as amino acid levels (mTOR), and energy status (AMPK) and activate downstream regulators of cellular growth and metabolism. The mTOR pathway integrates upstream signals of nutrient abundance and regulates most aspects of metabolism, in particular growth and proliferation. Genetic

manipulations that downregulate the activity of the mTOR pathway extend lifespan in yeast, worms, flies, and mice (Johnson et al. 2013). Additionally, downregulation of the mTOR pathway through rapamycin treatment extends lifespan in mouse models and is considered the most robust chemical intervention to extend lifespan (Harrison et al. 2009). The mTOR pathway is discussed in more detail in a later section.

The AMPK pathway acts by sensing energy scarcity and catabolism, and upregulation in response to low energy sources initiates signaling that promotes longevity. AMPK has been shown to downregulate mTOR activity in response to low cellular nutrient or energy availability (Alers et al. 2012). Chemical intervention with metformin, an AMPK upregulator, shows lifespan extension in both worms and mice (Anisimov et al. 2011; Onken & Driscoll 2010).

1.4 Down syndrome

1.4.1 Down syndrome; a precocious aging disorder

Down syndrome is the most common genetic form of intellectual disability and is caused by the triplication of human chromosome 21 (HSA21). This triplication event occurs in roughly 1 in 700 live births and impacts human development in diverse ways across many different organ systems. In addition to the developmental disruptions, individuals with DS experience an accelerated aging phenotype (Nakamura & Tanaka 1998; Patterson & Cabelof 2012; Zigman & Lott 2007). Along with the intellectual delay and accelerated aging, individuals with DS have an increased incidence of leukemia, diabetes, and autoimmune disorders, but a decreased risk of atherosclerosis and many solid

tumors that show increased incidence with age. People with DS begin to show the neuroanatomical changes associated with AD (amyloid plagues and neurofibrillary tangles) typically by their fourth decade of life. Many individuals with DS will develop AD by their 50s, and it is likely that all individuals with DS will develop AD as they age. The amyloid precursor protein (APP) gene is found on HSA21 and is trisomic in individuals with DS. APP encodes a protein that when proteolytically cleaved, produces the Aβ peptide, the major component of amyloid plaques in AD. One hypothesis is that individuals with DS are at an increased risk of early onset AD not only because of increased APP gene dosage, but also because they age prematurely (Chicoine & McGuire 1997; Lott & Head 2005; Patterson & Cabelof 2012).

Additionally, many biomarkers associated with aging, such as oxidative stress, accumulation of mutations, and altered DNA repair, are found in individuals with DS. Although marked improvements in life expectancy have been achieved, the life expectancy of individuals with DS remains significantly reduced, and risk of mortality is higher (Coppus et al. 2008). One reason for the extension of lifespan is that individuals with DS are no longer institutionalized and they have better access to improved medical care. Hematopoietic and neural stem cells taken from individuals with DS show changes characteristic of premature aging such as increased expression of pro-apoptotic genes, and inflammatory genes, and a down regulation of DNA repair genes (Cairney et al. 2009). Increased accumulation of altered aspartate residues in proteins, a phenomenon associated with cellular aging, has also been observed in DS (Galletti et al. 2007).

1.4.2 Mouse models of Down syndrome

Individuals with Down syndrome (DS) show a complicated and variable phenotype with a range of features, including intellectual disability, behavioral, psychiatric, and neurological problems. Given this complexity it is imperative that a model of DS be able to address this complexity in phenotypes. Models based on lower organisms and *in vitro* models have proven to be inadequate in representing the DS disease spectrum found in humans. Mouse models are well characterized higher organisms that allow for the study of many different phenotypic features of DS in a single organism. For example, intellectual, behavioral, cardiac, hematological, and skeletal disorders can all be expressed and studied in a mouse; this is not possible in *C. elegans* or *D. melanogaster*. Additionally, mouse models are well characterized and are used to study a wide range of pathologies such as Alzheimer's disease (AD), Parkinson's disease (PD), and Multiple Sclerosis (MS) amongst many others. Mouse models are used in drug development and drug testing. Mice have a relatively short lifespan and reproduce rapidly making them relatively inexpensive to house and maintain.

Figure 3. Trisomic Ts65Dn mouse (left) and Disomic littermate control (right).

Although, mouse models of human disorders will never fully represent the spectrum of pathology found in humans, they can serve as a surrogate for understanding

relevant pathways and gene aberrations *in vivo*. Currently, there are a number of mouse models of DS that carry a triplicated chromosomal region (mouse or human) that represent the triplicated genes in human DS (Vacano et al. 2012). Mice that are trisomic for various regions of HSA21 or the mouse chromosomal region of Mmu16 that are syntenic to HSA21 have been produced and represent human DS to different degrees (Figure 3) (Vacano et al. 2012). Mouse chromosomes 16, 17, and 10 carry all of the genes on HSA21, but they may not be completely analogous and may include copy number variations and regulatory sequences that affect the phenotype in a way that is not representative of DS (Sturgeon & Gardiner 2011).

1.4.3 Ts65Dn mouse model of DS, aging, and early onset Alzheimer's disease

The Ts65Dn mouse model of Down syndrome produced by Muriel Davidson and colleagues was a breakthrough in DS research (Davisson et al. 1990; Reeves et al. 1995). These mice were produced by irradiating the testes of male mice, breeding them, and screening the offspring for chromosomal rearrangements of Mmu16, the chromosome most homologous to HSA21. This mouse carries an extra chromosome that arose from translocation of part of Mmu16 to the centromeric region of Mmu17. The Ts65Dn mouse is trisomic for 100 genes homologous to the genes found on Hsa21 (Gardiner 2010). The mice are also trisomic for roughly 60 genes on Mmu17 (Duchon et al. 2011; Reinholdt et al. 2011). It is the most widely studied and characterized mouse model of DS because they exhibit many features common in people with DS. These include deficits in spatial learning

and memory beginning by 3 months of age. These deficits are minimized by 8 months of age, but begin a rapid decline as the mice age.

By 12 months of age, these changes have become readily apparent (Hyde & Crnic 2001). They exhibit a widespread impairment of cell proliferation in cerebellum, hippocampus, skin, and bone marrow (Contestabile, Fila, Bartesaghi, et al. 2009; Contestabile, Fila, Cappellini, et al. 2009; Jablonska et al. 2006).

Consistent with features of individuals with DS, the mice experience changes in development and aging such as congenital heart defects, myeloproliferative disorders, a decrease in bone density, and an altered incidence of solid tumor cancers (A. D. Williams et al. 2008; Blazek et al. 2011; Baek et al. 2009; Kirsammer et al. 2008). The Ts65Dn mice show signs of premature aging reminiscent of those associated with DS. They have an

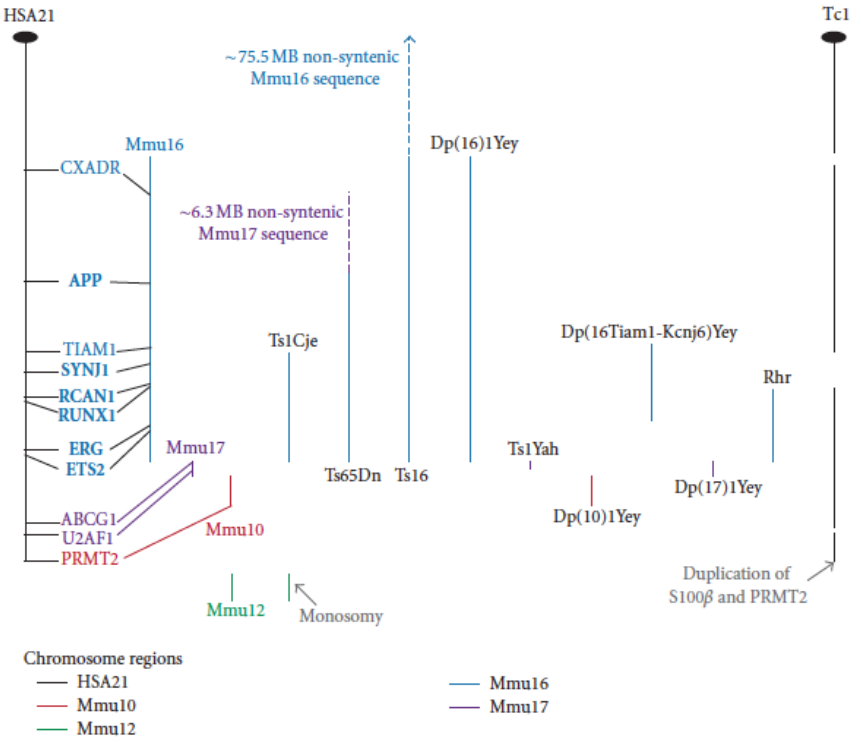

Figure 4. Chromosomal segments of different mouse models of trisomy of HSA21 the cause of human Down syndrome (From Vacano 2012).

increased risk of mortality and show age related declines in mobility and motor function and other features of aging not observed in littermate control (LMC) mice (Sanders et al. 2009). People with DS show many molecular and anatomical changes in the brain, most notably in hippocampus and cerebellum (Lott 2012). The mice lose functional basal forebrain cholinergic neurons, reminiscent of early onset AD (Granholm et al. 2000). Ts65Dn mice are trisomic for the APP gene and although they do not develop plaques and tangles, a recent study concluded that there is an age dependent dysregulation of APP metabolism in Ts65Dn mice (Choi et al. 2009). No abnormalities could be found in APP gene expression or APP metabolite levels in brains of 4-month old Ts65Dn mice. However, at 10 and 12 months of age, Ts65Dn mice showed elevated levels of APP and soluble APP metabolites. MRI studies reveal *in vivo* cholinergic changes possibly relevant to early onset AD in the brains of Ts65Dn mice (Chen et al. 2009). Trisomy of APP has been shown to be important for proper early endosome function in these mice (Salehi et al. 2006). Studies comparing cerebella from 3 and 10 month old Ts65Dn mice show that cerebellar abnormalities increase with age in these mice (Necchi et al. 2008). These investigators also reported that 10-month old Ts65Dn mice develop sporadic tremors and stereotypic behavior, which may reflect cerebellar anomalies. Degeneration is even more significant at 12 months of age (Lomoio et al. 2009). Some of the relevant changes observed in the Ts65Dn mice as they age are presented in Table 1.

Table 1. Features associated with aging in the Ts65Dn mouse model of DS

Parameter	3 – 6 months		10 – 15 months	References
Cerebellar Purkinje cell degeneration	No		Yes	Lomoio et al., 2009; Necchi et al., 2008
APP expression and metabolism	Normal		Abnormal	Choi et al., 2009
Context discrimination	Maximal		Deteriorated	Hyde and Crnic, 2001
Thrombocytosis	Present		Profound	Kirsammer et al., 2008
Cell proliferation in dentate gyrus	Normal		Decreased	Rueda et al., 2005
Response to physostigmine	Yes		No	Chang and Gold, 2008
Hippocampal cholinergic degeneration	No		Yes	Seo and Isacson, 2005
BFCN abnormalities	No		Yes	Granholm et al., 2000; Cooper et al., 2001

1.5 De novo purine biosynthesis pathway

Purines are essential building blocks for RNA and DNA synthesis, and regulate energy metabolism and transfer, and protein synthesis, function, and enzyme activity. Purines are also vital components of many essential coenzymes (NAD, NADH, FAD, Coenzyme A), and signaling molecules (cAMP, guanine nucleotides). The enzymatic steps of *de novo* purine biosynthesis convert PRPP (5-phospho-α-D-ribosyl-1-pyrophosphate) to IMP (inosine monophosphate), and an additional four steps convert IMP to AMP (adenosine monophosphate) or GMP (guanosine monophosphate) (Figure 5). In addition to ADSL and ATIC, 30 enzyme defects of purine and pyrimidine metabolism have been identified and 17 of these are known to cause human disease (Jurecka 2009). The clinical presentation of genetic disorders of purine metabolism includes a wide variety of symptoms, such as severe combined immunodeficiency, severe neurological defects, developmental delay, and abnormal brain development (Jurecka 2009; Jurecka et al. 2008;

Sempere et al. 2010). The consequences of inborn errors in purine metabolism are poorly understood, and misdiagnosis most likely results in underestimation of their incidence and prevalence (Jurecka 2009). In addition to the developmental consequences of inborn errors of metabolism, disruptions in the production of purines may play an important role in understanding aging and disrupted aging leading to disease (Figure 5). Some aspects of metabolomics and metabolic regulation can be studied more suitably in a cell based system rather than in an animal model. For example, examination of the cell autonomous effects of accumulation of particular metabolites can often be studied in cell culture model initially to gain insight into possible effects in an intact animal. For example, two of the intermediates of de novo purine synthesis, aminoimidazole carboxamide ribotide (AICAR, or ZMP) and succinyl aminoimidazole carboxamide ribotide (SAICAR) are known regulators of metabolism, ZMP as an agonist of AMPK and SAICAR as a regulator of pyruvate kinase form M2 (PKM2). Our lab has previously described isolation of mutant CHO-K1 cells that accumulate these intermediates, AdeI, which accumulates SAICAR, and AdeF, which accumulates ZMP. As part of our study of metabolic regulation, we carried out a molecular analysis of the AdeI mutant and also the AdeD mutant. These studies involved determination of the mutations in adenylosuccinate lyase (ADSL) in AdeI cells and in AdeD cells, deficient in SAICAR synthetase (Vliet et al. 2011; Duval et al. 2013). This work will be discussed further in Chapter Three.

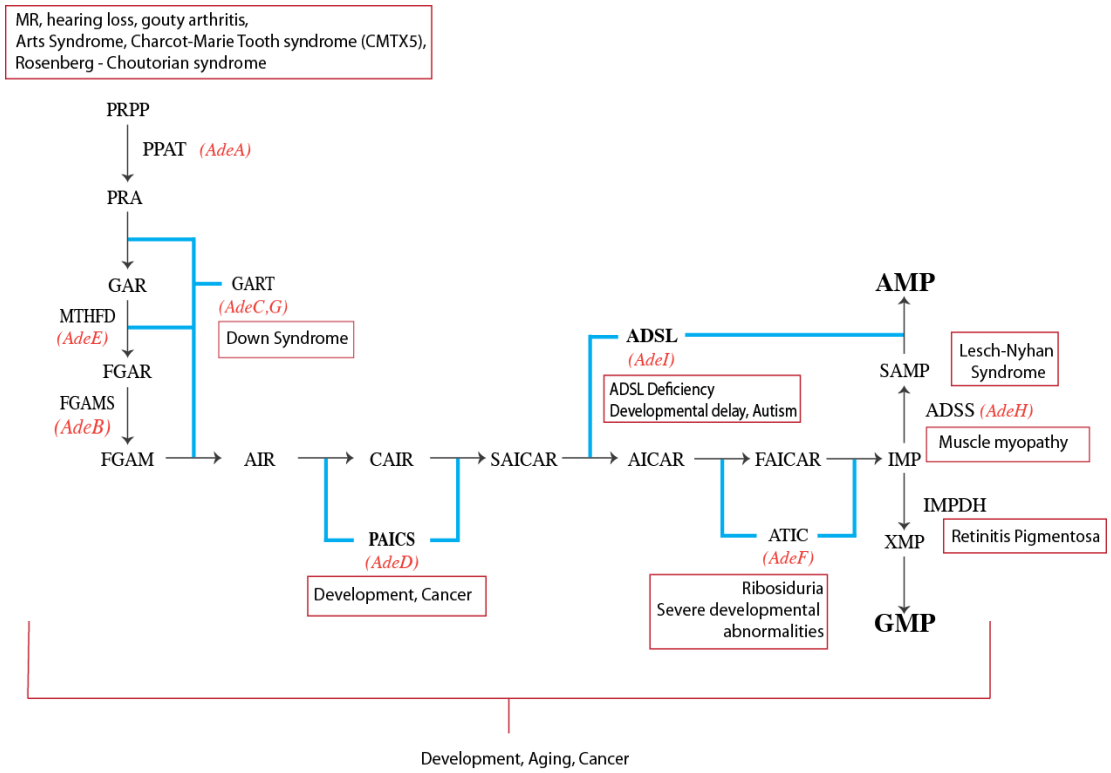

Figure 5. The de novo purine synthesis pathway showing relevant pathologies associated with disruption in the pathway and implications in development, and aging.

1.6 Metabolomics of Aging

1.6.1 Metabolomics

Metabolomics is the identification and quantification of small molecule (<1500 Da) metabolites and low molecular weight intermediates in a biological sample (Wishart 2010). The set of metabolites makes up the metabolome and can vary depending on the physiological, pathological, and developmental state of the cell, tissue, organ, or organism. The metabolome is also intimately connected to change in the genome, transcriptome, and proteome as they are often end products or intermediates of all biological reactions (Figure

5). According to the Human Metabolome Database (HMDB: http://www.hmdb.ca), there may be 41,993 identifiable metabolites, but currently there are roughly 3,033 identified and detected metabolites. There is a very limited database of brain metabolome studies, but if we assume that the closest surrogate is metabolites found in cerebrospinal fluid (CSF), the total number of metabolites detected is 440 (HMDB statistics). Global metabolomics attempts to identify and quantify all metabolites in a sample. Targeted metabolomics attempts to examine a particular subset of the metabolites in a sample. Despite the difficulties and limitations of the approach, the goal of metabolomics is to understand the changes in the metabolome and use these to identify key biomarkers and signaling pathways that are relevant to a pathological state. Methods for metabolomic analysis must be quantitative, selective, and sensitive. High sensitivity methods allow for the identification of low abundance metabolites; selectivity provides information to distinguish between two chemically similar metabolites; quantifiable results are critical for identifying relative changes in metabolite levels. Many metabolomics studies use high performance liquid chromatography (HPLC) as an initial

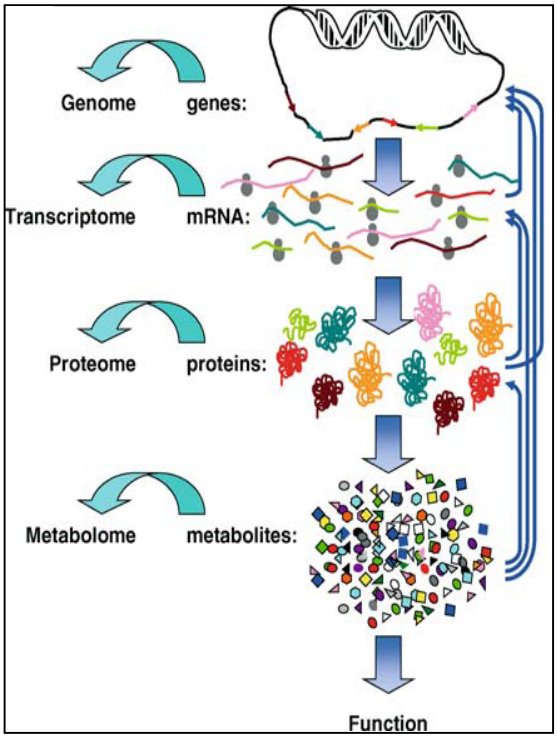

Figure 6. Systems biology levels and feedbacks.

separation method. There are various methods for metabolite detection after HPLC separation, but no method detects all metabolites (Wolfender 2009).

1.6.2 High pressure (performance) liquid chromatography (HPLC)

High performance liquid chromatography has become one of the most ubiquitous analytical techniques for the separation of molecules. Separation of nucleic acids (DNA, RNA), proteins, and different classes of metabolites are all possible by HPLC depending on the column and gradient methods employed. HPLC has become the dominant separation method in the study of metabolomics due to its ease of use and flexibility in separating many different metabolites. We employ reverse-phase chromatography, which separates molecules based on their hydrophobicity. The columns are comprised of porous silica beads with 18-carbon acyl chains, this is considered the stationary phase. The mobile phases consist of a primary aqueous phase to which a varying degree of solvents (ex: methanol, acetonitrile, isopropanol) are added to aid in the elution of hydrophobic molecules. In principle, hydrophilic compounds elute more quickly than hydrophobic compounds in reverse-phase chromatography. One strength of using a liquid chromatography based separation method is the ease at which the method can be modified in an experiment dependent manner. Downstream of the separation column different detectors are employed, such as mass spectroscopy (MS), nuclear magnetic resonance (NMR), and electrochemical detection (ECD). We have chosen to use electrochemical detection, specifically, a coulometric electrode array system (CEAS).

1.6.3 A brief history of electrochemical detection

With advances in separation technologies in column and mobile phase application, the limiting factor of HPLC as an analytical technique is the method of detection. The creation of the electrochemical detector helped usher in a new era of selectivity and sensitivity. Electrochemical detectors (ECD) were originally developed as a method to detect metabolites that function *in vivo* as a result of the electron transfer process, so it was reasonable to assume that those compounds could be monitored using the electron transfer process (McClintock et al. 1985). There have been many iterations of the ECD through the years including conductometric, potentiometric, oscillometric, and voltametric detectors. The most common form of ECD by far are the three voltametric detectors (amperometric, coulometric, and polarographic). I will not offer a discussion of the polarographic detector due to its difficulty of use (and rarity) due to poor peak shape and limits of detection, as well as the need to dispose of toxic "spent" mercury (Kemula 1952).

Amperometric ECD became the detection method of choice due to its increased sensitivity. It was used to measure neurotransmitters at the nanogram level in brain tissues (Riggin & Kissinger 1977; Kissinger 1989), as well as a method to detect other biochemical, environmental, and pharmaceutical metabolites (Jane et al. 1985; Musch et al. 1985; Radzik & Lunte 2006). One of the difficulties with amperometric detectors, in particular the early single-channel "low-volume" detectors, is the oxidation efficiency limit. Because the analytes must travel over a thin electrode, the efficiency is determined

by the amount of analyte that comes into contact with the electrode (Figure 4). This sensitivity and efficiency of the amperometric detector is inversely correlated with electrode chamber volume and flow rate. Advances have been made to amperometric sensitivity and efficiency. However, the development of the flow-through coulometric array by Wayne Matson revolutionized electrochemical detection (Matson et al. 1984).

The Flow-through Coulometric Electrode Array System (CEAS) was developed by Wayne Matson and features a graphite flow-through electrode that completely oxidizes an analyte as it passes through (Matson et al. 1984). Using an array of flow-through detectors co-eluting compounds can be resolved based on their redox potentials. Additionally, the flow-through design allows for >99% efficiency of detection due to its 3-dimensional design. Regardless of the direction a compound travels through the detector, it will encounter the working electrode surface (Figure 4). Another benefit of the flow-through CEAS is that response of the detector can be related to the quantity of the analyte undergoing reduction or oxidation, and Faraday's law can be applied (Equation 1) (Kristal, Shurubor, Kaddurah-Daouk & Matson 2007a).

$$Q = n \cdot F \cdot N$$

Q = Charge transferred (Coulombs); n = number of electrons transferred (equivalents/mole); F = Faraday's constant (Coulombs/equivalent); N = moles of reactant (mole)

The peak area is measured in charge (current over time), therefore, using Faraday's equation, if the amount injected is known the peak area can be predicted. Conversely, if the peak area is known, the amount added can be calculated. Taken together, this

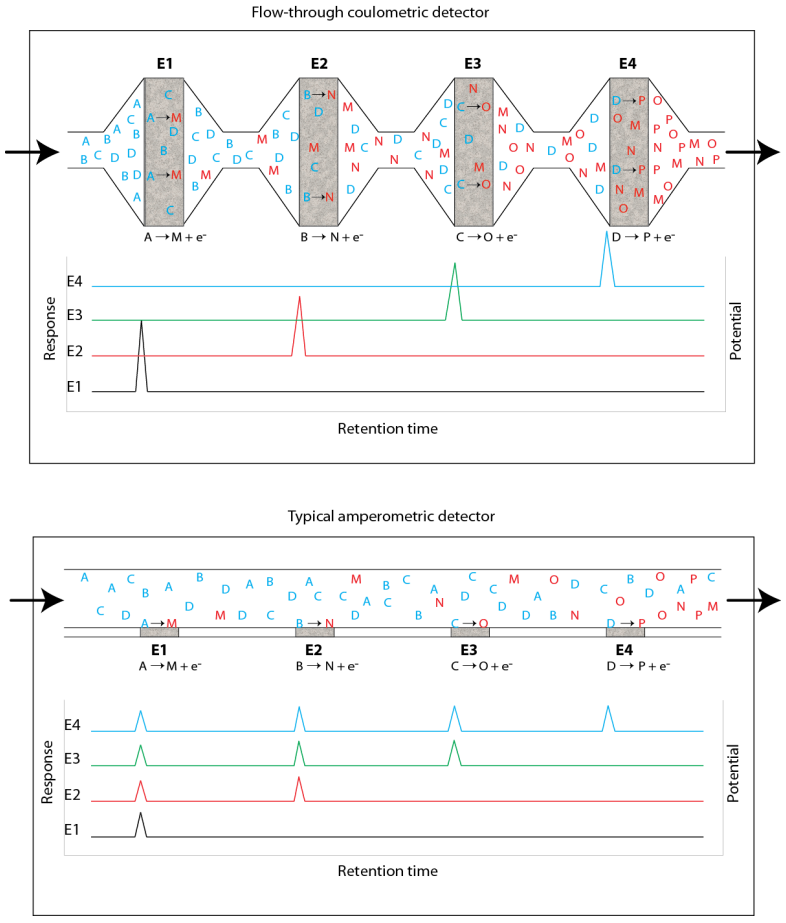

Figure 7. Illustration of a 4-channel flow-trhough coulometric electrode array system (CEAS) Top, and a typical amperometric detector. CEAS provides 100% oxidation of samples as they pass through the electrode, amperometric detectors have a lower efficiency due to the flow-over set up.

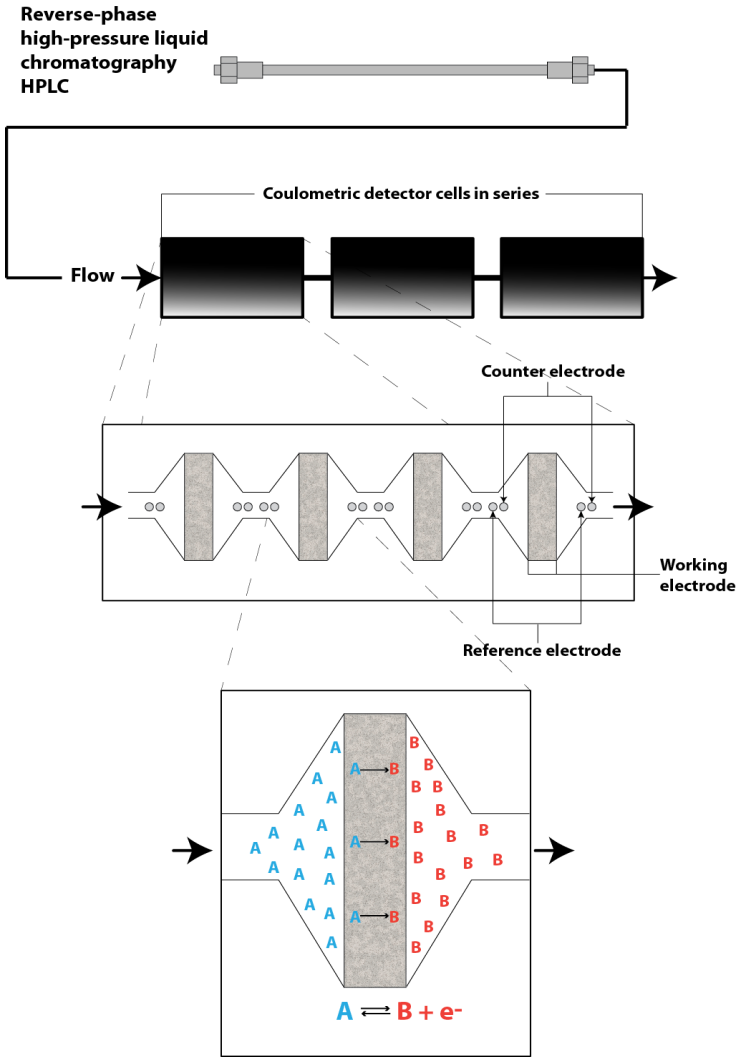

Figure 8. Diagram of HPLC and flow-through coulometric electrode array system (CEAS). Notice that each cell contains four detector channels allowing for progressively higher potentials to be used, essentially giving the capability of 12 independent electrochemical detectors.

demonstrates that the flow-through CEAS detection system offers the most sensitivity, selectivity, and is extremely quantitative when compared to other electrochemical detectors. We have chosen HPLC coupled CEAS as our metabolomics platform due to the minimal signal to noise ratio, high sensitivity, and quantitative nature (Figure 5). It has

also been used as a platform to study aging and caloric restriction (Kristal, Shurubor, Kaddurah-Daouk & Matson 2007b).

1.6.4 Disadvantages of electrochemical detection as a metabolomics platform

There are distinct disadvantages when comparing ECD to MS and NMR when used as metabolomics detection platforms. The first, and arguably the most significant is that ECD does not give any direct structural information about the individual metabolite. This requires additional work to identify the detected metabolites. Other groups are attempting to address this by coupling MS to ECD resulting in the combination of benefits from each platform (Bird et al. 2012). This deficiency is easily overcome by the creation of a "database" of known metabolites that can be used to help identify metabolites of interest. This is an intensive procedure requiring standards be run on the method of choice and the "spiking", which is the addition of a known concentration of standard to a tissue sample, to correctly identify peaks.

The second disadvantage is that ECD is limited in its sample throughput. For example, our current system has a run time of roughly 3 hours per sample. This presents a few problems regarding throughput, obviously the time to analyze a high number of samples rapidly, but also the possible degradation of sample metabolites over time in the samples waiting to be analyzed. Unfortunately, we cannot the remedy the time to analyze individual samples. The goal is to separate and detect with the best separation possible in a reproducible manner. Therefore, modifying the gradient profile will diminish this in favor of rapid throughput. This was adapted to be an exploratory method, therefore, we

are not concerned with how many samples can be processed in a short amount of time. In the future, we could modify the method to focus on given metabolites of interest. The other issue regarding the prolonged nature of our method and sample degradation is the volatile nature of some metabolites. If we allow samples to wait to be analyzed, they may degrade giving us a false concentration. We determined the length of time a sample can be viably stored at 4°C, and extract only the number of samples that will allow the final sample to sit for a safe period of time.

Another disadvantage is the chromatographic drift occuring over time that complicates the analysis. In particular, this can disrupt the pattern recognition we perform to explore global metabolite changes in the mice. However, we take great care to make large batches of mobile phases and mix these so that there is a homogenous quality of mobile phases throughout the analysis. We also use algorithms that mathematically stretch or compress the chromatograms.

The final disadvantage may also be an advantage depending on your perspective. The ECD platform can only detect reduction-oxidation active compounds. The method is based on electrochemical exchange of electrons, therefore if a metabolite is not redox active it will not be detected. We can perform a derivatization of molecules before analysis if we are interested in redox inactive compounds. We do not do any derivatization of any metabolites in the current study. It has been hypothesized that there may be over 3500 detected metabolites in the brain. Many of these compounds are redox active as many signaling molecules and reactions are part of oxidation/reduction reactions. By using ECD and detecting redox active compounds, we may increase the probability of finding a change

in a metabolite that is critical in signaling or brain function by reducing the detection burden of trying to identify a large number of metabolites.

1.6.5 Advantages of electrochemical detection as a metabolomics platform

There are also distinct advantages of the ECD platform that make it ideal for the analysis of brain metabolites. The CoulArray ECD is a highly sensitive method of detection with a sub-nano level capability of detection. Some labs have reported sub-pico level detection, however, as with most platforms, these are limited by signal to noise issues. Other platforms, specifically MS, have achieved progressively and rapidly lower detection limits that easily rival those of ECD. Currently, our limit of detection is between 1-10 ng of metabolite.

As discussed briefly above (in disadvantages), the ECD platform gives great specificity and selectivity for redox active metabolites. Most metabolites of many major biochemical pathways are redox active. It does not detect inert metabolites and allows us to focus on the reactive metabolites with a greater signal to noise with high quantitative precision. The ECD coupled HPLC method allows us to separate molecules based on HPLC method, in our case by hydrophobicity (reversed-phase HPLC) as well as by electrochemical potential. Each ECD array contains four electrochemical cells (we currently employ 3 cells giving us the power of 12 detectors) and each can be set at sequentially higher voltage potentials. Redox active compounds are differentially active, that is they have a distinct "oxidation" potential. We set each of our detectors at a progressively higher voltage and this allows us to detect co-eluting metabolites based on

electrochemical potential. The probability of metabolites having a similar retention time and electrochemical potential is low. Therefore, as a tool for the discovery of metabolomic changes in brain tissue and as an exploratory method to analyze these changes in a highly quantitative manner, electrochemical detection is more than adequate.

1.6.6 High Energy Focused Microwave

To understand quantitative metabolic changes in the brain, it is imperative to harvest brains in such a way that the *in vivo* state is preserved. An inherent difficulty in studying metabolomics, particularly in the aged brain, is the acquisition of quality and pathologically relevant tissue. Many different methods of euthanasia have been proposed to be proficient at extracting tissue in a manner that preserves the *in vivo* status of metabolites. Typically, these methods involve various protocols of euthanasia followed by decapitation and flash freezing the brain in liquid nitrogen to halt metabolic activity. The limiting factor is the time between euthanasia and the submersion of the tissue in liquid nitrogen. It has been shown that the method of euthanasia can influence the brain metabolome (Hunsucker et al. 2008). The use of anesthetics before euthanasia is common and is used to prevent pain or distress in the animals. However, the introduction of anesthetics can have important effects on the animal's physiology causing alterations to the metabolomer. Therefore, finding a method that will allow for rapid and humane euthanization of the mice, does not require the use of anesthetics, and preserves the metabolome of the brain tissue in a way that represents a live animal is important.

We employ high-energy focused microwave irradiation (HEFM) applied directly to the brain. This results in immediate death and arrests brain metabolic and enzymatic processes essentially instantaneously. This method does not use anesthetics or sedatives and requires very little handling of the mice. Levels of lipids, neurotransmitters, peptides, and neurometabolites as well as post-translational modifications including phosphorylation state of proteins can all be preserved and detected. The conservation of the metabolome and the protein state more accurately reflect the *in vivo* situation after HEFM irradiation when compared to other methods. This instantaneous arrest of metabolic and enzymatic activity ensures that the metabolite state and the protein phosphorylation state are preserved. Both are crucial since we will be studying the mTOR pathway (a multi-kinase pathway) and preservation of the state of protein phosphorylation is crucial as well as the brain metabolome.

Previously, our lab has used this method to assess the significant changes in the brain proteome of mice euthanized by HEFM and decapitation; we showed preservation of the *in vivo* state when HEFM was used in lieu of cervical dislocation (Hunsucker et al. 2008). Protein phosphorylation was markedly different in HEFM samples, versus cervical dislocation samples. Using difference gel electrophoresis (DIGE) to analyze the cerebellar and hippocampal proteome of the Ts65Dn mice compared to LMC at 6 and 12 months, we showed that there are more significant changes to the proteome in response to the age of the mice compared to changes we see due to trisomy (Vacano et. al., in preparation). Our preliminary results show that there are significant changes to the proteome and strongly suggest that there will be changes in the brain metabolome associated with aging.

There is a concern that HEFM and the heat required to halt the enzymatic activity may be altering the metabolome through derivation of the molecules. This is a valid concern and one that we do not dispute. However, other detection methods (fluorescence detection) require that samples be derivatized with a fluorescent tag and this does not compromise the validity of the method. Therefore, we do not feel this is an issue with our instrument.

To determine if we were creating *de novo* metabolites or derivitized molecules from HEFM euthanization we compared metabolic profiles of mice euthanized by HEFM and cervical dislocation (CD) followed by decapitation. We found that the profiles from mice euthanized by HEFM differed from those euthanized by CD and decapitation (Figure 8). These chromatographic profiles show that concentration levels of specific metabolites detected consistently change between euthanization method. However, we do not see the creation of any new peaks or shifting of peaks found in the CD mice when compared to profiles of the HEFM mice. This is strong evidence that HEFM euthanization does not derivitize any metabolites, at least not in a significant way. Obviously, to be certain that the chemical nature of the metabolites was not being altered a comparison through a method allowing structural analysis would need to be done. This also provides evidence that HEFM is preserving the metabolites in a way that represents the living state.

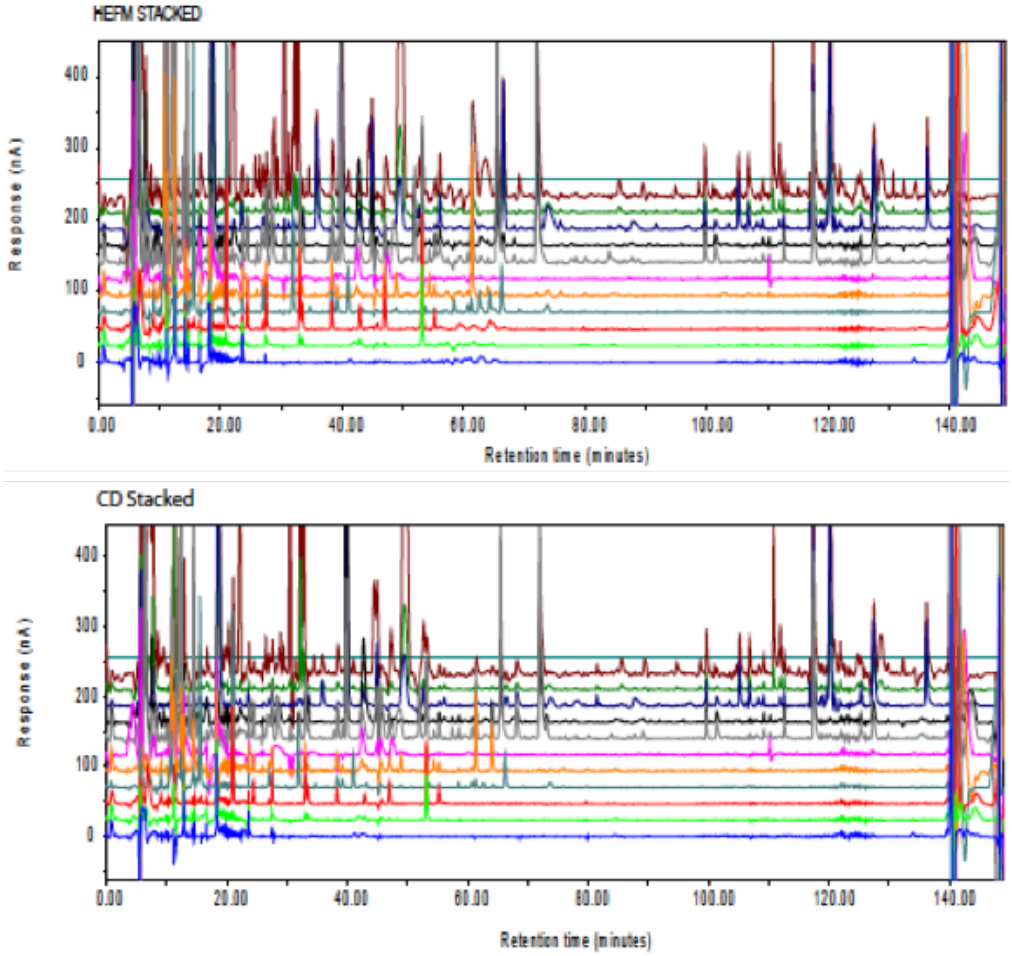

Figure 9. HPLC-EC chromatogram of 2 mice comparing different euthanization methods. The top shows the profile of a mouse euthanized by high energy focused microwave, the bottom a mouse euthanized by cervical dislocation and decapitation.

The following chapters will describe metabolomics studies in a mammalian model of DS, aging, and Alzheimer's disease using both targeted and global metabolomic profiling to elucidate changes associated with DS, and aging. We also aimed to determine if prolonged treatment with rapamycin can ameliorate the changes we see in the mice due to a triplicated chromosome and aging. Also discussed is the study of the DNPS in a CHO model system. We analyze and characterize two genetic mutations in the pathway associated with phosphoribosylaminoimidazole carboxylase/phosphoribosyl amino-imidazole succinocarboxamide synthetase (PAICS).

Both the mammalian and cellular model organisms can provide deep insight into metabolic pathways and the molecules that regulate the aging process as well as different disorders and pathologies. We employ the HPLC coupled electrochemical detector extensively in both the study of the metabolomics changes in the Ts65Dn mouse model as well as in the study of the DNPS. Much of the system validation was done using the CHO cell lines and led to several successful lines of study. For example, the machine was used to create a sensitive kinetic assay to measure the bi-functional enzyme adenylosuccinate lyase (ADSL) and the conversion of both substrates (SAICAR and SAMP) simultaneously (Ray 2012). This work, in addition to the previous work in our lab on the ADSL protein, led to collaborations with the Max Planck Institute for Evolutionary Anthropology. This collaboration has found interesting results using an ancestral version of the ADSL protein.

Taken together, the following work attempts to integrate metabolomics studies to understand metabolism in both a mammalian model and a cellular model.

Chapter Two

Brain metabolomics of long-term rapamycin treatment in the Ts65Dn mouse model of Down syndrome, aging, and early onset Alzheimer's disease

Abstract

Aging is often associated with impaired cognition and a progressive loss of organ function over time accompanied by an increased susceptibility for many disorders, including Alzheimer's disease (AD), Parkinson's disease (PD), heart disease, osteoporosis, type II diabetes, and many forms of cancer. Interventions that can increase the healthspan of an individual are of the utmost importance. With a rapidly aging population, the negative impacts of aging and age-related disorders is a major cause of increased human suffering both for affected individuals and for families and caregivers. Metabolic changes are also apparent in normal aging, but may increase in magnitude or nature with accompanying disease states or with accelerated aging. Thus, studying aging in a disease state, or in a disorder characterized by accelerated aging, will facilitate identification of these changes. Down syndrome (DS) is an intellectual disability characterized by premature aging. We hypothesize that trisomy of chromosome 21 (HSA21) causes disruption of the metabolome leading to an accelerated aging phenotype. In the Ts65Dn mouse model of DS, a premature

aging phenotype is also observed. We used the TS65Dn mouse model to study the metabolic changes associated with trisomy, and how these change with age. An initiative by the National Institute on Aging (NIA) Interventions Testing Program testing the efficacy of rapamycin treatment demonstrated that mice treated with rapamycin showed a significant increase in lifespan and healthspan. Therefore, we hypothesize that treatment of the Ts65Dn mouse model of premature aging and DS with rapamycin will ameliorate the accelerated aging phenotype in the Ts65Dn mouse model of DS.

1.0 Introduction

Aging is often associated with impaired cognition and a progressive loss of organ function over time. Though subtle in normal aging, this shift from fully-functional to failing-to-function is associated with an increased susceptibility for many disorders, including Alzheimer's disease (AD), Parkinson's disease (PD), heart disease, osteoporosis, type II diabetes, and many forms of cancer. Many theories of aging such as telomere shortening, oxidative stress, mitochondrial dysfunction, and inflammation have been investigated using a reductionist approach. All are likely contributors to the progressive decline in function associated with aging, and it is clear that they are not mutually exclusive. Hence, aging is not only complex, but is the single largest risk factor for many human diseases. Understanding the basic mechanisms involved in normal aging as well as aging associated with or accompanying disease states is critical for the design of novel and effective treatment strategies that not only prolong lifespan, but also increase healthspan.

Caloric restriction (CR) and dietary restriction (DR) without starvation have been shown to significantly extend healthspan by decreasing the onset of age-associated pathologies including cancer, cardiovascular disease, diabetes, and cognitive decline (Weindruch et al. 1986; Masoro 2005; Kennedy et al. 2007). Interventions that can increase the healthspan of an individual are of the utmost importance. With a rapidly aging population, the negative impacts of aging and age-related disorders is a major cause of increased human suffering both for affected individuals and for their families and caregivers. In addition, the costs associated with care and medicines for the elderly have increased substantially. Reducing the susceptibility to age-related disease would

significantly reduce human suffering and the cost burden on individuals as well as on the healthcare system. An initiative by the National Institute on Aging (NIA) Interventions Testing Program testing the efficacy of rapamycin treatment demonstrated that mice treated with rapamycin showed a significant increase in lifespan, even when treatment was administered late in life (Harrison et al. 2009; Miller et al. 2011). Later studies have now shown that treatment with rapamycin ameliorates many age-associated pathologies including heart disease, AD, PD, dysregulated immune function, and diabetes (reviewed in (Johnson et al. 2013)). Rapamycin is also being investigated as a treatment for a variety of cancers more common in older individuals. Most of these conditions are accompanied by metabolic changes, and how rapamycin brings about these changes is under intense study but not yet completely understood.

1.1 DS and Ts65Dn mice as models of premature aging

DS is the most common genetic cause of intellectual disability (1/700 live births) and includes an accelerated aging phenotype (Nakamura & Tanaka 1998; Patterson & Cabelof 2012; Zigman & Lott 2007). In addition to intellectual delay and accelerated aging, individuals with DS have an increased incidence of leukemia, and diabetes but a decreased risk of atherosclerosis and many solid tumors that show increased incidence with age (Yang and Reeves 2011, Yang 2016). These last two features strongly suggest that there are metabolic differences in people with DS. People with DS begin to show the neuroanatomical changes associated with AD (amyloid plagues and neurofibrillary tangles) typically by age 40. Many individuals with DS will develop AD by their 50s, and

it is likely that all individuals with DS will develop AD as they get older. The amyloid precursor protein (APP) gene is found on HSA21 and is trisomic in individuals with DS. APP encodes a protein that when proteolytically cleaved, produces the Aβ peptide, the major component of amyloid plaques in AD. One hypothesis is that individuals with DS are at an increased risk of early onset AD not only because of increased APP gene dosage, but because they age prematurely (Chicoine & McGuire 1997; Lott & Head 2005; Patterson & Cabelof 2012).

Additionally, many biomarkers associated with aging, such as oxidative stress, accumulation of mutations, and altered DNA repair, are found in individuals with DS. Although marked improvements in life expectancy have been achieved, the life expectancy of individuals with DS remains significantly reduced, and risk of mortality is higher (Coppus et al. 2008). Hematopoietic and neural stem cells taken from individuals with DS show changes characteristic of premature aging such as increased expression of pro-apoptotic genes, and inflammatory genes, and a down regulation of DNA repair genes (Cairney et al. 2009). Increased accumulation of altered aspartate residues in proteins, a phenomenon associated with cellular aging, has also been observed in DS (Galletti et al. 2007).

The Ts65Dn mouse model of Down syndrome is trisomic for most of the region of mouse chromosome 16 (Mmu16) homologous to HSA21 (Davisson et al. 1990; Reeves et al. 1995). Ts65Dn mice show signs of premature aging reminiscent of those associated with DS. They have an increased risk of mortality and show age related declines in mobility and motor function and other features of aging not observed in littermate control (LMC)

mice (Sanders et al. 2009). They exhibit a widespread impairment of cell proliferation in cerebellum, hippocampus, skin, and bone marrow (Contestabile, Fila, Bartesaghi, et al. 2009; Contestabile, Fila, Cappellini, et al. 2009; Jablonska et al. 2006). They are also resistant to certain solid tumors as they age and may promote survival in models mouse models of cancer (Satgé & Vekemans 2011; Yang & Reeves 2011).

Ts65Dn mice have spatial learning and memory deficits that involve the hippocampus and have structural alterations in the hippocampus that are similar to those seen in DS, and that worsen with age (Holtzman et al. 1996; Rueda et al. 2005). Ts65Dn mice show learning and memory deficits at 3 months of age compared to LMC mice.

These are minimized by 8 months, and then rapidly worsen, becoming readily apparent by 12 months of age (Hyde & Crnic 2001). Along with loss of learning and memory, the mice lose functional basal forebrain cholinergic neurons, reminiscent of early onset AD (Granholm et al. 2000). Ts65Dn mice are trisomic for the APP gene and although they do not develop plaques and tangles, a recent study concluded that there is an age dependent dysregulation of APP metabolism in Ts65Dn mice (Choi et al. 2009). No abnormalities could be found in APP gene expression or APP metabolite levels in brains of 4-month old Ts65Dn mice. However, at 10 and 12 months of age, Ts65Dn mice showed elevated levels of APP and soluble APP metabolites. MRI studies reveal *in vivo* cholinergic changes possibly relevant to early onset AD in the brains of Ts65Dn mice (Yuanxin Chen et al. 2009). Trisomy of APP has been shown to be important for proper early endosome function in these mice (Salehi et al. 2006). Studies comparing cerebella from 3 and 10 month old Ts65Dn mice show that cerebellar abnormalities increase with age in these mice

(Necchi et al. 2008). These investigators also reported that 10-month old Ts65Dn mice develop sporadic tremors and stereotypic behavior, which may reflect cerebellar anomalies. Degeneration is even more significant at 12 months of age (Lomoio et al. 2009). Some of the relevant changes observed in the Ts65Dn mice as they age are presented in Table 1.

1.2 mTOR and aging

Rapamycin is a macrocyclic lactone metabolite produced by the soil bacterium *Streptomyces hygroscopicus* on the island of Rapa Nui. Rapamycin forms an intracellular complex with its receptor FK506-binding protein, FKBP12, which binds to the c-terminus region of the mechanistic target of rapamycin (mTOR), effectively inhibiting mTOR enzyme activity. Mechanistic target of rapamycin (mTOR) is a protein kinase, which acts as a central regulator of eukaryotic growth and division in response to nutrient and growth factor signals. It is the primary component of two heteromeric complexes, mTORC1 and mTORC2. mTORC2 is rapamycin insensitive, and includes mTOR, rapamycin-insensitive companion of mTOR (Rictor), and mLST8. mTORC2 has been shown to be important for actin cytoskeleton regulation (Loewith et al. 2002; Jacinto et al. 2004). mTORC1 is a complex of three proteins: mTOR, regulatory associated protein of mTOR (Raptor) and mLST8. mTORC1 is rapamycin sensitive, and treatment with rapamycin causes down regulation of mTOR activities in cell growth and metabolism. Intra and extra-cellular signals are integrated through mTOR. Metabolic signaling integrated through mTOR is initiated by four major inputs; growth factors, nutrients, energy, and hypoxia. The initial

downstream effectors of mTOR are p70 ribosomal protein S6 kinase (S6K) and the eukaryotic translation initiation factor 4E-binding protein stimulating translation and recruitment of translational machinery (4EBP; (Fang et al. 2001). These initiate a host of downstream effects that include mitochondrial metabolism, lipogenesis, RNA transcription, protein translation, and angiogenesis.

Regulation of cell growth and division in response to cellular energy and nutrient availability through TOR has been proposed as a mechanism for increased longevity and extension of healthspan in invertebrate models (Kapahi et al. 2004; Kaeberlein et al. 2005; Hansen et al. 2007). The mTOR pathway may also hold clues to ameliorating the effects of aging and age-related diseases. Although inhibition of mTOR produces some negative effects, such as glucose intolerance and insulin resistance in mice, the benefits in models of aberrant aging are impressive. These include a delayed progression of disease in models of AD, protection against dopaminergic neuron loss in models of PD, and rescue of learning and memory in aged mice (Spilman et al. 2010; Majumder et al. 2011; Halloran et al. 2012; Majumder et al. 2012). Halloran *et al.* describes the measurement of brain metabolites using HPLC coupled Coulochem II detection, the precursor to the more robust CoulArray detection platform, which we employed. Rapamycin treatment in a mouse model of aortic constriction shows reduced hypertrophy (Shioi 2003), and reduces cardiomyopathy in a lamin A/C progeria model (Ramos et al. 2012). Additionally, mice fed rapamycin late in life showed improved cardiac contractile function, reduced inflammation, and increased anti-hypertrophic signaling versus controls (Flynn et al. 2013).

1.3 Ts65Dn model system

We propose an unbiased, global metabolomic analysis of electrochemically active compounds in the cortex and cerebellum of the Ts65Dn mouse and LMC. While genome, transcriptome and proteome analyses are valuable, the metabolome may be more closely associated with phenotype. Metabolomic analysis, therefore, may provide the best characterization of age-related decline. Additionally, metabolomic analysis should facilitate characterization of interactions between complex genetic and proteomic factors and how changes in these interactions may lead to loss of homeostasis and disease. There may be conserved molecular targets, pathways, and interactions important to maintaining stability in homeostasis. Identification of these critical targets may lead to new treatment options.

We expect to see metabolic changes in both Ts65Dn and LMC mice as they age, and further expect metabolic differences due to Ts65Dn trisomy. However, the Ts65Dn is not an inbred strain of mice, so these changes may not be limited to only our study and possibly represent the human population more robustly. Changes in LMC mice would be associated with normal aging, while changes in Ts65Dn mice would include changes due to trisomy and premature aging, such as increased neurodegeneration, as well.

For the observed changes to be relevant to aging or to trisomy, treatments that ameliorate aging should be helpful to both the Ts65Dn and LMC, while treatments that ameliorate the effects of trisomy will be helpful to Ts65Dn mice. These changes could extend lifespan or health span and possibly prevent or reverse the deleterious aspects of the

genotype of the Ts65Dn mice. We hypothesize that supplementation with rapamycin will alter the metabolome of Ts65Dn and LMC mice, and ameliorate the consequences of aging in both. Previous studies with rapamycin on other mouse models, including models of aging, heart disease, PD, and neurodegeneration (including AD) have shown encouraging results (Tain et al. 2009; Spilman et al. 2010; Majumder et al. 2011; Wilkinson et al. 2012; Halloran et al. 2012).

1.4 Method of euthanasia

To understand quantitative metabolic changes in the brain, it is imperative to harvest brains in such a way that the in vivo state is preserved. We will employ high-energy focused microwave irradiation (HEFM) applied directly to the brain. This results in immediate death and arrests brain metabolic and enzymatic processes essentially instantaneously. Levels of lipids, neurotransmitters, peptides, and neurometabolites as well as post-translational modification including phosphorylation state of proteins more accurately reflect the *in vivo* situation after HEFM irradiation versus other methods. This instantaneous arrest of metabolic and enzymatic activity ensures that the metabolite state and the protein phosphorylation state are preserved. Both are crucial since we will be studying the mTOR pathway (essentially a multi-kinase pathway) and preservation of the state of protein phosphorylation is crucial. Previously, our lab has used this method to assess the significant changes in the brain proteome of mice euthanized by HEFM and decapitation; we showed preservation of the *in vivo* state when HEFM was used in lieu of cervical dislocation (Hunsucker et al. 2008). Protein phosphorylation was markedly

different in HEFM samples, versus cervical dislocation samples. Using difference gel electrophoresis (DIGE) to analyze the cerebellar and hippocampal proteome of the Ts65Dn mice compared to LMC at 6 and 12 months, we showed that there are more significant changes to the proteome in response to the age of the mice compared to changes we see due to trisomy (in preparation). Our unpublished results (Vacano et. al., in preparation) show that there are significant changes to the proteome and strongly suggest that there will be changes in the brain metabolome associated with aging.

1.5 Choice of metabolomic method

Metabolomics is the identification and quantification of all small molecule (<1500 Da) metabolites in a biological sample (Wishart 2010). Current estimates are that there may be about 3000 known endogenous metabolites in mammals, and likely more that have not yet been detected. Global metabolomics attempts to identify and quantify all metabolites in a sample. Targeted metabolomics attempts to examine a particular subset of the metabolites in a sample. Methods for metabolomic analysis must be quantitative, selective, and sensitive. High sensitivity methods allow for the identification of low abundance metabolites; selectivity provides information to distinguish between two chemically similar metabolites; quantifiable results are critical for identifying relative changes in metabolite levels. Many metabolomics studies use high performance liquid chromatography (HPLC) as an initial separation method. There are various methods for metabolite detection after HPLC separation, but no method detects all metabolites (Wolfender 2009).

We analyzed the metabolic changes accompanying aging using HPLC coupled with electrochemical detection (HPLC-EC) using flow-through coulometric electrochemical cells. This method allows for the quantitative detection of several hundred metabolites in about two hours and has been used to study aging and DR in rodents (Shi et al. 2002) and neurodegenerative disorders in rodents and in humans (Stack et al. 2008; Rozen et al. 2005). HPLC-EC is extremely sensitive, (some compounds can be detected in femtomole amounts), quantitative, and has a dynamic range of ~6 orders of magnitude. This allows for the detection of a wide range of metabolites including lipids, neurotransmitters, some amino acids, intermediates in glutathione synthesis and purine and pyrimidine synthesis, and many other compounds relevant to critical metabolic pathways. For a method to be clinically useful it must be high-throughput and relatively robust. Sample collection should be minimally intrusive and rapid for accurate analysis. We propose analysis of both brain and blood samples, but for clinical applications, analysis of blood biomarkers would be the most reasonable choice. HPLC-EC has been employed in the search for blood biomarkers for PD; we would like to establish a similar approach (Bogdanov et al. 2008). Sample preparation for analysis by HPLC-EC is quite simple, involving metabolite extraction with cold acetonitrile acidified with 0.4% acetic acid, which has been found to yield highly reproducible results with blood, serum, plasma, brain, and mitochondria (Kristal et al., 2007).

An obvious strength of the method is the ability for a 2-dimensional separation based on retention time (HPLC) and electrochemical potential. The detector consists of 3 electrochemical cells with 4 coulometric channels each for a total of 12 autonomous

electrochemical detectors. Each can be set to a progressively higher electrochemical potential and will allow for separation and identification of metabolites with similar retention times based on their electrochemical properties (Figure 1). These cells have an upper limit of about 900 mV but we have the capability to detect molecules with oxidation potentials of 1700 mV with a boron-doped diamond amperometric cell. Figure 1 also demonstrates our ability to detect several hundred peaks using our current method. Unfortunately, the method of detection provides little structural information. However, this can be remedied by the use of known standards. Dr. Wayne Matson, the inventor of the flow-through coulometric cell, has kindly provided us with the set of standards they use in their brain metabolomics research.

2.0 Methods

2.1 Mouse Handling and Care

The care of the animals and the procedures for their use follow the many recommendations for the use of mice in gerontological research (Miller & Nadon 2000). All experiments were approved by the University of Denver Animal Care and Use Committee. We treated mice with rapamycin, an immunosuppressant previously shown to increase longevity and health in aged mice (Harrison et al. 2009; Miller et al. 2011). We chose three age groups (6, 12, and 18-month), see below for reasoning. Each received a diet containing microencapsulated rapamycin, or control diet without rapamycin starting at 4 months of age. For each age group we will have two cohorts, trisomic and disomic littermate controls (LMC).

- 6 – month

  The 6-month time point was chosen as this is the age when the mice have reached their cognitive peaks.

- 12 – month

  By 12 months the Ts65Dn mice begin to experience delays in learning, and memory behavior.

- 18 – month

  After 18-months the mice have deteriorated significantly and have severe declines in learning, and memory behavior as well as survival

In the literature, the number of Ts65Dn mice used in similar analysis to those we chose are in the range of 10-15 mice, achieving statistical significance of $p<0.05$ (Reeves et al. 1995; Kirsammer et al. 2008; Lockrow et al. 2009). Given the variability of the assays we are fully aware that there will be some attrition, particularly in the 18-month group. Trisomic males are sterile, therefore, we used males for analysis. Trisomic females were required for breeding to maintain the colony and were not used in the analysis. We expected 15 trisomic and 15 LMC per testing group to be sufficient to detect differences similar to those seen in the literature. Therefore, we determined we would need 180 male mice, 90 trisomic and 90 LMC. This was calculated as follows: 3 age groups x 15 mice = 45 trisomic mice and the same number of LMC (45 mice x 2 = 90 mice). We treated both the trisomic and LMC with either rapamycin containing diet or control diet (90 mice x 2 = 180 mice). Roughly 30% of each litter is trisomic and half are expected to be male. This required the production of 600 offspring to obtain 90 trisomic Ts65Dn males (600 x 0.5 x

0.3 = 90). The average litter size is 5 mice and the typical Ts65Dn female will provide, on average, 4 litters. Therefore, we expected to need 35 trisomic Ts65Dn females and 35 B6EiC3Sn C57BL/6JEi x C3H/HeSnJ F1 males. All our breeder mice were purchased from Jackson Labs. Over a three year period, we used roughly 638 mice, 600 experimental, and 38 male breeders purchased from Jackson Labs.

The University of Denver Natural Sciences and Mathematics Animal Facility is AAALAC accredited and is supervised by the University of Denver Institutional Animal Care and Use Committee (IACUC). The Facility is under the supervision of the University of Denver veterinarian, Dr. Ron Banks, who is available at all times. A full-time animal care technician performs routine cage cleaning, feeding, and watering, and daily health and welfare checks. If animals exhibit distress, injury, or infection the technician and veterinarian will recommend proper treatments (antibiotics, analgesics) to remedy the situation. If the welfare of the animal is at risk the veterinarian may intervene and terminate the study. We do not use any surgical procedures.

Paired matings (one male and one female) were used to breed the mice. The male and female were continually housed together in order to generate multiple litters. Bedding squares were placed in cages with all breeding and pregnant mice so that females can nest throughout pregnancy and until weaning. Mice were weaned when they are able to reach food and water sources and feed themselves (typically 19 to 21 days of age). If one or more mice in a litter appeared smaller than normal at weaning (as determined by the researcher performing the weaning) a few pieces of moistened food were placed in the bottom of the new cage to ensure access to food and water during the first few days after weaning.

Weaned mice were housed in same-sex littermate groups. If weaned mice appeared to be fighting or barbering excessively, they were separated and individually housed. Any mouse with minor skin abrasions or cuts were treated with a small amount of topical antibiotic and were carefully monitored to insure that the cuts heal. Mice housed singly were given bedding squares to provide environmental enrichment in the absence of littermates.

A maximum of five adult mice or a single breeding pair with pre-weaned young are maintained per polycarbonate cage (50 square inche floor area). Cages are washed once a week and filled with an appropriate amount of sterilized white pine shavings. Water bottles were replaced with clean bottles weekly and filled with acidified (pH 2.8-3.2) water. Cage lids are covered with a snap-on non-woven polyester flat filter. Food hoppers, which are attached to the cage lids, were filled weekly. On a daily basis (Monday through Sunday), animal care technicians check to determine the mice have sufficient food and water, bedding is not excessively wet or dirty, and mice appear in good condition. All mice are transferred into clean housing weekly.

a. Blood sample collection.

   Blood was collected by maxillary venipuncture from unanesthetized mice. Anesthetics are not administered because 1) experienced researchers can perform this technique rapidly and effectively; 2) the risk associated with administration of anesthesia exceeds the temporary discomfort associated with the withdrawal of up to 400 µl of blood using a microhematocrit tube; and 3) published evidence suggests that anesthetics can alter blood chemistry. This will likely affect our metabolomic

analyses, which is extremely sensitive. All animals that were bled were checked during the next week for signs of infection or damage caused by the sampling procedure.

b. Ear notching

A small 1-2 mm punch was used to produce a small hole near or notch at the edge of the mouse's ear. A small notch was taken a notch taken from the left ear for genotyping, which is necessary to identify trisomic mice from LMC. Notches (1-3) will be taken to identify each mouse in a cage. We have found this method of identification to be less problematic than ear tags, which can be torn out.

c. The Ts65Dn mouse model used for these experiments were maintained by crossing Ts65Dn females to C57BL/6JEi x C3H/HeSnJ (B6EiC3Sn) F1 males. The recessive retinal degeneration 1 mutation (Pdebrd1) is segregating in this model. The mutation causes retinal degeneration, which can be evaluated using an ophthalmoscope. The procedure involves restraining the mouse by hand (holding the scruff of the neck), and applying a drop of 1% atropine sulfate (which dilates the iris) to one eye. The mouse is then returned to its cage for five minutes, and is then restrained, again by hand. The ophthalmoscope evaluation involves shining a light into the eye, and looking into the dilated eye with a lens, to visually evaluate retinal degeneration. This procedure is necessary so that we can evaluate whether the blind mice have altered biomarkers when compared to sighted mice. We do not expect metabolomic profiles to be altered by the Pdrbrd1 gene, but can check this easily by examining the mice for retinal degeneration.

Table 1. Final rapamycin treatment groups and final number of subjects

Diet	**Control**			**Rapamycin**		
Group	6 month	12 month	18 month	6 month	12 month	18 month
Disomic	14	15	14	14	13	13
Trisomic	14	14	7	15	12	10

2.2 Microencapsulated rapamycin diet and control diet

The National Institute of Aging (NIA) Interventions Testing Program (ITP) was created to find lifespan and healthspan extending treatments, in particular those that have received FDA approval for other treatments. Rapamycin was determined to increase lifespan in mice when treated late in life (600 day old mice) (Harrison et al. 2009). We obtained the same diet formulation that was used by the three independent locations of the original NIA-ITP study. The rapamycin (from LC Labs, Woburn, MA) was microencapsulated by Southwest Research Institute (San Antonio, TX), using a spinning disk atomization coating process with the enteric coating material Eudragit S100 (Röhm Pharma, Germany). The coating increases the fraction of rapamycin that survives the food preparation process by 3- to 4-fold. It also protected the agent from digestion in the stomach increasing adsorption (Nadon et al. 2008). Rapamycin (14 ppm) is incorporated into 5LG5 mouse chow. Control diet contains the Eudragit S100 entieric coating without rapamycin.

2.3 High-Energy Focused Microwave

We use high-energy focused microwave irradiation (HEFM) applied directly to the brain. This results in immediate death and arrests brain metabolic and enzymatic processes essentially instantaneously. This method does not use anesthetics or sedatives and requires very little handling of the mice.

Once the mice have reached the appropriate age they are scheduled for euthanization. To account for circadian changes in the metabolome every mouse was sacrificed between 1 pm and 4 pm. The mice were removed from the mouse facility several hours before and kept in a dimly lit room with the cages covered. A final weight for each mouse was measured and the mice were returned to their respective cages. The mice were placed in a mouse holder to keep them properly aligned and motionless during the procedure. Placing the mouse properly in the holder is crucial to ensuring accurate results with the microwave device. The microwave beam must pass through the brain tissue to halt all metabolic activity. Once the mouse has been euthanized, the mouse is removed from the holder and the temperature of the brain is taken using an electronic thermometer with a needle probe. All the mice received a microwave dose that heated the brain to between 85 ^{o}C and 95 ^{o}C, which ensures the cessation of enzymatic activity.

Once the mice have been euthanized the mouse is decapitated using a small animal guillotine (Kent Scientific). An incision through the midline of the scalp is made from the caudal end of the head to the rostral using sharp dissecting scissors. The scalp is pulled towards the ears and a similar incision is made through the midline of the brain. The skull is peeled away and the cerebellum is removed, placed in a microcentrifuge tube and flash

frozen in liquid nitrogen. The anterior portion of the brain is removed and placed in a separate microcentrifuge tube and flash frozen in liquid nitrogen. The samples are stored in -80 ^{o}C until metabolites are purified from them.

2.4 Metabolite extraction from brain samples

Sample preparation for analysis by HPLC-EC is quite simple, involving metabolite extraction with cold acetonitrile acidified with 0.4% acetic acid, which has been found to yield highly reproducible results with blood, serum, plasma, brain, and mitochondria (Kristal et al., 2007).

For metabolite extraction 16 mg of each brain were taken and homogenized in 1 mL of acidified acetonitrile and finely chopped using dissecting scissors. The samples were further homogenized using sonication (Branson Sonifier Cell Disrupter 185). The homogenized samples were centrifuged at 14,000 x g for 5 minutes. The supernatant was taken and frozen at -80°C for one hour. The pellets were saved for protein analysis used to normalize the data against. The frozen samples were placed into a speedvac concentrator and lyophilized for 2 hours (until all the acidified acetonitrile is removed). The samples were resuspended in 200 μL of mobile phase A and centrifuged at 14,000 x g for 15 minutes. Cerebellar samples followed the same extraction protocol, however, the entire cerebellum was extracted with 750 μL due to varying and limited tissue availability.

2.5 HPLC coupled electrochemical detection of brain metabolites

We analyzed metabolic changes accompanying aging using HPLC coupled with electrochemical detection (HPLC-EC) using flow-through coulometric electrochemical cells. This method allows for the quantitative detection of several hundred metabolites in about two hours and has been used to study aging and DR in rodents (Shi et al. 2002) and neurodegenerative disorders in rodents and humans (Stack et al. 2008; Rozen et al. 2005).

For the separation of metabolites from blood and brain samples, we employed reversed-phase HPLC with a gradient profile. Mobile phase A was primarily aqueous and consisted of 10 g/L pentane sulfonic acid (PCA), 1% methanol (MeOH), 1 mg/L citric acid, pH 2.85. Mobile phase B consisted of 50 mM lithium acetate (LiAc), 80% methanol, 10% acetonitrile, 10% isopropanol, pH 5.0. Both mobile phase solutions were filtered through 0.2 μm filters.

Table 2. Gradient protocol of the HPLC – EC system used to separate and detect tissue metabolites

Time (min)	Flow rate (mL · min $^{-1}$)	Mobile phase B (%)
0	0.750	0
40	0.750	12
47	0.750	20
74	0.530	48
120	0.740	100
127	0.900	100
133	0.900	100
140	0.750	0

Samples were kept at 4^{o} C until 30 μL are injected into the HPLC system using an ESA autosampler (model 542) and separated through a Tosoh Bioscience TSKgel guard cartridge and two TSKgel ODS-80T$_m$ C-18 columns (250 mm x 4.6 mm ID, 5 μm) in series to maximize theoretical plates. A column temperature of 30^{o} C was maintained throughout the analysis. The analytes were detected using a CoulArray HPLC system (model 5600A, ESA) with three coulometric detector modules. Each electrochemical cell contained four flow-through coulometric detectors in series.

Cell one (channels 1-4) was set to a range of potentials from 0 – 300 mV in 100 mV increments. Cell two - four (channels 5-12) were set to a range of potentials from 375 – 900 mV in 75 mV increments. The CoulArray software was used for baseline correction and analysis.

2.6 Protein Sample Preparation

The pellet from the metabolite extracted samples were resuspended in cell lysis buffer (10 mM Tris-HCl pH 8.3, 10 mM KCl, 2 mM EDTA, 1 mM DTT, 4% glycerol) with Inhibitor Protease Cocktail Tablets (Roche). The homogenate was centrifuged at 16,000 x g for 30 min. The supernatant was removed and placed into a fresh microcentrifuge tube. The protein concentration was determined by BSA protein concentration colorometric assay (Thermo Scientific) using standard procedures and measured on using Gen5 software.

2.7 Analysis of chromatographic profiles

Once the samples have been separated and detected, the raw data files (chromatograms) were batch analyzed. This involves the CoulArray software applying a proprietary algorithm to the chromatograms to flatten the baselines. As described in the Introduction, there was inherent drift in the channels, particularly when a gradient to 100% solvent mobile phase is involved. The software also determined peaks based on preset parameters. We set our peak parameters conservatively to ensure we stay above noise. The parameters we set are height threshold, a peak must reach a height of 0.005nA to be

considered a peak. A peak width minimum of 0.05 seconds was set as well. Once the peaks have been batch analyzed, they can be manually curated for known peaks, or be analyzed by the pattern recognition software.

2.8 Data analysis

2.8.1 Pattern recognition for global metabolomics analysis

Chromatographic peaks are input into the pattern recognition wizard, which is part of the CoulArray Software package. Once the peaks were loaded, a pooled sample was used as a reference sample. The pooled sample is sample comprised of 4 samples representing each group. The software takes the mean of the 12 channels in the pooled reference sample and matches these with each subsequent individual sample. The samples are manually curated and the alignment was checked for each sample. Only once each sample has been aligned with the reference sample was the algorithm applied. The final computed pattern recognition output gives data values that were deviation from the pooled reference sample over a given time, which was determined by the compression factor. Our compression factor is 20x. These data were imported into excel and the mean of sample duplicates (or triplicate in some cases) is calculated. These data were then normalized to protein concentration in mg to give a final value that can be considered the change in signal per mg of protein, this was considered a significant feature.

2.8.2 Significant feature

The pattern recognition software identifies significant features over a given segment of retention time. This feature was not a peak, rather a change in the signal pattern during that time duration or segment of the chromatogram. This will capture segments of peaks, but does not recognize peaks. Therefore, when discussing significant features in pattern recognition analysis we are describing the pattern of the chromatogram at different time intervals, not specific metabolites or compounds that recognized as peaks.

2.8.3 Targeted metabolite changes

We use targeted metabolite profiling to determine changes to disease or pathway relevant metabolites. As stated previously, targeted metabolomics using electrochemical detection is difficult because we do not obtain any structural information. To identify unknown peaks, we separate and detect standards using the same system. Once a standard was identified we spike tissue samples with the known standards and measure the change in peak area. In the CoulArray Software a peak table is created. The peak table acts at the metabolite library or database. This library was used by the software to identify peaks when each chromatogram was analyzed. Many of our standards were graciously donated by Wayne and Samantha Matson.

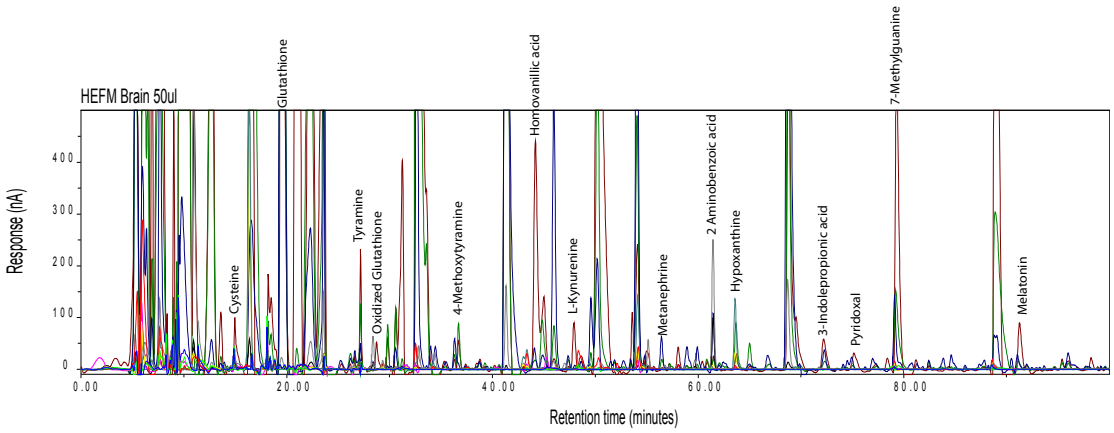

Figure 1. Representative chromatographic trace showing targeted metabolites.

2.8.4 Statistical analysis

We utilized MetaboAnalyst software to perform both univariate and multivariate analysis. MetaboAnalyst is web-based pipeline for the analysis of large and complex metabolomics data sets and provides comprehensive interpretation and visualization of the data. The analysis of the data includes two functional steps. The first was the data processing step, which includes different options for data filtering, normalization, and transformation. The second step was the actual data analysis, and visualization.

The normalized data are broken into relevant groupings to analyze the different experimental questions. For example, to understand the changes associated with the karyotype of the mice, we compare the data from disomic and trisomic mice on control diet. These data are then input into the software and a quality check was performed. During this step, missing values are replaced by null (N). Next we mean-center transform the data. This does not alter the variability of the data distribution; it just shifts the data to an arbitrary starting point.

2.8.5 Univariate analysis

Univariate methods are the most common methods of exploratory data analysis. For two group analysis we employed t-test, fold-change analysis, and volcano plots to show the relationship between features identified by the pattern recognition software and help identify patterns in those features. For analysis of more than two groups, we used analysis of variance (ANOVA).

2.8.6 Multivariate analysis

Two different multivariate analysis, principal component analysis (PCA) and partial least squares – discriminant analysis (PLS-DA), are used to identify sources of variance (PCA) in the data and the relatedness (PLS-DA).

2.8.7 Clustering analysis

Hierarchical cluster analysis (HCA) was performed to search for patterns in the data. In HCA each sample begins as an individual cluster and the algorithm combines them until all samples are clustered into a single large cluster, this shows

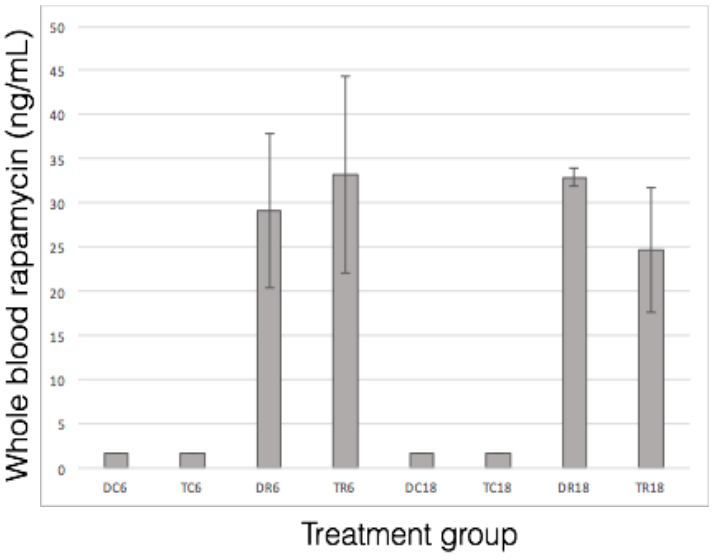

Figure 2. Whole blood rapamycin concentrations in Ts65Dn mice fed microencapsulated rapamycin (DR, TR) or control diet (DC, TC).

similarity of samples based on their significant features. Our HCA method uses the Ward clustering algorithm and Euclidean distance similarity measure.

3.0 Results

3.1 Global metabolomics – long-term rapamycin treatment

Mouse blood was collected into lavender capped EDTA tubes for analysis of rapamycin concentration in whole blood. The analysis was performed by Dr. Martin Javors at the University of Texas Health Sciences Center San Antonio (UTHSCSA). After consulting with Dr. Javors, four blood samples from each set (DC, DR, TC, TR) and at the two time points (6- and 18-month) were delivered for analysis. The results show that the mice fed microencapsulated rapamycin diet had elevated levels of rapamycin (Figure 2). The control mice had rapamycin levels below the limit of detection (1.56ng/mL) (Figure 2). The 18-month trisomic mice fed rapamycin diet had a lower level of rapamycin compared to the other mice on the treatment, however, this is insignificant and could be due to the mice eating less food compared to the younger mice.

3.2 Global metabolomics – general health of long-term rapamycin treatment

Weights of the mice were taken before they were euthanized to determine if there is an age-related loss in weight (Figure 3). As expected, the trisomic mice are significantly smaller than the disomic mice (Figure 3). The mice also show a reduction in weight as they age, this is part of typical aging in both humans and mice. The disomic mice also

show a significant loss of weight on rapamycin diet compared to those on control diet, this was not seen in trisomic mice (Figure 3).

Routine blood samples were taken from the mice for comprehensive blood analysis, including complete blood count (CBC) and blood chemistry (Table 3). Every four months starting at 6-months of age blood was collected from the mice by maxillary venipuncture and collected into lavender capped EDTA tubes for CBC and yellow capped tube for blood chemistry analysis. The blood was delivered to IDEXX Laboratories Inc. for analysis. The comprehensive blood analysis showed that the mice were in generally good health and did not show any significant changes in the different components of the analysis. This was true as the mice aged. Rapamycin diet also did not alter the blood chemistry or CBC in a way that would indicate poor or failing health. Additionally, we did not see a difference in the blood analysis between disomic and trisomic mice indicating poor or failing health. However, there are interesting changes in glucose and cholesterol levels in the mice. Glucose levels have been reported to increase in mice that receive short-term rapamycin

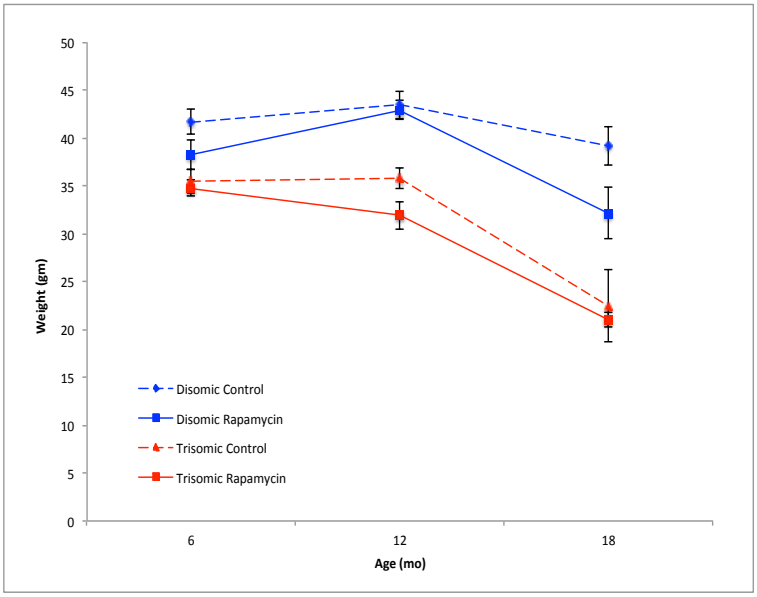

Figure 3. Age-related weight loss in the Ts65Dn mice. Weights of trisomic (red) and disomic (blue) mice on rapamycin (solid line) or control diet (dashed line).

treatment. Our blood analysis showed a similar increase in blood glucose levels in the mice receiving the rapamycin diet when compared to those on control diet (Figure 4). We do not see a difference between disomic and trisomic mice (fed control diet), indicating that this is due to the rapamycin diet, not karyotype of the mice (Figure 4).

Table 3. Complete blood count (CBC) and blood chemistry analysis performed by IDEXX Laboratories Inc.

Comprehensive Blood Chemistry		Complete Blood Cell Count	
ALKALINE PHOSPHATASE	GLUCOSE	WBC	MYELOCYTE
SGPT (ALT)	CALCIUM	RBC	PROMYELOCYTE
SGOT (AST)	PHOSPHORUS	Hgb	POIKILOCYTES
CPK	BICARBONATE	MCV	ANISOCYTES
ALBUMIN	CHLORIDE	MCH	METAMYELOCYTE
TOTAL PROTEIN	POTASSIUM	MCHC	MONOCYTE
GLOBULIN	SODIUM	NRBC	EOSINOPHIL
TOTAL BILIRUBIN	A/G RATIO	NEUTROPHIL	BASOPHIL
DIRECT BILIRUBIN	B/C RATIO	LYMPHOCYTE	
BUN	INDIRECT BILIRUBIN		
CREATININE	NA/K RATIO		
CHOLESTEROL			

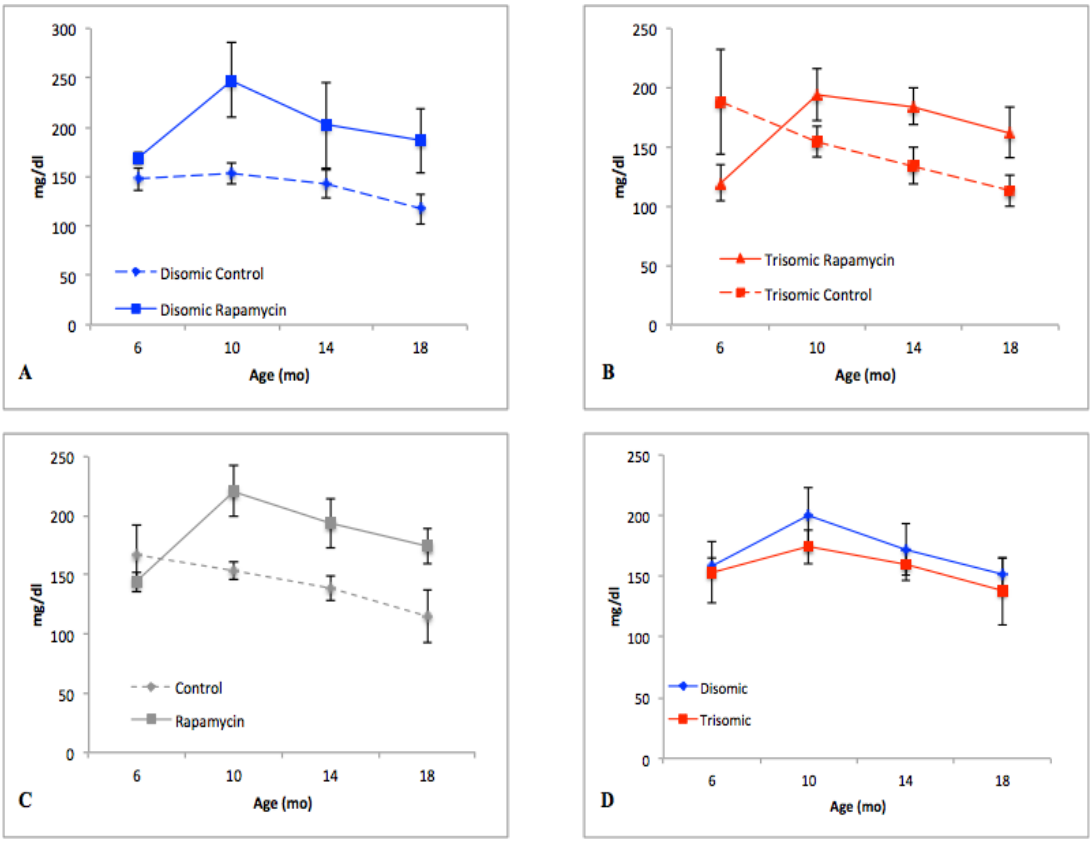

Figure 4. Blood glucose levels in mice receiving control diet or rapamycin diet A) Shows the blood glucose levels in disomic mice either on rapamycin diet or control diet, B) shows the same comparison in trisomic mice. C) Compares the mice either receiving rapamycin diet or control diet and D) shows the comparison between karyotype of the mice, these indicate the increase in blood glucose is due to diet.

When we compared the disomic mice on control diet to the mice on rapamycin diet we notice an initial rapid increase in blood glucose, however, after prolonged treatment with rapamycin, we see a decrease in the glucose levels (Figure 4). We also see a shift in the cholesterol levels of the mice, however, unlike the glucose levels, this appears to be caused by the karyotype of the mice rather than the diet (Figure 5). When the cholesterol levels are broken out by treatment, there is no difference between rapamycin and control diet groups (Figure 5). However, when the mice are isolated by karyotype, the trisomic

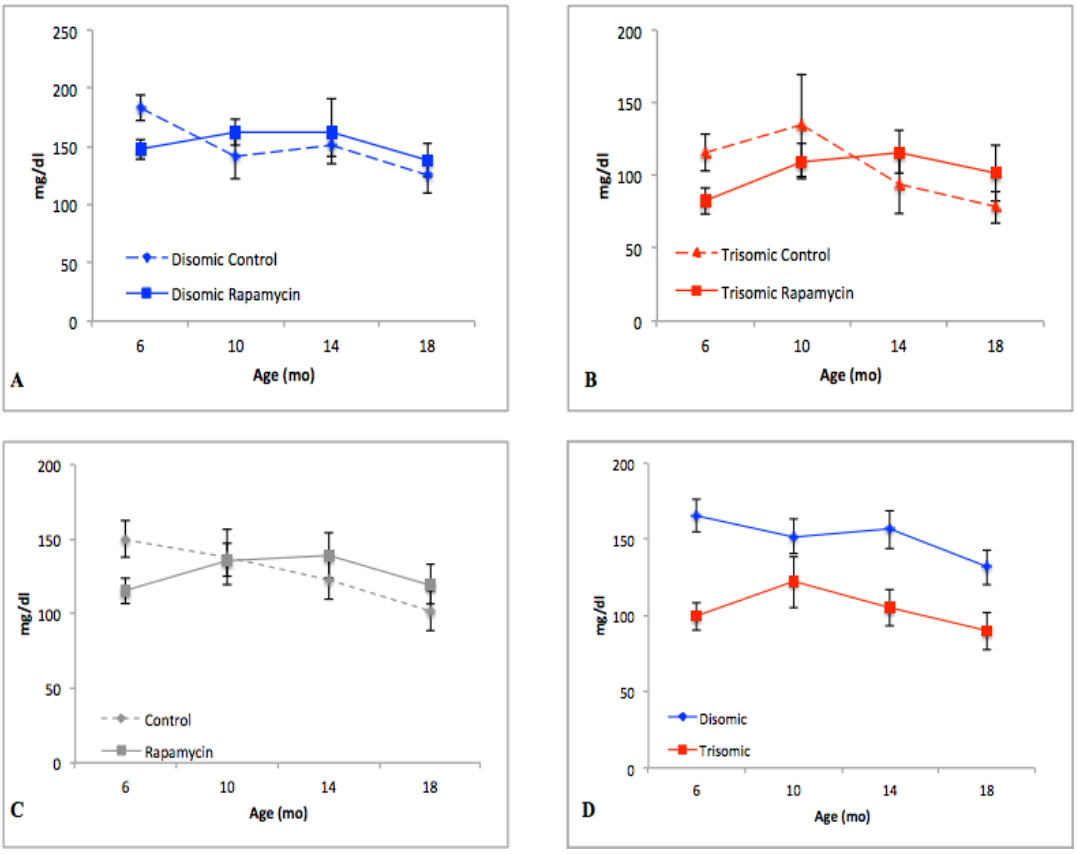

Figure 5. Blood cholesterol levels in mice receiving control diet or rapamycin diet A) Shows the cholesterol levels in disomic mice either on rapamycin diet or control diet, B) shows the same comparison in trisomic mice. C) Compares the mice either receiving rapamycin diet or control diet and D) shows the comparison between karyotype of the mice, these indicate the decrea se in cholesterol is due to karyotype of the mice.

mice have lower levels of cholesterol compared to disomic mice (Figure 5). Although the mice experience a higher glucose level, or changes in cholesterol levels, we do not believe this alters their survival.

Although, this was not a typical aging study in which the mice are allowed to age until time of death, we performed a Kaplan - Meier survival plot to determine the probability of survival through the duration of the study (Figure 6). A higher rate of mortality occurred in the trisomic mice receiving the control diet, in particular as they aged. Observationally, the trisomic mice on control diet appeared more fragile than their disomic

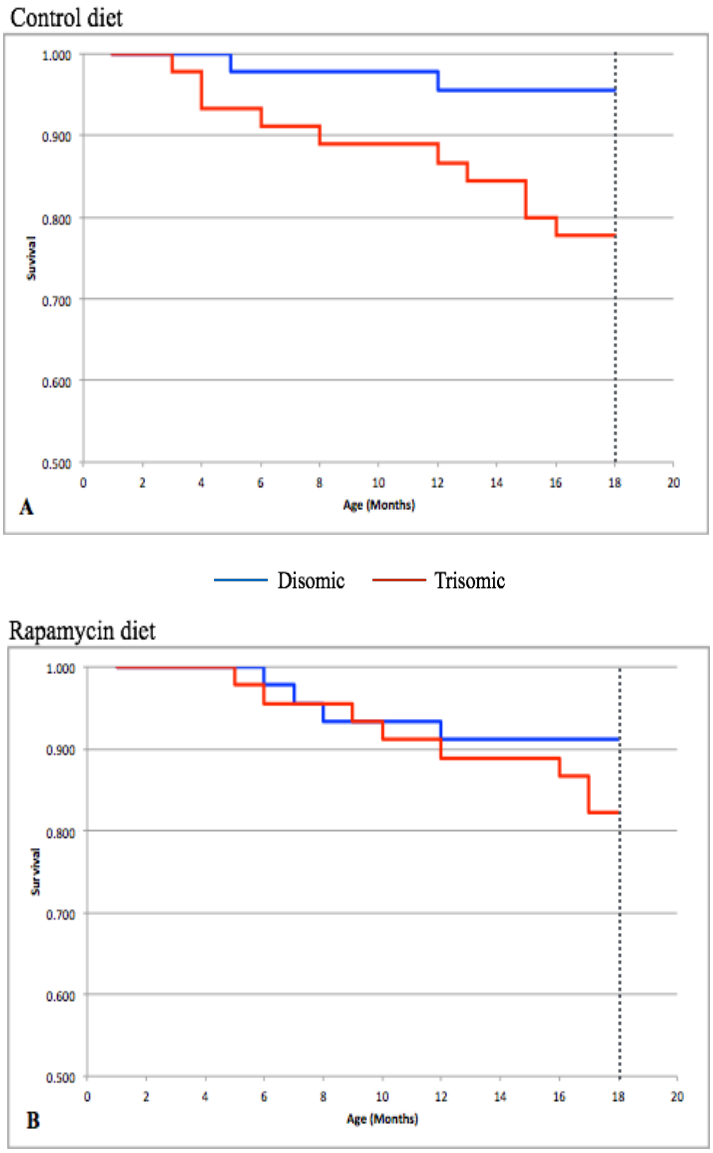

Figure 6. Kaplan – Meier survival plots.

Kaplan Meier survival plots showing the probability of survival for mice on control diet (A) and the mice on rapamycin diet (B). The dotted line shows the end of the diet study when mice were sacrificed. Although not a typical aging study the probability of survival deceases in the trisomic control diet mice.

counterparts as well as the trisomic mice on rapamycin diet. Trisomic mice on rapamycin diet appear to have a higher survival probability (Figure 6). Interestingly, we also see reduction in the probability of survival in disomic mice receiving rapamycin diet (Figure 6).

It has been reported that the Ts65Dn mice have reduced cerebellum size that corresponds to the precocious aging phenotype. We measured the cerebellum protein content after extraction of metabolites. Protein content was used as a surrogate for

cerebellar size, the higher protein content corresponds to a larger size of cerebellum. The trisomic Ts65dn mice show a reduced cerebellum compared to the disomic mice (Figure 7). The comparison between disomic and trisomic mice may not be a fair comparison other than to illustrate that the disomic mice are larger, as shown by the mouse weights. However, comparing the intragroup cerebellar sizes between young (6-month) and old (18-month) groups is relevant. The trisomic mice show an age-related reduction in size of cerebellum determined by total protein content and rapamycin treatment appears to rescue this age-related decline (Figure 7). The disomic mice do not show this age-related decline in cerebellar size, this may be because compared to the trisomic mice they are not aged.

Taken together these data show that the mice on the microencapsulated rapamycin diet and control diet are in general healthy. There are some changes, such as increase in glucose in mice treated with rapamycin, and lowered cholesterol in mice that are trisomic

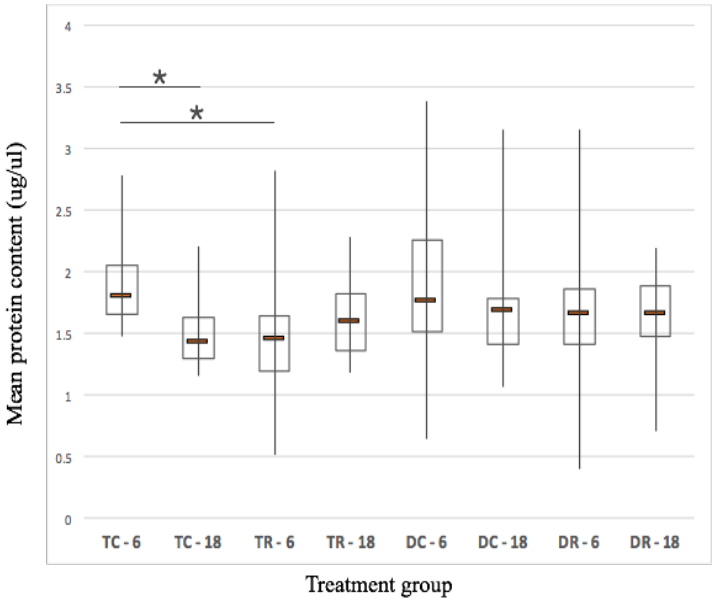

Figure 7. Changes in cerebellar size by age and treatment of Ts65Dn mice. Total cerebellar protein as a surrogate for cerebellar size for 6 and 18 month mice. Disomic control (DC)), Disomic rapamycin (DR), Trisomic control (TC), Trisomic rapamycin (TR).

for Mmu16. These changes have been previously documented in other studies of rapamycin treatment (glucose increase) or with the use of the Ts65Dn mouse (cholesterol levels). These data also demonstrate that there are age-related declines in the trisomic mice and that rapamycin in the diet is having an effect on the physiology.

3.3 Targeted metabolomics analysis

To identify specific metabolite changes in the brains of the Ts65Dn mouse model of DS, aging, and early-onset Alzheimer's disease we prepared a set of known standards that can be separated using HPLC and detected by electrochemical detection (Table 4) (Figure 1). These metabolites represent a variety of disease relevant pathways, including catecholamine biosynthesis, purine biosynthesis, tryptophan and tyrosine metabolism, and glutathione metabolism in addition to others. We also identify 150 peaks that are consistently changed but have not been identified using electrochemical detection.

3.3.1 Targeted metabolomic changes due to trisomy of Mmu16

To determine if there are changes to specific metabolites relevant to trisomy of Mmu16 and human DS, we compared samples from mice fed control diet and identified changes between disomic and trisomic mice. To determine if there are significant changes in detected peaks between disomic and trisomic mice we used a t-test analysis. The 6-month mice show 8 compounds that are significantly changed between disomic and trisomic mice (Figure 8). The increase in homovanillic acid (HVA) in trisomic mice compared to disomic mice is interesting, previous studies show individuals with DS have

elevated levels of HVA (Figure 8) (Kay et al. 1987; Schapiro et al. 1987). We also see a decrease in 4-hydroxybenzoic acid (4-HBA) levels and guanosine levels in trisomic mice. 4-HBA is often used as an indicator for ROS (hydroxyl) stress (Liu et al. 2002). Guanosine is an important purine metabolite and plays an important role in information and energy transfer.

Table 4. Library of metabolites detectable by HPLC-EC.

Metabolite	HMDB	PubChem	KEGG
Ortho-Hydroxyphenylacetic acid	HMDB00669	11970	C05852
3,4-Dimethoxyphenylethylamine	HMDB41806	8421	
3-Hydroxyanthranilic acid	HMDB01476	86	C00632
Hydroxykynurenine	HMDB00732	89	C02794
3-Methoxytyramine	HMDB00022	1669	C05587
Hydroxyphenyllactic acid	HMDB00755	9378	C03672
4-Hydroxybenzoic acid	HMDB00500	135	C00156
p-Hydroxyphenylacetic acid	HMDB00020	127	C00642
5-Methoxydimethyltryptamine	HMDB02004	1832	C08309
5-Methoxytryptophan	HMDB02339	151018	
5-Hydroxy-L-tryptophan	HMDB00472	144	C01017
6-Hydroxydopamine	HMDB01537	4624	
6-Hydroxymelatonin	HMDB04081	1864	C05643
7-Methylguanine	HMDB00897	11361	C02242
N-Acetylserotonin	HMDB01238	903	C00978
2-Aminobenzoic acid	HMDB01123	227	C00108
Ascorbic acid	HMDB00044	54670067	C00072
Cysteine	METPA0075	NA	C00736
3,4-Dihydroxybenzeneacetic acid	HMDB01336	547	C01161
Dopamine	HMDB00073	681	C03758
Epinephrine	HMDB00068	5816	C00788
Oxidized glutathione	HMDB03337	975	C00127
Glutathione	HMDB00125	124886	C00051
Guanine	HMDB00132	764	C00242
Guanosine	HMDB00133	6802	C00387
4-Hydroxy-3-methoxybenzenemethanol	HMDB32012	62348	C06317
Homogentisic acid	HMDB00130	780	C00544
Homovanillic acid	HMDB00118	1738	C05582
Homoveratric acid	HMDB00434	7139	
Hypoxanthine	HMDB00157	790	C00262
3-Indolepropionic acid	HMDB02302	3744	
L-Kynurenine	HMDB00684	161166	C00328
Melatonin	HMDB01389	896	C01598
Metanephrine	HMDB04063	21100	C05588
N-Methylserotonin	HMDB04369	150885	C06212
Norepinephrine	HMDB00216	439260	C00547
Normetanephrine	HMDB00819	1237	C05589
Pyridoxal	HMDB01545	1050	C00250
Tryptophanol	HMDB03447	10685	C00955
Tyramine	HMDB00306	5610	C00483
Uric acid	HMDB00289	1175	C00366
Vanillic acid	HMDB00484	8468	C06672
Vanillylmandelic acid	HMDB00291	736172	C05584
Xanthine	HMDB00292	1188	C00385
Xanthosine	HMDB00299	64959	C01762

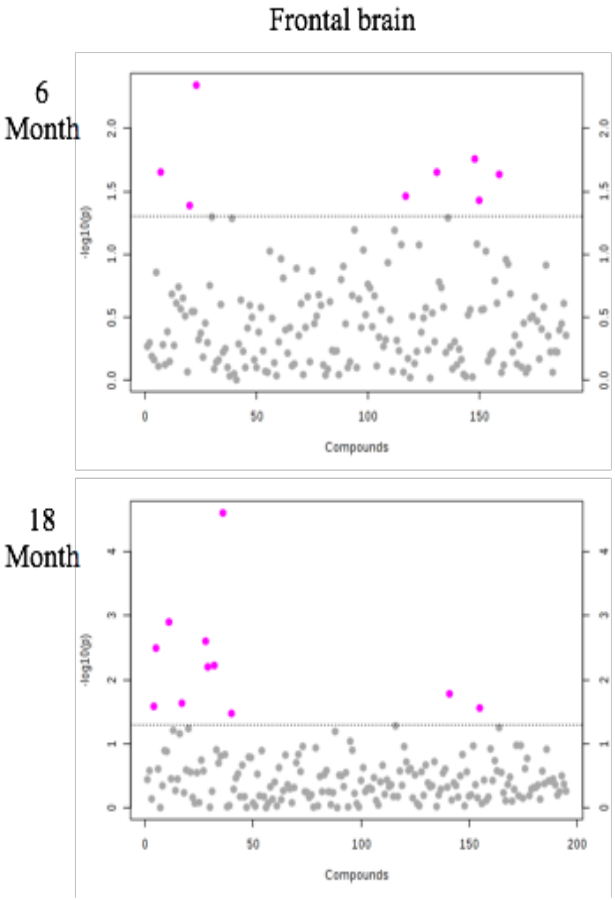

Compound	p.value	$LOG_{10}(p)$
Homovanillic acid	0.004543	2.3427
unk109	0.017505	1.7568
4-Hydroxybenzoic acid	0.022274	1.6522
unk092	0.022298	1.6517
unk120	0.023222	1.6341
unk078	0.034579	1.4612
unk111	0.037333	1.4279
Guanosine	0.041021	1.387

Compound	p.value	$LOG_{10}(p)$
Norepinephrine	2.46E-05	4.6098
5-Hydroxy-L-tryptophan	0.0012496	2.9032
Homovanillic acid	0.0024944	2.603
3-Methoxytyramine	0.0031932	2.4958
L-Kynurenine	0.0059742	2.2237
Homoveratric acid	0.0062851	2.2017
unk096	0.016558	1.781
Ascorbic acid	0.02324	1.6338
Hydroxykynurenine	0.025988	1.5852
unk110	0.027637	1.5585
Tyramine	0.033577	1.474

Figure 8. Significantly changed compounds detected by HPLC-EC. Metabolites that are significantly changed in mice fed control diet. Comparison is between disomic and trisomic mice illustrating changes that are possibly associated with Mmu16. Tables show the metabolites that are detected and p-values (>0.05). Red highlights show changed metabolite in both 6- and 18-month mice. Blue highlight shows AD associated metabolite (REF).

The mice treated with microencapsulated rapamycin do not show this increase in HVA or the decrease in 4-HBA and guanosine. There are several changes associated with rapamycin treatment, however these are not currently in our library of detectable metabolites and are labeled as unkX (unknown, X indicating the peak number)

(Appendix 1). In the 18-month mice comparing the differences between disomic and trisomic mice fed control diet we see 11 significantly changed metabolites ($p < 0.05$), again HVA is changed and we find a significant change in levels of L-kynurenine among others (Figure 8). These changes illustrate the dynamic nature of the brain as the mice age. Changes in L-kynurenine and HVA have been associated with a host of neurodegenerative disorders, including AD, so it is important that we see an increase in these as the mice age possibly indicating early AD pathology (Figure 9).

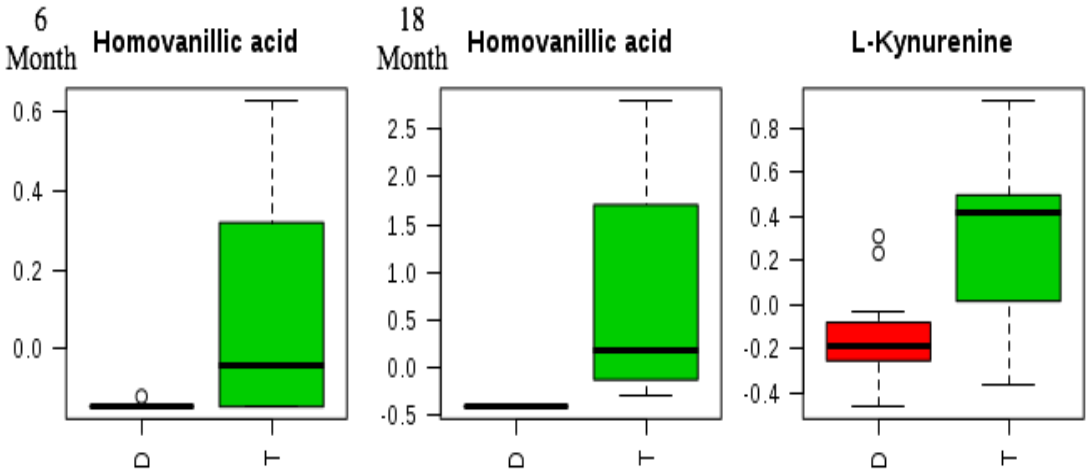

Figure 9. Changes in homovanillic acid levels in young and old disomic (red) and trisomic (green) mice. Elevation of L-kynurenine in 18-month mouse brains. L-kynurenine is not elevated in 6-month mice.

To determine if these changes are associated with DS we performed a metabolite set enrichment analysis (MSEA), this is a technique similar to gene set enrichment analysis, to determine if the changes we see in our metabolites are pathologically relevant. We compare our data to a database of known metabolite changes. Unfortunately, a mouse brain specific database does not exist so we cross-referenced our metabolite changes

against human cerebrospinal fluid to determine if there were any pathologies relevant to our metabolites (Figure 10). This is also used as a test of our model system, we would expect DS to be at, or near, the highest hits when we screen our metabolite changes in the T65Dn mouse model of DS, this is what we see (Figure 10).

3.3.2 Targeted metabolomic profile changes due to rapamycin treatment.

Similar to the global metabolomic data analysis, we want to determine if there are changes in the metabolites due to prolonged rapamycin treatment. The global metabolomic changes showed the appearance of a "sensitivity" to rapamycin treatment in the trisomic mice due to the high number of features that were significantly changed, in particular in the 6-month mice. Our targeted analysis reveals some interesting changes. 6-month mice fed control diet compared to mice on diet containing microencapsulated rapamycin have elevated HVA and norepinephrine in trisomic mice (Figure 11). The upregulation of HVA and norepinephrine is conserved in the 18-month mice and is expected considering the above analysis of changes associated with karyotype of the mice, in which HVA was elevated in the trisomic mice fed control diet (Figure 12). We also see many changes associated with rapamycin treatment, most of which are in unidentified peaks. It is important to note that rapamycin has been shown to rescue dopaminergic neurons which may increase dopamine levels and reduce HVA levels (Tain et al. 2009).

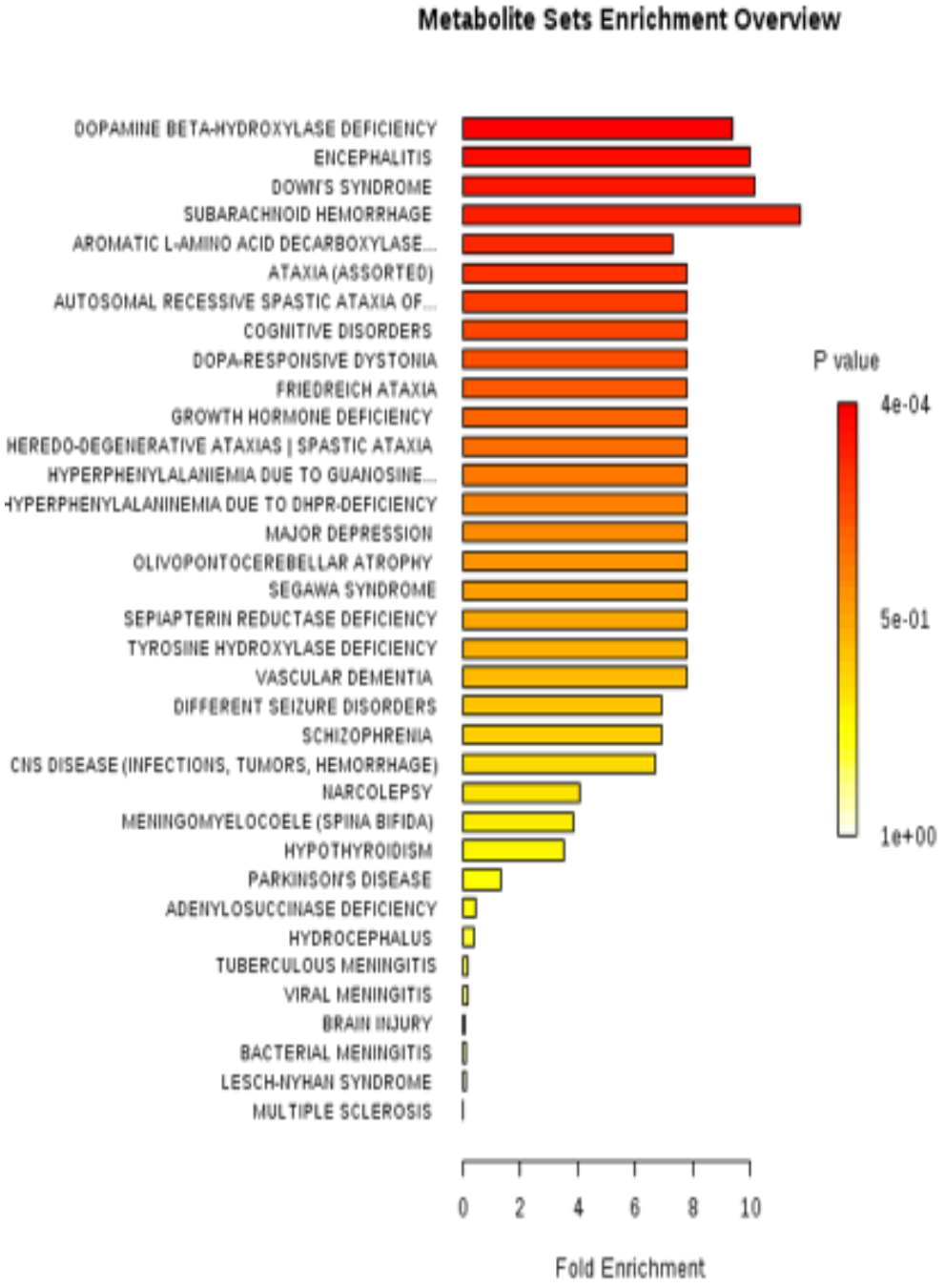

Figure 10. Metabolite set enrichment analysis (MSEA) of metabolite changes between disomic and trisomic mice fed control diet. Queried against human cerebrospinal fluid (CSF) database due to lack of brain metabolite database.

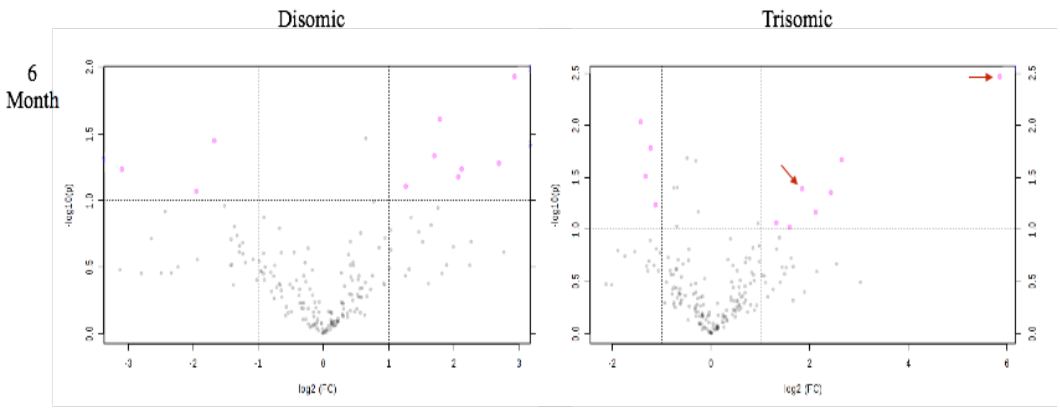

Compounds	FC	log2(FC)	p.value	LOG10(p)
unk046	7.6383	2.9332	0.01173	1.9307
unk049	3.4537	1.7882	0.024475	1.6113
unk057	0.31311	-1.6752	0.035545	1.4492
unk109	3.2526	1.7016	0.046224	1.3351
Pyridoxal	6.4728	2.6944	0.05244	1.2803
unk045	4.349	2.1207	0.05793	1.2371
unk059	0.11713	-3.0938	0.058179	1.2352
unk076	4.1957	2.0689	0.066573	1.1767
unk098	2.4047	1.2658	0.078209	1.1067
unk093	0.25836	-1.9525	0.08546	1.0682

Compound	FC	log2(FC)	p.value	LOG10(p)
Homovanillic acid	57.845	5.8541	0.0033882	2.47
unk109	0.37109	-1.4302	0.0091762	2.0373
unk097	0.42742	-1.2263	0.01649	1.7828
unk095	6.2739	2.6494	0.021337	1.6709
unk055	0.39783	-1.3298	0.030782	1.5117
Norepinephrine	3.5982	1.8473	0.040531	1.3922
unk083	5.3908	2.4305	0.04415	1.3551
unk103	0.45867	-1.1245	0.057952	1.2369
unk100	4.3466	2.1199	0.068474	1.1645
unk015	2.5057	1.3252	0.086575	1.0626
unk081	3.0171	1.5932	0.094767	1.0233

Figure 11. Changes in targeted metabolites due to rapamycin diet. Both disomic and trisomic mice receive either control diet or diet containing rapamycin. Volcano plots and corresponding tables show significantly changed metabolites in 6-month disomic and trisomic mice comparing control diet and rapamycin diet.

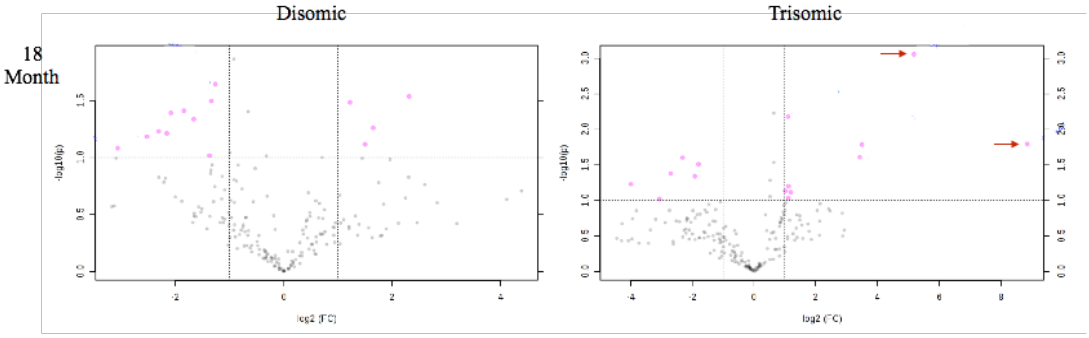

Compound	FC	log2(FC)	p.value	LOG10(p)
unk035	0.32078	-1.6403	0.012466	1.9043
5-Methoxydimethyltryptamine	0.41676	-1.2627	0.022812	1.6418
unk070	4.9886	2.3186	0.029203	1.5346
unk023	0.3958	-1.3372	0.032126	1.4931
Melatonin	2.3417	1.2275	0.032899	1.4828
6-Hydroxydopamine	0.27836	-1.845	0.038987	1.4091
unk107	0.23545	-2.0865	0.04067	1.3907
unk098	0.31563	-1.6637	0.046257	1.3348
unk043	3.1522	1.6564	0.055187	1.2582
unk110	0.20207	-2.3071	0.059029	1.2289
unk011	0.22356	-2.1612	0.061616	1.2103
unk077	0.17354	-2.5266	0.065674	1.1826
unk034	2.8359	1.5038	0.076691	1.1153
unk073	0.11931	-3.0672	0.082952	1.0812
3,4-Dimethoxyphenylethylamine	0.38673	-1.3706	0.096421	1.0158

Compounds	FC	log2(FC)	p.value	LOG10(p)
Norepinephrine	36.44	5.1874	0.00088046	3.0553
N-Methylserotonin	2.1412	1.0984	0.0066318	2.1784
Homovanillic acid	465.54	8.8628	0.016124	1.7925
6-Hydroxymelatonin	11.323	3.5012	0.016368	1.786
unk064	10.779	3.4301	0.024731	1.6068
unk116	0.20027	-2.32	0.025041	1.6013
unk034	0.28742	-1.7988	0.030906	1.51
unk010	0.15363	-2.7025	0.041967	1.3771
unk028	0.26424	-1.9201	0.045695	1.3401
unk071	0.062684	-3.9958	0.059154	1.228
Normetanephrine	2.1718	1.1189	0.063048	1.2003
p-Hydroxyphenyllactic acid	2.0184	1.0132	0.073419	1.1342
Cysteine	2.2838	1.1914	0.076629	1.1156
4-Hydroxybenzoic acid	2.164	1.1137	0.092641	1.0332
unk076	0.11883	-3.073	0.095562	1.0197

Figure 12. Changes in targeted metabolites due to rapamycin diet. Both disomic and trisomic mice receive either control diet or diet containing rapamycin. Volcano plots and corresponding tables show significantly changed metabolites in 18-month disomic and trisomic mice comparing control diet and rapamycin diet.

When we analyze the differences between disomic and trisomic mice fed rapamycin diet we see that the increase in HVA and epinephrine is not significant (Figure 13). Importantly, we see that most of the changes are in unknown peaks, some of which are conserved between 6-month and 18-month mice (Figure 13). It will be important in future work to identify these unknown peaks.

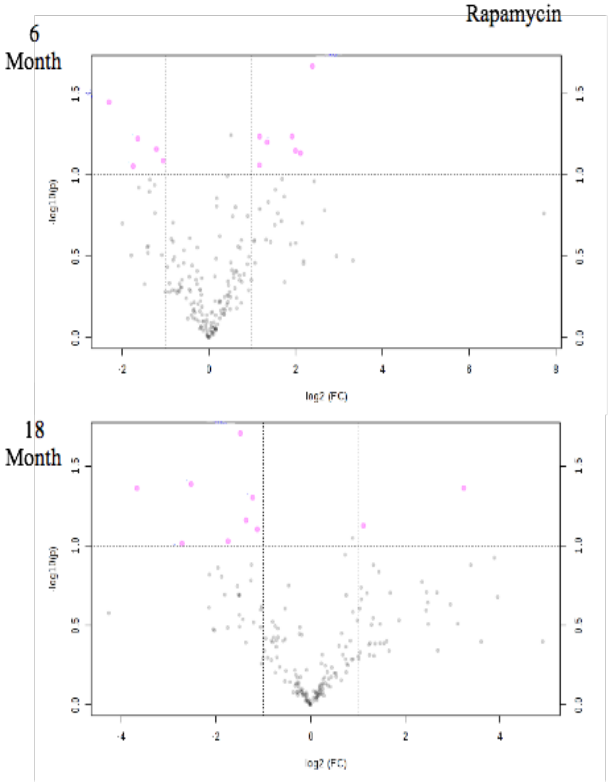

Compounds	FC	log2(FC)	p.value	LOG10(p)
unk100	5.232	2.3874	0.021354	1.6705
unk120	0.20273	-2.3023	0.035465	1.4502
unk092	3.7849	1.9202	0.057597	1.2396
unk020	2.2529	1.1718	0.057656	1.2392
unk076	0.32121	-1.6384	0.059458	1.2258
unk089	2.5327	1.3407	0.062552	1.2038
unk109	0.43258	-1.209	0.068992	1.1612
unk095	3.998	1.9993	0.070462	1.152
unk090	4.331	2.1147	0.072914	1.1372
unk103	0.48298	-1.05	0.0815	1.0888
unk051	2.2453	1.1669	0.086435	1.0633
unk122	0.29785	-1.7473	0.087927	1.0559

Compounds	FC	log2(FC)	p.value	LOG10(p)
unk034	0.35786	-1.4825	0.019693	1.7057
unk067	0.17414	-2.5217	0.041043	1.3868
unk013	9.4077	3.2338	0.043455	1.362
unk039	0.079024	-3.6616	0.04357	1.3608
unk106	0.42849	-1.2227	0.049972	1.3013
unk099	0.38843	-1.3643	0.069132	1.1603
5-Methoxydimethyltryptamine	2.1633	1.1132	0.074839	1.1259
unk092	0.45831	-1.1256	0.078869	1.1031
unk076	0.29849	-1.7443	0.093571	1.0289
unk101	0.15221	-2.7159	0.09677	1.0143

Figure 13. Volcano plots and associated tables representing changes between disomic and trisomic mice fed rapamycin diet. Targeted metabolomic changes showing the comparison of disomic and trisomic mice on rapamycin diet. Importantly, the increase in HVA and norepinephrine are no longer significant in rapamycin fed trisomic mice.

3.3.3 Targeted metaboomic profile changes due to age

To determine if there are age related differences between the groups we performed an ANOVA with a Tukey's post-hoc analysis. We already see that there are changes associated with age when the analysis was performed to search for changes associated with trisomy of Mmu16 (Figure 8) and again when analyzing changes due to rapamycin treatment (Figures 11 and 12). However, we want to see how these changes are associated between all treatment groups within each age group. In the 6-month ANOVA analysis there are 7 metabolites that are significantly changed (Figure 14). Four of these changes are of interest, including norepinephrine and HVA, which have shown to be elevated in trisomic CSF. Strikingly, both norepinephrine and HVA are reduced in mice treated with rapamycin, this is the first example of rapamycin treatment reducing HVA and norepinephrine. Additionally, we see that rapamycin treatment appears to elevate the levels of dopamine in both the disomic and trisomic mice (Figure 14). As previously, noted, rapamycin has been shown to rescue dopaminergic neurons increasing dopamine levels (Tain et al. 2009). There is also an increase in L-kynurenine levels associated with rapamycin treatment (Figure 14). In the 18-month mice we see more significantly changed metabolites when compared to the 6-month mice (Figure 15). Many of these are implicated in changes in brain chemistry (kynurenine, HVA, 3-methoxytyramine, and norepinephrine) (Figure 15).

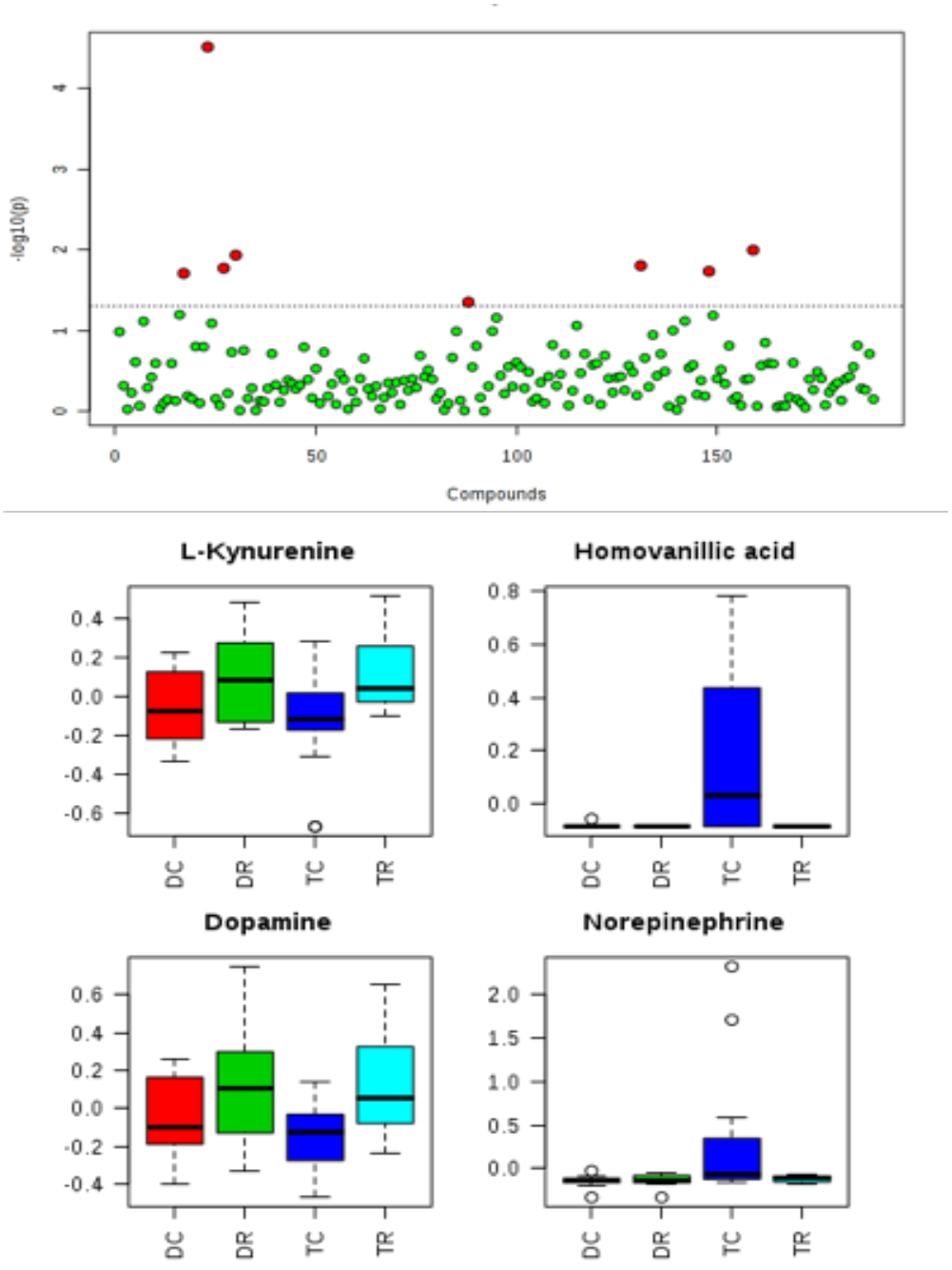

Figure 14. ANOVA of all groups in the 6-month set showing significantly changed metabolites in red (Tukey's post-hoc). Box and whisker plots of metabolites of interest.

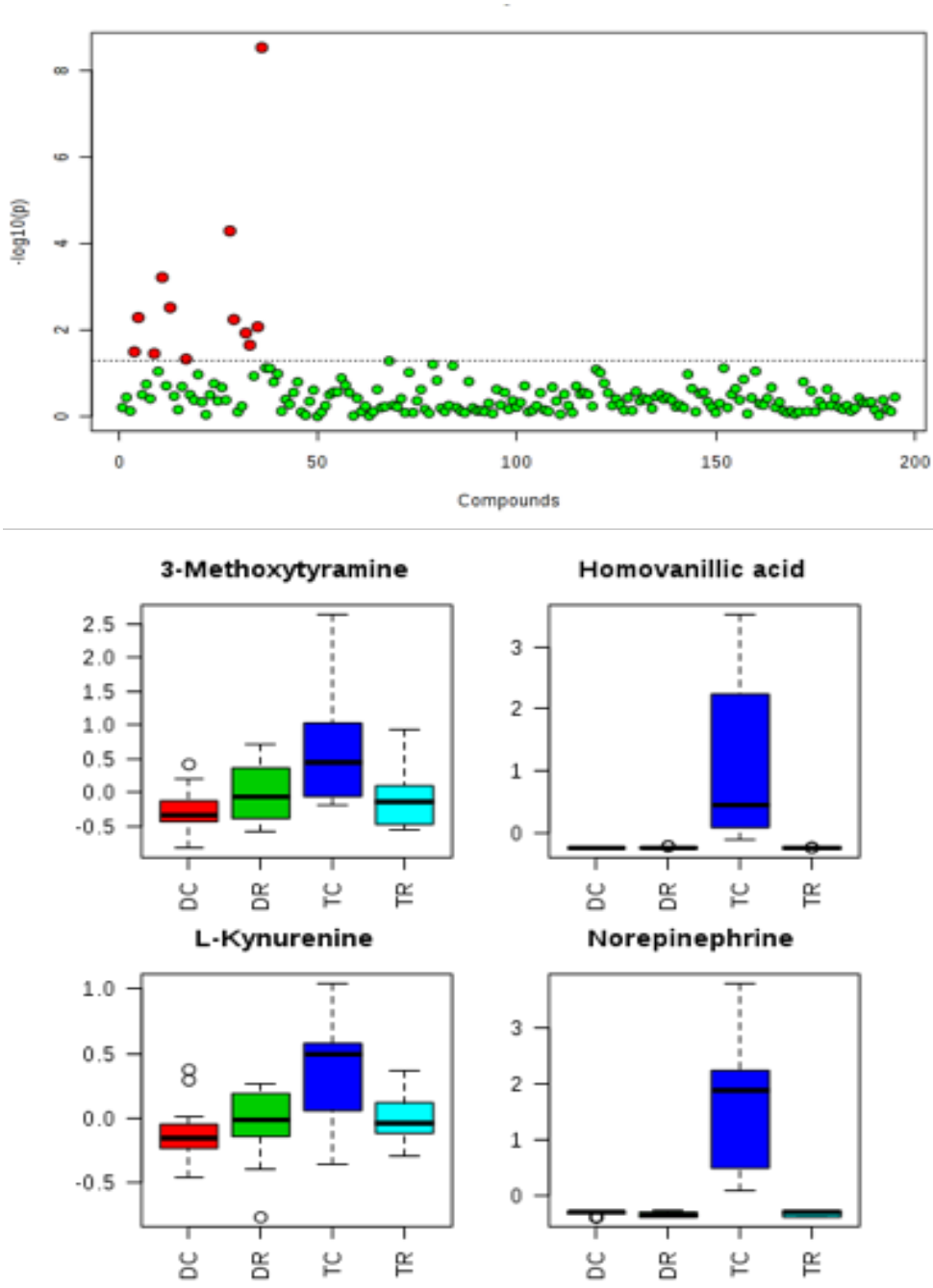

Figure 15. ANOVA of all groups in the 18-month set showing significantly changed metabolites in red (Tukey's post-hoc). Box and whisker plots of metabolites of interest.

3.4 Metabolomic changes associated with the trisomy of Mmu16

To determine if there are changes in patterns between global metabolomic profiles due to karyotype of the mice, we performed pattern recognition analysis on the chromatographic profiles of disomic and trisomic mice on control diet. We analyzed both cerebellar profiles and frontal brain profiles.

Initial fold change analysis showed that there were many significant feature changes of 10-fold or in trisomic mice when compared to disomic mice fed control diet (Appendix 1, section 1). It is interesting to note that a comparison of trisomic mice to disomic mice on control diet indicates that most of the changes are up-regulated, especially in the 18 month mice, and may represent changes due to triplication of Mmu16 genes (Appendix 1, section 1). A t-test was performed and features with a p-value > 0.01 (Log_{10} (p) = 2) are deemed significantly changed between disomic compered to trisomic mice (Figure 16). There are more features that are significantly changed in the 6-month groups when compared to the 18-month in both frontal brain and cerebellar groups (Figure 16). There also appears to be more features in the cerebellum that are significantly changed (Figure 16).

To further explore the relationship between karyotype of the mice, volcano plots displaying the fold-change (> 10-fold) and p-value (p > 0.05, Log_{10} (p) = 1) are created. These plots show the significantly changed features and the direction of the fold change in these features (Figure 17). Again, there appear to be more changes in the cerebellum compared to the frontal brain, especially in the 18-month mice. Also of note, the 18-month

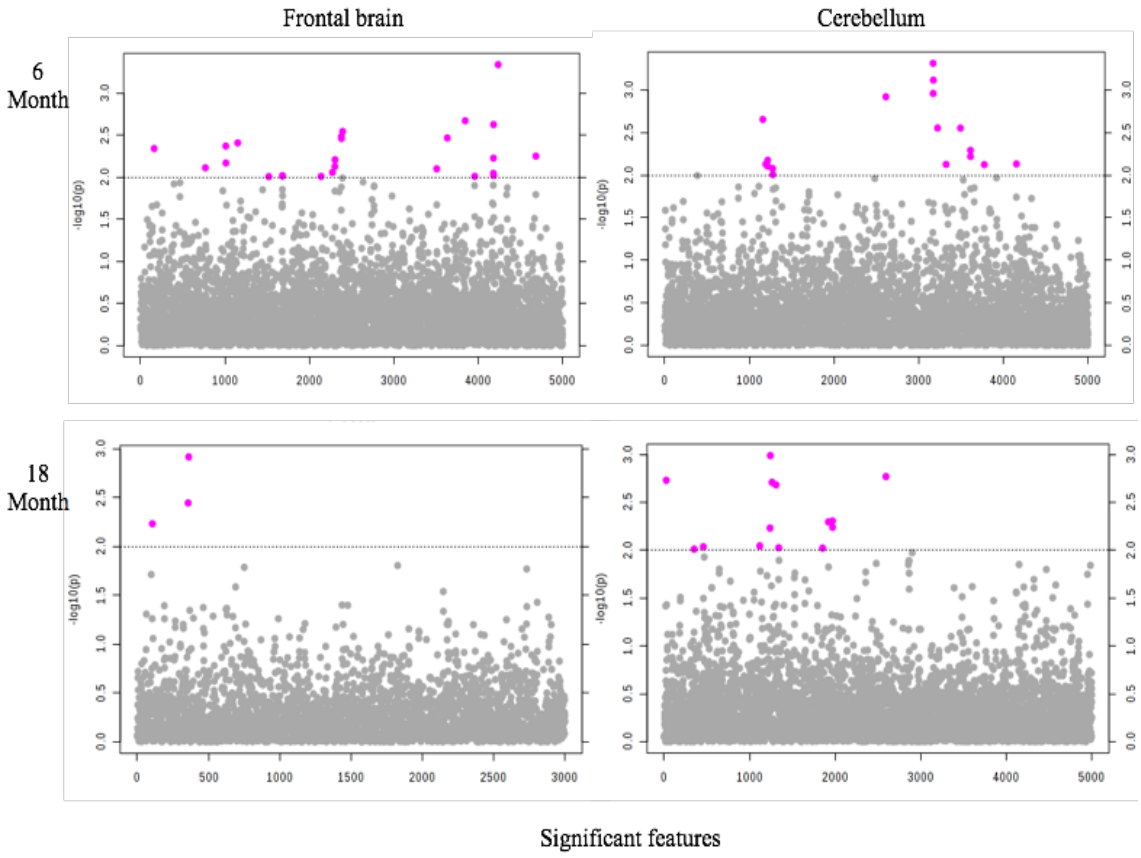

Figure 16. Features that are significantly changed between disomic and trisomic mice. Features that are significantly changed between disomic and trisomic mice at 6-months and 18-months. Comparison is between disomic and trisomic mice fed control diet.

cerebellum showed changes that resemble a down-regulation of trisomic signals (shown by the pink signals to the right of midline (Figure 17).

Using hierarchical cluster analysis (HCA) to search for patterns in the 6 month groups comparing disomic and trisomic mice fed control diet indicates a pattern in cerebellar samples. The top 25 features based on t-test p-value show no pattern emerging from the frontal brain groups at 6- and 18-months of age fed control diet (Figure 18). The cerebellum samples in both 6- and 18-month groups fed control diet begin to show a coordinated pattern that appears to become more striking at 18 months (Figure 18). The

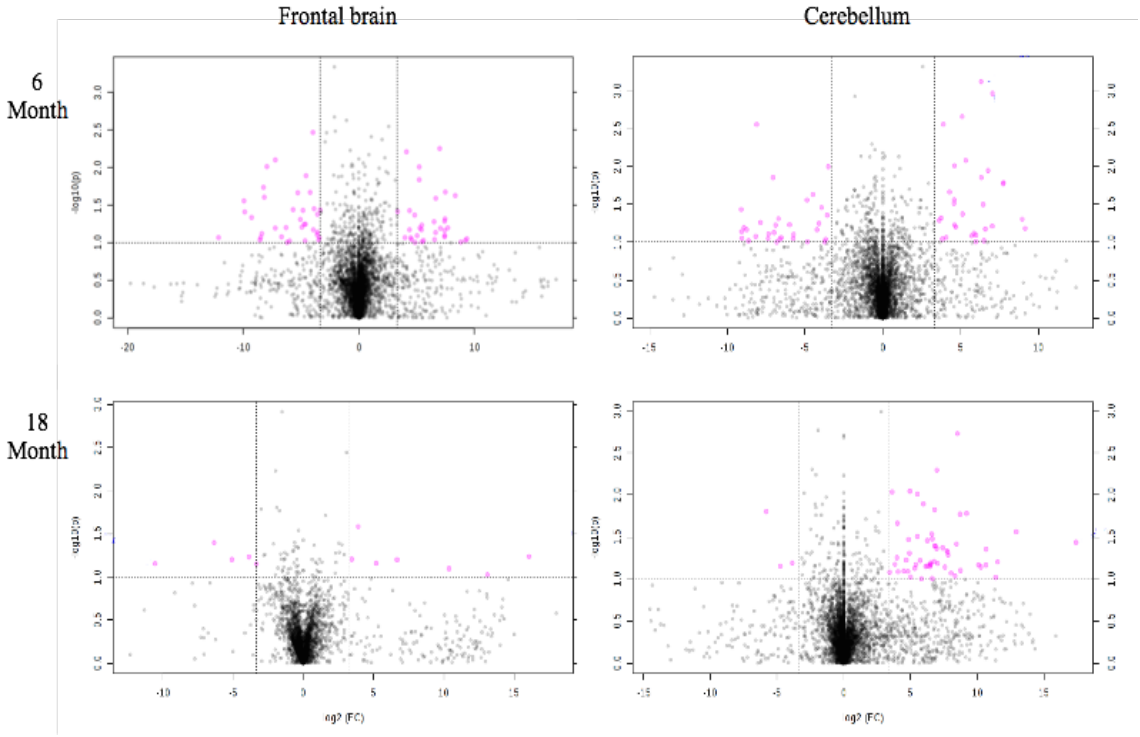

Figure 17. Volcano plots analyzing changes due to karyotype of the mice
Volcano plots showing the relationship between fold-change and t-test p-value. These show the relationship between disomic and trisomic mice on control diet in frontal brain and cerebellum at different ages.

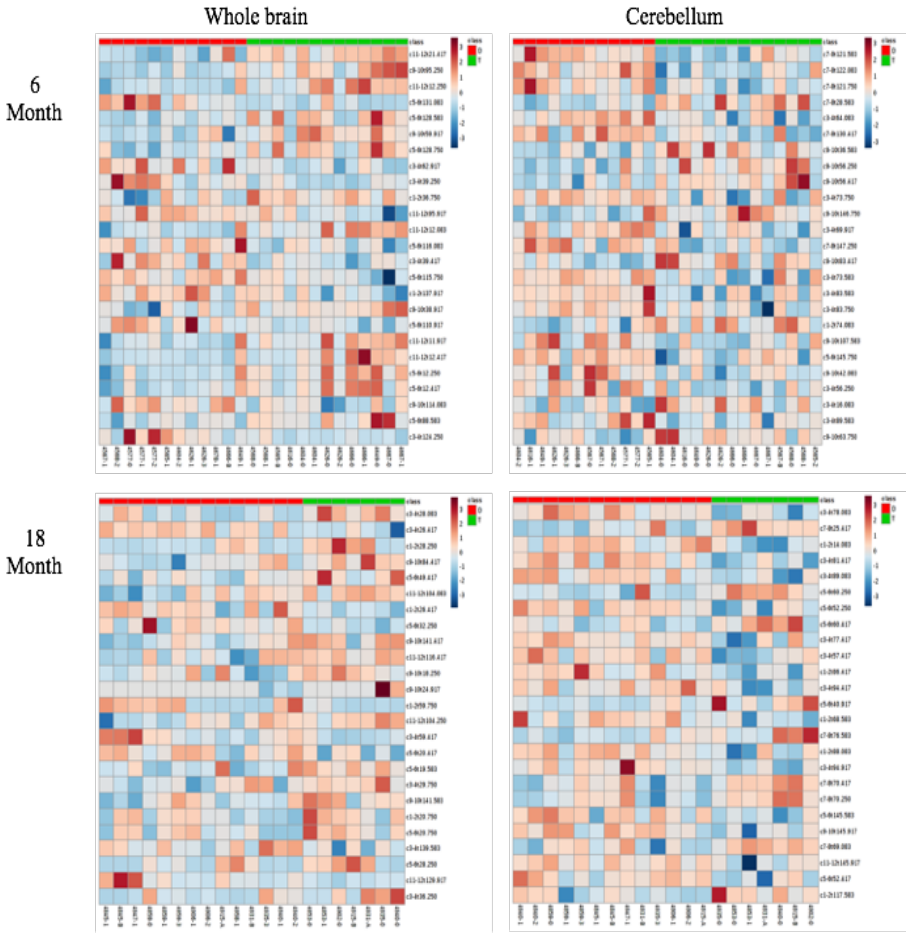

Figure 18. Hierarchical cluster analysis heatmaps.
HCA heatmaps are used to search for the emergence of patterns in the data. These compare disomic mice to trisomic mice on either control diet or rapamycin diet and at 6 months and 18 months of age.

pattern shows many features being down-regulated in trisomic mice compared to disomic mice (Figure 18). Tables of significant features found by t-test and volcano plot analysis along with other data analysis, including PCA and PLS-DA can be found in Appendix 1.

Taken together, these data show that there is little difference created by the karyotype of the mice that contribute to significant changes in the patterns of chromatographic data. These data also suggest that the cerebellum may have a more coordinated effect of trisomy. This may be caused by the heterogeneity of the frontal brain samples which include many different cells types from many distinct brain regions. The cerebellum is a more homogenous sample, so these changes may be more clear due to the more uniform nature of the cerebellar samples.

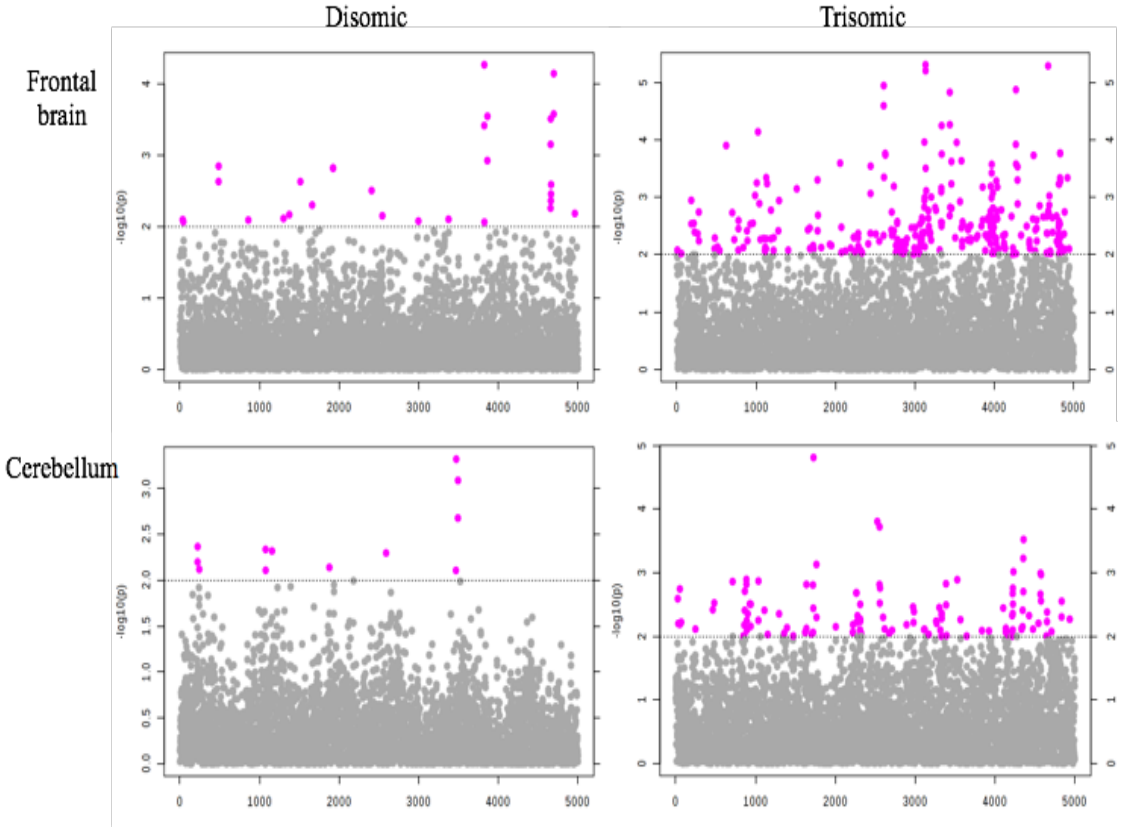

Figure 19. Significant changes in metabolomic profiles of 6-month mice due to rapamycin treatment. Comparison of control diet and rapamycin diet in disomic and trisomic mice as well as brain region by t-test ($p > 0.01$).

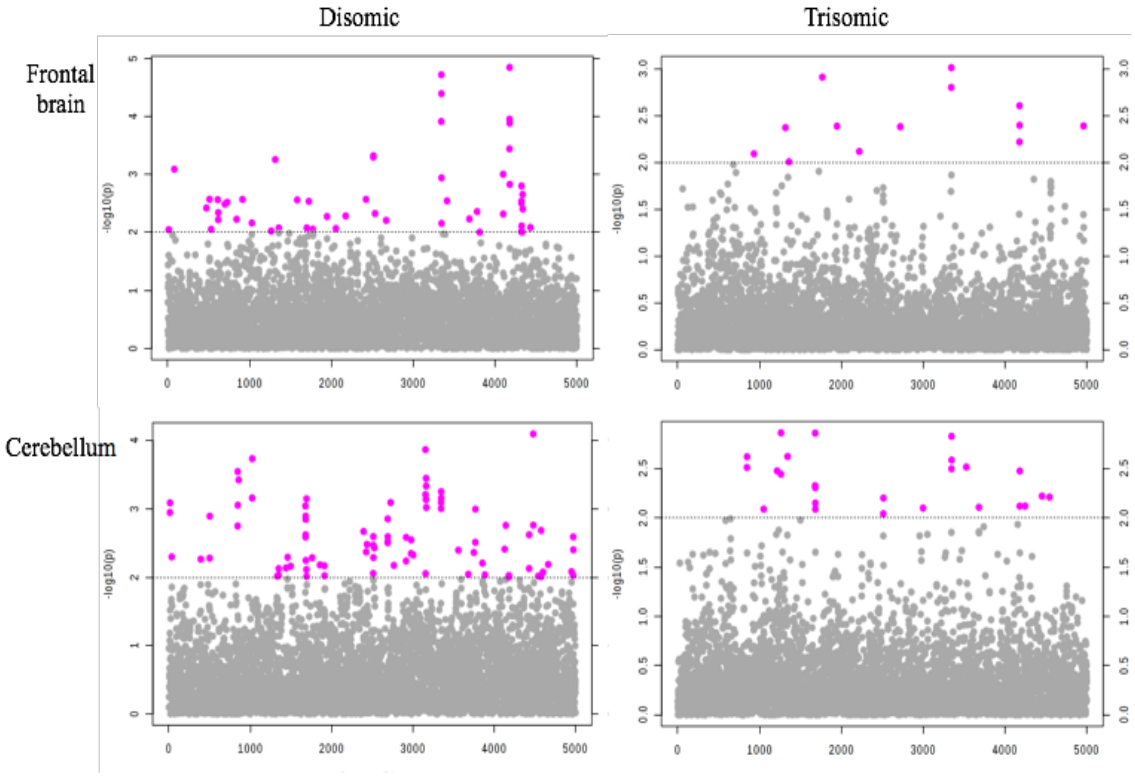

Figure 20. Significant changes in metabolomics profiles of 18-month mice due to rapamycin treatment. Comparison of control diet and rapamycin diet in disomic and trisomic mice as well as brain region by t-test ($p > 0.01$).

3.4.1 Global metabolomic changes due to rapamycin treatment

To understand if there are changes associated with rapamycin treatment we analyzed the chromatographic profiles of mice fed microencapsulated rapamycin. We performed similar analysis to the mice fed control diet to try and determine if rapamycin treatment had an effect on the global metabolic patterns and if these patterns differ between disomic and trisomic mice. There are many features that show a greater than 10-fold change when treated with rapamycin compared to control diet (Appendix 1, section 2). Interestingly, in 6-month mice the greatest number of significantly changed features seem

to be in trisomic mice, with fewer significant changes in disomic mice when comparing rapamycin to control diet (Figure 19). Unexpectedly, the number of significant features in 18-month mice are diminished when compared to the 6-month samples, more striking is the trisomic mice have fewer significant features than the disomic mice (Figure 20). Volcano plots that represent the relationship between fold change (>10-fold) and p-value ($p > 0.05$, Log_{10} (p) = 1) identify the same trend as the t-test plots, there are more significantly changed peaks in the trisomic samples compared to the disomic samples, and these are changed by a greater amount (Figure 21). Additionally, the appearance of a trend showing a down-regulation of rapamycin related metabolite features in the trisomic mice

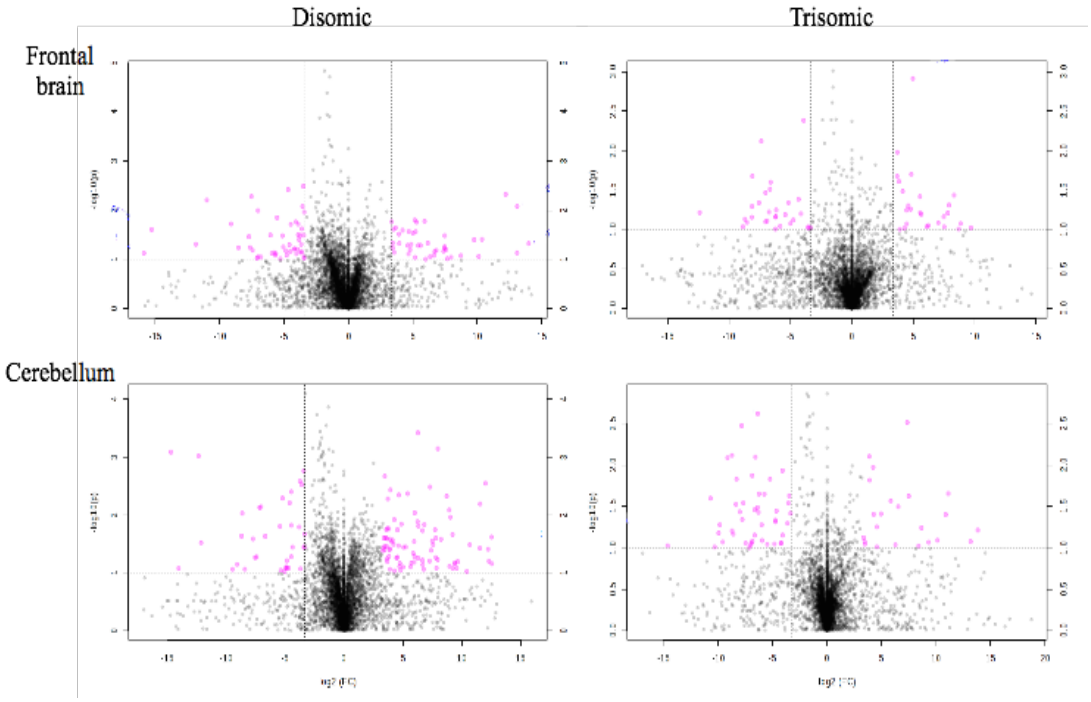

Figure 21. Volcano plots of 6-month mice fed rapamycin diet.
These plots illustrate the relationship between fold change and p-value in 6-month rapamycin fed mice. The comparison in each is between control and rapamycin significant features

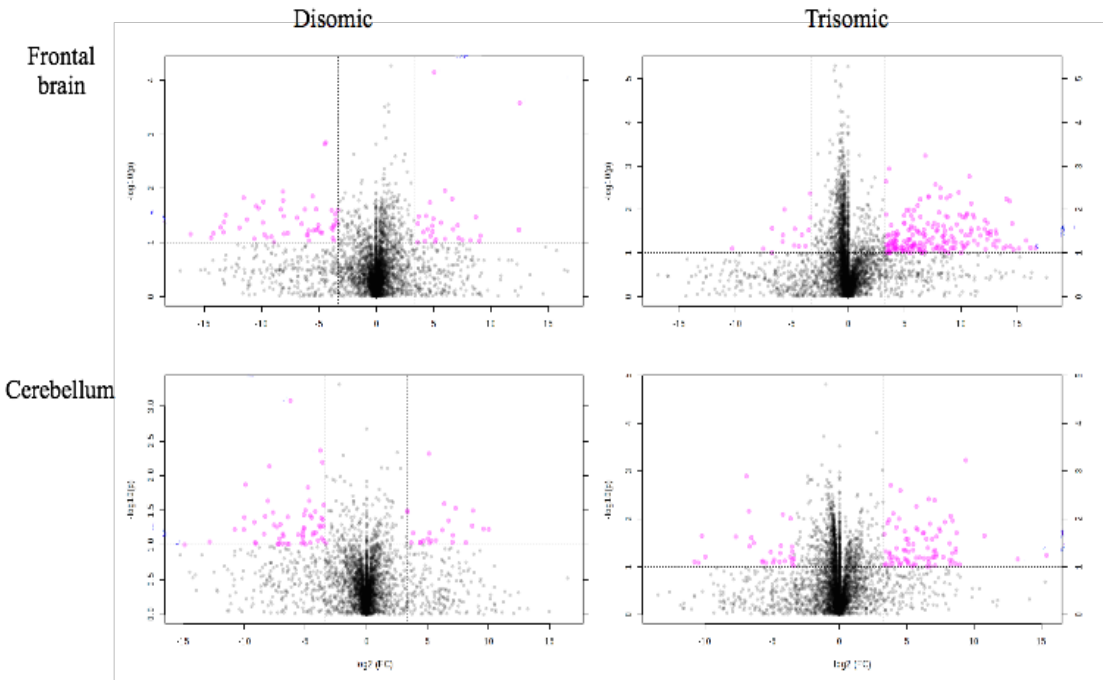

Figure 22. Volcano plots of 18-month mice fed rapamycin diet. These plots illustrate the relationship between fold change and p-value. Comparison is between control and rapamycin fed mice at 18-months.

(greater density to the right of midline) and the opposite effect in the disomic samples (greater density of features to the left of midline) (Figure 21). Volcano plot analysis of the (18-month groups show fewer features that are significant ($p > 0.05$, $Log_{10}(p) = 1$) and the fold change of these is lower (Figure 22). Taken together these data indicate that there are global metabolomics changes associated with rapamycin treatment, and this change appears to be stronger in samples from frontal brain and cerebellum of mice with trisomy Mmu16. Tables of significant features found by volcano plot analysis can be found in Appendix 1.

4.0 Discussion

4.1 Global metabolomics – long-term rapamycin treatment

We treated the Ts65Dn mouse model of DS, aging, and early onset Alzheimer's disease with microencapsulated rapamycin. To ensure that the mice were receiving adequate levels of rapamycin bloods collected on the day of euthanization were sent to the University of Texas Health Sciences Center San Antonio to the lab of Dr. Martin Javors for analysis. Dr. Javors detects rapamycin using MS. We sent four blood samples from four different mice in each group (6- and 18-month: trisomic control, disomic control, trisomic rapamycin, disomic rapamycin). The results were more than conclusive that our mice fed microencapsulated rapamycin had adequate levels in their blood. There is a slight reduction (not significant) in the 18-month rapamycin treated trisomic mice, this is possibly due to reduced food intake. An additional factor to consider is that mice were housed together, often up to 4 mice in a single cage. Ensuring that each mouse received the diet in sufficient amounts was not done, however, we did not have any mice perish from starvation, therefore we can confidently assume that all mice were consuming the diet and rapamycin.

4.2 Global metabolomics – general health of long-term rapamycin treatment

We treated the Ts65Dn mouse model of DS, aging, and early onset Alzheimer's disease with rapamycin, an immunosuppressant previously shown to increase longevity and healthspan in evolutionarily divergent species, including mice. The mice were treated starting at 4 months of age and were sacrificed at 6 an 18 months. To determine the health

of long-term rapamycin treatment we analyzed CBC and blood chemistry of the mice every four months. We did not see any significant changes that would indicate a decrease in the health of the mice or illness. Short-term rapamycin treatment in mice has previously been associated with an increase in glucose load. Long-term treatment shows an initial increase in glucose levels, often to pre-diabetic levels followed by a decrease in glucose, possibly due to a homeostasis mechanism that compensates for this chronic increase in glucose (Fang & Bartke 2013). We treated mice for up to 14 months with rapamycin. Our data indicate elevated glucose levels in the first several months of rapamycin treatment followed by a decrease towards normal levels in disomic mice. This response is slower in trisomic mice, perhaps this may be an interplay between rapamycin treatment and a slower or weaker homeostatic response due to trisomy Mmu16.

Our comprehensive blood analysis also revealed an increase in cholesterol levels in disomic mice. The data indicate that this is due to karyotype of the mice and not due to rapamycin treatment. The lower cholesterol levels in the trisomic mice is interesting that individuals with DS show a reduced incidence of heart attacks and cardiovascular disease, as well as reduced levels of hypertension (Murdoch et al. 1977; Brattström et al. 1987; Ylä-Herttuala et al. 1989). There is also evidence that rapamycin treatment reverses age related heart dysfunction (Flynn et al. 2013).

Body weights of the mice were taken the week they were sacrificed to determine if there were age-associated weight changes while on the diet. As expected we see a typical decrease in body weight as the mice age, in particular the trisomic mice have a significant decrease in weight at 18 months. The disomic mice do not show this significant decrease

in weight at 18 months, perhaps this is because the disomic mice have not reached advanced age. The trisomic mice are a model of premature aging in addition to DS, therefore at 18 months they have deteriorated significantly. A typical mouse can survive up to 36 months, therefore the disomic mice may be middle aged and have not experienced an age related decline. Interestingly, disomic mice fed rapamycin show a reduction in body weight at 18 months on rapamycin diet when compared to those on control diet. We expected to see an aggressive age-associated loss of weight in the Ts65Dn mice at 18-months. Rapamycin is considered a mimetic of caloric restriction, or dietary restriction, which results in weight loss in mammalian model systems, including non-human primates (Ross et al. 2015). Other mouse models have shown a variety of responses to rapamycin treatment to glucose tolerance and insulin sensitivity (Lamming et al. 2013; Krebs et al. 2007; Schindler et al. 2014). Laboratory mice are considered by some to be surrogates for a modern western lifestyle that is characterized by ample food supply and a mostly sedentary lifestyle and rapamycin treatment may act in a way to reduce weight, especially in individuals that cannot safely exercise or diet (Moore et al. 2011; Aoyagi et al. 2015). Previous studies show a decrease in brain region size in the Ts65Dn mouse model (Contestabile, Fila, Bartesaghi, et al. 2009; Usowicz & Garden 2012; Das et al. 2013). We measured total cerebellum protein as a surrogate for cerebellum size to determine if there are age-related changes associated with karyotype of the mice, and if rapamycin treatment ameliorates this deterioration. Previous studies show that individuals with DS have a decreased cerebellar volume in addition to changes in action potentials and excitability (Usowicz & Garden 2012). We did not perform any learning and behavior tests on our mice, but our

measurements of cerebellum size show a significant age-related decline in the control fed Ts65Dn mice. Mice on rapamycin diet have a reduced cerebellum size, but do not show the age-related decline. In other mouse models of neurodegenerative diseases rapamycin has been shown to be neuroprotective and in some cases has ameliorated some of the cognitive declines associated with the progression of disease (Santini et al. 2009; Malagelada et al. 2010; Spilman et al. 2010; Maiese 2015).

4.3 Targeted metabolomic changes due to karyotype

To identify specific changes in metabolites that we can detect using electrochemical detection we created a library of known compounds detectable on our system (Table 4). Analysis of these changes revealed that in mice fed control diet have enrichment of metabolites that are consistent with metabolite changes in human DS as well as other DS relevant pathologies (Cognitive disorders, hypothyroidism). We identify changes in metabolite levels of known metabolites from our library as well as several unknowns that change in trisomy as well (Appendix 1). Two important changes we see in the comparison of karyotype are the elevation of homovanillic acid and the decrease of 4-hydroxybenzoic acid and guanosine. The increase in homovanillic acid (HVA) in trisomic mice compared to disomic mice is interesting, individuals with DS have elevated levels of HVA (Figure 14) (Kay et al. 1987; Schapiro et al. 1987). However, this increase in HVA doesn't appear to be the cause of cognitive deficiencies, rather may be related to altered turnover of monoamines in the brain. Homovanillic acid is a dopamine metabolite and is altered in neurodegenerative diseases such as Parkinson's disease, and in schizophrenics

(Bacopoulos et al. 1979; LeWitt et al. 1992; Loeffler et al. 1995). The hypothesis is that neurodegeneration and loss of dopaminergic neurons alter the dopamine metabolism in brains and CSF resulting in the accumulation or loss of abundant dopamine metabolites. In mice treated with microencapsulated rapamycin comparing disomic and trisomic mice we do not see the same elevation in HVA in the trisomic samples (Appendix 1). We do see a change in several metabolites, however, none of these are currently in our library. Identifying these might produce novel biomarkers or therapy targets. The fact that there is a reduction in the HVA levels in the rapamycin treatment is intereting and may be a significant finding. Other studies of rapamycin have shown the neuroprotective effects, in particular in dopaminergic neurons (Tain et al. 2009).

We also detect the reduction in 4-hydroxybenzoic acid (4-HBA) and guanosine in trisomic mice when compared to disomic mice fed control diet. 4-HBA has been used as a marker for hydroxyl radicals (conversion of 4-HBA to 3,4-dihydroxybenzoic acid (3,4-DHBA)) (Liu et al. 2002). This decrease in 4-HBA might indicate an increased oxidative environment in trisomic brains. Guanosine is an important and abundant molecule in the brain, which can be phosphorylated to GMP, GDP, GTP. Reductions could indicate disruptions in the de novo purine synthesis pathway and inborn errors of purine metabolism, which are often characterized by developmental delays (Wevers et al. 1999; Jurecka 2009). Guanosine also plays a neuroprotective role in the brain, possibly through modulation of glutamatergic neurotransmission (Dal-Cim et al. 2016). The increase in metabolites associated with neurodegeneration (HVA) and an increased oxidative

environment (4-HBA) combined with the reduction of a neuroprotective agent (guanosine) may provide a signature for DS related neuroanatomical deficiencies.

4.3.1 Targeted metabolomic changes due to rapamycin treatment

When we compared the disomic mice treated with control diet or rapamycin diet we see several changes, unfortunately, most of these are in metabolites that are currently not in our library of detectable compounds. Considering the trends in the global metabolomcs analysis (fewer changes in disomic mice treated with rapaycin) we are not surprised that we find the disomic mice have fewer changes in specific metabolites. The trisomic mice have far more changes in specific metabolites than the disomic mice. The trisomic mice show increases in dopamine, L-kynurenine, and N-methyserotonin when treated with rapamycin. As previously stated, rapamycin has been shown to be a neuroprotecant in mouse models of Parkinson's disease (PD) and Alzheimer's disease (AD) (Tain et al. 2009; Spilman et al. 2010). This may be through the stabilization of dopamine metabolism or through the preservation of dopaminergic neurons.

L-kynurenine is a critical tryptophan metabolite and occurs in neurodegenerative disorders such as PD, AD, Huntington's disease (HD), multiple sclerosis (MS), amyotrophic lateral sclerosis (ALS) (Maddison & Giorgini 2015). It can act as a neuroprotective agent as kynurenic acid or as a neurotoxic agent when metabolized to quinolinic acid, 3-hydroxyanthranilic acid, or 3-hydroxykynurenine (Sundaram et al. 2014). In different concentrations, these metabolites can have effects on neurotransmission, particularly through NMDA and AMDA receptors (Bohár et al. 2015).

Perhaps more interesting in the trisomic mice treated with rapamycin, we do not see the increase in HVA. We also do not see the reduction of 4-HBA and guanosine. Taken together, the increase in potentially neuroprotective metabolites (L-kynurenine and guanosine) and the loss of an oxidative environment (4-HBA) may promote protective effects in the brain. Obviously, these will have different effects in different neuronal cell types as well as in different neuronal cell population in specific regions of the brain, but they provide a potential target to explore mechanisms of the precocious aging phenotype of the DS brain.

As the mice age the appearance of more significantly changed metabolites associated with trisomy of Mmu16 appear (Appendix 1) in addition to the ones changed in 6-month mice. This may indicate that the effects of trisomy become compounded as the mice age. The appearance of 3-hydroxykynurenine in addition to the L-kynuenine may indicate that the mice are experienced altered kynurenine metabolism towards the neurotoxic. The activation of the kynurenine pathway (upregulation of L-kynurenine and related metabolites) may be the result of abberant tryptophan signaling that may be the result of inflammation (Yiquan Chen & Guillemin 2009; Zuo et al. 2016). One of the most potent stimulators of the tryptophan and kynurenine pathway is interferon-γ (Yiquan Chen & Guillemin 2009). Four of the six interferon receptors are located on HSA21 as well as Mmu16 (Maroun 1980). The kynurenine pathway results in the production of nicotinamide adenine dinucleotide (NAD^+). NAD acts as an important regulator of transcription and is central in metabolism. Modulation of NAD has been implicated in DR and may play a role in health and disease {Moroz:2014ih, Lin:2003et} These results in dysregulated and

hyperactive immune function through the interferon signaling pathway. Hyperactive interferon signaling may result in a number of different morbidities experienced by individuals with DS, including cognitive deficits as well as the myeloproliferative disorders, and autoimmune disorders.

4.4 Global changes due to karyotype

To elucidate changes in the global metabolomic profiles caused by triplication of Mmu16 we compared frontal brain and cerebellum samples from mice fed control diet so we could isolate changes in trisomic mice when compared to disomic mice. There are changes in both frontal brain and cerebellum associated with trisomy of Mmu16. These are diminished as the mice age and at 18 months, the mice have far fewer significantly changed features in frontal brain, however there are still a large number changed in cerebellum. This may be due to the fact that we homogenize the entire frontal portion of the brain (everything forward of the cerebellum). There are both age and karyotype related changes in specific brain regions such as the hippocampus (Mann 1988; Insausti et al. 1998; Costa & Grybko 2005; Mann et al. 1985). We may be diluting these changes by not performing region specific metabolomics. The cerebellar tissue is a more homogenous cellular population; therefore, we may not be diluting these signatures.

4.4.1 Global changes due to rapamycin treatment

We examined the changes in global metabolomics profiles that may be caused by long-term treatment with microencapsulated rapamycin. We analyzed samples from both

the frontal brain and the cerebellum to compare pattern recognition signatures in disomic and trisomic mice. We see that there are significant changes in the younger mice that seem to be isolated primarily to the trisomic mice. This may be due to the sensitivity of the trisomic mice to an immunosuppressant drug. It has been shown in the past that both to individuals with DS and mouse models of DS have dysregulated immune signaling, possibly due to the triplication of interferon receptors in HSA21 and Mmu16 (Maroun 1980). Interestingly, the number of significant features are diminished in the 18-month samples. There could be homeostasis response after prolonged treatment that normalizes the metabolomics profiles over time. The mTOR signaling pathway appears to be upregulated in brains of individuals with DS with and without AD pathology and may lead to a decrease in autophagy and a hyper-phosphorylation of tau through RCAN1 and increase in oxidative stress (Perluigi et al. 2014; Tramutola et al. 2016).

Chapter Three

Genetic and metabolomic analysis of AdeD and AdeI mutants of de novo purine biosynthesis: cellular models of de novo purine biosynthesis deficiency disorders

*This work has been published:
Genetic and metabolomic analysis of AdeD and AdeI mutants of de novo purine biosynthesis: cellular models of de novo purine biosynthesis deficiency disorders.
Duval N, Luhrs K, Wilkinson TG 2nd, Baresova V, Skopova V, Kmoch S, Vacano GN, Zikanova M, Patterson D. Mol Genet Metab. 2013 Mar;108(3):178-89. doi: 10.1016/j.ymgme.2013.01.002.

Abstract

Purines are molecules essential for many cell processes, including RNA and DNA synthesis, regulation of enzyme activity, protein synthesis and function, energy metabolism and transfer, essential coenzyme function, and cell signaling. Purines are produced via the *de novo* purine biosynthesis pathway. Mutations in purine biosynthetic genes, for example phosphoribosylaminoimidazole carboxylase/phosphoribosylaminoimidazole succinocarboxamide synthetase (PAICS, E.C. 6.3.2.6/E.C. 4.1.1.21), can lead to developmental anomalies in lower vertebrates. Alterations in PAICS expression in humans have been associated with various types of cancer. Mutations in adenylosuccinate lyase (ADSL, E.C. 4.3.2.2) or 5-aminoimidazole-4-carboxamide ribonucleotide formyltransferase/IMP cyclohydrolase (ATIC, E.C. 2.1.2.3/E.C. 3.5.4.10) lead to inborn errors of metabolism with a range of clinical symptoms, including developmental delay, severe neurological symptoms, renal stones, combined immunodeficiency, and autistic

features. The pathogenetic mechanism is unknown for any of these conditions, and no effective treatments exist. The study of cells carrying mutations in the various *de novo* purine biosynthesis pathway genes provides one approach to analysis of purine disorders. Here we report the characterization of AdeD Chinese hamster ovary (CHO) cells, which carry genetic mutations encoding p.E177K and p.W363* variants of PAICS. Both mutations impact PAICS structure and completely abolish its biosynthesis. Additionally, we describe a sensitive and rapid analytical method for detection of purine *de novo* biosynthesis intermediates based on high performance liquid chromatography with electrochemical detection. Using this technique, we detected accumulation of AIR in AdeD cells. In AdeI cells, mutant for the ADSL gene, we detected accumulation of SAICAR and SAMP and, somewhat unexpectedly, accumulation of AIR. This method has great potential for metabolite profiling of *de novo* purine biosynthesis pathway mutants, identification of novel genetic defects of purine metabolism in humans, and elucidating the regulation of this critical metabolic pathway.

1.0 Introduction

Purines are essential building blocks for RNA and DNA synthesis, and regulate energy metabolism and transfer, and protein synthesis, function, and enzyme activity. Purines are also vital components of many essential coenzymes (NAD, NADH, FAD, Coenzyme A), and signaling molecules (cAMP, guanine nucleotides). The enzymatic steps of *de novo* purine biosynthesis convert PRPP (5-phospho-α-D-ribosyl-1-pyrophosphate) to IMP (inosine monophosphate), and an additional four steps convert IMP to AMP (adenosine monophosphate) or GMP (guanosine monophosphate) (Figure 1). Recent evidence demonstrates that the proteins carrying out *de novo* purine biosynthesis form a multienzyme complex, the purinosome, which is induced by acute requirement for purines (An et al. 2008; Deng et al. 2012; Baresova et al. 2012). Formation of the purinosome can be disrupted by mutations in ADSL (E.C. 4.3.2.2) and ATIC (E.C. 2.1.2.3/E.C.3.5.4.10), with severe developmental consequences in humans (Baresova et al. 2012). In addition to ADSL and ATIC, 30 enzyme defects of purine and pyrimidine metabolism have been identified and 17 of these are known to cause human disease (Jurecka 2009).

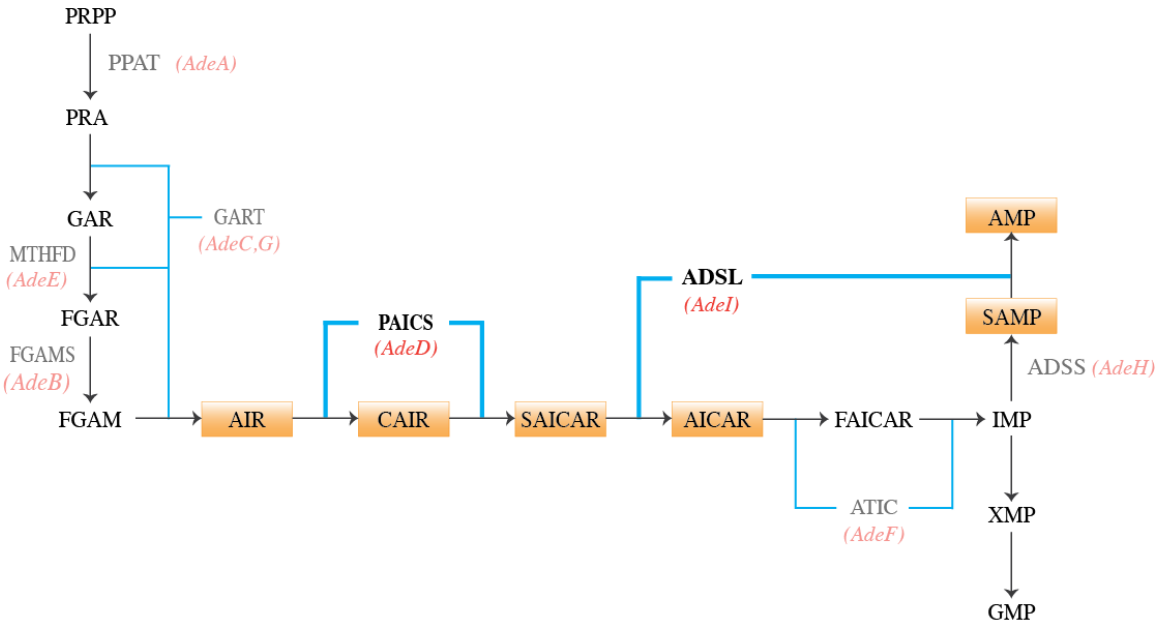

Figure 1. The de novo purine biosynthesis pathway. Ten enzymatic steps produce IMP, and four additional steps produce either AMP or GMP. Orange boxes indicate pathway intermediates of interest. Red italics indicate CHO cell mutations, and affected enzymatic steps. Enzymes are indicated in gray text, and enzymatic steps are indicated (blue lines).

The clinical presentation of genetic disorders of purine metabolism includes a wide variety of symptoms, such as severe combined immunodeficiency, severe neurological defects, developmental delay, and abnormal brain development (Jurecka 2009; Jurecka et al. 2008; Sempere et al. 2010). The consequences of inborn errors in purine metabolism are poorly understood, and misdiagnosis most likely results in underestimation of their incidence and prevalence (Jurecka 2009).

One approach utilized in the analysis of *de novo* purine biosynthesis and the role of the purinosome is the use of mammalian cells with mutations in the genes encoding enzymes of the pathway. These can be cells isolated from individuals with inborn errors of purine metabolism as reported previously (Zikanova et al. 2010; Baresova et al. 2012),

or experimentally derived cells which carry mutations in *de novo* purine biosynthesis genes. We have previously reported the isolation and initial characterization of Chinese hamster ovary cell (CHO-K1) mutants presumably defective in each of the seven proteins required for *de novo* AMP synthesis (Tu & Patterson 1977; Patterson 1975). Here we report the further characterization of two of these, AdeD and AdeI. AdeD is deficient in bifunctional phosphoribosylaminoimidazole carboxylase/phosphoribosylaminoimidazole succinocarboxamide synthetase (PAICS, E.C. 6.3.2.6/E.C. 4.1.1.21) activity, responsible for conversion of AIR (5-aminoimidazole ribotide) to CAIR (5-amino-4-carboxyimidazole ribotide) and conversion of CAIR to SAICAR (5-amino-4-imidazole-N-succinocarboxamide ribotide). AdeI is deficient in bifunctional adenylosuccinate lyase (ADSL) activity, responsible for conversion of SAICAR to AICAR (5-amino-4-imidazolecarboxamide ribotide) and conversion of SAMP (adenylosuccinate) to AMP (adenosine monophosphate). We previously characterized AdeI, and presented evidence that AdeI is a useful model for the cellular consequences of ADSL deficiency (Vliet et al. 2011).

The metabolic intermediates SAICAR (the product of PAICS and a substrate for ADSL) and AICAR (the product of ADSL) regulate the expression of purine pathway genes in yeast cells (Benoıt Pinson et al. 2009). When purine levels are deficient, accumulated AICAR enhances binding of pho2p, pho4p, and bas1p transcription factors to purine and phosphate pathway gene promoters (Benoıt Pinson et al. 2009). SAICAR enhances pho2p and bas1p binding, which specifically positively regulates purine regulon genes (Benoıt Pinson et al. 2009). Whether these intermediates have similar effects in

mammalian cells is not known. AICAr (the riboside form of AICAR) is a potential antitumor agent and promotes apoptosis in aneuploid cells (Tang et al. 2011; Rattan et al. 2005). Administration of AICAr to sedentary mice mimicked the effects of exercise, resulting in increased oxidative biomarkers in cultured skeletal muscle cells and enhanced running endurance (Narkar et al. 2008). It has also been demonstrated that inhibition of adenylosuccinate lyase activity by SAICAR results in skeletal muscle dysfunction (Swain et al. 1984). These findings show that altering the balance of SAICAR and AICAR disrupts cellular functions, including energy metabolism and the regulation of nucleotide synthesis and phosphate consumption.

In addition to its role in supplying the substrate for ADSL, PAICS is of interest because mutations in PAICS cause errors in vertebrate embryonic development (Ng et al. 2009), and because PAICS shows elevated expression in numerous cancers, and may be an important target for anticancer therapies (Zaza et al. 2004; Sun et al. 2004). PAICS overexpression is likely due to the increased proliferation of tumor cells and consequent increased demand for purine nucleotides. Since the two steps catalyzed by PAICS in vertebrates are catalyzed by three enzymes (PurK, PurE, and PurC) in bacteria, and the mechanism of catalysis is different, PAICS is a target for development of antimicrobial drugs (Firestine et al. 2009). If the PAICS deficiency observed in AdeD is due to mutation in the PAICS gene, it could serve as a mammalian cell culture model for analysis of the mechanism of mammalian PAICS catalysis, which should be informative in the development of antimicrobials or vaccines that target SAICAR synthesis (Jackson et al. 1999), the role of PAICS mutations in abnormal development, and cancer metabolism.

Disruption of *de novo* purine biosynthesis can result in the accumulation of intermediary metabolites in cells and body fluids. The detection of these intermediates is difficult, which is problematic for studying *de novo* purine biosynthesis and identifying inborn errors of purine metabolism. This may be why mutations in PAICS have not yet been found in humans. A previous study used high performance liquid chromatography (HPLC) coupled with pulsed amperometry detection to detect phosphoribosylglycinamide (GAR), the product of the second step of *de novo* purine biosynthesis. This suggests that electrochemical detection may be feasible for detection of *de novo* purine biosynthesis pathway intermediates (Taha & Deits 1993). Since the system described requires gradient elution and has limited dynamic range, we used HPLC coupled coulometric detection (HPLC-EC) to analyze intermediate accumulation in AdeD and AdeI cells. Coulometric detection has a number of advantages over amperometric detection, including increased sensitivity, dynamic range, and simplicity of quantitation (Matson et al. 1984).

Here we report the identification of the mutations in AdeD cells in the PAICS gene and their effect on PAICS mRNA and protein expression. Moreover, we report the comparative analysis of AdeD and AdeI intermediate accumulation using HPLC-EC. This method readily detects accumulation of AIR in AdeD cells and SAICAR and SAMP in AdeI cells and, somewhat unexpectedly, accumulation of AIR in AdeI cells.

2.0 Materials and Methods

2.1 Identification and analysis of PAICS mutations

2.1.1 Identification of PAICS mutations in AdeD by RT-PCR

Total RNA was isolated from CHO-K1 and AdeD cells using the RNAqueous4PCR kit (Ambion). AdeD and CHO-K1 cDNA was prepared from the isolated total RNA using the RETROscript kit (Ambion). The PAICS cDNA was amplified with appropriate PCR primers (Table 1) using the Expand Hi-Fidelity PCR kit (Roche) and thermocycler parameters: 95° C for 5 minutes, (95° C for 30 seconds, 60° C for 30 seconds, and 72° C for 30 seconds) for 35 cycles, and 72° C for 7 minutes. PCR products were analyzed by TAE agarose gel electrophoresis. Single bands were excised from the gel and the PCR product was purified using the Zymoclean Gel DNA Recovery kit (Zymo Research). DNA concentration was estimated using TAE agarose gel electrophoresis by comparison with Low Mass DNA or High Mass DNA ladders (Invitrogen). DNA samples containing ~60 ng/kb fragment length were sequenced by the University of Colorado Cancer Center DNA Sequencing and Analysis Core.

PAICS Primers

Primers	5' - 3' Sequence	Purpose
245_PAICS_CHO_F	GGGAGACTGCTTTCATTGCACCCCA	RT-PCR & Sequencing
1509_PAICS_CHO_R	TCAGCCTCTGGTGTGCTGAGGTTAC	
406_PAICS_CHO_F	AATGACCCGCAGTGGTCTGAGGAGC	
1510_PAICS_CHO_R	CTCAGCCTCTGGTGTGCTGAGGTT	
1095_PAICS_CHO_R	GGATGACCACACATCCTGAGCACCC	
807_PAICS_CHO_F	AGTGCTGATGGGTTCCACTTCTGAC	
1265_PAICS_CHO_R	TCTCTGATTTTCTTGTCAGCTTGCTTT	
5U-PAICS-1F	GCGCTGCTTCTCTTTCCCGCGCC	
T7	TAATACGACTCACTATAGGG	pTarget Sequencing
pTarget.seq	TTACGCCAAGTTATTTAGGTGACA	
VP1.5	GGACTTTCCAAAATGTCG	pCMV6-hPAICS Sequencing
XL39	ATTAGGACAAGGCTGGTGGG	
5U-IF-PAICS-4F	CGTGATATCTTTCCCTGCGTTGCGCCGCCCTTTCC	CHO PAICS Cloning
3U-IF-PAICS-4R	GTCGACGGTACCCCCTTTCTGCCTCAGCCTCTGGTGTGC	
CHO_PAICS_F1	CTGATGGGTTCCACTTCTGACCTTG	qPCR
CHO_PAICS_R1	GCCATCGCCTTCATACTCTGCTT	
CHO_ACTB_F1	CTTCGCGGGCGACGATGCT	
CHO_ACTB_R1	GGCCCATGCCCACCATCACG	

Table 1. Primers used in this study.

Sequence alignment with BLAST (Becker et al. 2011; Altschul et al. 1990) using the Mus musculus PAICS cDNA sequence (NCBI NM_025939.2) identified a CHO PAICS cDNA sequence, JP049561.1. Primers for RT-PCR were designed using the JP049561.1 sequence, however, nucleotides +1 to +217 were missing from the 5′- end. A reference CHO PAICS cDNA sequence was constructed by adding 431 nt from a predicted sequence for CHO PAICS (NCBI XM_003513528.1, 2168 bp) onto the 5′-end of JP049561.1. All PAICS RT-PCR primers (Table 1) were numbered relative to the +1 nucleotide in the XM_003513528.1 sequence. The PAICS amino acid sequence derived from JP049561.1 is identical to that from XM_003513528.1, except JP049561.1, like human, mouse, and rat PAICS sequence, has a K at p.418, while XM_003513528.1 has a Q at this position. The resulting CHO reference sequence was used to perform alignments

with sequencing data from CHO-K1 and AdeD cDNA. The Needle program at EBI was used for pairwise alignments with our CHO reference sequence. After identification of polymorphisms in the CHO-K1 and AdeD RT-PCR data, sequencing reads were translated in all reading frames to determine whether any SNP resulted in an amino acid change.

2.1.2 Cloning of PAICS from CHO-K1 and AdeD cDNA.

PAICS was amplified from CHO-K1 and AdeD cDNA using the same PCR protocol described above for RT-PCR. However, the Expand Hi-Fidelity Long Template PCR kit (Roche) was used instead of the Expand Hi-Fidelity Template PCR kit (Roche), following the manufacturer's protocol. The In Fusion PCR primers for PAICS are 5U-IF-PAICS-4F and 3U- IF-PAICS-4R (Table 1). The PCR reactions were cleaned using Nucleospin Plasmid (Clontech).

The pTarget vector (Promega) was linearized overnight with *Sma I* restriction endonuclease and cleaned. The DNA concentration of linearized pTarget and PAICS AdeD PCR product was determined by gel electrophoresis as described earlier. The In Fusion HD Cloning Kit (Clontech) was used to ligate the PAICS AdeD In Fusion RT-PCR products into the pTarget vector.

2.1.3 Mini-preps and DNA sequencing of PAICS-AdeD and PAICS-CHO-K1-pTarget Clones

Mini-preps of plasmid DNA from ampicillin-resistant clones were performed using the Nucleospin Plasmid (Clontech) kit. TAE agarose gel electrophoresis was used to

estimate the size of plasmids recovered from PAICS-AdeD-pTarget and PAICS-K1-pTarget clones, and to estimate DNA concentration. DNA sequencing was performed using the T7, pTarget seq, 807F, 1095R, and 1265R CHO PAICS primers (Table 1). Samples were sequenced by the University of Colorado Cancer Center DNA Sequencing and Analysis Core.

2.1.4 Maxi-prep of PAICS-K1-pTarget, E177K-PAICS-pTarget, and W363Stop-PAICS-pTarget plasmids

DNA maxi preps were performed using the Nucleobond Xtra Midi Plasmid DNA Purification kit (Clontech) according to the manufacturer's protocol, with some modifications. The kit comes with a filter to clarify cell lysates simultaneous with column purification. We clarified cell lysates by centrifugation at 12,000 × g (8,500 RPM) for 50 minutes in a Sorvall RC-5B Superspeed Centrifuge, followed by filtration. The plasmid DNA was concentrated and desalinated using the NucleoBond Finalizer Plasmid DNA Concentration and Desalination kit (Clontech). The quality and quantity of plasmid DNA was quantified by UV spectroscopy at 260 and 280 nm.

2.1.5 Transfection of cDNA expression plasmids PAICS-K1-pTarget, E177K-PAICS-pTarget, and W363Stop-PAICS-pTarget into AdeD.

For each plate, 500 µl OptiMEM I reduced serum medium (Gibco), 20 µl Lipofectamine 2000 (Invitrogen), and 8 µg total DNA were combined according the manufacturer's protocol (Invitrogen Lipofectamine 2000). The transfection mixture was

added to confluent 60mm plates of AdeD cells and incubated overnight at 37° C, 5% CO_2. After 24 hr, the medium was replaced with F12 medium supplemented with 10% FCS, Normocin (100 μg/ml), and 3×10^{-5} M adenine. After an additional 24 hr, the medium was changed to F12 medium containing Geneticin (400 μg/ml) for selection of pTarget-transfected cells and supplemented with 10% FCS, Normocin (100 μg/ml), and 3×10^{-5} M adenine. The purine requirement of AdeD cells stably transfected with wild type (WT) and mutant PAICS plasmid cDNAs was assessed by plating cells into α-MEMFCM10 with or without 1×10^{-4} M hypoxanthine.

2.2 Analysis of PAICS protein from CHO-K1 and AdeD cells

2.2.1 Protein Extraction

CHO-K1, AdeD and AdeI mutant cells were grown in F12 supplemented with 10% fetal calf serum (FCS), Normocin, and 3×10^{-5} M adenine when necessary. Confluent 60 mm plates of cells were rinsed with 1X PBS and the plates were scraped using cell scrapers. The total volume of extracted material was centrifuged for 10 minutes at 2,000 RPM at 4° C. The pelleted cells were resuspended in buffer (10 mM Tris-HCl pH 8.3, 10 mM KCl, 2 mM EDTA, 1 mM DTT, 4% glycerol) with Inhibitor Protease Cocktail Tablets (Roche) and lysed by sonication twice for 15 seconds at 40 W. The homogenate was centrifuged for 20 minutes at 17,000 × *g* at 4° C and protein in supernatant was measured by Bradford assay (Sigma).

2.2.2 Western Blot Analysis for PAICS protein

Total CHO-K1, AdeD, and AdeI protein (20 μg/lane) was separated by SDS-PAGE (10% gel) for 4 hours at 130 V. The gel was wet-blotted to PVDF membrane in blotting buffer (48 mM Tris, 39 mM glycine, 1.3 mM SDS, 20% methanol) at 100 mA constant current for 2 hours. The blot was blocked overnight at 4° C in block solution (5% BSA, 1X PBS, 0.05% Tween-20, pH 7.4) followed by a 3 hour incubation in anti-PAICS antibody (Sigma-Aldrich HPA035895) diluted 1:150 in block solution. This was followed by five washes (1, 3, 5, 10 and 15 minutes) in wash solution (1X PBS/0.05% Tween-20). The blot was then incubated in goat anti-rabbit IgG-HRP conjugate (Pierce-Thermo Scientific 31460) diluted 1:10,000 in block solution for 40 minutes followed by five washes in wash solution. Blots were treated with chemiluminescent SuperSignal West Femto Maximum Sensitivity Substrate (Thermo Scientific) and visualized on a Syngene Genomic and Proteomic Gel Documentation System (Syngene, Cambridge, UK). The blot was rinsed in 1X PBS and incubated in mouse monoclonal anti-GAPDH antibody (Sigma-Aldrich G8795) diluted 1:10,000 in block solution for 90 minutes, followed by five washes. The blot was then incubated in goat anti-mouse IgM-HRP conjugate (Pierce-Thermo Scientific 31440) diluted at 1:20,000 in block solution for 40 minutes, followed by five washes and visualized as described above.

2.2.3 Expression levels of PAICS transcript in CHO cells

PAICS expression levels in CHO cells (AdeD and CHO-K1) were determined by quantitative PCR (qPCR) and ΔΔCt analysis. Total RNA isolation and subsequent cDNA

synthesis was carried out as described above (methods 2.1). The cDNA was used as a template in 25 ul reactions using the iQ SYBER Green Supermix kit (BioRad) with 500 nM CHO specific PAICS primers (Table 1). The qPCR cycling conditions were as follows: 95° C for 5 min followed by 35 cycles of denaturation at 95° C for 10 seconds, annealing at 60° C for 30 seconds followed by SYBER Green data collection, and extension at 72° C for 30 seconds. CHO beta-actin was amplified as a reference control using specific primers (Table 1).

2.3. HPLC-EC Analysis of CHO mutant intermediate accumulations

2.3.1 Accumulation of intermediates

CHO-K1 and the various adenine-requiring mutants were grown in 60 mm dishes in αMEM supplemented with 10% fetal calf serum (FCS), 3×10^{-5} M adenine, and 100 µg/mL Normocin. Accumulation of intermediates was induced by growth in purine-free medium (purine starvation) as follows. Medium in confluent plates was replaced with either fresh αMEM containing 10% FCM (twice dialyzed FCS), Normocin, and 10^{-4} M adenine (which we have previously shown drastically reduces *de novo* purine biosynthesis in CHO cells) or with fresh αMEM containing FCM and Normocin but *lacking* adenine. The cells were then incubated for 4-6 hours. After incubation plates were washed twice with 1 ml cold 1X PBS then incubated for 30 minutes in 500 µl of 80% ethanol at 4° C. The plates were scraped using cell scraper and the ethanol/extract mixture was transferred to 1.5 ml microcentrifuge tube and centrifuged for 10 minutes at 14,000 × g at 4^{o} C. The supernatant was transferred to a microcentrifuge tube and immediately frozen at -80^{o} C.

The frozen extracts were dried under a vacuum in a SpeedVac. The concentrated samples were resuspended in 200 µl HPLC grade water [ultrapure (18.2 MΩ cm) water, which was filtered through 0.2 µm filter and polished through a C18 Sep-Pak column]. Resuspended samples were centrifuged for 15 minutes at 14,000 × g at 4^{o} C to remove any remaining cellular debris prior to analysis.

2.3.2 HPLC-EC Analysis

Separation and measurement of CHO mutant intermediate accumulation was performed using reverse phase HPLC-EC with a TSKgel ODS-80Tm C-18 column (250 mm x 4.6 mm ID, 5 µm) protected by Tosoh Bioscience TSKgel guard cartridge. A column temperature of 35° C was maintained throughout the analysis. A mobile phase consisting of 50 mM lithium acetate, 2% acetonitrile, 5 mM tetrabutyl ammonium phosphate (TBAP), pH 4.8 was delivered isocratically at a flow rate of 0.7 ml/min. Sample extracts and standards were kept at 10° C until a 20 µl aliquot of each sample was injected using an ESA autosampler (model 542). After injection and separation, analytes were detected using a CoulArray HPLC system (model 5600A, ESA) with three electrochemical detector modules. Each module contains four flow-through coulometric detectors in series set to a range of potentials from 0 – 900 mV in 100 mV increments. Also in series with the coulometric detectors was a UV detector set at 240 nm. ESA CoulArray software was used for baseline correction and analysis of all samples.

3.0 Results

3.1 Identification of the PAICS mutations in AdeD cells

We have shown previously that AdeD cells apparently accumulate AIR, due presumably to mutation of the PAICS gene (Patterson 1975). The cDNA coding region for CHO-K1 and mouse PAICS is 1278 nucleotides long with 426 codons including the TAA stop codon. Sequencing of PAICS RT-PCR products from CHO-K1 and AdeD cells provided approximately 80% of the PAICS cDNA sequence. Comparison to our reference PAICS cDNA sequence revealed two sequence variants unique to AdeD, and one sequence variant common to both AdeD and CHO-K1 (Table 2). This latter variant is p.I237V (c.A709G), located in the loop between β14 and α5. A BLAST search reveals that most organisms (including mouse and human) have a V at this position, and we tentatively hypothesize that V is the correct residue in CHO cells. Interestingly, p.237 is missing in

PAICS cDNA Sequence Polymorphisms

	Primers			
Cell Line	**RT-PCR**	**Sequencing**	**Verified Sequence**	**Polymorphisms**
K1	245F/1265R	1095R	244-1015	A709G
	245F/1265R	807F	863-1263	ND
	5U-1F/1095R	1095R	433-883	A709G
	807F/1509R	807F	926-1278	ND
AdeD	245F/1509R	1095R	277-1016	G529A, A709G
	245F/1265R	1265R	716-1166	G1088A
	5U-1F/1095R	1095R	483-883	G529A, A709G
	807F/1509R	807F	883-1278	G1088A

Table 2. Identification of polymorphisms in CHO-K1 and AdeD PAICS cDNA by RT-PCR. The polymorphisms are p.E177K (c.G529A), p.W363 (c.G1088A), and p.I237V (c.A709G). ND indicates no polymorphisms detected.*

the structure of human PAICS (2H31.pdb); "Asp221-Thr238 were not visible in the electron density map and assumed being disordered in the crystal" (Li et al. 2007). This suggests that the region containing p.237 is quite flexible, and that replacement of valine with isoleucine (a conservative change) would have little effect on the monomer structure.

The two variants found only in AdeD PAICS are p.E177K (c.G529A), located in α4, and p.W363* (c. G1088A), located in α9. The AdeD and CHO-K1 cDNAs were ligated into pTarget and sequenced. The sequences were compared to the PAICS reference sequence described earlier (431 nt from a predicted CHO-K1-PAICS sequence stitched to the 5′-end of JP049561.1). Our CHO-K1 PAICS sequence is presented (see Figure 2) and differs from our reference sequence at c.G-5A (upstream of the coding region), c.A153G (a silent mutation), and c.A709G (p.I237V). In CHO-K1, it is possible that one PAICS allele has isoleucine at p.237 and the other has valine. The PAICS sequence in our pTarget clone has p.237V. Both JP049561.1 and XM_003513528.1 have c.A709 (p.I237), however valine is evolutionarily conserved at p.237 (Li et al. 2007).

We hypothesized that the two PAICS variants in AdeD represent two different PAICS alleles. To test this, we ligated AdeD PAICS cDNA into pTarget and isolated subclones for sequencing. Some subclones contained the c.G529A (p.E177K) variant, and some contained the c.G1088A (p.W363*) variant. The c.A709G (p.I237V) variant was present only in c.G529A (p.E177K) subclones (Figure 3 A). None of the PAICS-AdeD-pTarget clones had the wild type sequence. The PAICS cDNA sequence of K1, and both AdeD alleles in our pTarget clones have been deposited in GenBank (NCBI accession

numbers KC176530, KC176531, and KC176532). The AdeD p.E177K allele (KC176531) is referred to as "allele 1" and the p.W363* allele (KC176532) is referred to as "allele 2".

3.2 The mutations in AdeD lead to lack of detectable PAICS protein

The p.W363* PAICS variant would be expected to be incapable of producing a full-length protein. However, to address the possibility that the p.E177K variant produces a full-length inactive protein, we carried out western blot analysis of protein extracts from CHO-K1 and AdeD. The result demonstrates that CHO-K1 contains PAICS protein as expected. However, AdeD does not contain detectable levels of PAICS protein (Figure 4). We also assessed whether PAICS is present in AdeI, which has a mutation in ADSL, the next enzyme in the *de novo* purine biosynthetic pathway. PAICS is abundant in AdeI cells. Two bands of similar molecular weight were detected, possibly representing different PAICS isoforms.

CHO-K1 PAICS

```
                                M  A  T  A  E  V  L  N  I  G  R  K   12
-26 tctacacctccttcccaccagagataatggcgacagctgaggtactgaacattgggagaa

     L  Y  E  G  K  T  K  E  V  Y  E  L  L  D  N  P  G  K  V  L   32
 35 aactctatgagggtaagacaaaagaagtctatgaattgttagataatccaggaaaagtcc

     L  Q  S  K  D  Q  I  T  A  G  N  A  A  R  K  N  H  M  E  G   52
 95 tcctgcagtccaaggaccagattacagcaggaaatgcagctagaaagaaccatatggagg

     K  A  A  I  S  N  K  I  T  S  C  I  F  Q  L  L  Q  D  A  G   72
155 gcaaagctgcaatctccaataagattaccagctgtatttttcagttgttacaggatgccg

     I  K  T  A  F  T  K  K  C  G  E  T  A  F  I  A  P  Q  C  E   92
215 gTATCAAAACTGCTTTCACCAAGAAATGTGGGGAGACTGCTTTCATTGCACCCCAATGCG

     M  I  P  I  E  W  V  C  R  R  I  A  T  G  S  F  L  K  R  N  112
275 AAATGATTCCAATTGAATGGGTGTGCCGAAGAATAGCAACTGGATCTTTTCTCAAAAGGA

     P  G  V  K  E  G  Y  K  F  Y  P  P  K  V  E  M  F  F  K  D  132
335 ACCCTGGTGTAAAGGAAGGGTATAAATTTTACCCACCAAAAGTAGAGATGTTCTTCAAGG

     D  A  N  N  D  P  Q  W  S  E  E  Q  L  I  A  A  K  F  C  F  152
395 ATGATGCCAATAATGACCCGCAGTGGTCTGAGGAGCAGCTCATTGCTGCAAAGTTCTGCT

     A  G  L  V  I  G  Q  T  E  V  D  I  M  S  H  A  T  Q  A  I  172
455 TTGCTGGACTTGTTATAGGCCAGACTGAAGTTGACATCATGAGTCATGCTACCCAAGCTA

     F  E  I  L  E  K  S  W  L  P  Q  N  C  T  L  V  D  M  K  I  192
515 TATTTGAAATCCTGGAGAAGTCCTGGCTTCCCCAGAACTGTACACTGGTTGATATGAAGA

     E  F  G  V  D  V  T  T  K  E  I  V  L  A  D  V  I  D  N  D  212
575 TTGAATTTGGTGTTGATGTAACCACCAAAGAGATTGTTCTGGCTGATGTTATTGATAATG

     S  W  R  L  W  P  S  G  D  R  S  Q  Q  K  D  K  Q  S  Y  R  232
635 ATTCCTGGAGACTCTGGCCATCAGGGGATCGGAGCCAGCAGAAAGACAAACAGTCTTACC

     D  L  K  E  V  T  P  E  G  L  Q  M  V  K  K  N  F  E  W  V  252
695 GTGACCTCAAGGAAGTAACTCCGGAAGGACTGCAGATGGTAAAGAAGAACTTTGAGTGGG

     A  D  R  V  E  L  L  L  K  S  D  S  Q  C  R  V  V  V  L  M  272
755 TTGCAGATCGAGTGGAGTTACTCCTGAAGTCAGATAGTCAGTGCAGGGTTGTAGTGCTGA

     G  S  T  S  D  L  G  H  C  E  K  I  K  K  A  C  G  N  F  G  292
815 TGGGTTCCACTTCTGACCTTGGTCACTGTGAGAAAATTAAAAAGGCTTGTGGAAACTTCG

     I  P  C  E  L  R  V  T  S  A  H  K  G  P  D  E  T  L  R  I  312
875 GGATTCCATGTGAACTTCGAGTAACATCTGCCCATAAAGGACCGGATGAAACTTTGAGGA

     K  A  E  Y  E  G  D  G  I  P  T  V  F  V  A  V  A  G  R  S  332
935 TTAAAGCAGAGTATGAAGGCGATGGCATACCTACTGTATTTGTCGCAGTGGCTGGCAGAA

     N  G  L  G  P  V  M  S  G  N  T  A  Y  P  V  I  S  C  P  P  352
995 GCAATGGTTTGGGCCCAGTGATGTCTGGTAATACTGCATATCCGGTTATCAGCTGTCCCC

     I  T  P  D  W  G  A  Q  D  V  W  S  S  L  R  L  P  S  G  L  372
1055 CCATCACACCAGACTGGGGTGCTCAGGATGTGTGGTCATCCCTTCGACTGCCCAGTGGTC

     G  C  S  T  I  L  S  P  E  G  S  A  Q  F  A  A  Q  I  F  G  392
1115 TTGGCTGTTCAACTATACTTTCTCCAGAAGGATCCGCCCAGTTTGCTGCTCAGATATTTG

     L  Y  N  H  L  V  W  A  K  L  R  A  S  I  L  N  T  W  I  S  412
1175 GGTTATACAACCATTTGGTATGGGCCAAACTTCGAGCAAGCATTCTTAACACATGGATAT

     L  K  Q  A  D  K  K  I  R  E  C  N  L                      425
1235 CTTTAAAGCAAGCTGACAAGAAAATCAGAGAATGCAATTTATAAAAAAA
```

Figure 2. DNA sequence of PAICS-K1 cloned into pTarget. The adenine in the start (ATG) codon is designated +1. Mutations identified in AdeD are underlined: c.G1088A (p.W363) and c.G529A (p.E177K). PAICS DNA sequence in capital letters represents the truncated cDNA sequence. PAICS DNA sequence from the predicted sequence is in lowercase letters. Our K1 PAICS sequence is presented and differs from our **XM_003513528.1**: **JP049561.1** reference sequence at c.G-5A and c.A153G (a silent mutation). The valine (V) at position p.237 (c.A709G) differs from the published K1 PAICS, **JP049561.1**, which when translated has isoleucine (I) at this position.*

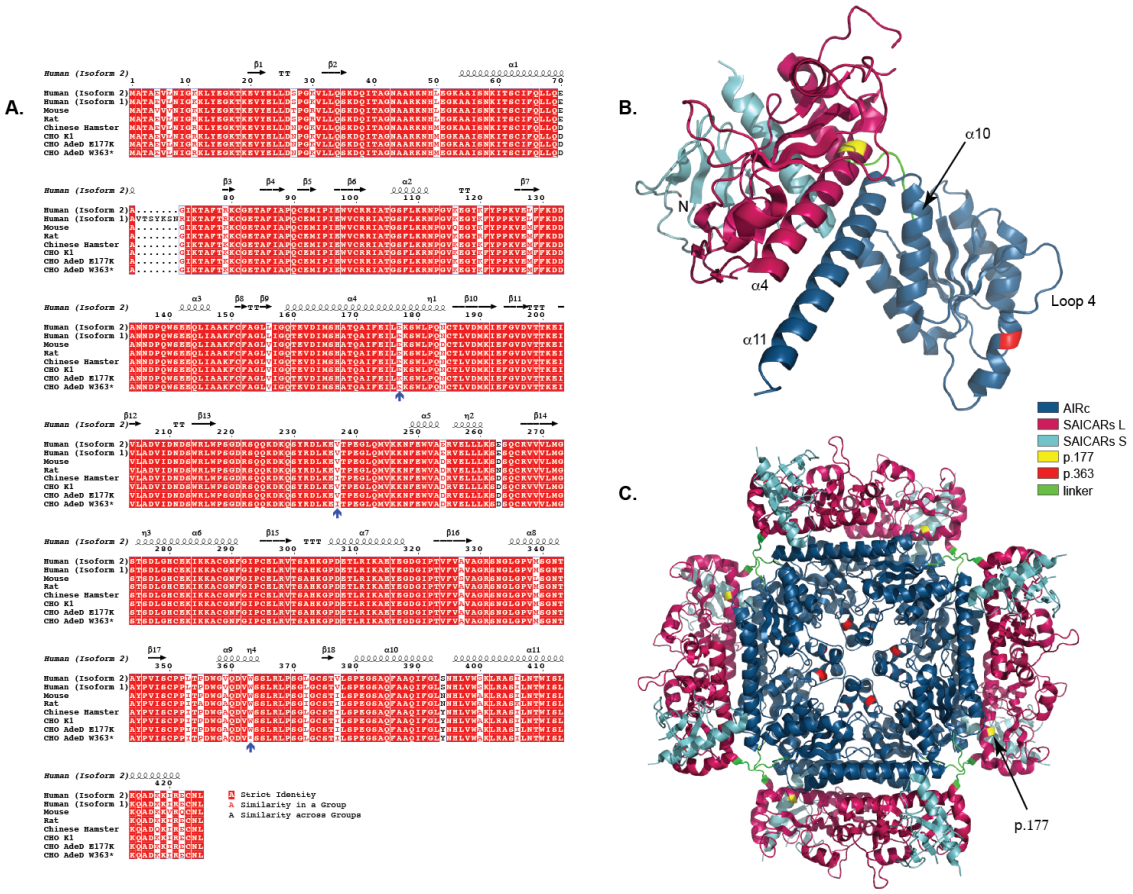

*Figure 3. COBALT alignment of PAICS protein sequences using Genbank IDs. The Genbank IDs for the amino acid sequences are Human (Isoform 2): **119220557**, Human (Isoform 1): **119220559**, Mouse: **13385434**, Rat: **18266726**, Chinese Hamster: **354503014**. CHO K1, CHO AdeD E177K, and CHO AdeD W363* are described in this report. The E177K, I237V, and W363* mutations are indicated by blue arrows. Secondary sequence is indicated above the aligned sequences. This representation of the aligned sequences was created using the Espript program (http://espript.ibcp.fr/ESPript/ESPript/).*

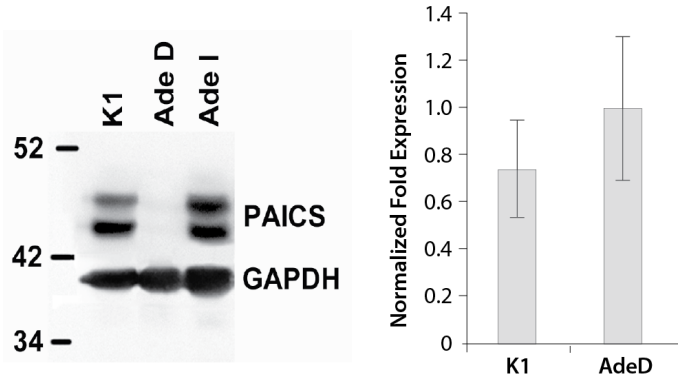

Figure 4. Protein and RNA expression patterns of CHO-K1 and AdeI mutant.
A) Western blot of CHO-K1, AdeD, and AdeI protein.
B) qPCR analysis of PAICS mRNA levels in CHO-K1 and AdeD cells.

3.3 AdeD produces abundant amounts of PAICS mRNA

We performed qPCR to determine the level of PAICS mRNA in AdeD and CHO-K1 cells. Figure 5 shows the relative fold expression of PAICS mRNA in CHO-K1 and AdeD cells. There was no significant difference in PAICS transcript levels in AdeD cells compared to CHO-K1.

3.4 Alleviation of the purine requirement of AdeD cells by transfection with CHO-PAICS cDNA

To confirm that the AdeD mutations inactivate PAICS, we constructed vectors with wild type (WT) and both mutant PAICS. We then transfected AdeD cells with each of the PAICS vectors. As expected, transfection with WT PAICS cDNA rescued the AdeD purine requirement, but transfection with either mutant clone did not. This demonstrates that the mutations in AdeD inactivate PAICS (Figure 6).

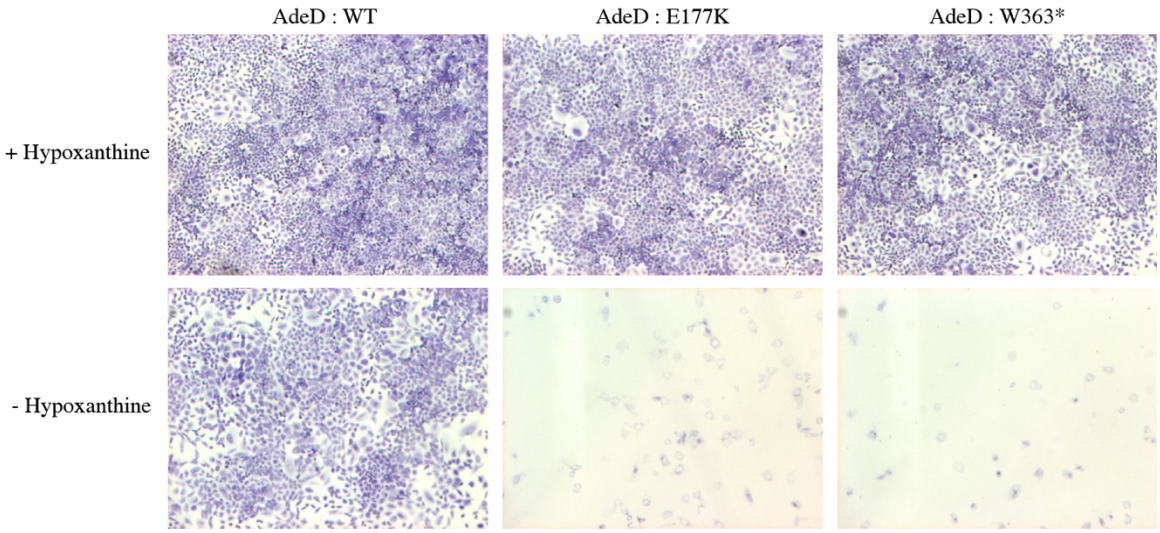

Figure 5. Cell growth of AdeD cells stably transfected with WT and mutant PAICS (E177K and W363X) cDNA plasmids. Purine requirement was assessed by plating cells into supplemented (+Hypoxanthine) or purine deficient (-Hypoxanthine) aMEMFCM10 medium.

3.5 HPLC-EC analysis of AdeI and AdeD intermediate accumulation

We previously demonstrated that AdeD cells accumulate an intermediate presumed to be AIR (Patterson 1975). To confirm that this intermediate is indeed AIR, we devised a simple method for detecting AIR that does not depend on radioisotopic labeling. Using HPLC-EC, we found that AdeD accumulates two compounds upon incubation in purine-free medium. To determine whether one of these is AIR, we performed HPLC-EC analyses employing standard AIR (validated by mass spectroscopic analysis, using a method devised in our laboratory to be described elsewhere) and demonstrated that AIR co-elutes, and co-oxidizes, with one of the two compounds. The purine deprived cells show accumulation of a major peak with a retention time of 5 minutes when compared with adenine supplemented cells (Figure 7 A, B). The addition of AIR to the AdeD sample from cells incubated in purine-free media does not yield a new peak, but instead increases the

intensity of an existing peak. AIR standard alone yields a significant peak with the same 5-minute retention time and the same oxidation pattern.

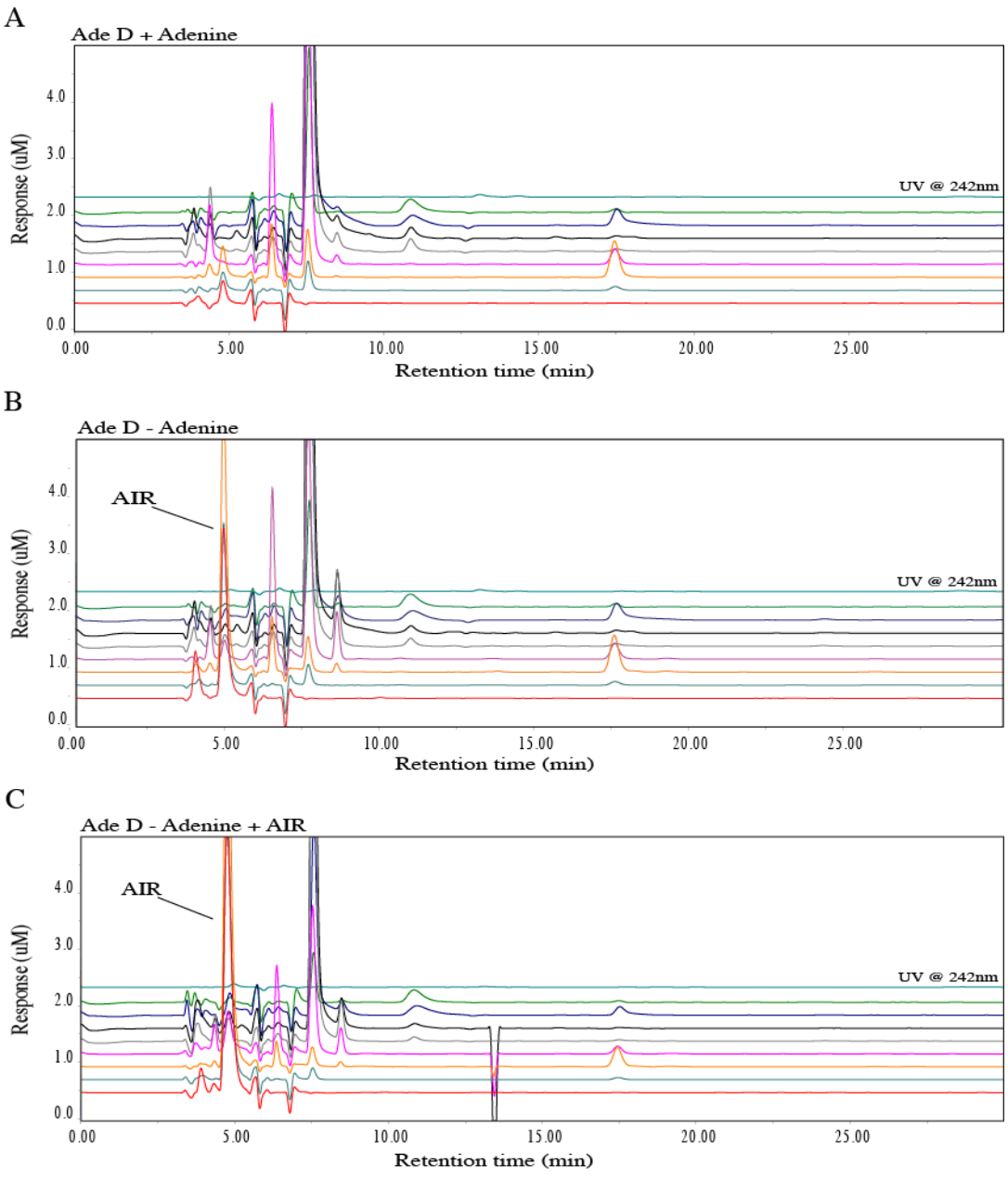

Figure 6. Metabolomic analysis of AdeD (PAICS) mutant CHO cell starvation. The traces show the baseline profile of AdeD unstarved (A) and the accumulation of a peak at 5 minutes with a maximum peak height in the 400 mV EC channel in the starved sample (B). This peak corresponds to the appearance of a peak at 5 minutes with the same peak profile in the Ade D sample spiked with AIR standard (isolated by Zikanova) (C).

Similarly, we examined the accumulation of purine intermediates in AdeI cells. When cultured in purine-free media, AdeI cells accumulate a compound identified as SAICAR (Figure 8 B, C). They also accumulate an additional compound that appears from retention time and oxidation characteristics to be the same compound accumulated by purine-depleted AdeD. Co-chromatography of AdeI extracts with standard AIR confirms that AdeI, like AdeD, accumulates AIR (Figure 8 D). There are no differences detected in the intermediate accumulation of starved versus unstarved CHO-K1 cells.

4.0 Discussion

Analysis of AdeD PAICS cDNA sequences revealed two sequence variants, p.E177K and p.W363* which map to separate alleles. AdeD was produced by treatment of CHO cells with EMS, which induces point mutations, consistent with our characterized (point) mutants. The CHO-K1 variants c.G-5A and c.A153G probably have no consequence for PAICS protein structure and function. One is upstream of the start codon and the other is silent. The c.G-5A and c.A153G variants differ from the predicted CHO PAICS sequence (NCBI XM_003513528.1, 2168 bp).

Except for p.W363* (AdeD), p.E177K (AdeD), and p.I237V [AdeD (the p.I237V allele) and CHO-K1], no other differences were found comparing our AdeD and CHO-K1 PAICS sequences to JP049561.1. These three variants were identified both by RT-PCR and by sequencing the inserts of pTarget clones containing the PAICS cDNA from either CHO-K1 or AdeD cells. Transfection of AdeD cells with WT and mutant PAICS vectors demonstrates that WT PAICS cDNA rescues the AdeD purine requirement, but

transfection with either mutant cDNA does not. Western blot analysis demonstrated expression of PAICS protein in CHO-K1 and in AdeI, but not in AdeD. These results and the observed abundance of PAICS mRNA in AdeD cells strongly suggests that both the mutations observed in PAICS lead to production of truncated and/or unstable protein.

The p.E177K substitution is located in the SAICARs domain of PAICS in an alpha helical (α4) region of the protein important for interaction of the SAICARs and AIRc domains as well as maintenance of SAICARs structure (Figure 3). It may also play a role in substrate channeling within PAICS (Li et al. 2007). The fly, frog, chicken, cattle, mouse, and human PAICS all have p.E177 in the α4 helix (Li et al. 2007). At physiological pH, glutamate (E) is negatively charged. In the structure for human PAICS (2H31.pdb, Li et al. 2007), p.E177 is extremely close to p.R102 (arginine), which is located next to β6, between β6 and α2. Arginine is positively charged, and it is possible that attraction between p.E177 and p.R102 in the wild type protein may play a role in stabilizing PAICS monomer structure. If this is the case, p.K177 (lysine) would be disruptive; it is positively charged, so rather than attraction between it and p.R102, it would most likely repel p.R102. In addition, K has a longer side chain than E, so steric hindrance may also be a destabilizing factor. This is consistent with the possibility that the mutation affects the folding of AdeD PAICS, thus leading to an unstable protein. Indeed, analysis of this mutation using PoPMuSiC 2.1 calculates a ΔΔG of 0.41 and predicts that this is a destabilizing mutation for PAICS (Yves Dehouck et al. 2009; Dehouck et al. 2011).

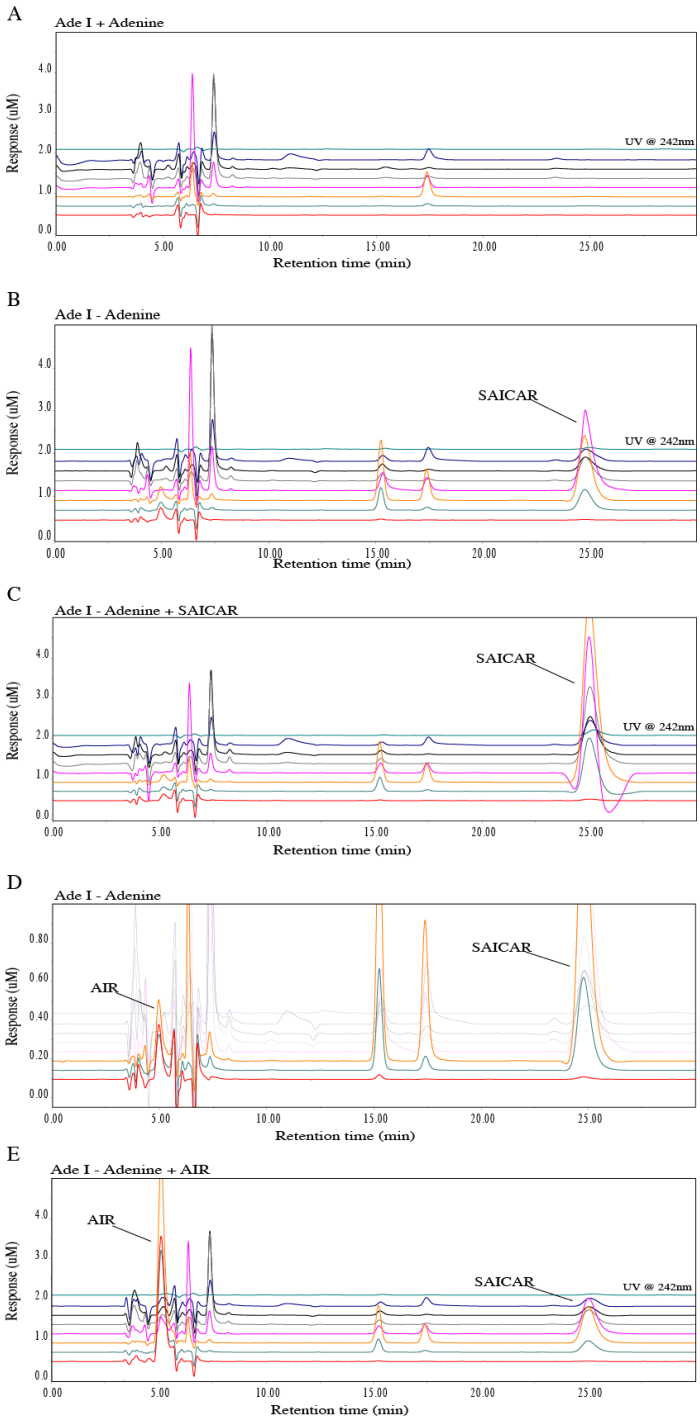

Figure 7. Metabolomic analysis of the AdeI (ADSL) CHO cell starvation. The traces show the baseline profile of AdeI unstarved (A) and the accumulation of a peak at 25 minutes in the starved sample (B). This corresponds to a peak in the unstarved sample spiked with a SAICAR standard (C). Additionally, a small peak at 5 minutes reminiscent of AIR accumulated in small concentrations in the AdeI starved samples. This suggests that accumulation of SAICAR may inhibit the function of PAICS resulting in AIR accumulation (D). This peak corresponds to AIR in starved AdeI cells spiked with AIR (E).

It is unlikely that the p.W363* mutant monomer could participate in the octameric form of the PAICS protein since structures beyond the carboxyl end of p.362, such as the α10 and α11 helices believed to form the dyad symmetry interface crucial for assembly of the octamer, and loop 4, which forms part of the AIRc active site (Li et al. 2007), would be absent. The seven-turn α11 helix interacts with the six-turn α4 helix in a coiled coil, so this interaction would be absent as well (Figure 3). AIRc activity and assembly of an octamer would be highly unlikely (Li et al. 2007).

Previously, we characterized mutations in AdeI (A291V in ADSL) and AdeC and AdeG (both deficient in trifunctional GART activity) (Vliet et al. 2011; Knox et al. 2008). Here we report characterization of two sequence variants, p.E177K and p.W363*, in two PAICS alleles that are responsible for the purine auxotrophy observed in AdeD. Thus, defined mutants exist in 3 of the 6 proteins required for *de novo* purine biosynthesis in mammalian cells. We are currently characterizing the mutations in the other mutant CHO cell lines (Figure 1).

We have reported previously that isolates of AdeC and AdeG produce markedly reduced or undetectable levels of trifunctional GART (triGART) protein and also of monofunctional GARS (Brodsky et al. 1997). In addition we have published evidence that CHO-K1 AdeB mutants produce undetectable levels of FGAMS (phosphoribosylformylglycinamidine) (Barnes et al. 2001; Patterson et al. 1999). We have also reported a mutant CHO-K1 cell that overproduces FGAMS (Barnes et al. 2001). Deng et al. (Deng et al. 2012) recently presented evidence supporting the hypothesis that triGART and FGAMS are core components of the purinosome and that PPAT and FGAMS

interact intracellularly, a hypothesis we proposed previously on the basis of somatic cell genetic evidence (Oates et al. 1980). These mutations, resulting in altered levels of *de novo* purine biosynthesis proteins, serve as important model systems for analysis of purinosome formation and function. We show here that AdeD cells produce undetectable levels of PAICS protein. This collection of mutants should be helpful in analyzing the formation and functioning of the purinosome. For example, Deng et al. (Deng et al. 2012) hypothesize that PAICS, ADSL, and ATIC interact individually with the core purinosome but may also interact with each other. Clearly, interactions between ADSL and PAICS cannot take place in AdeD cells since there is no detectable PAICS protein. It would be important to know what the consequences are for other protein-protein interactions relevant to the purinosome.

One difficulty in analysis of *de novo* purine biosynthesis is that robust methods that are not reliant on the use of radioisotopes to detect and quantify pathway intermediates from small samples of cells are not readily available. Our analysis of AdeD and AdeI demonstrates the utility of HPLC-EC for these studies. The method has provided convincing evidence that AdeD cells incubated in purine-free conditions accumulate AIR, the initial substrate of the bifunctional enzyme PAICS (Figure 7 B, C). Similarly, HPLC-EC readily detects accumulation of SAICAR in AdeI cells (Figure 8 B, C).

HPLC-EC has provided new insights into intermediate accumulation under conditions of purine depletion. For example, AdeI cells incubated in purine-free media accumulate AIR in addition to SAICAR. AdeI cells have virtually undetectable levels of ADSL activity. It is not clear whether cells from ADSL deficiency patients accumulate

AIR or not, since these cells all have significant residual ADSL activity. If AIR does accumulate in these cells, it may potentially play a role in pathogenetic mechanisms of ADSL deficiency.

HPLC-EC analysis demonstrates that AdeD and AdeI cells accumulate a second compound that was not identified. The *de novo* pathway suggests that this compound may be carboxy-AIR (CAIR), the substrate of the second sequential step catalyzed by PAICS. However, the lack of detectable PAICS protein argues against this interpretation. Other possibilities are that the compound may be aminoimidazole riboside, or aminoimidazole, or an earlier intermediate in the pathway.

HPLC-EC offers many advantages for these analyses. Samples undergo redox reactions with 100% efficiency, and the series of incremental voltages allows for high specificity and resolution of co-eluting compounds. HPLC-EC is also extremely sensitive, capable of detecting 1-10 pg of a given compound. Detection of SAICAR is about 200 times more sensitive by EC than by UV. Detection of AIR by UV is possible, but absorption is relatively low. The molar extinction coefficient for AIR (250 nm, pH 6) is 4170 M^{-1} cm^{-1} (Meyer et al. 1992). Our results demonstrate the utility of HPLC-EC as a detection method for investigating the *de novo* purine biosynthesis pathway and detecting its intermediates. We are currently investigating detection of other *de novo* purine biosynthesis intermediates using HPLC-EC.

Current clinical methods used to test for purine intermediate accumulation generally detect dephosphorylated compounds in bodily fluids. HPLC-EC is sufficiently sensitive that it can likely be used to detect the true pathway intermediates in clinically

relevant samples such as skin biopsies, fibroblast cultures, or small blood samples. Additionally, HPLC-EC methods could be devised to detect dephosphorylated compounds. These possibilities are currently under study.

Acknowledgments

This work was supported by grants from the Bonfils-Stanton Foundation and the Ludlow-Griffith Foundation to DP, and Partners in Scholarship and Summer Research Grants to KL. VB, VS, SK and MZ were supported by the by Charles University institutional programs PRVOUK-P24/LF1/3, UNCE 204011 and SVV2012/ 2645, and by grants LH11031 from The Ministry of Education of Czech Republic and P305/12/P419 from the Czech Science Foundation. The University of Colorado Cancer Center DNA Sequencing and Analysis Core is supported by NIH-NCI grant P30 CA 046934.

Future Directions

We performed a metabolomic analysis of the Ts65Dn mouse model of DS, aging, and early onset Alzheimer's disease. The goal was to search for age-associated changes in the mice that are related to the triplication of the Mmu16 chromosome. Additionally, we treated the mice with rapamycin, an FDA approved immunosuppressant drug with pro-longevity properties, and tried to elucidate the changes in the metabolome due to treatment. We find that there are changes to the metabolome of the Ts65Dn mice caused by the triplication of Mmu16. These changes may promote the developmental delays that individuals with DS experience as well as the changes they encounter as they progress to old age. Considering metabolomics as a fingerprint of phenotype, these changes may reflect the end product of the developmental delays and could be used as a biomarker for discovering therapeutics. With this in mind, it will be important to discover if these metabolome changes reflect by-products of disrupted development and aging, or if they actively contribute to the phenotype by creating a neurotoxic environment.

Our study also revealed that long-term treatment with rapamycin ameliorates the changes seen in the mice that may be promoting the disruption in development and aging. When trisomic mice are treated with rapamycin, the metabolites we see increased are no longer in abundant levels, this indicates that rapamycin may be having a beneficial effect.

Both individuals with DS and the Ts65Dn mice have dysregulated immune function, possibly due to the triplication of four of six interferon receptors causing hyperactivity. Chronic treatment with an immunosuppressant such as rapamycin may help to ameliorate this disrupted immune function. We identify changes that implicate a change in tryptophan metabolism, which is regulated by interferon gamma signaling. Interferon gamma is triplicated in DS. Future studies could focus on the changes that occur through interferon gamma signaling and determining if these cause a change in the metabolites we see upregulated.

Most importantly, in the future, attempting to identify the unknown metabolites we find changed in the different groups will be of importance. Of these, the most valuable may be Unk76, which appears to be coupled to rapamycin treatment. Perhaps using MS to determine what this metabolite is may help give more insight to the pathways disrupted in the Ts65Dn mice as well as in individuals with DS. It may also prove to be a novel metabolite that can be used as a target for therapeutics.

In addition to this work, determining if these changes occur in the cerebellum and blood samples we collected. This may help to identify possible blood biomarkers for DS and aging.

We also performed a metabolomic and biochemical characterization of the PAICS enzyme of the DNPS. This enzyme has been implicated as a possible anti-cancer drug target. Further analysis of the PAICS enzyme using human cells or mouse models with a similar approach to the Ts65Dn rapamycin study may help to further this line of research.

Appendix 1
Supplement to Chapter 2

Section 1 – 6-month frontal brain pattern recognition analysis

The following are supplemental data plots for 6-month frontal brain samples.

Comparison of disomic and trisomic mice fed control diet.

Control diet

Fold change (>10)

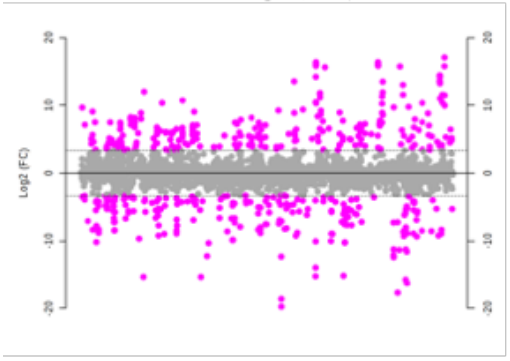

Volcano plot

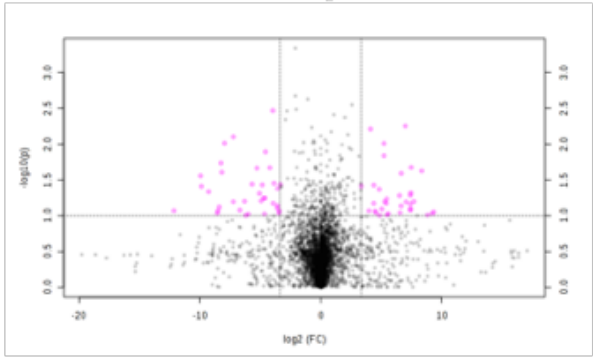

All features

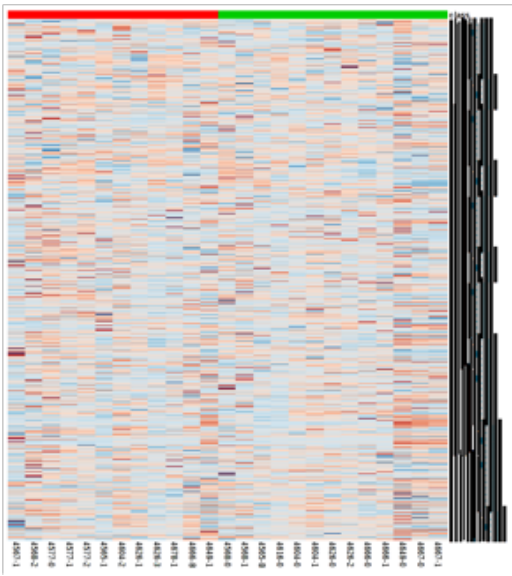

Top 25 features by t-test

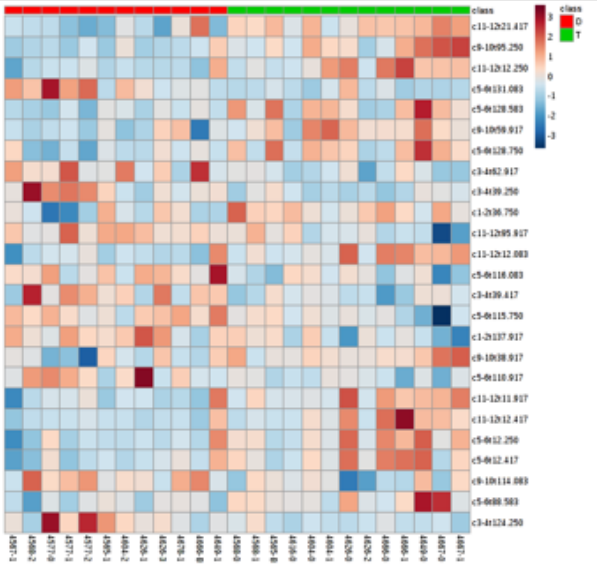

Control diet

PCA pairwise

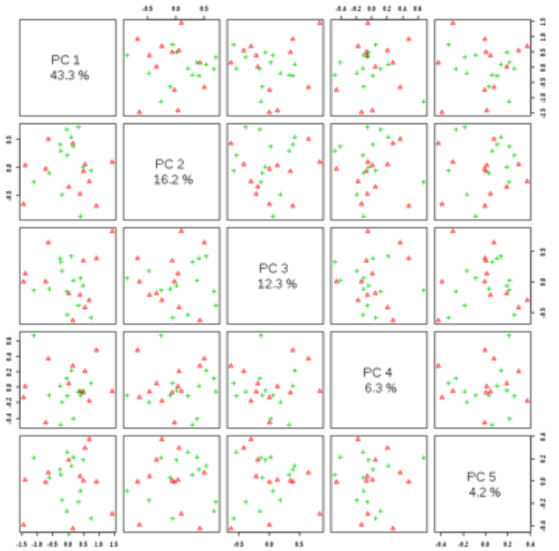

PCA scores

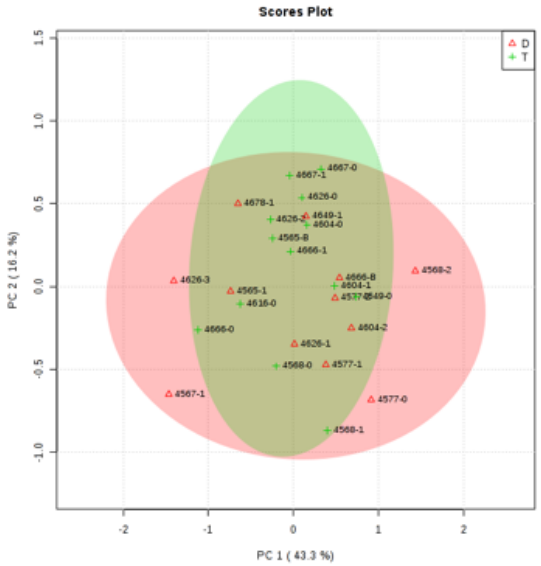

Control diet

PLS-DA pairwise

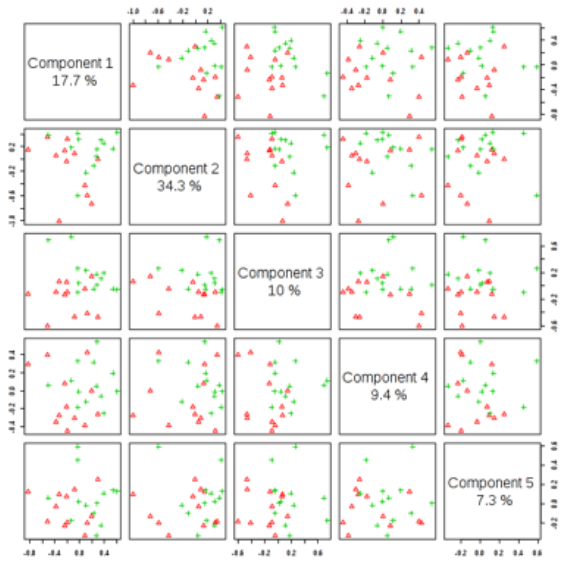

PLS-DA scores

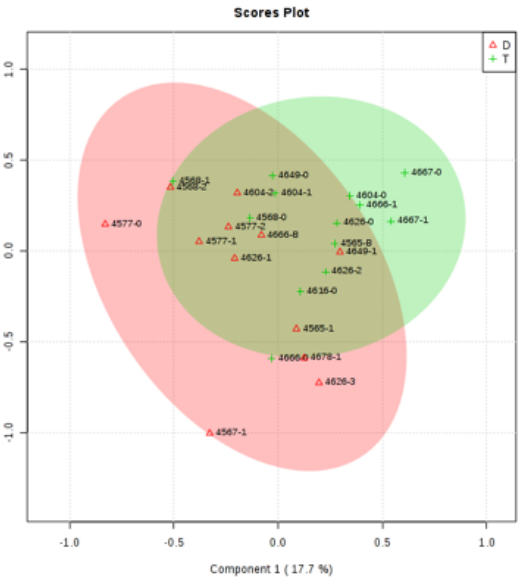

Comparison of disomic and trisomic mice fed microencapsulated rapamycin diet

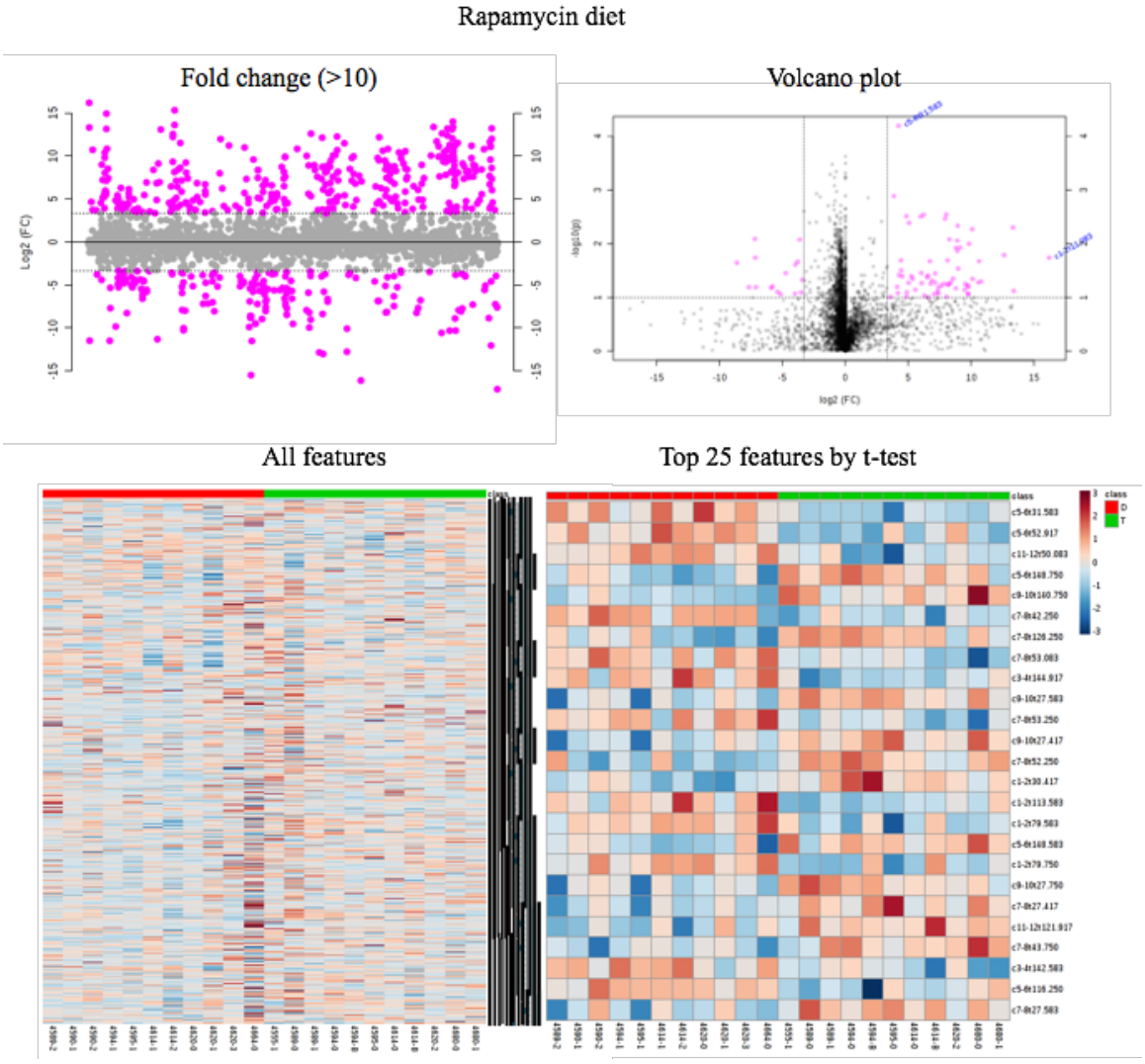

Rapamycin diet

PCA pairwise

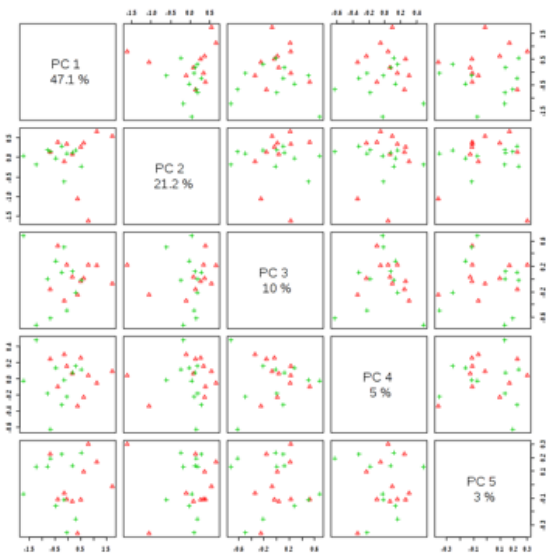

PCA scores

Rapamycin diet

PLS-DA pairwise

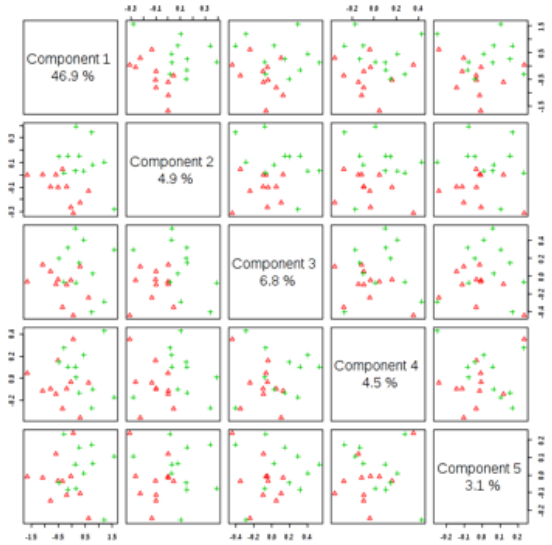

PLS-DA scores

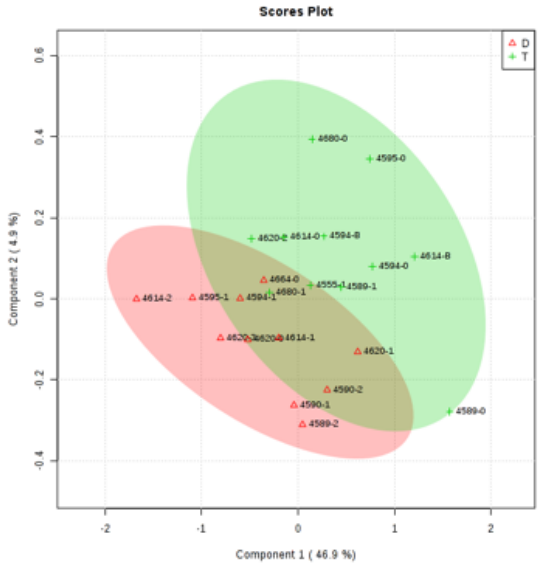

Comparison of control diet and microencapsulated rapamycin diet in disomic mice

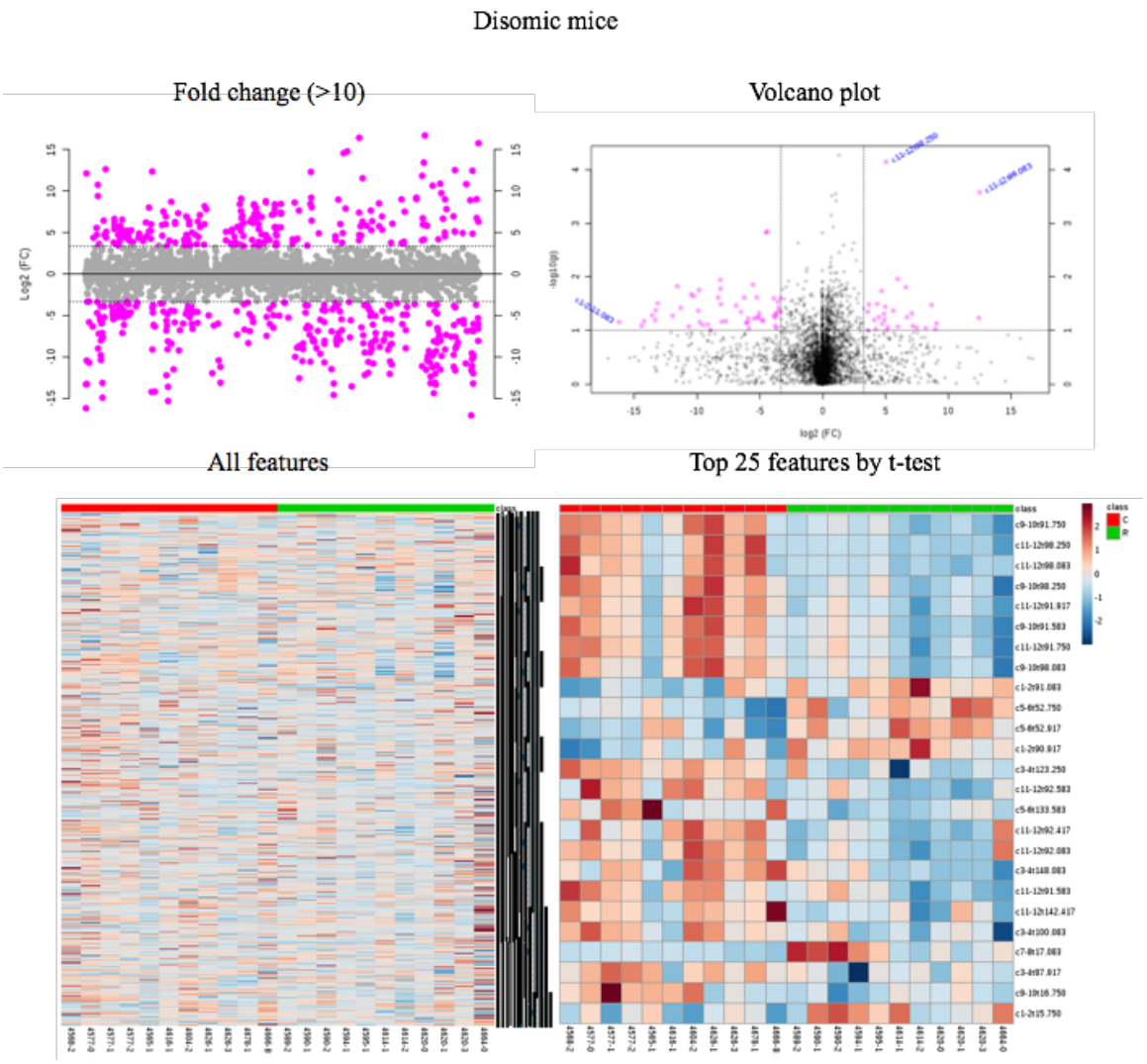

Disomic mice

PCA pairwise

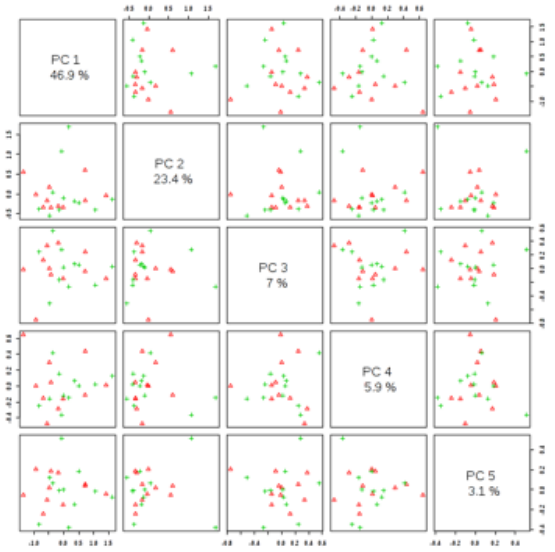

PCA scores

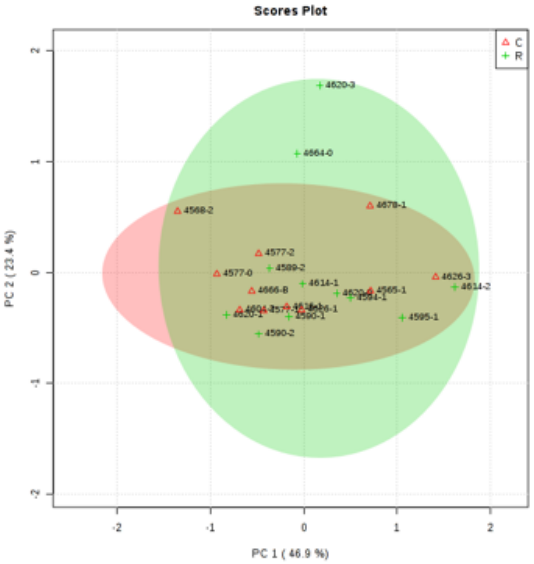

Disomic mice

PLS-DA pairwise

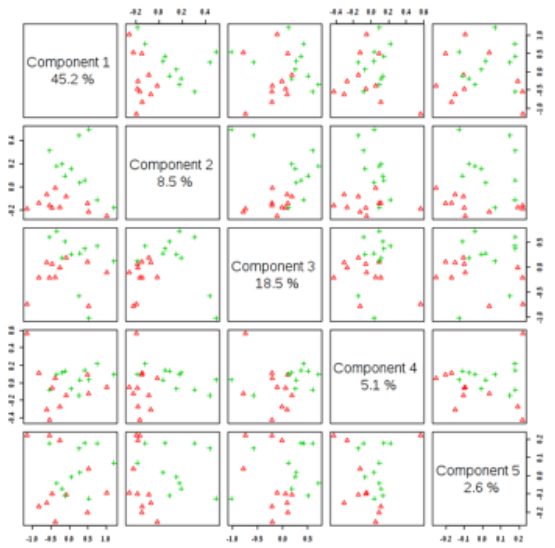

PLS-DA scores

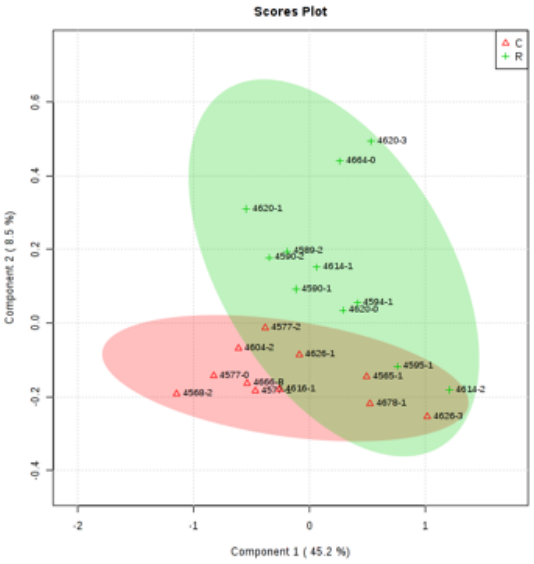

Comparison of control diet and microencapsulated rapamycin diet in trisomic mice

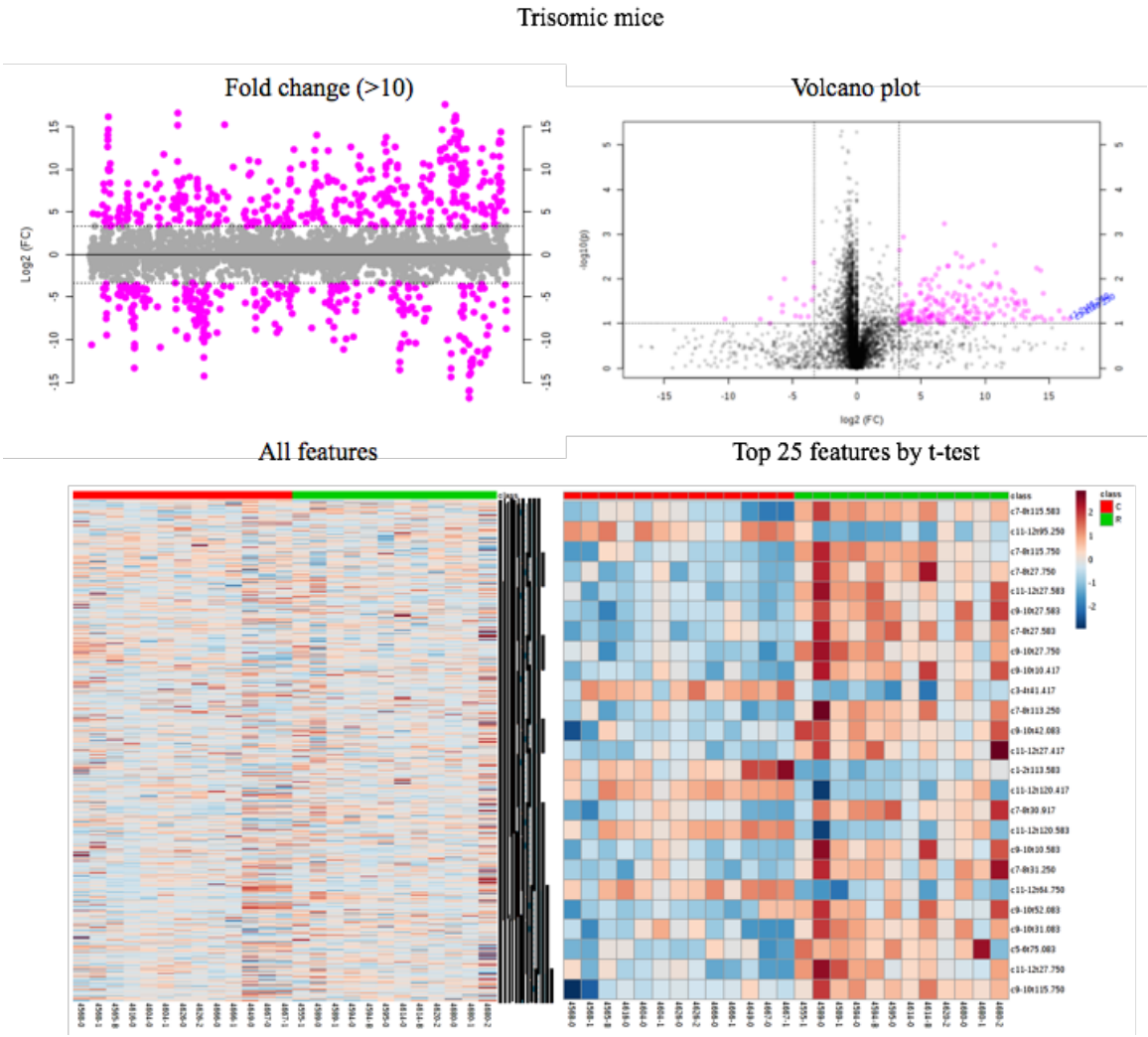

Trisomic mice

PCA pairwise

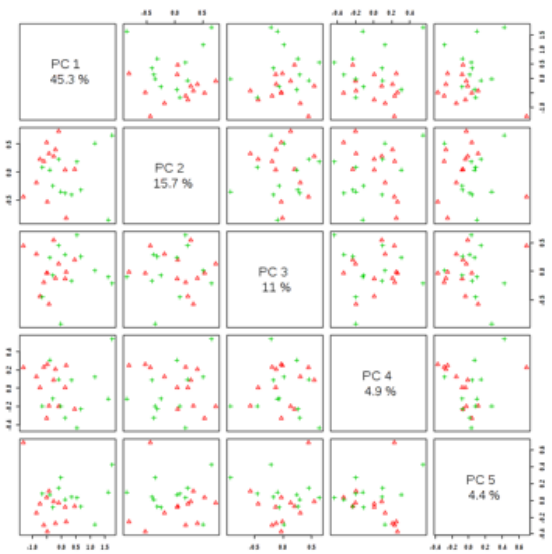

PCA scores

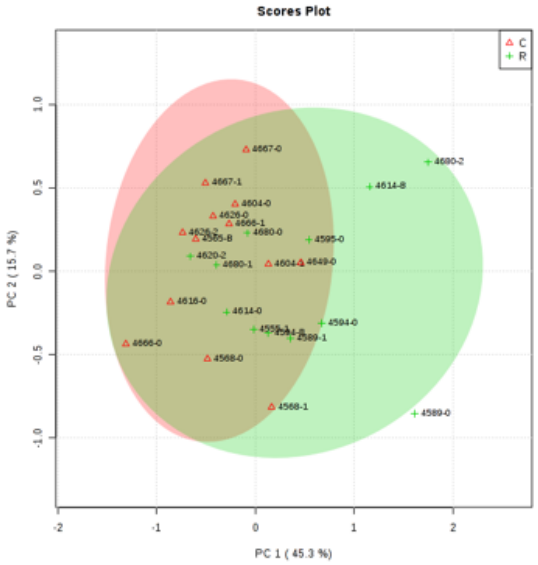

Trisomic mice

PLS-DA pairwise

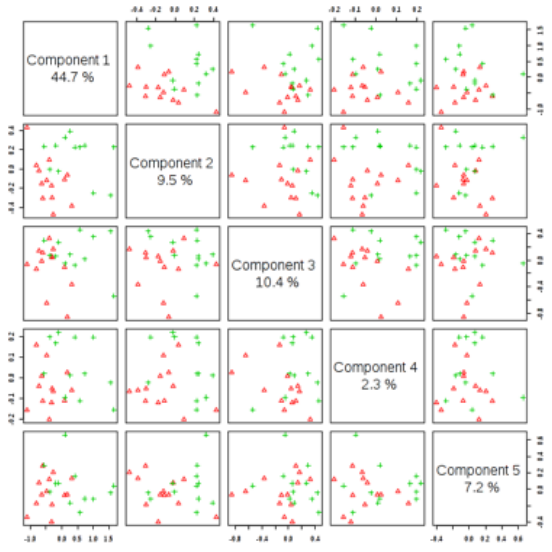

PLS-DA scores

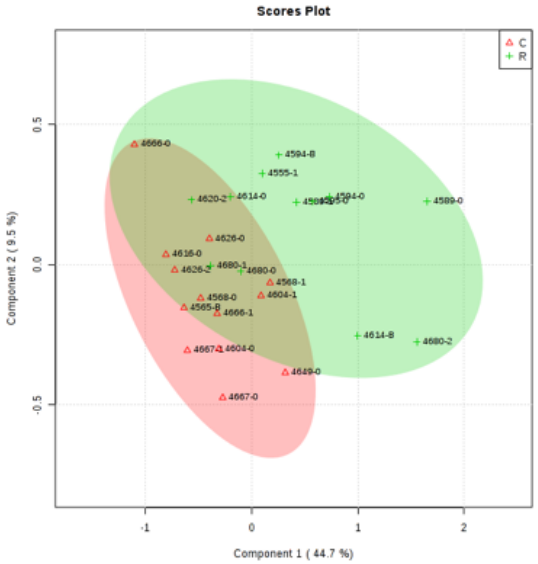

Section 2 – 18-month frontal brain pattern recognition analysis

The following are supplemental data plots for 18-month frontal brain samples.

Comparison of disomic and trisomic mice fed control diet.

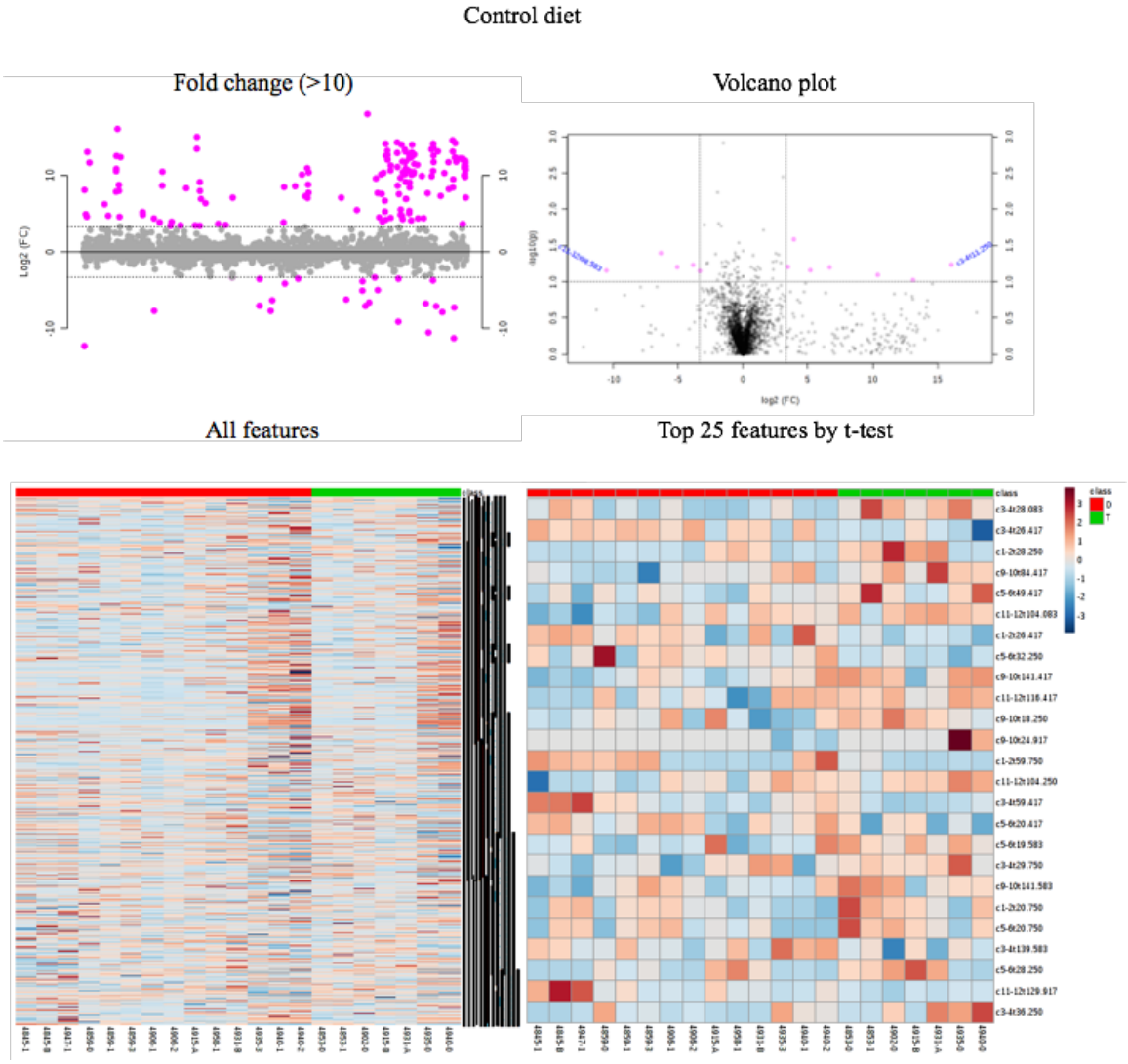

Control diet

PCA pairwise

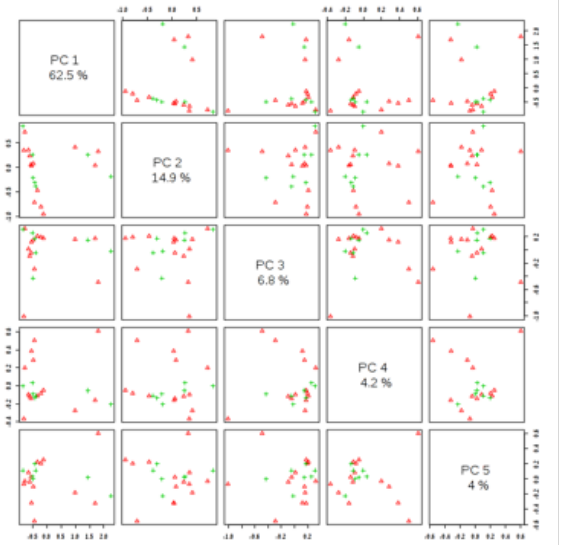

PCA scores

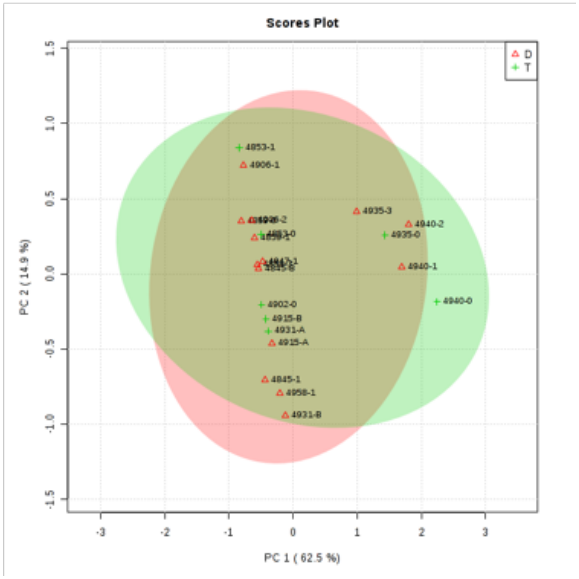

Control diet

PLS-DA pairwise

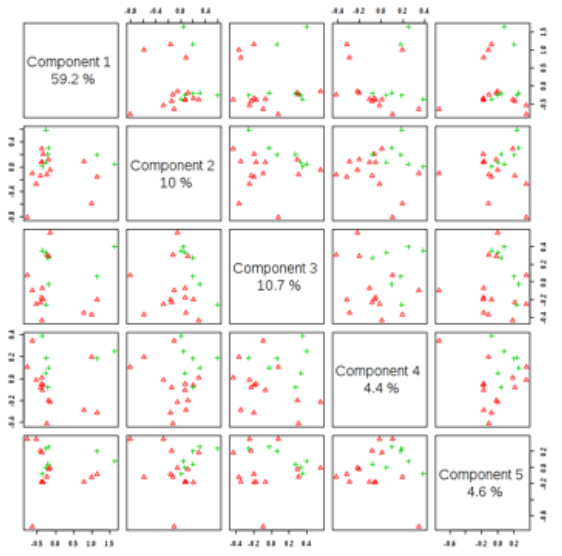

PLS-DA scores

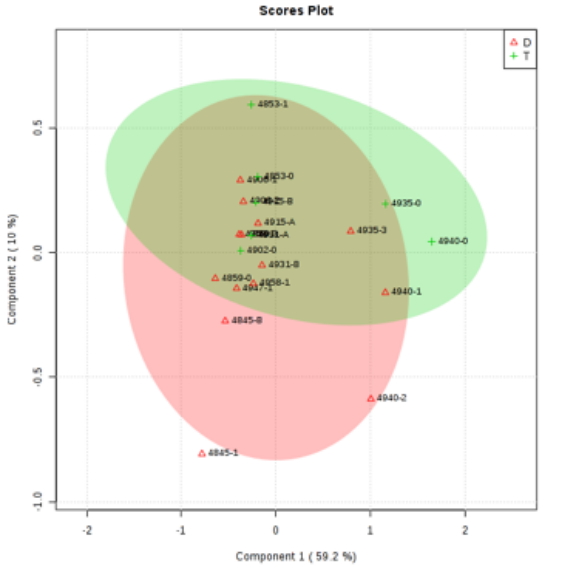

Comparison of disomic and trisomic mice fed microencapsulated rapamycin diet.

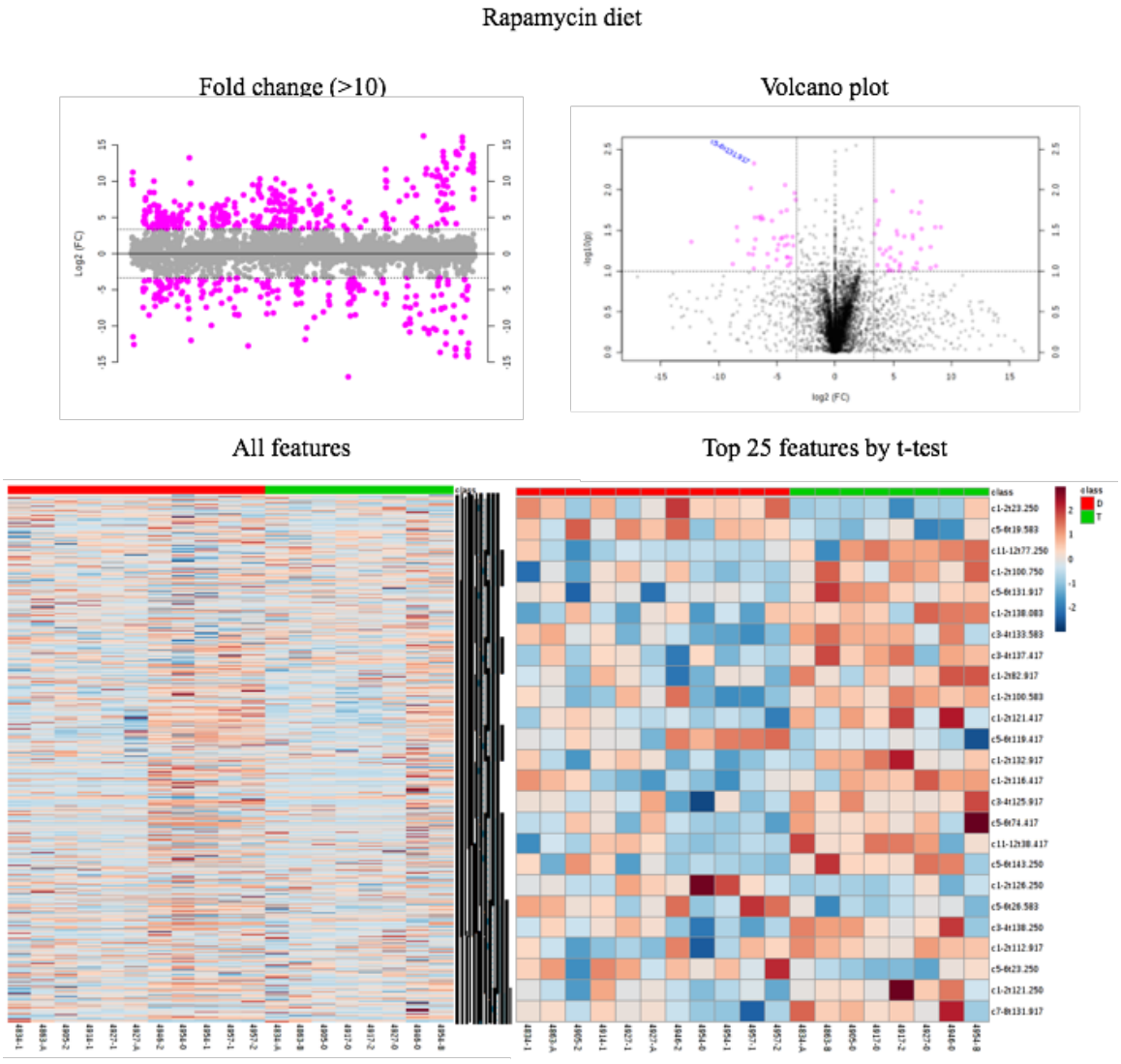

Rapamycin diet

PCA pairwise

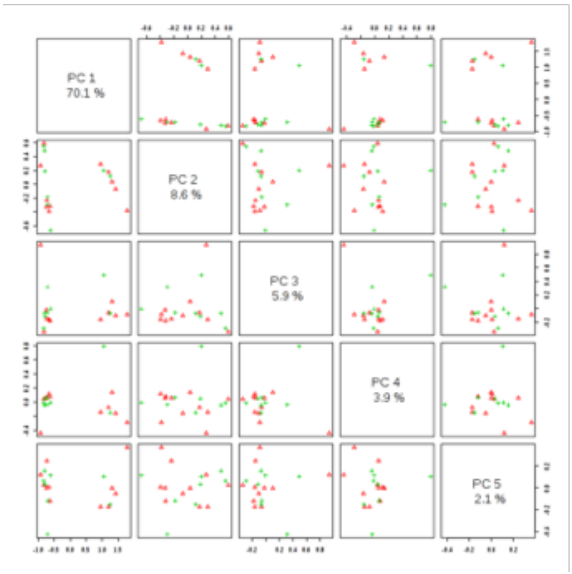

PCA scores

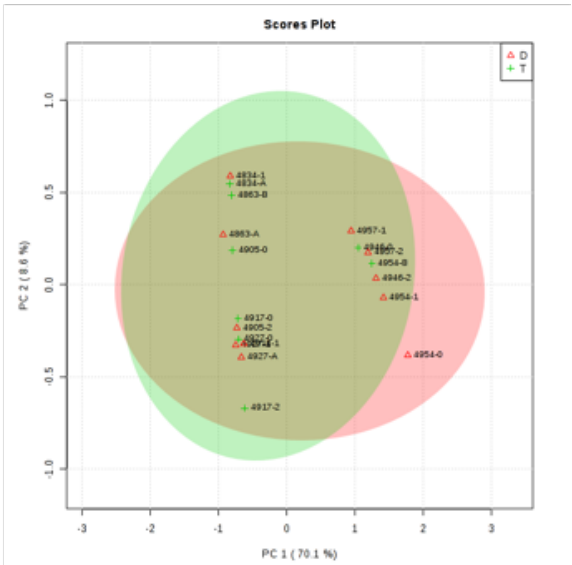

Rapamycin diet

PLS-DA pairwise

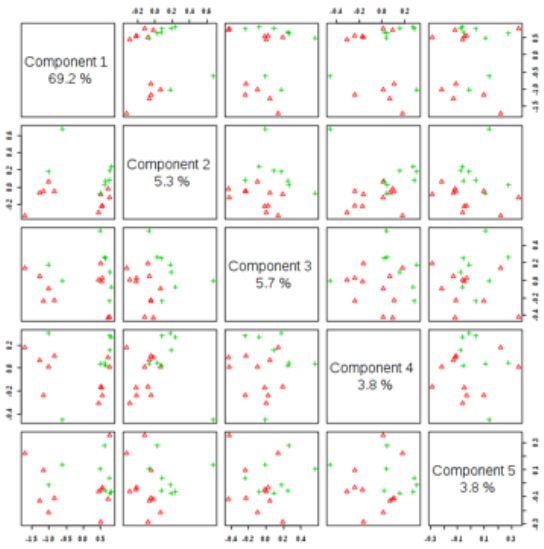

PLS-DA scores

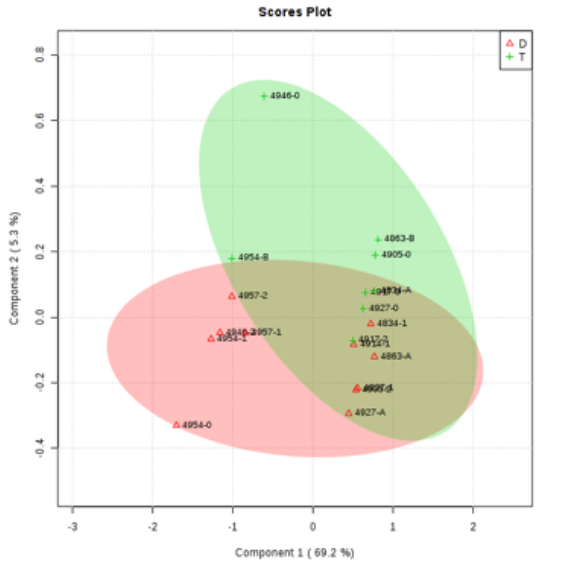

Comparison of control diet and microencapsulated rapamycin diet in disomic mice

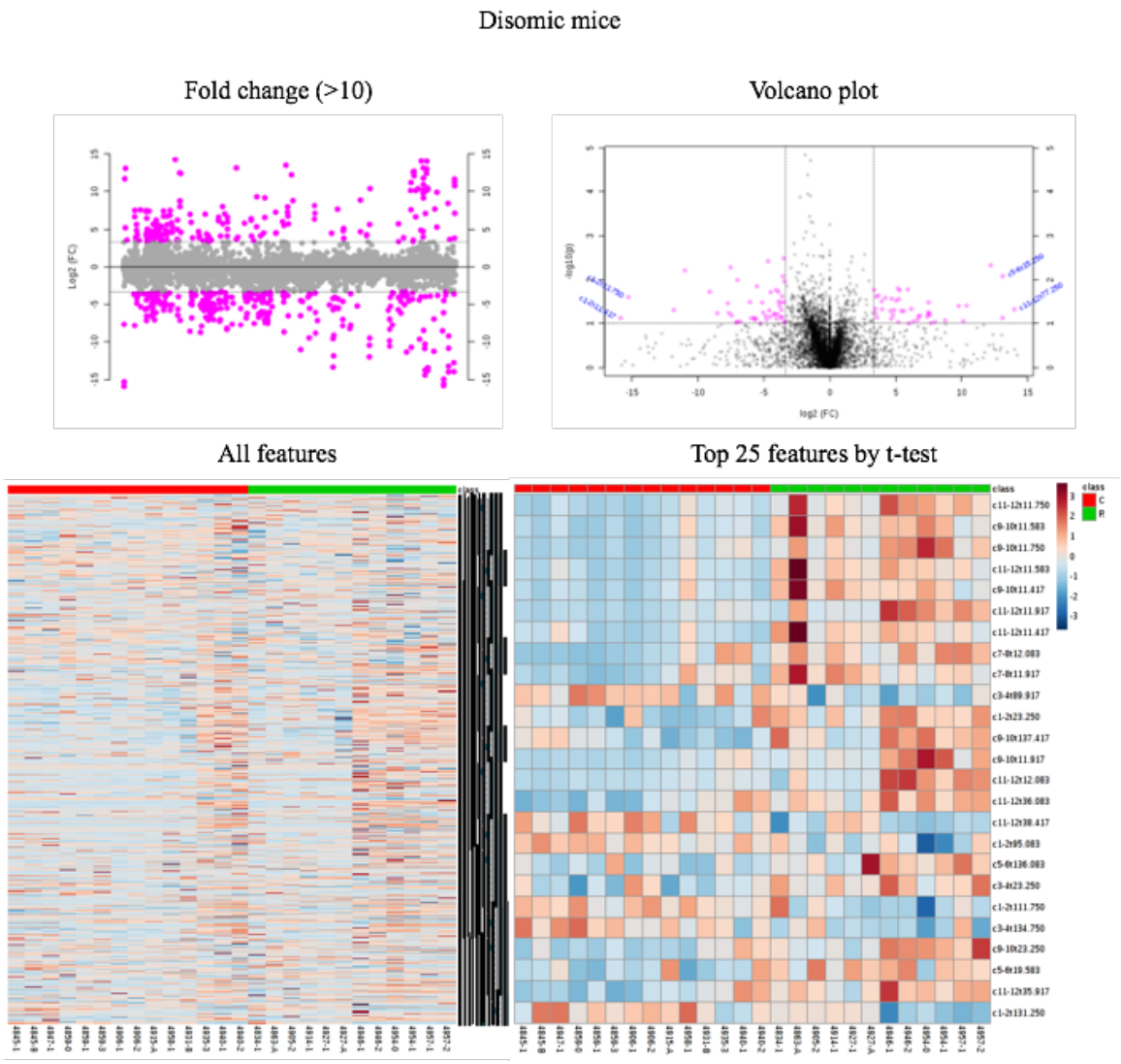

Disomic mice

PCA pairwise

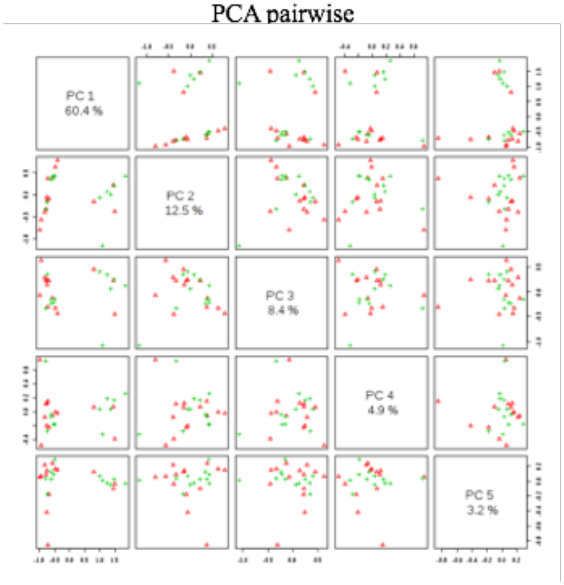

PCA scores

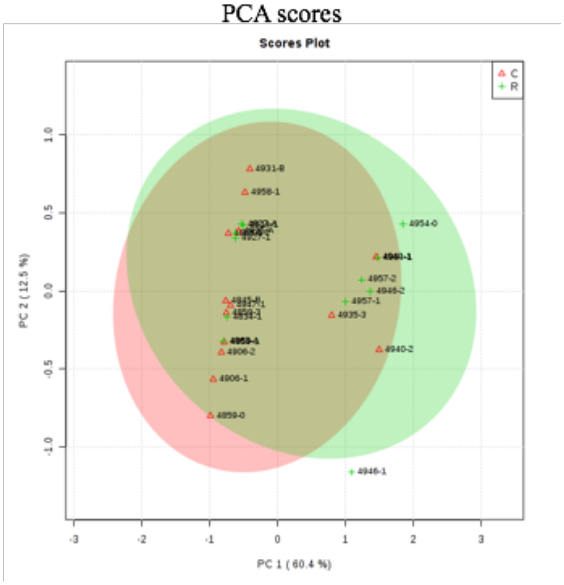

Disomic mice

PLS-DA pairwise

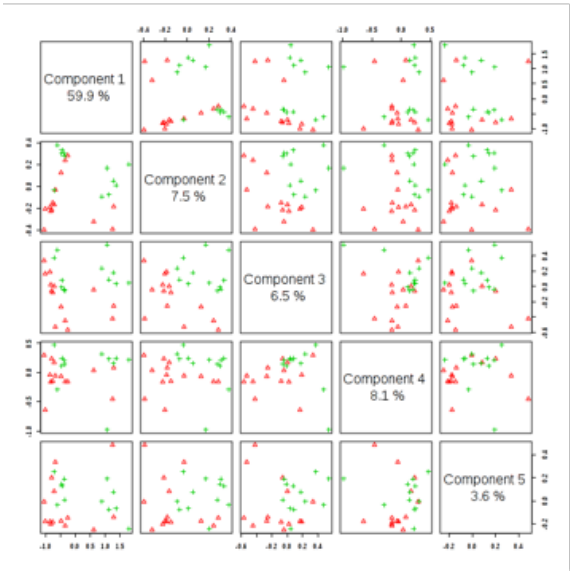

PLS-DA scores

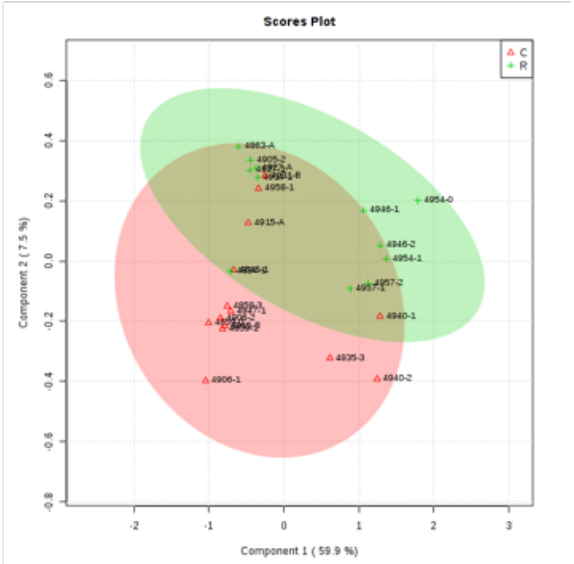

Comparison of control diet and microencapsulated rapamycin diet in trisomic mice

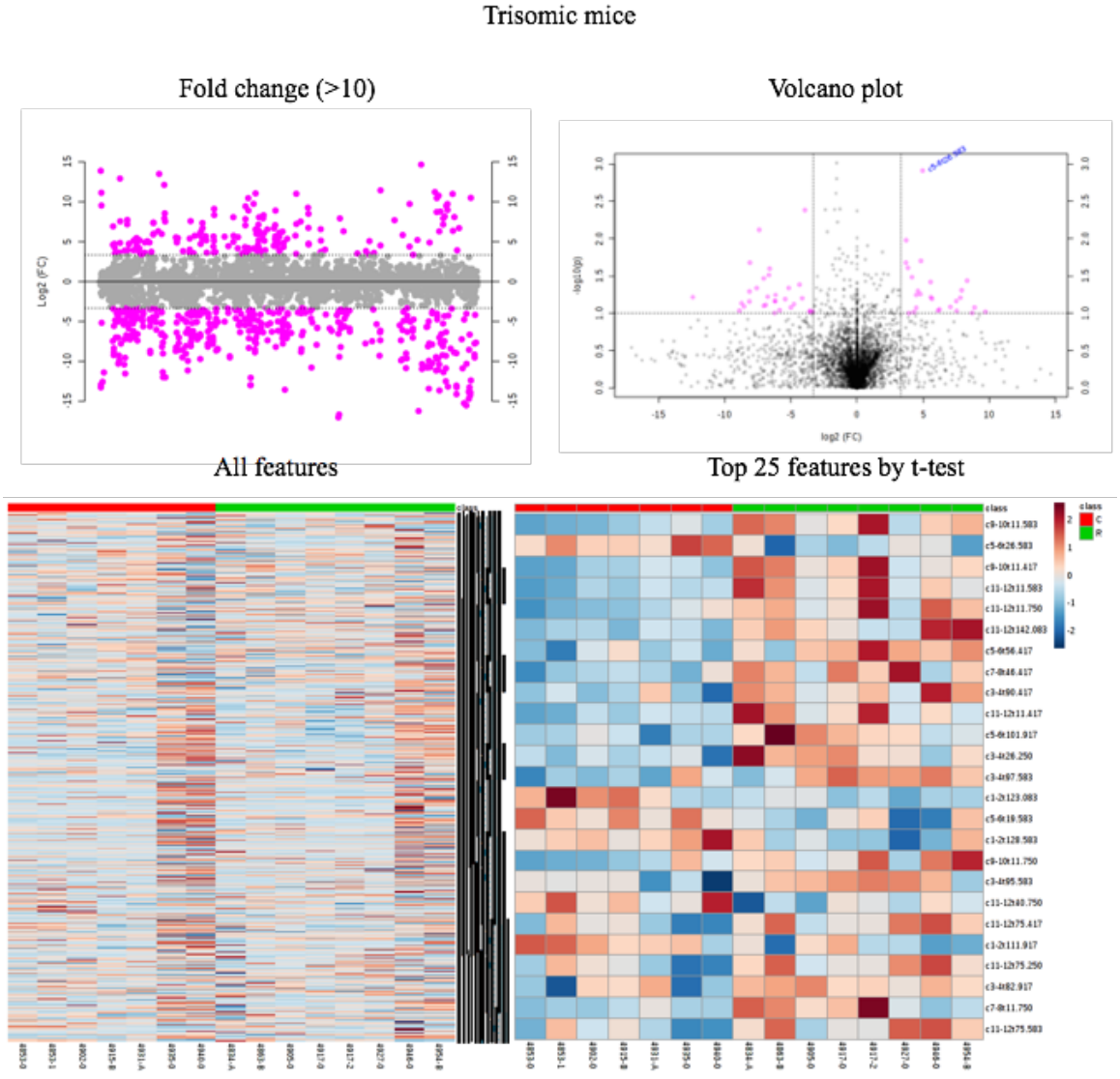

Trisomic mice

PCA pairwise

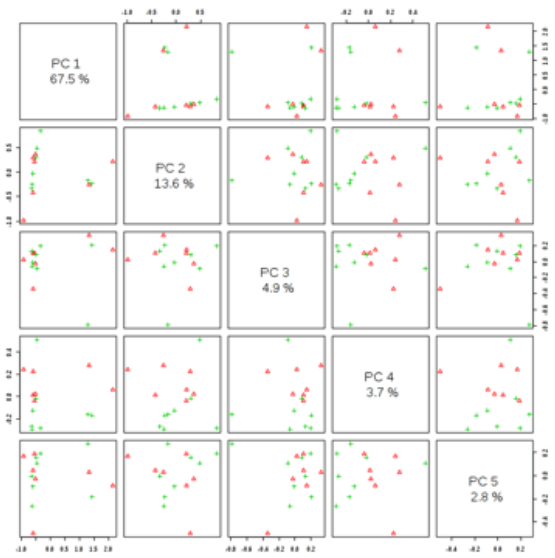

PCA scores

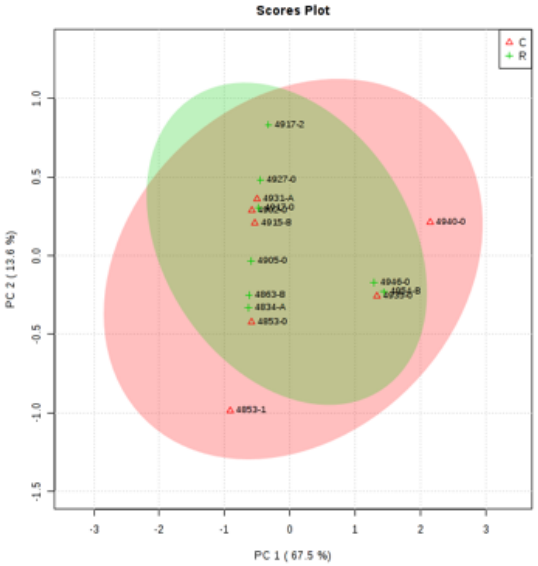

Trisomic mice

PLS-DA pairwise

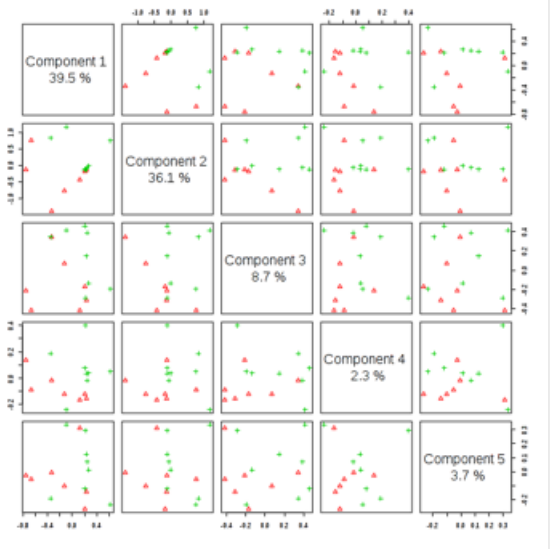

PLS-DA scores

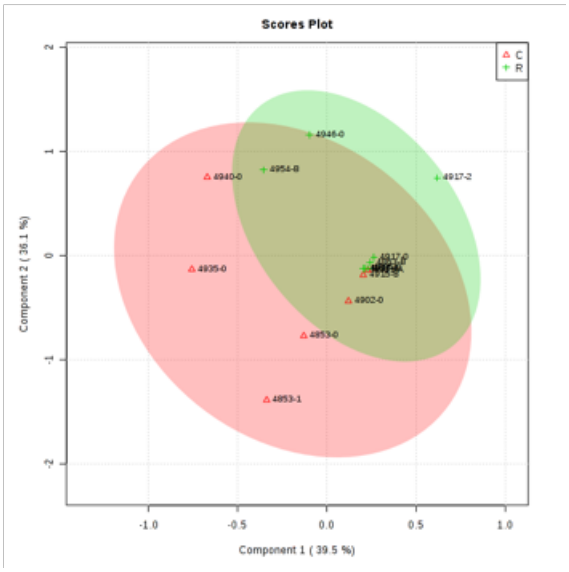

Section 3 – 6-month cerebellum pattern recognition analysis

The following are supplemental data plots for 6-month cerebellum brain samples.

Comparison of disomic and trisomic mice fed control diet.

Control diet

Fold change (>10)

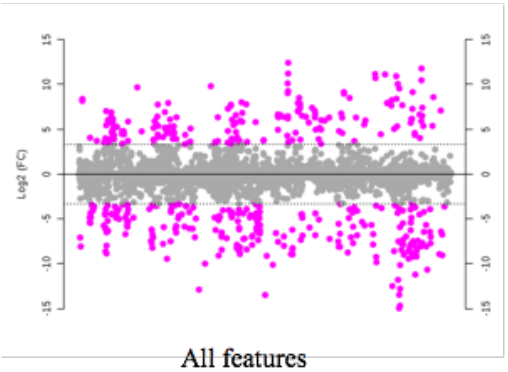

Volcano plot

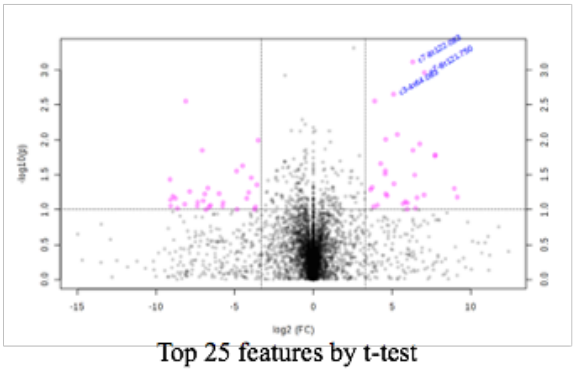

All features

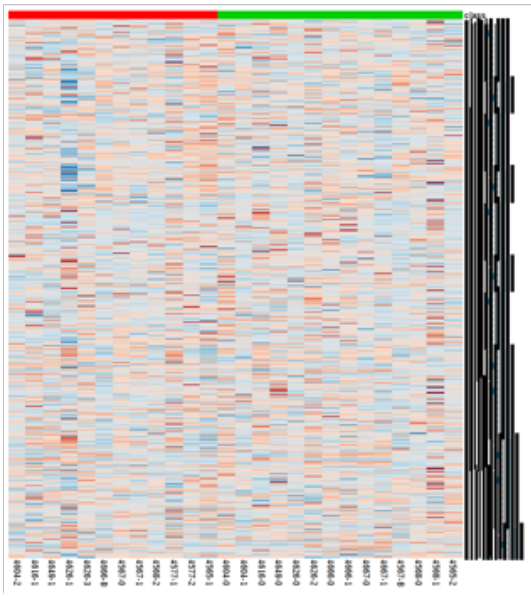

Top 25 features by t-test

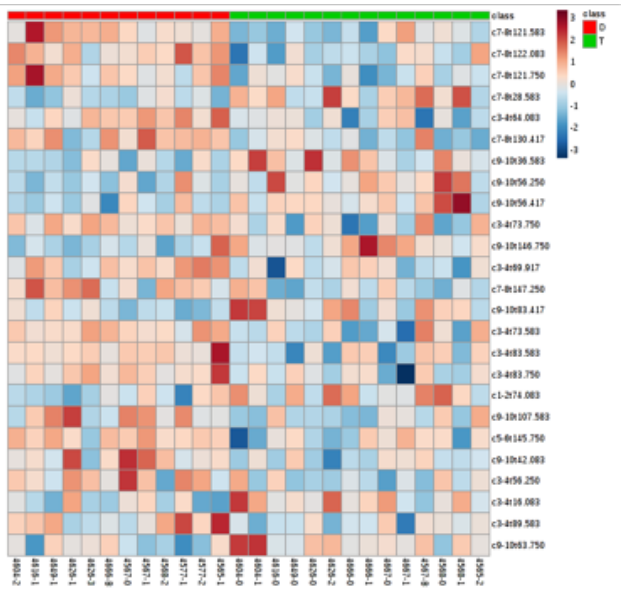

Control diet

PCA pairwise

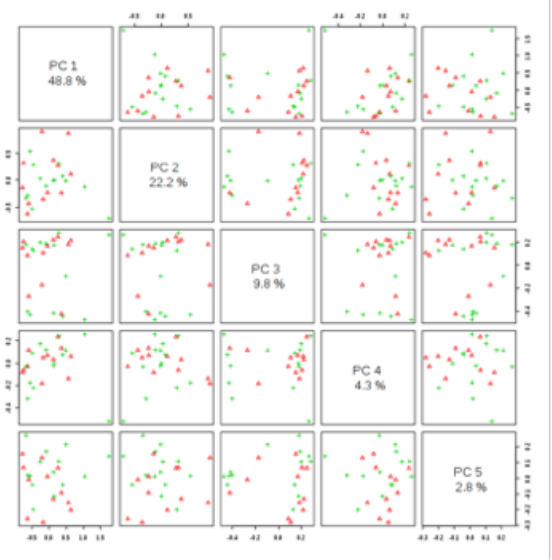

PCA scores

Control diet

PLS-DA pairwise

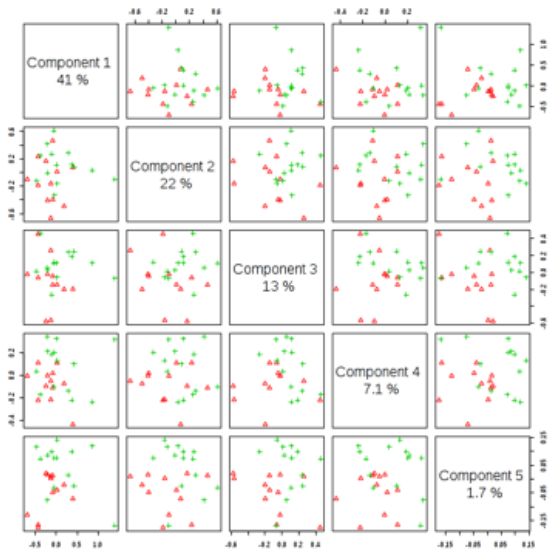

PLS-DA scores

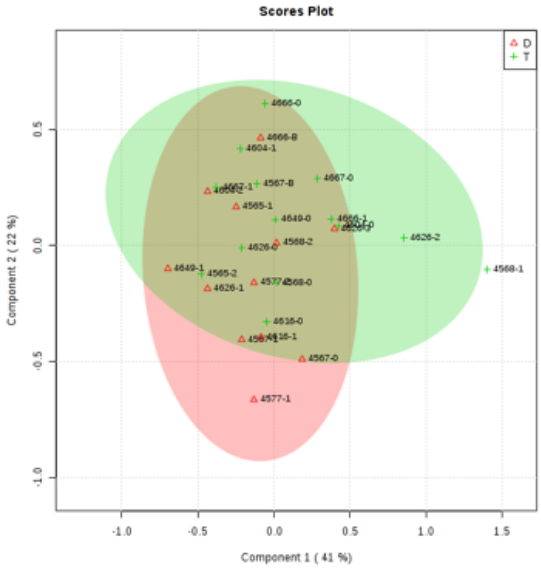

Comparison of disomic and trisomic mice fed microencapsulated rapamycin diet.

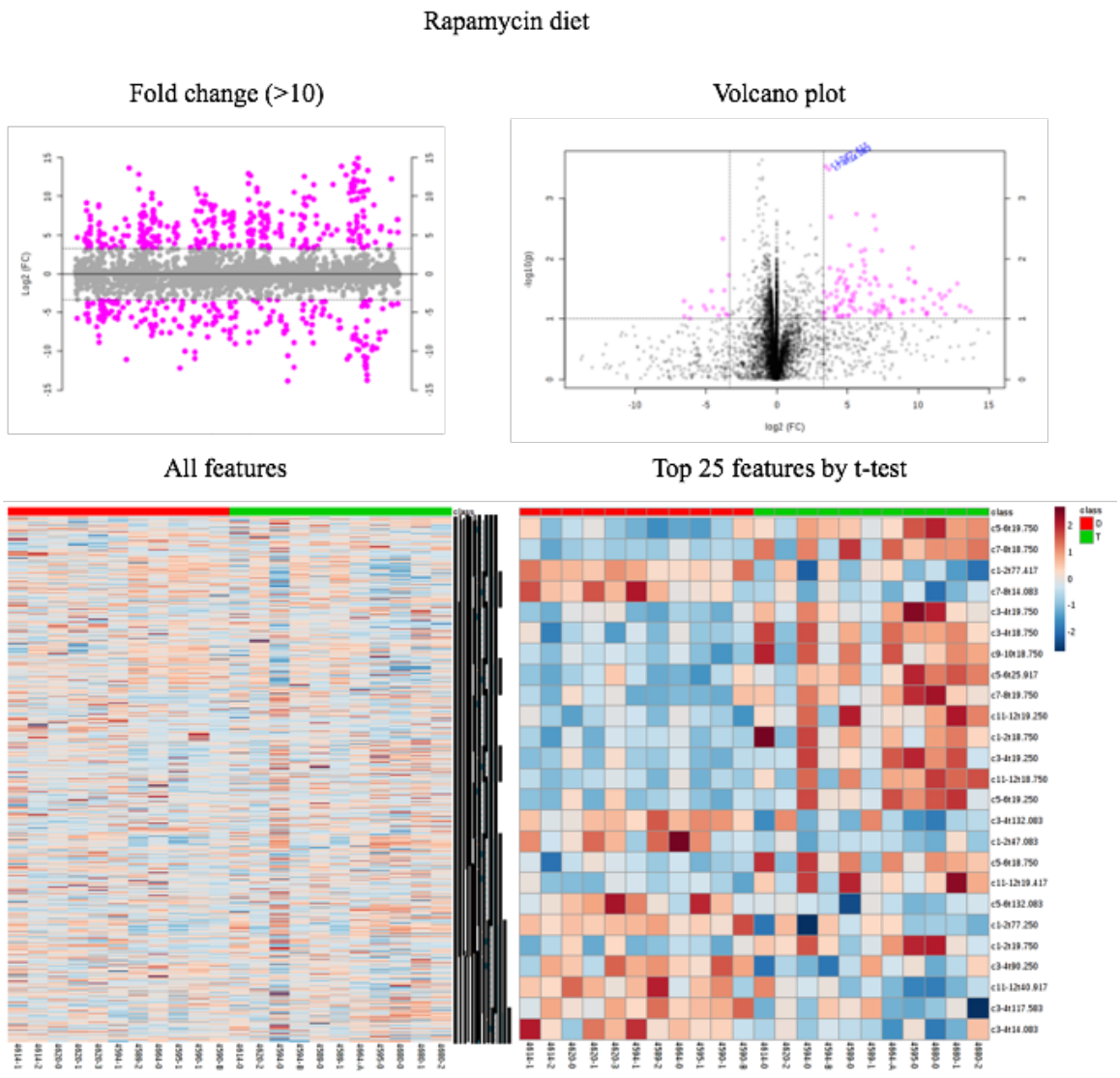

Rapamycin diet

PCA pairwise

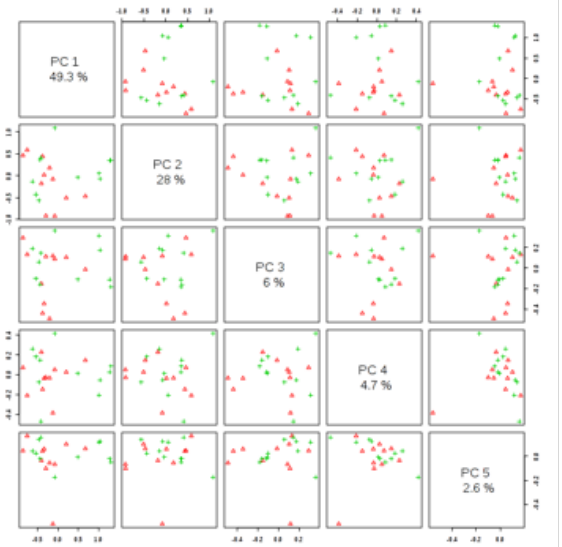

PCA scores

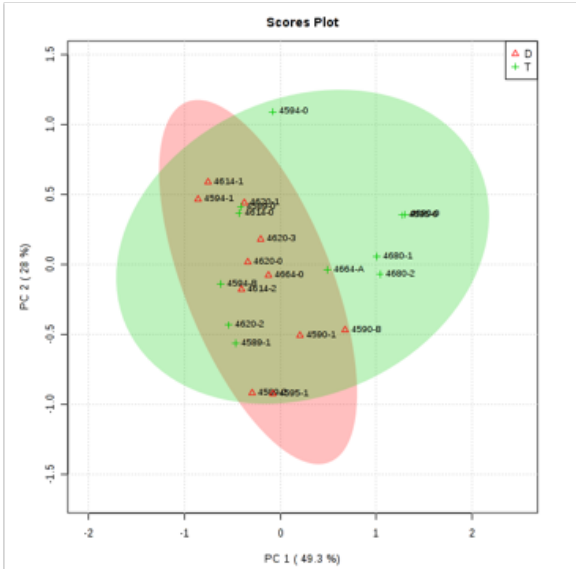

Rapamycin diet

PLS-DA pairwise

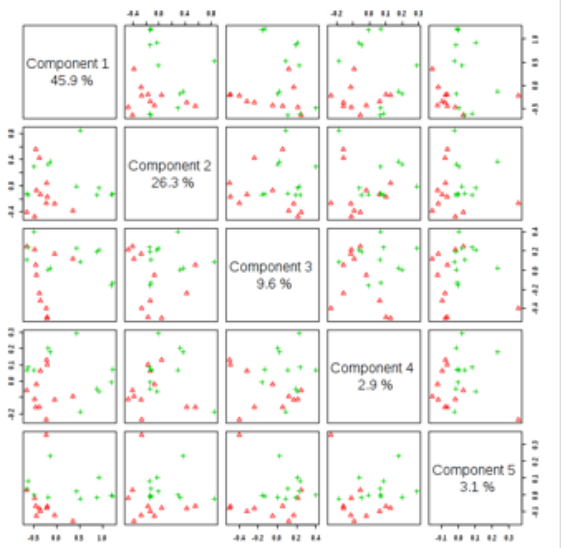

PLS-DA scores

Comparison of control diet and microencapsulated rapamycin diet in disomic mice

Disomic mice

Fold change (>10)

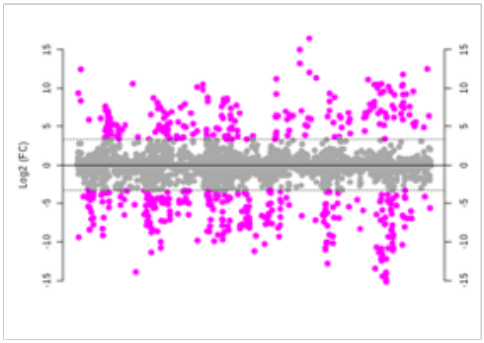

Volcano plot

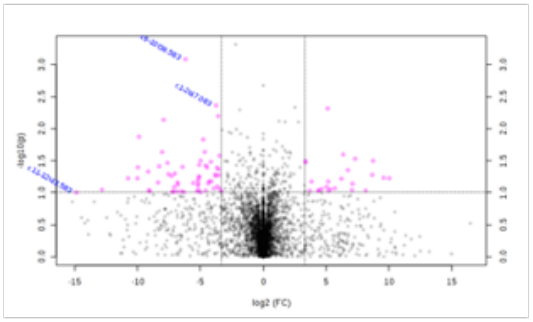

All features

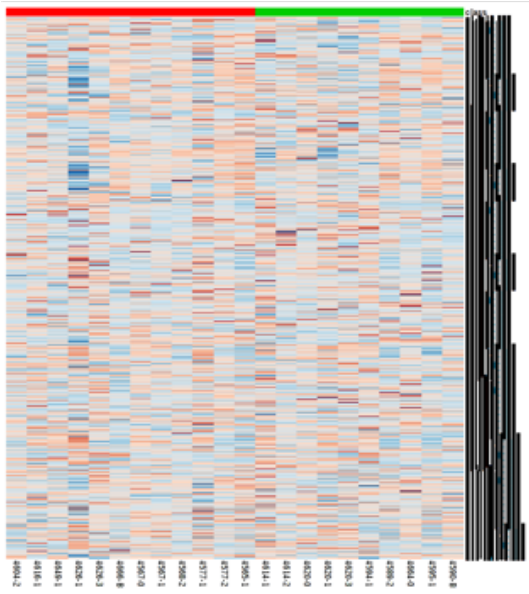

Top 25 features by t-test

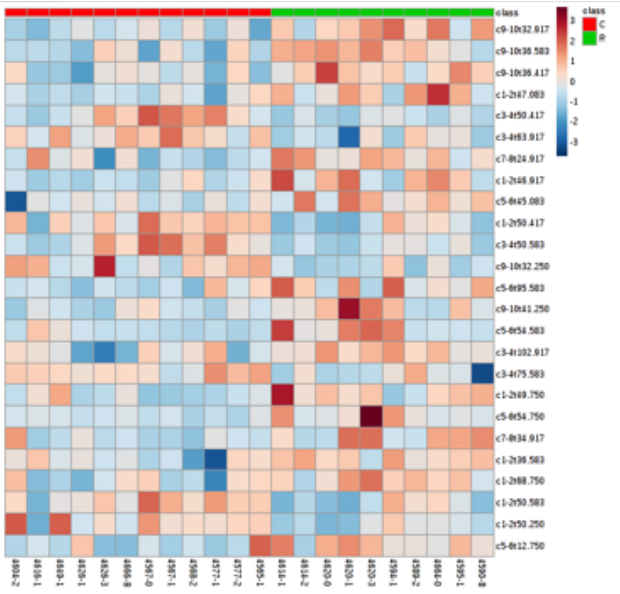

Disomic mice

PCA pairwise

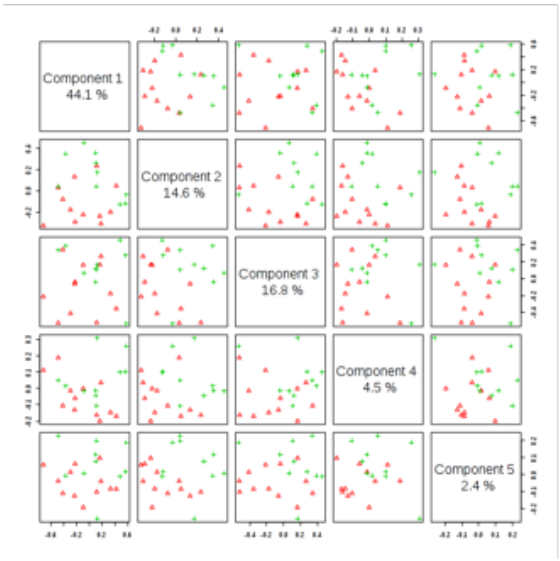

PCA scores

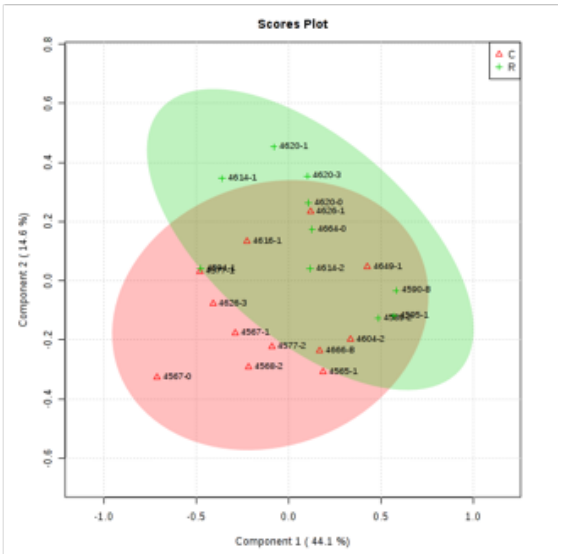

Trisomic mice

PLS-DA pairwise

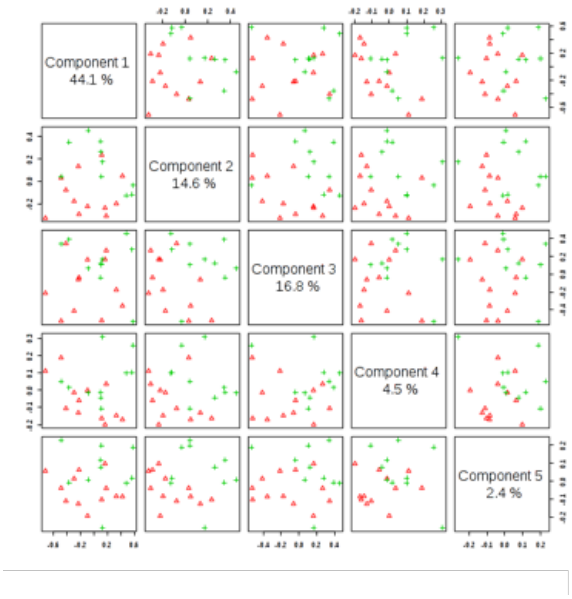

PLS-DA scores

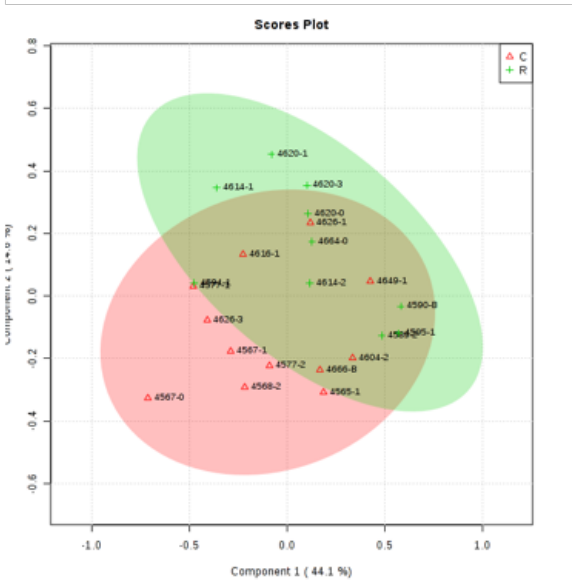

Comparison of control diet and microencapsulated rapamycin diet in trisomic mice

Trisomic mice

Fold change (>10)

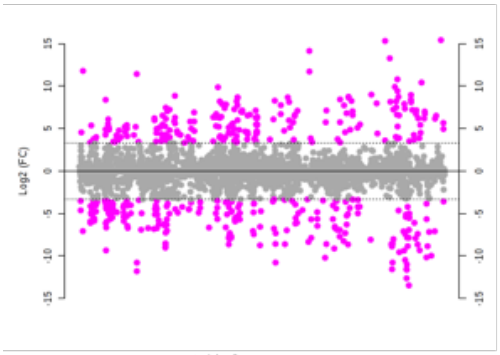

Volcano plot

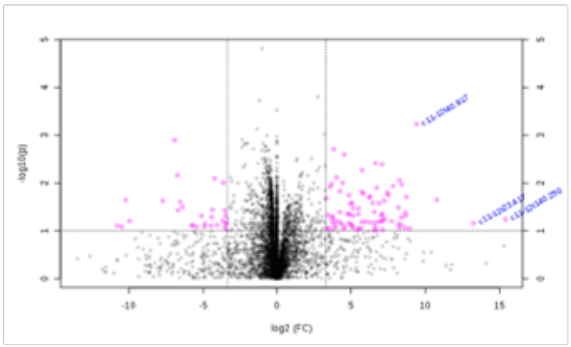

All features

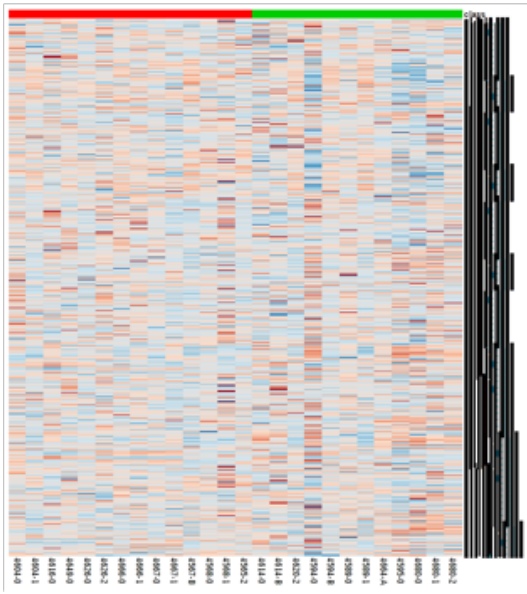

Top 25 features by t-test

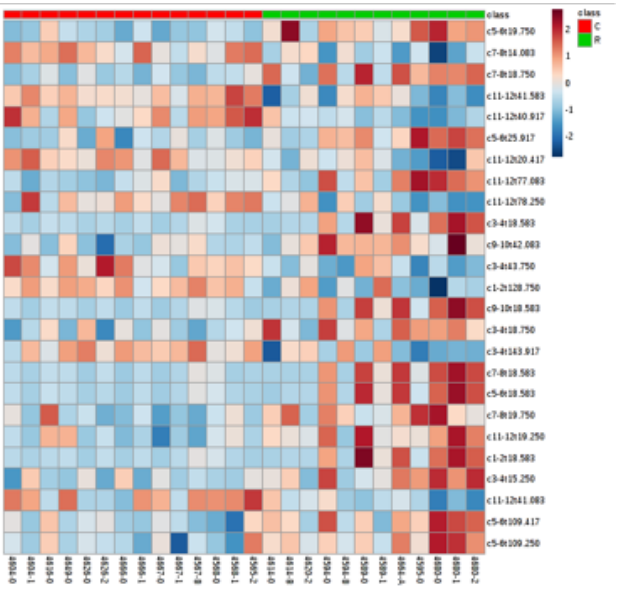

Trisomic mice

PCA pairwise

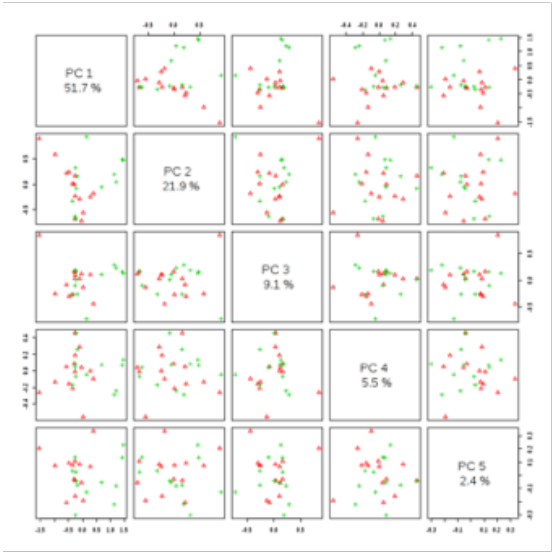

PCA scores

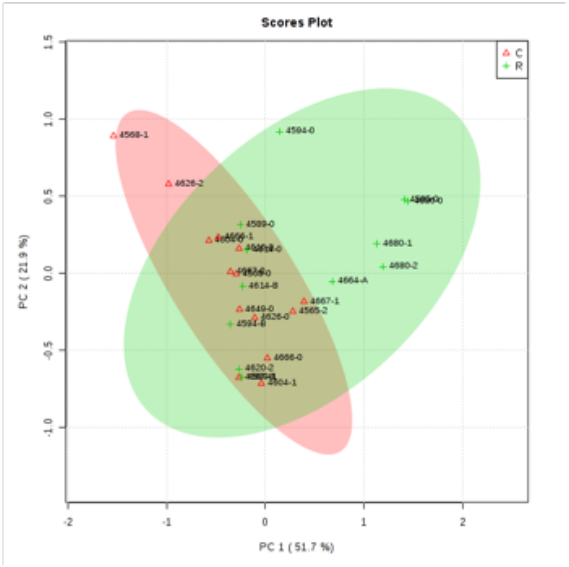

Trisomic mice

PLS-DA pairwise

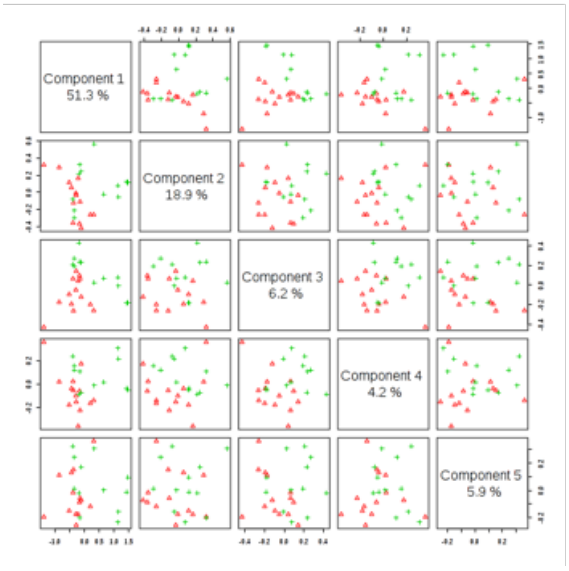

PLS-DA scores

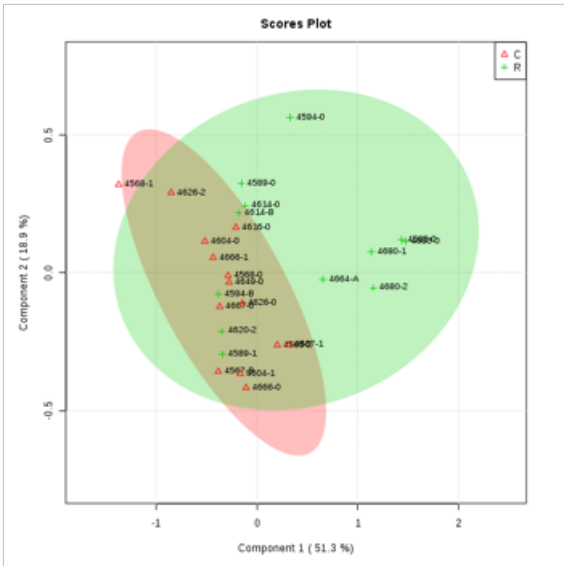

Section 4 – 18-month cerebellum pattern recognition analysis

The following are supplemental data plots for 18-month cerebellum brain samples.

Comparison of disomic and trisomic mice fed control diet.

Control diet

Fold change (>10)

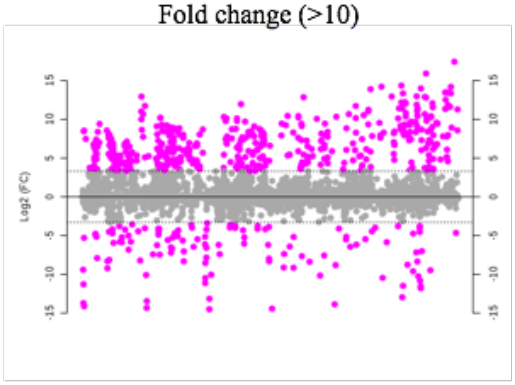

Volcano plot

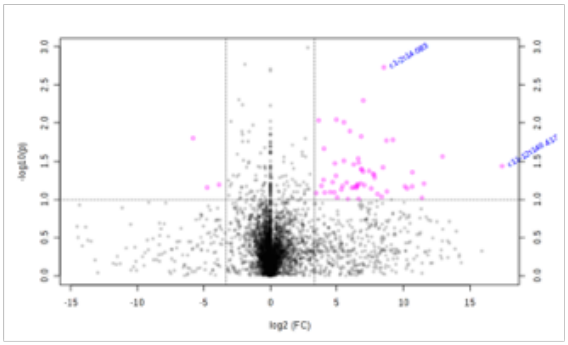

All features

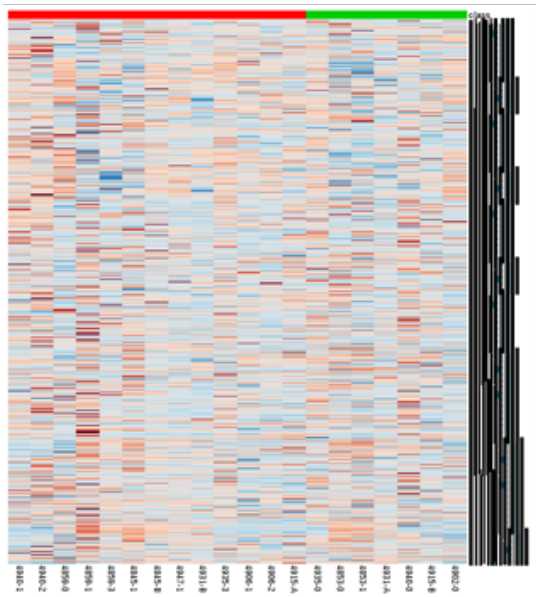

Top 25 features by t-test

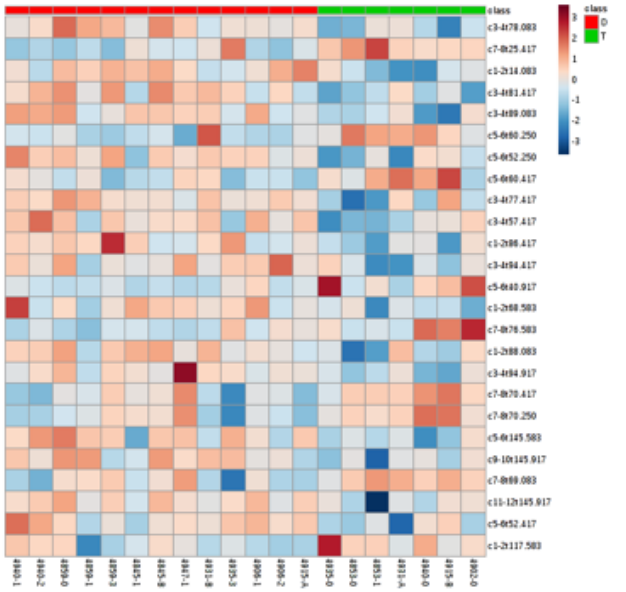

Control diet

PCA pairwise

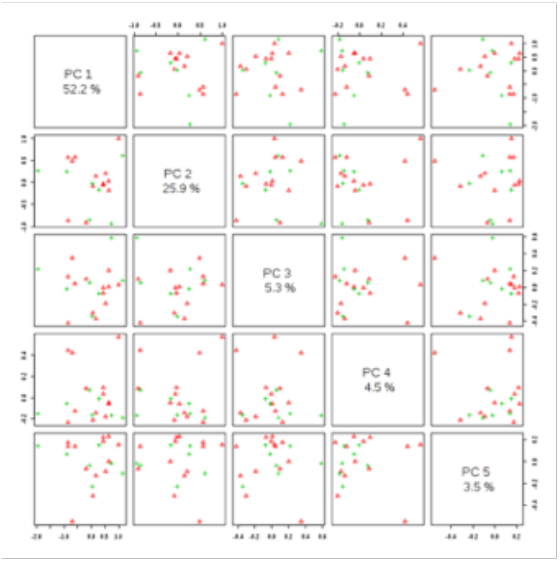

PCA scores

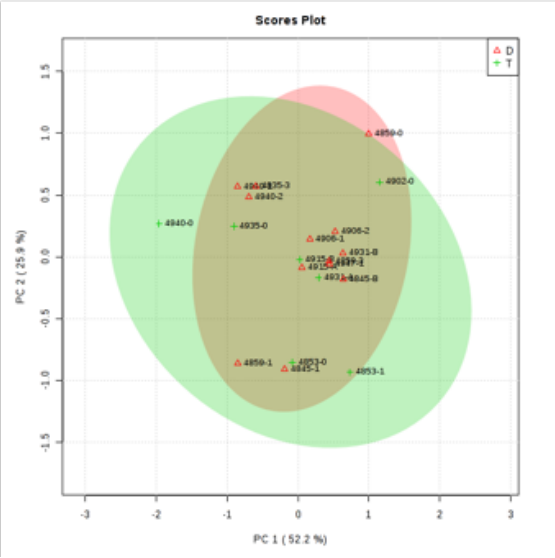

Control diet

PLS-DA pairwise

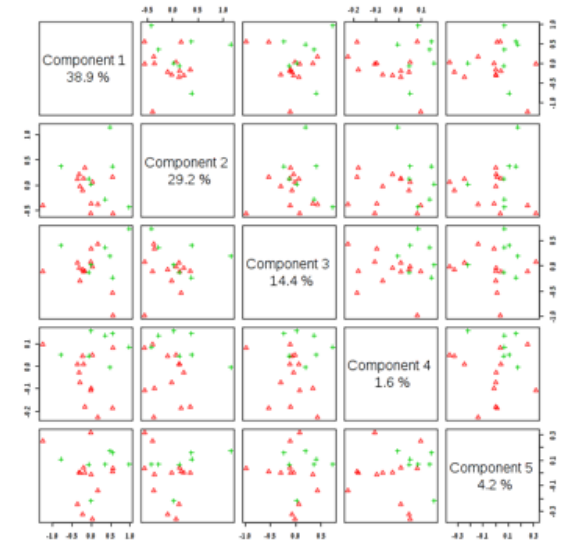

PLS-DA scores

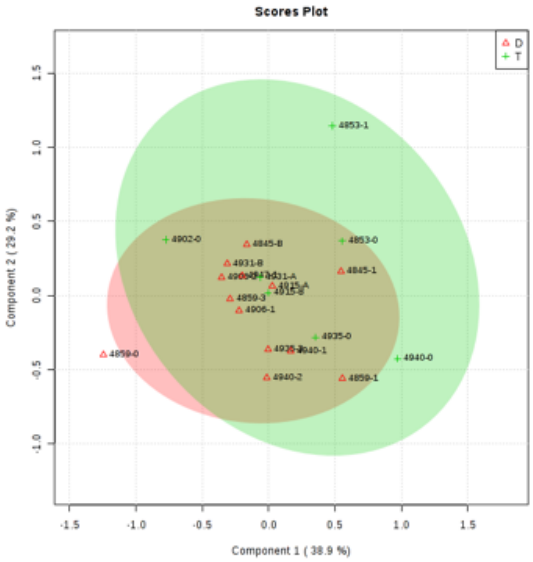

Comparison of disomic and trisomic mice fed microencapsulated rapamycin diet.

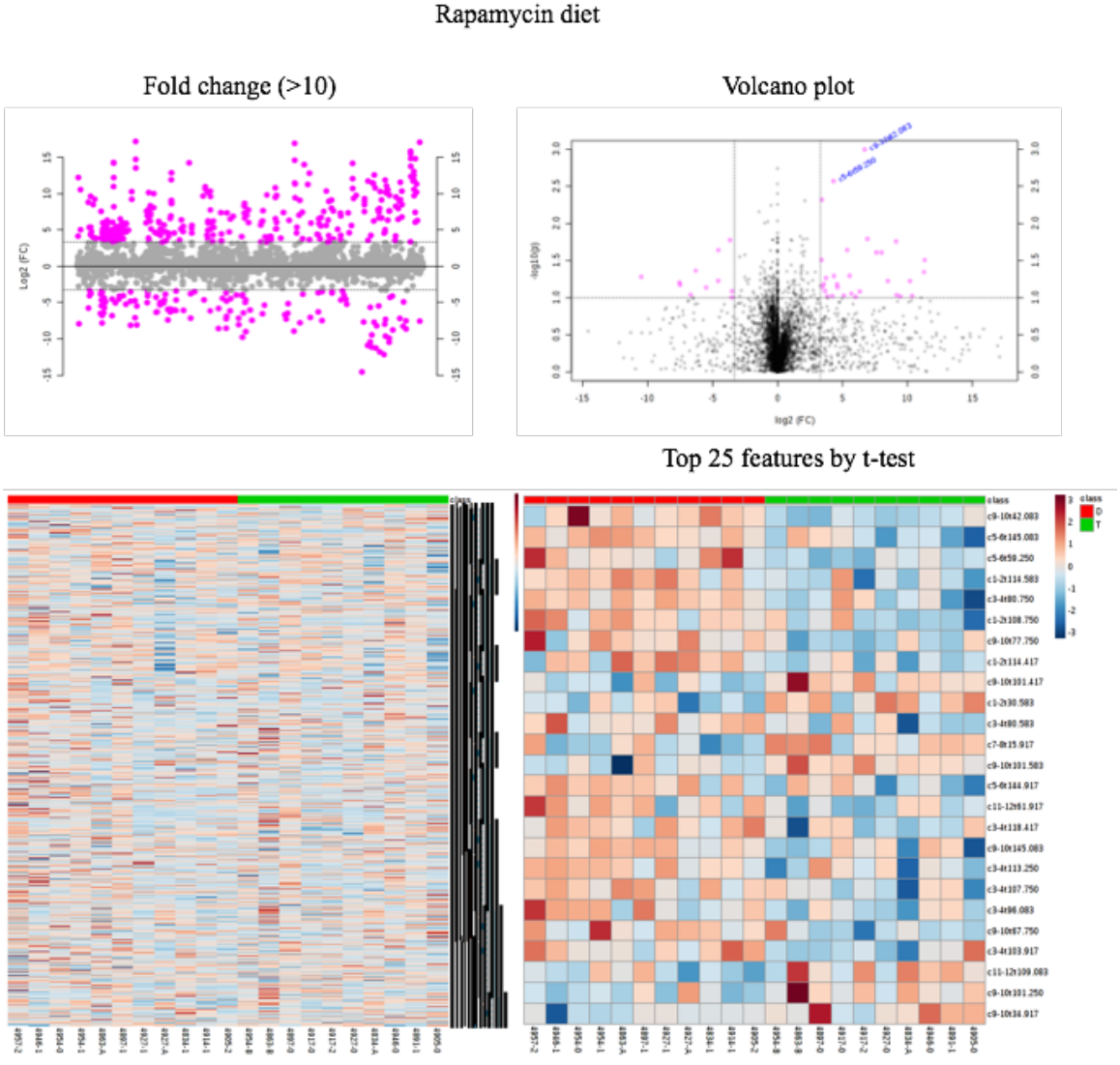

Rapamycin diet

PCA pairwise

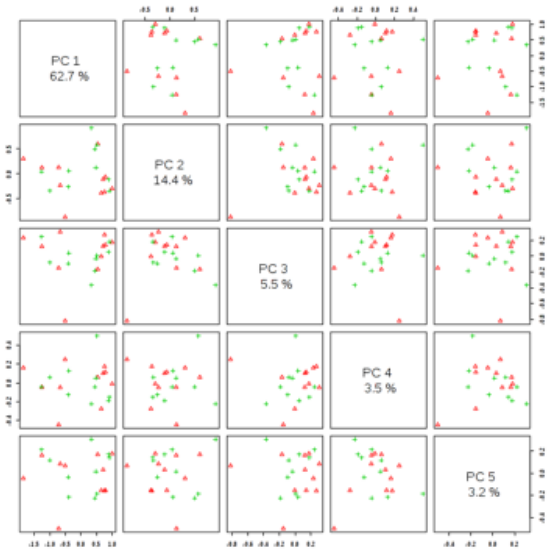

PCA scores

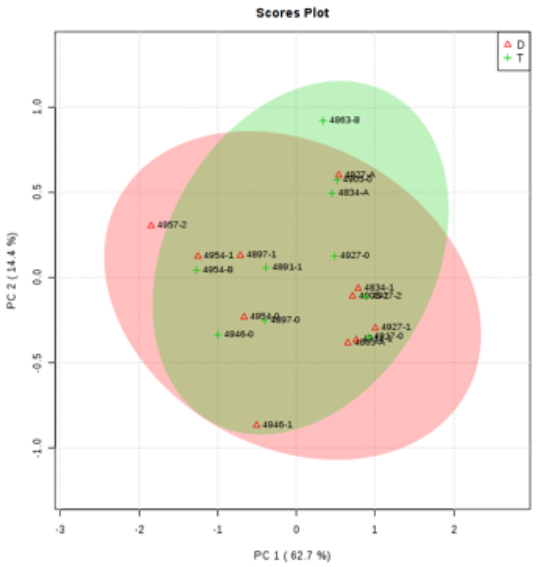

Rapamycin diet

PLS-DA pairwise

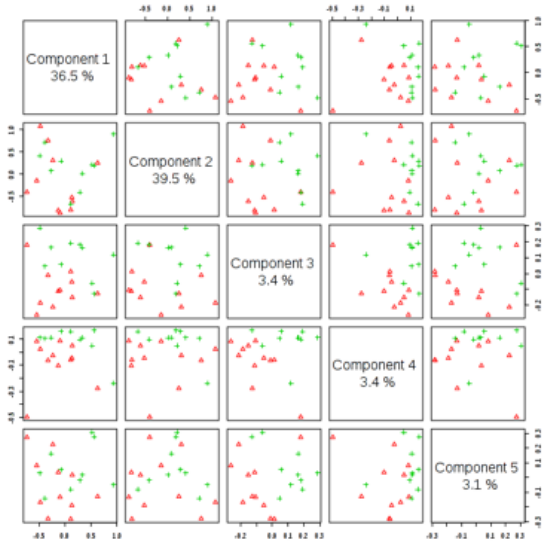

PLS-DA scores

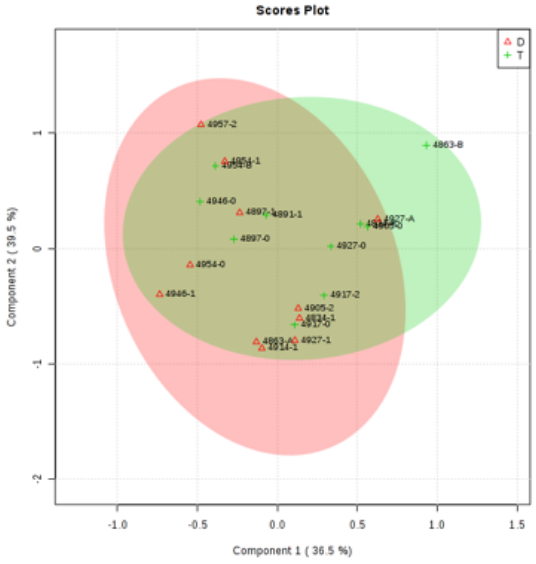

Comparison of control diet and microencapsulated rapamycin diet in disomic mice

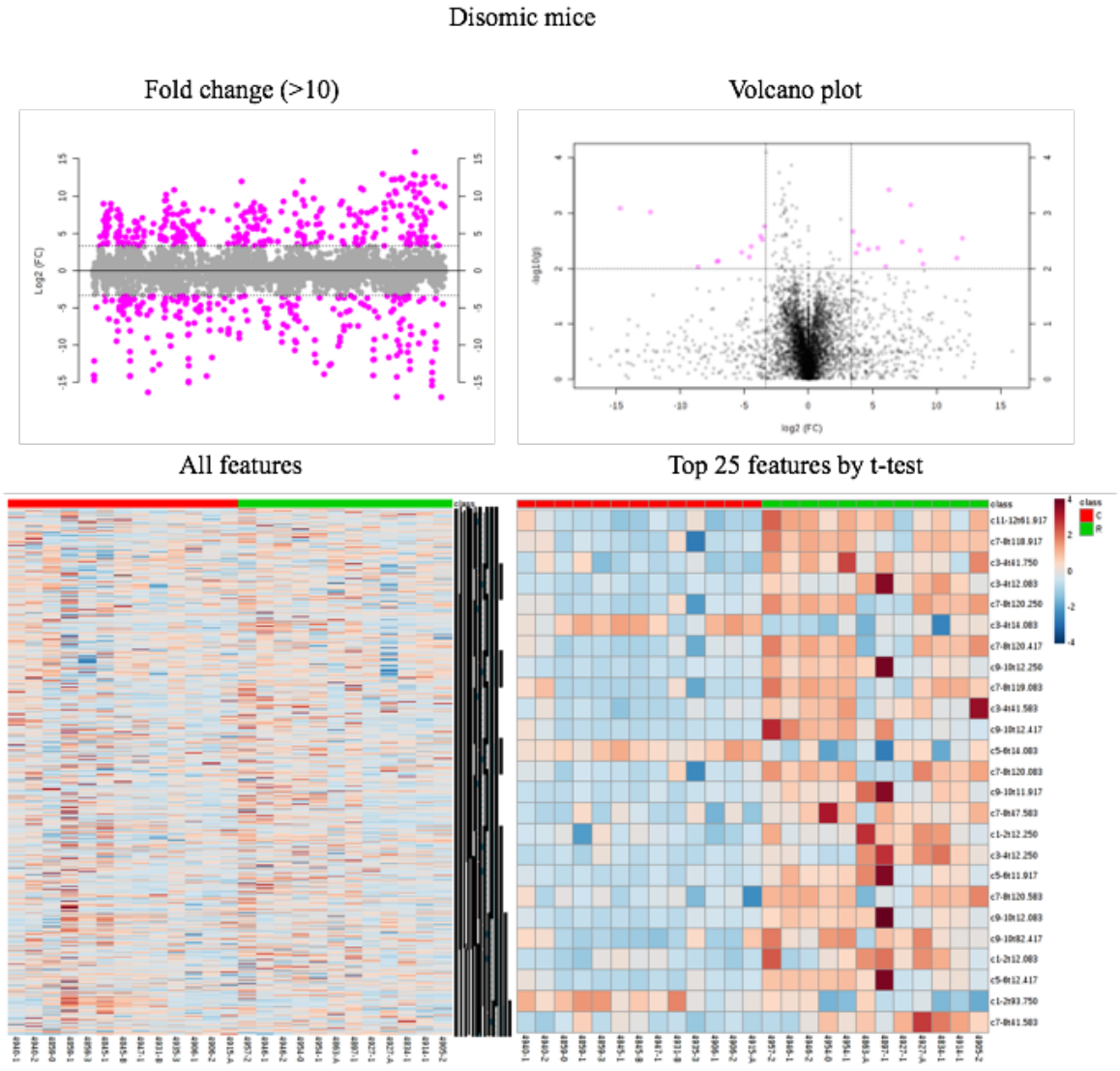

Disomic mice

PCA scores

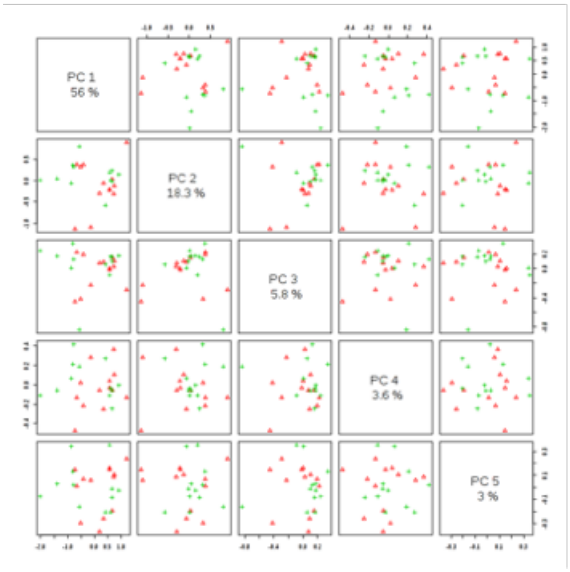

Disomic mice

PLS-DA pairwise

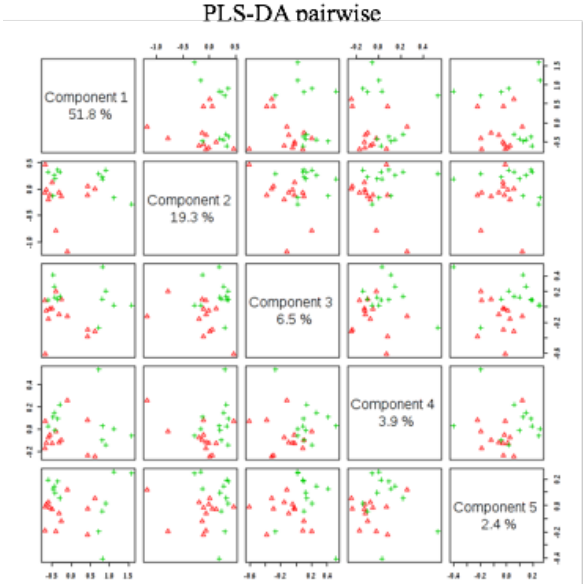

PLS-DA scores

Comparison of control diet and microencapsulated rapamycin diet in trisomic mice

Trisomic mice

Fold change (>10)

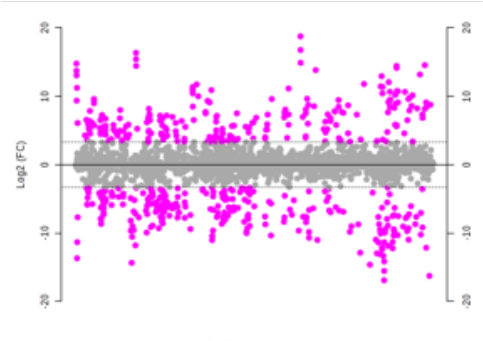

Volcano plot

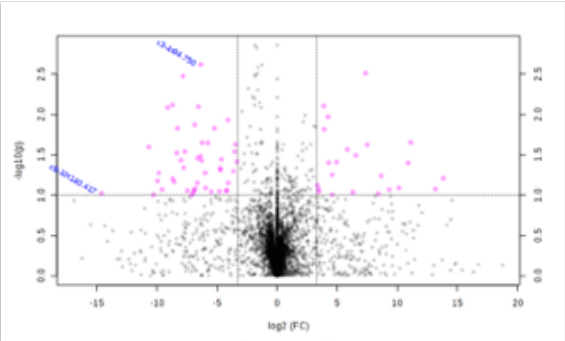

All features

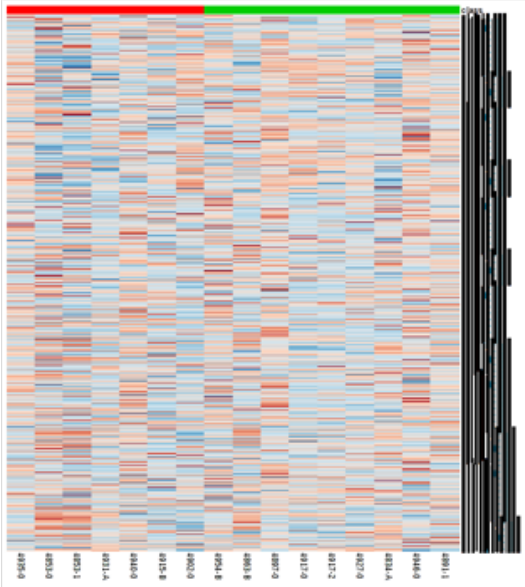

Top 25 features by t-test

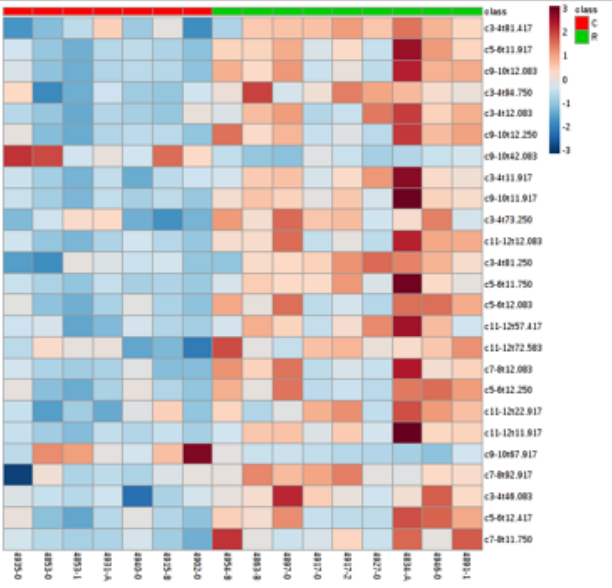

Trisomic mice

PCA pairwise

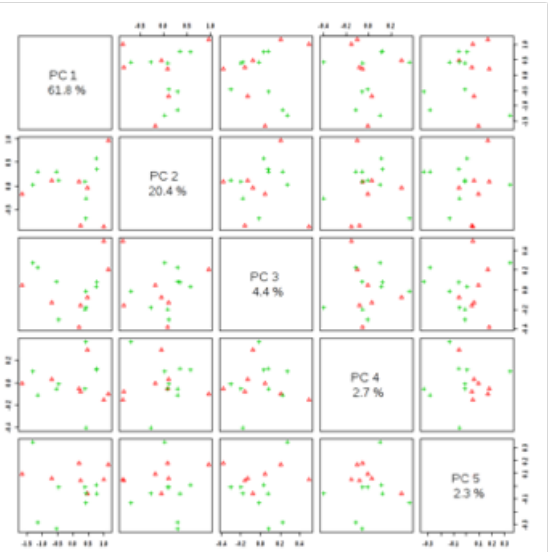

PCA scores

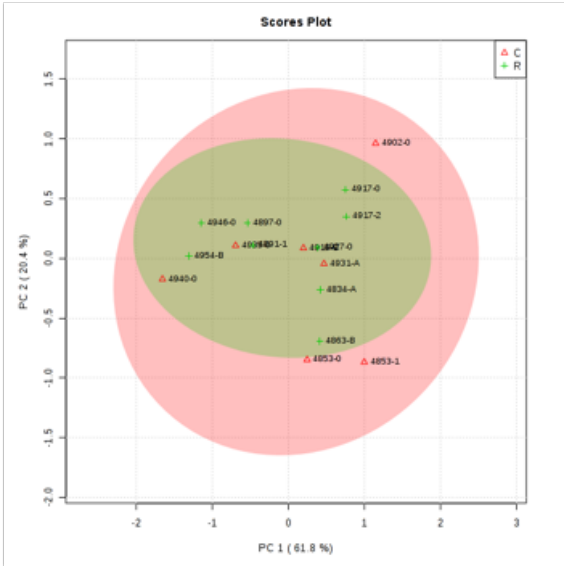

Trisomic mice

PLS-DA pairwise

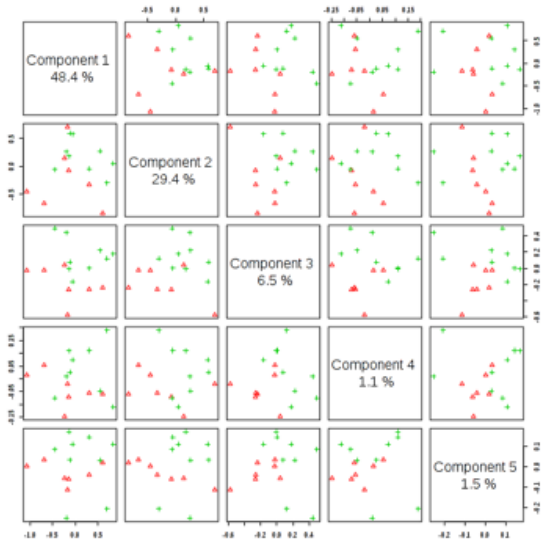

PLS-DA scores

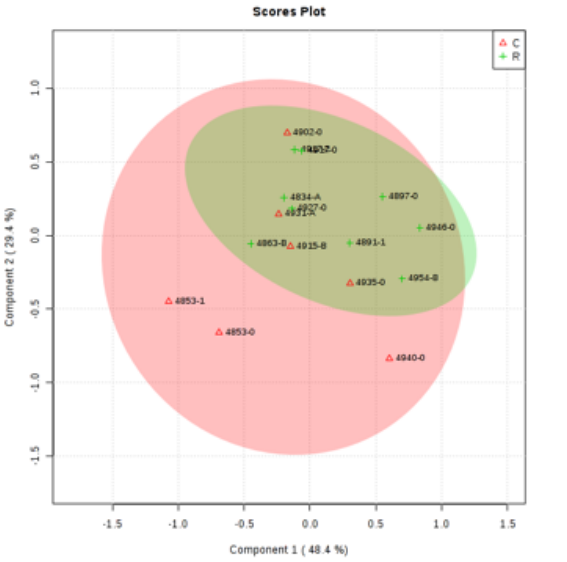

Section 5 – 6-month frontal brain targeted metabolomics analysis

The following are supplemental data plots for 6-month frontal brain samples

Comparison of disomic and trisomic mice fed control diet.

Control diet

Fold change (>10)

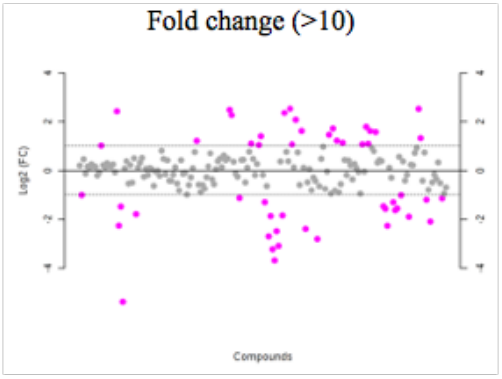

t-test

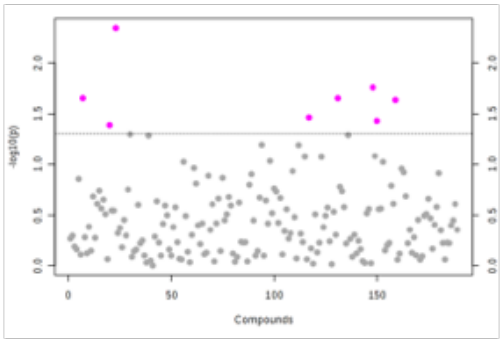

PCA pairwise

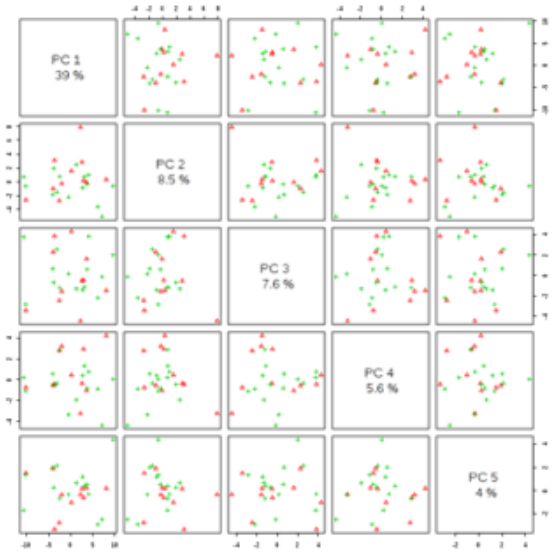

PLS-DA pairwise

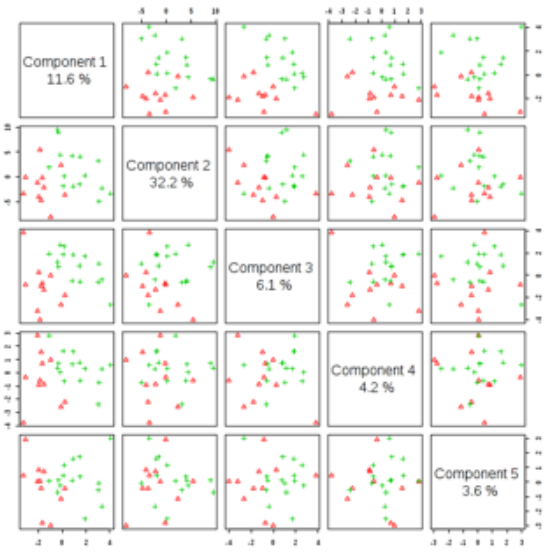

Control diet

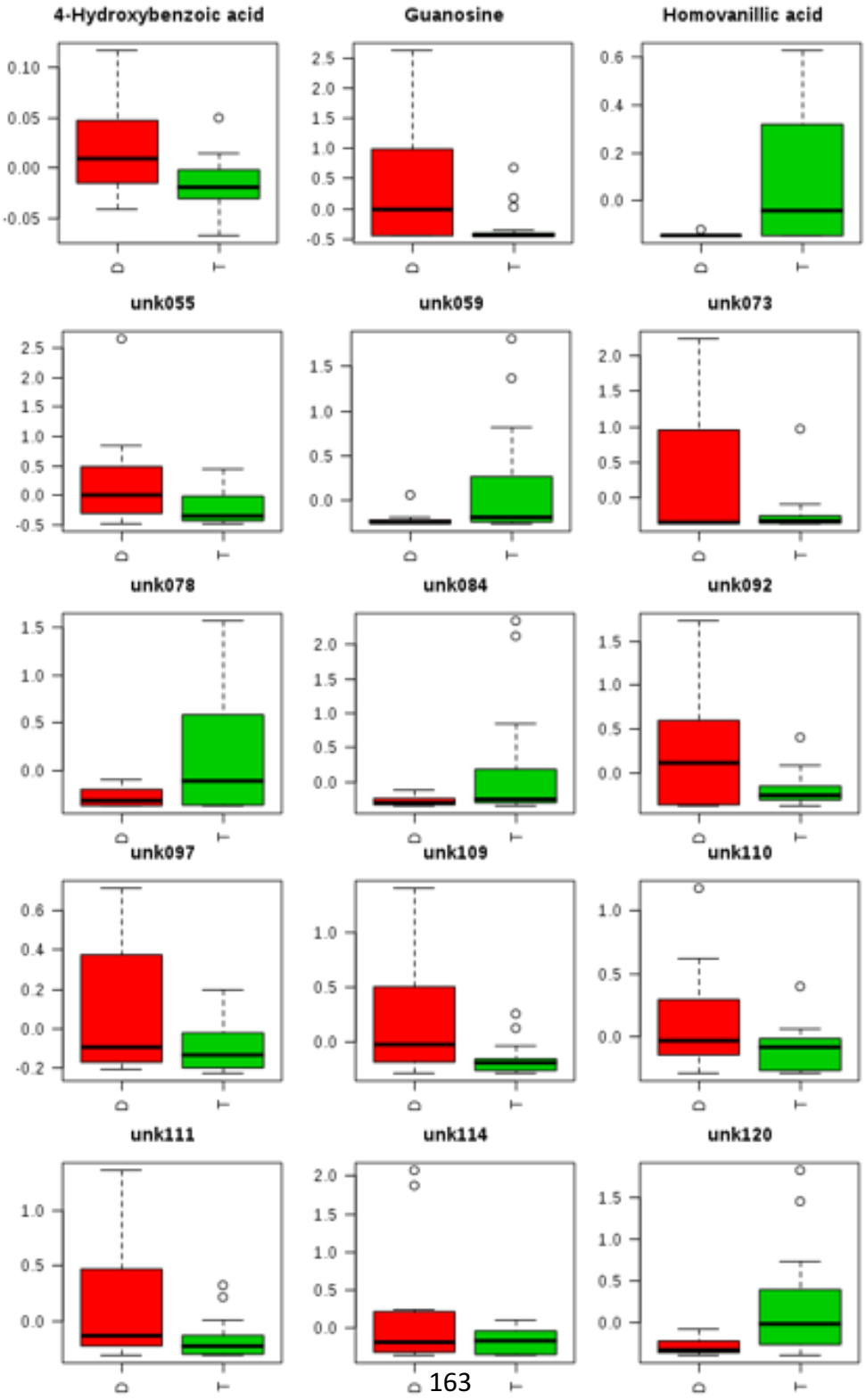

Comparison of disomic and trisomic mice fed microencapsulated rapamycin diet.

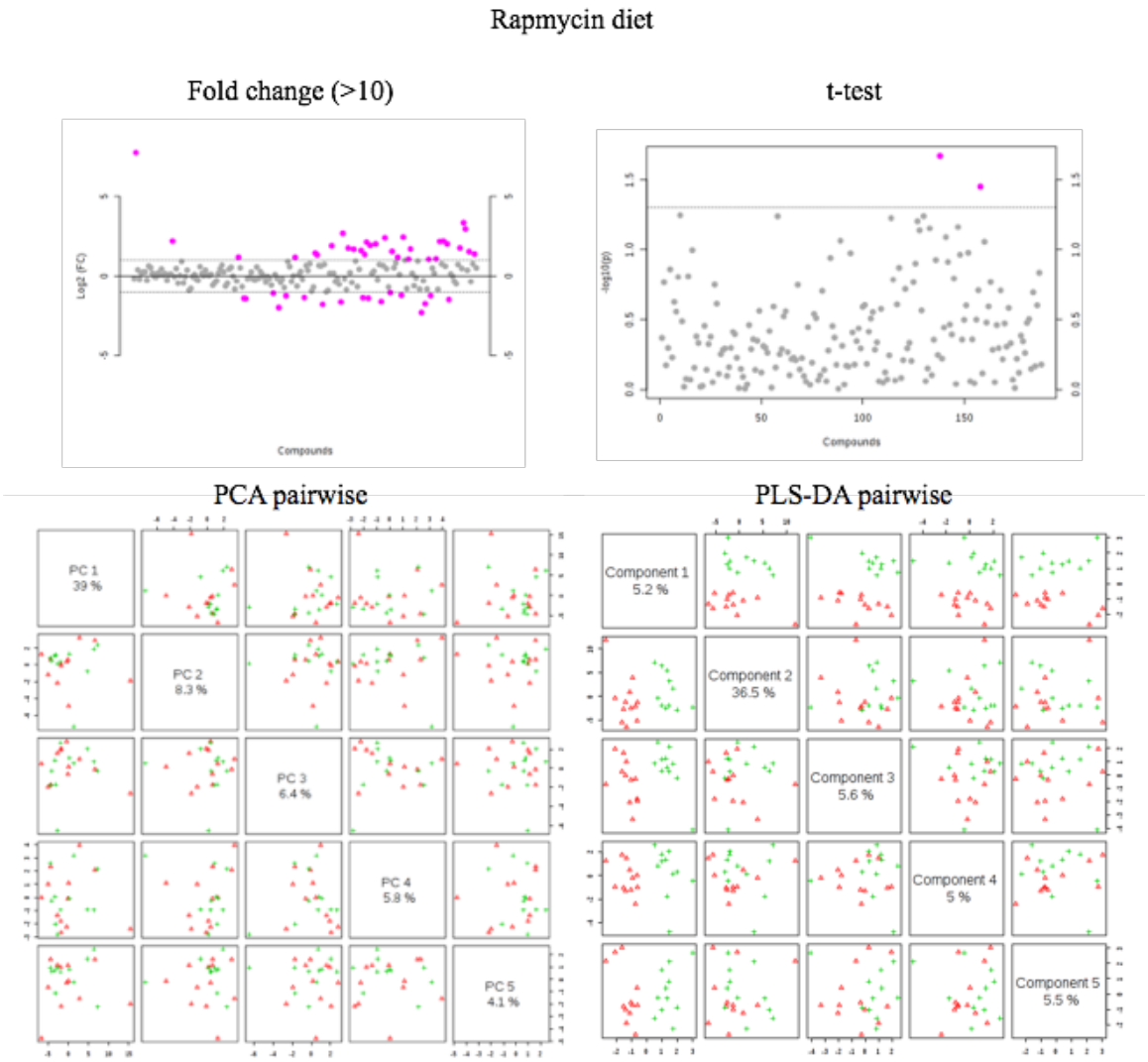

Rapamycin diet

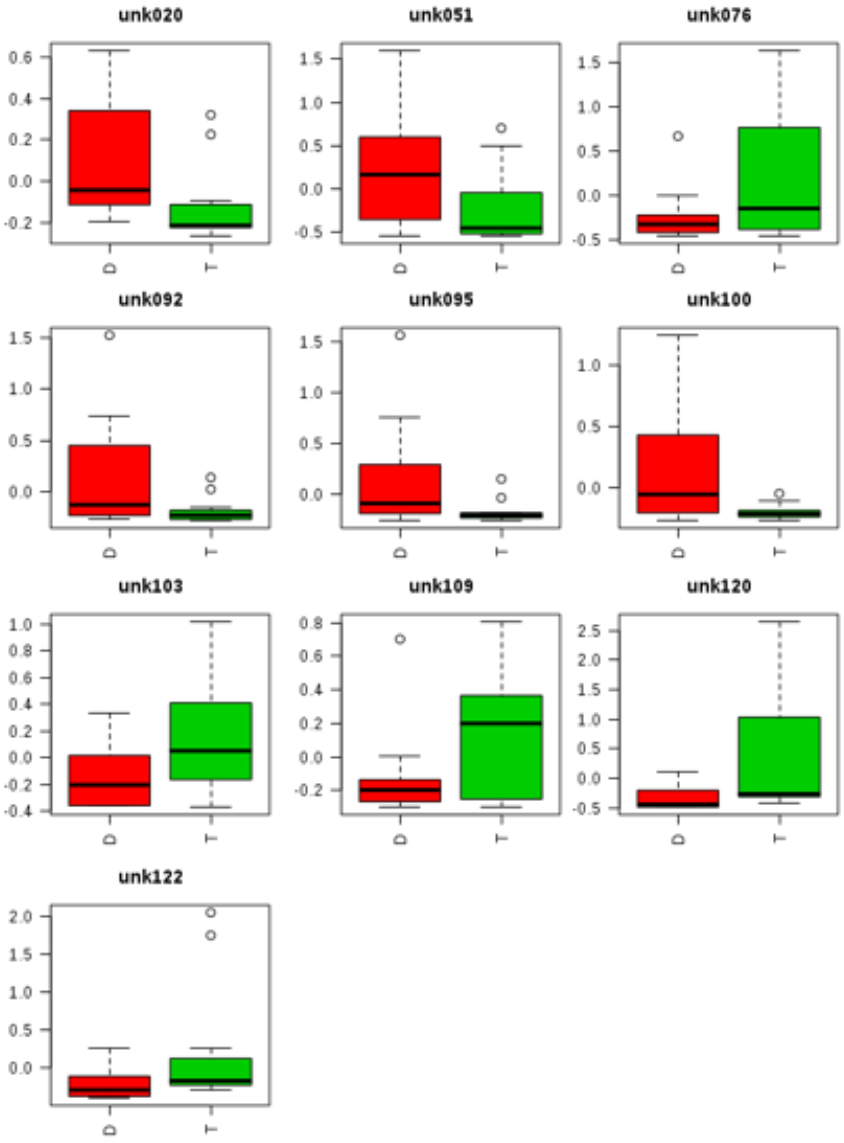

Comparison of control diet and microencapsulated rapamycin diet fed to disomic mice.

Disomic mice

Fold change (>10)

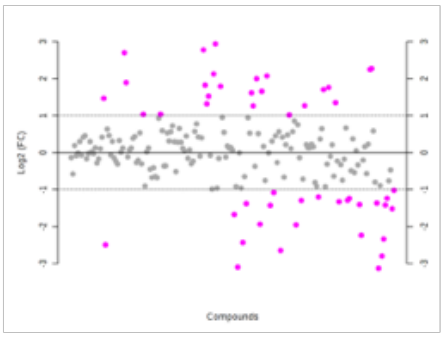

t-test

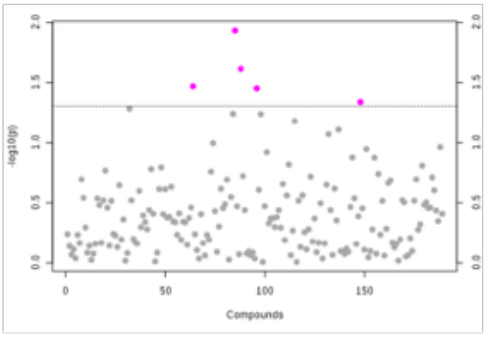

PCA pairwise

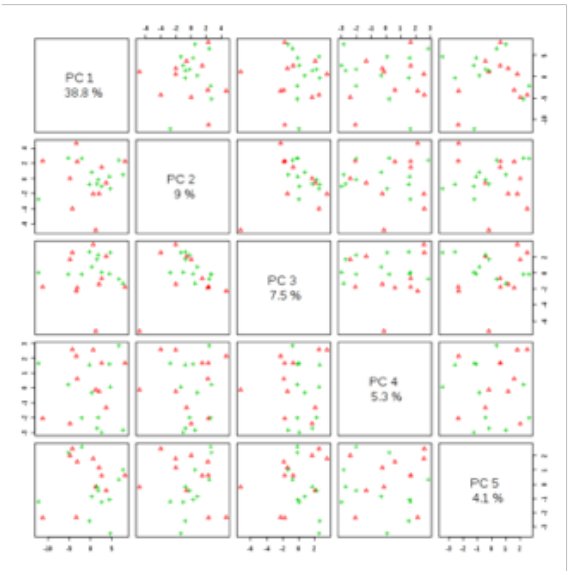

PLS-DA pairwise

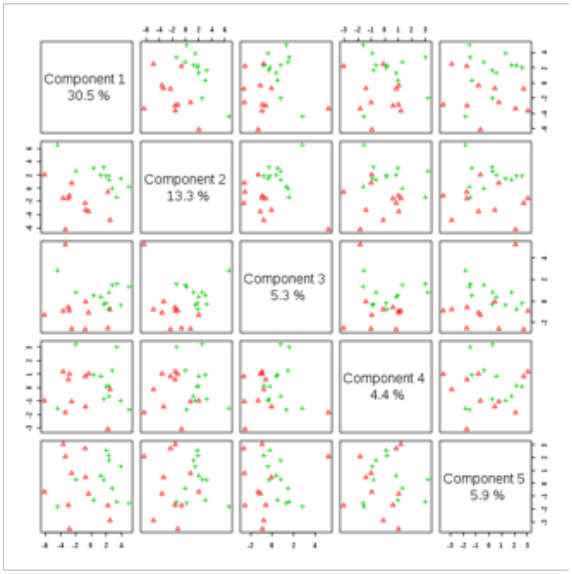

Disomic mice

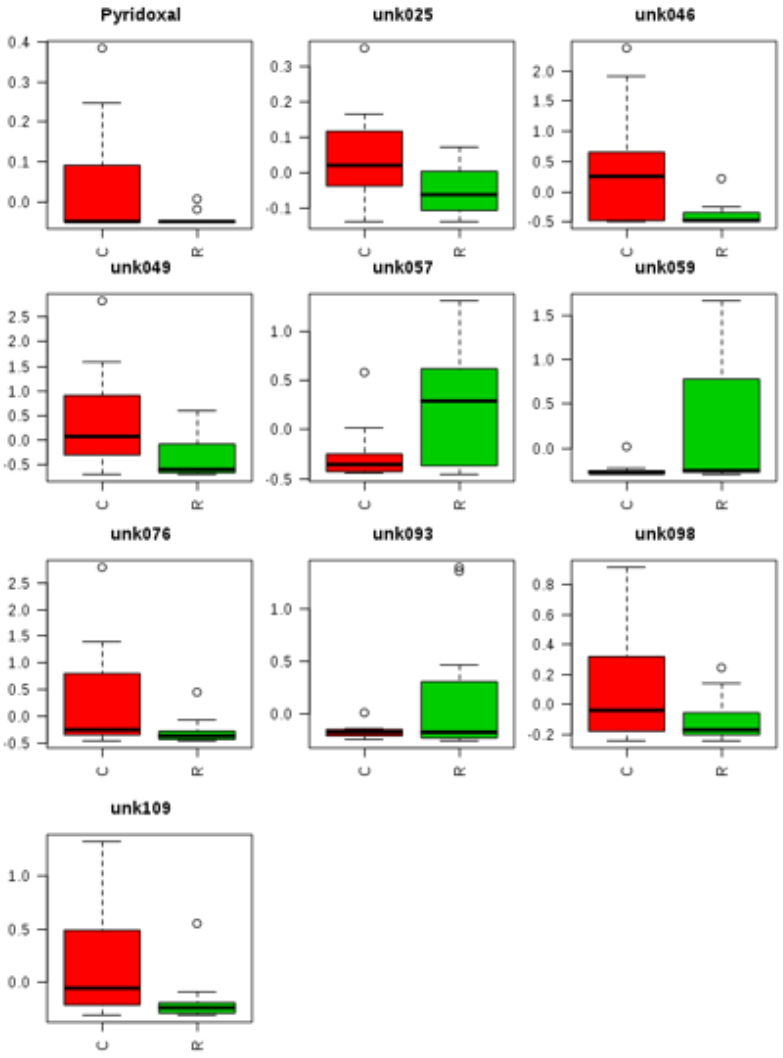

Comparison of control diet and microencapsulated rapamycin diet fed to trisomic mice.

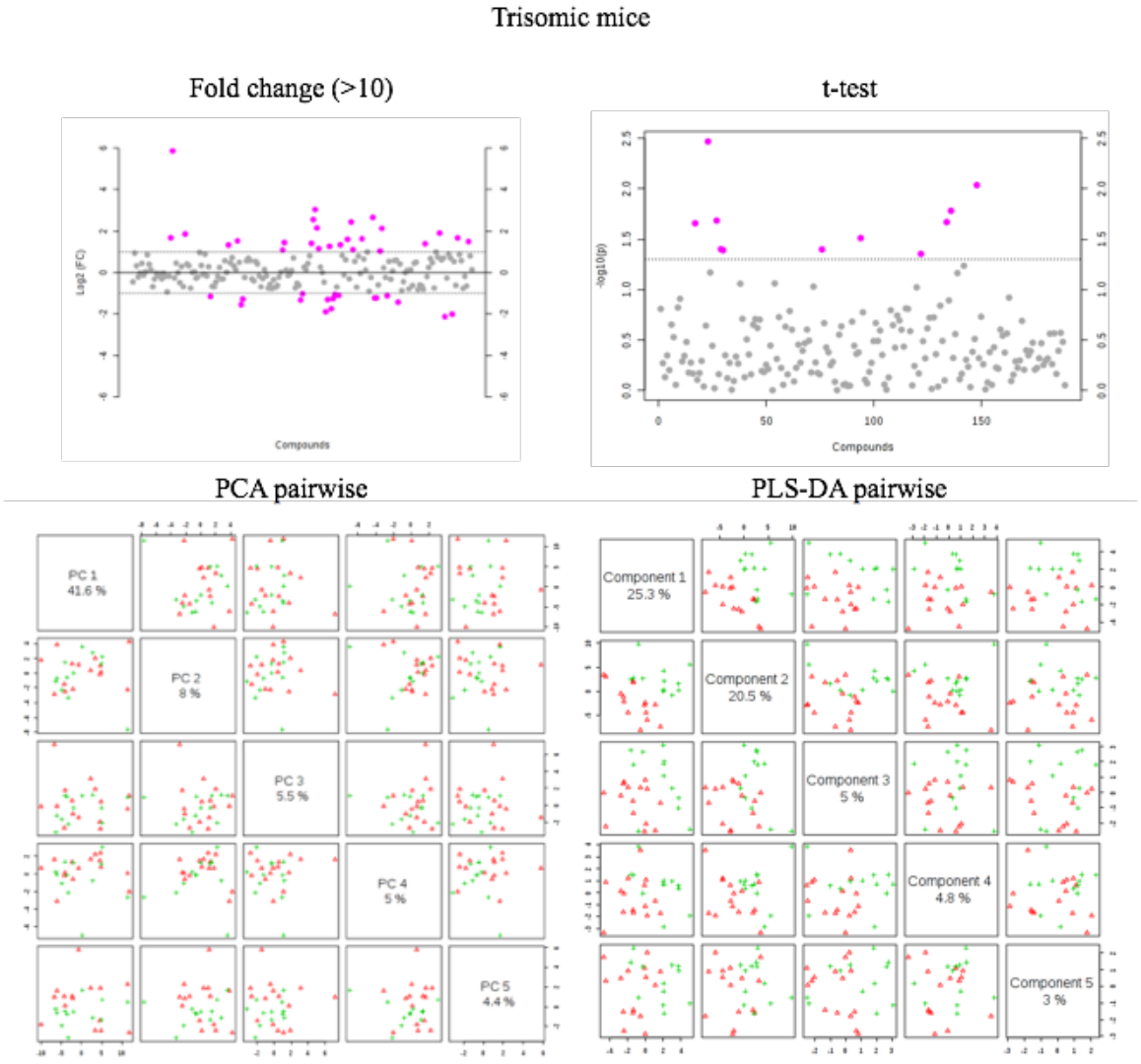

Trisomic mice

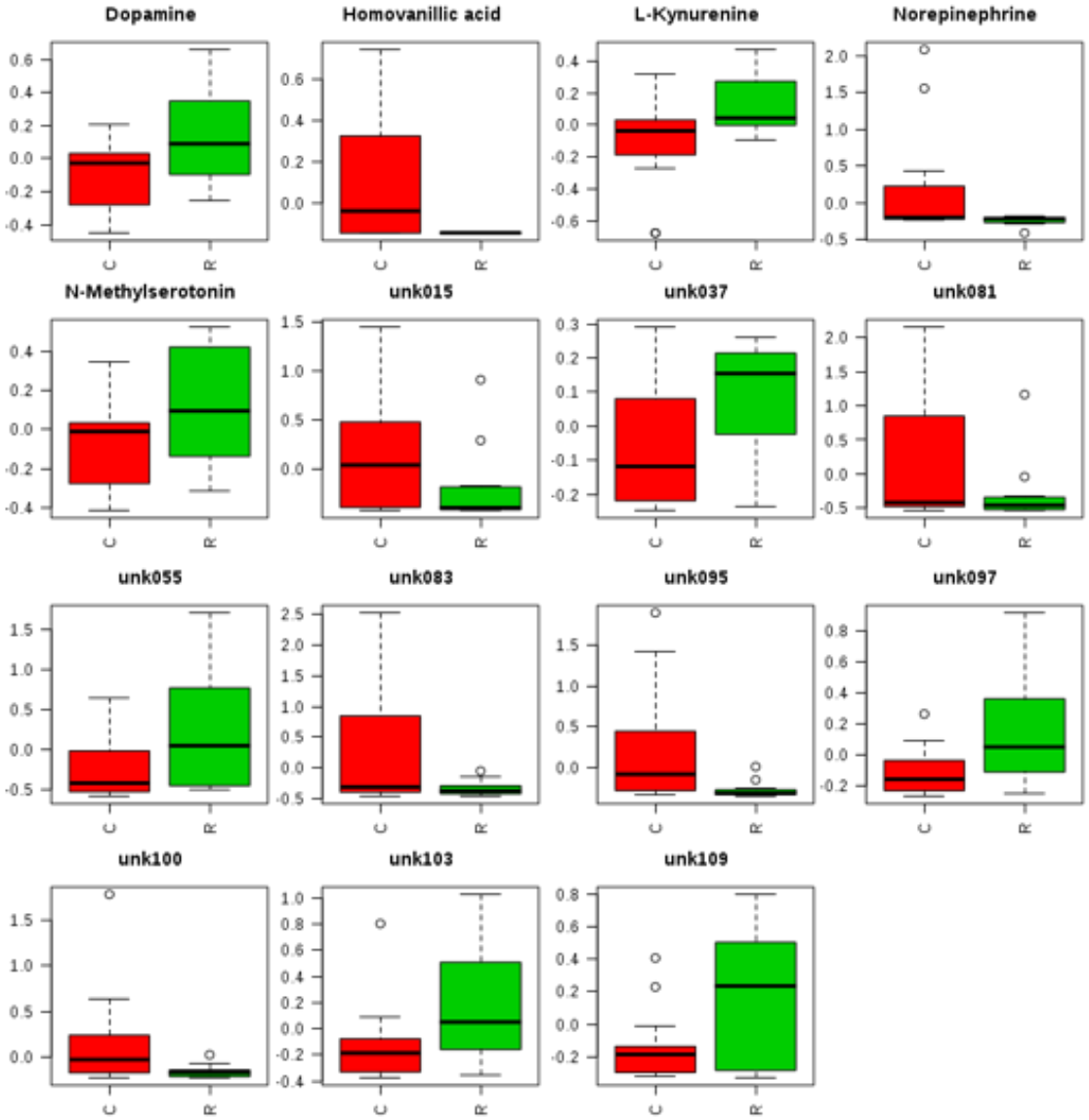

Section 6 – 18-month frontal brain targeted metabolomics analysis

The following are supplemental data plots for 18-month frontal brain samples

Comparison of disomic and trisomic mice fed control diet.

Control diet

Fold change (>10)

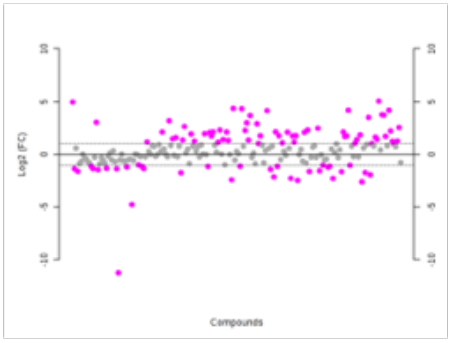

t-test

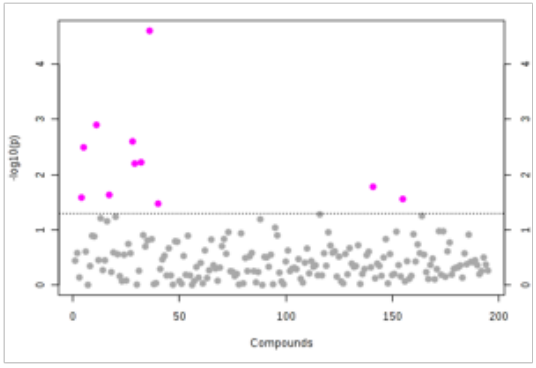

PCA pairwise

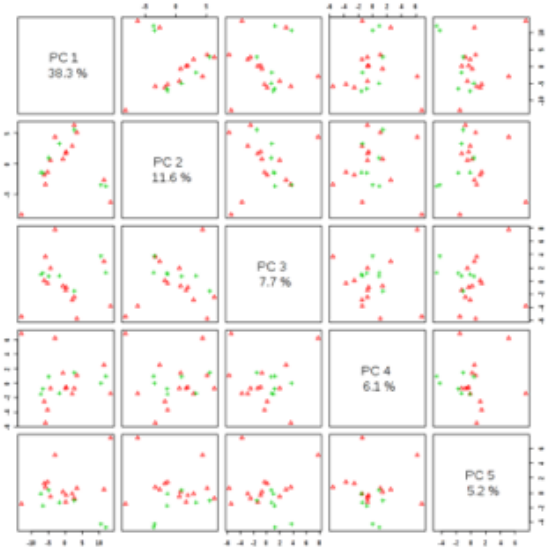

PLS-DA pairwise

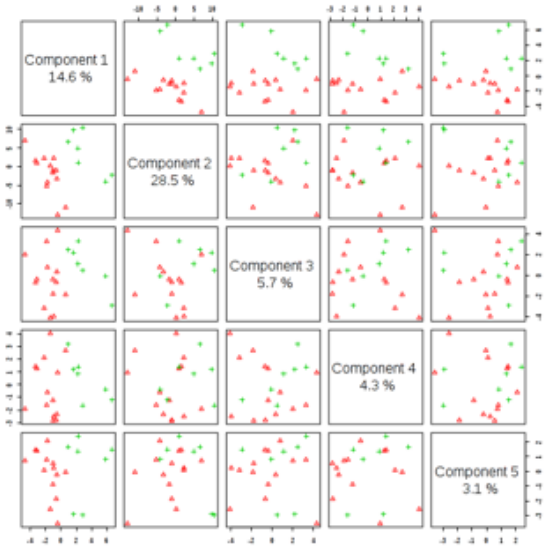

Control diet

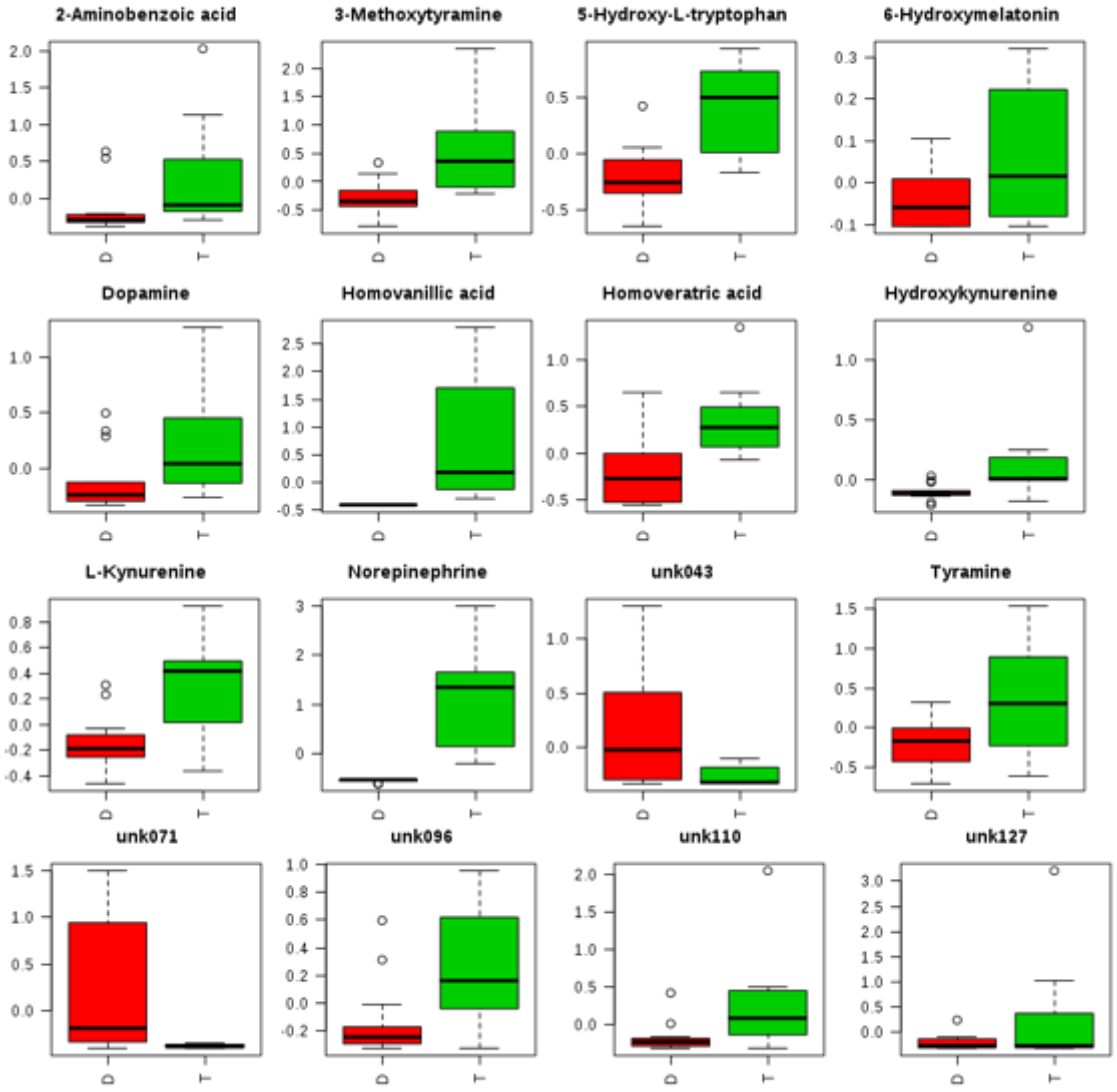

Comparison of disomic and trisomic mice fed microencapsulated rapamycin diet.

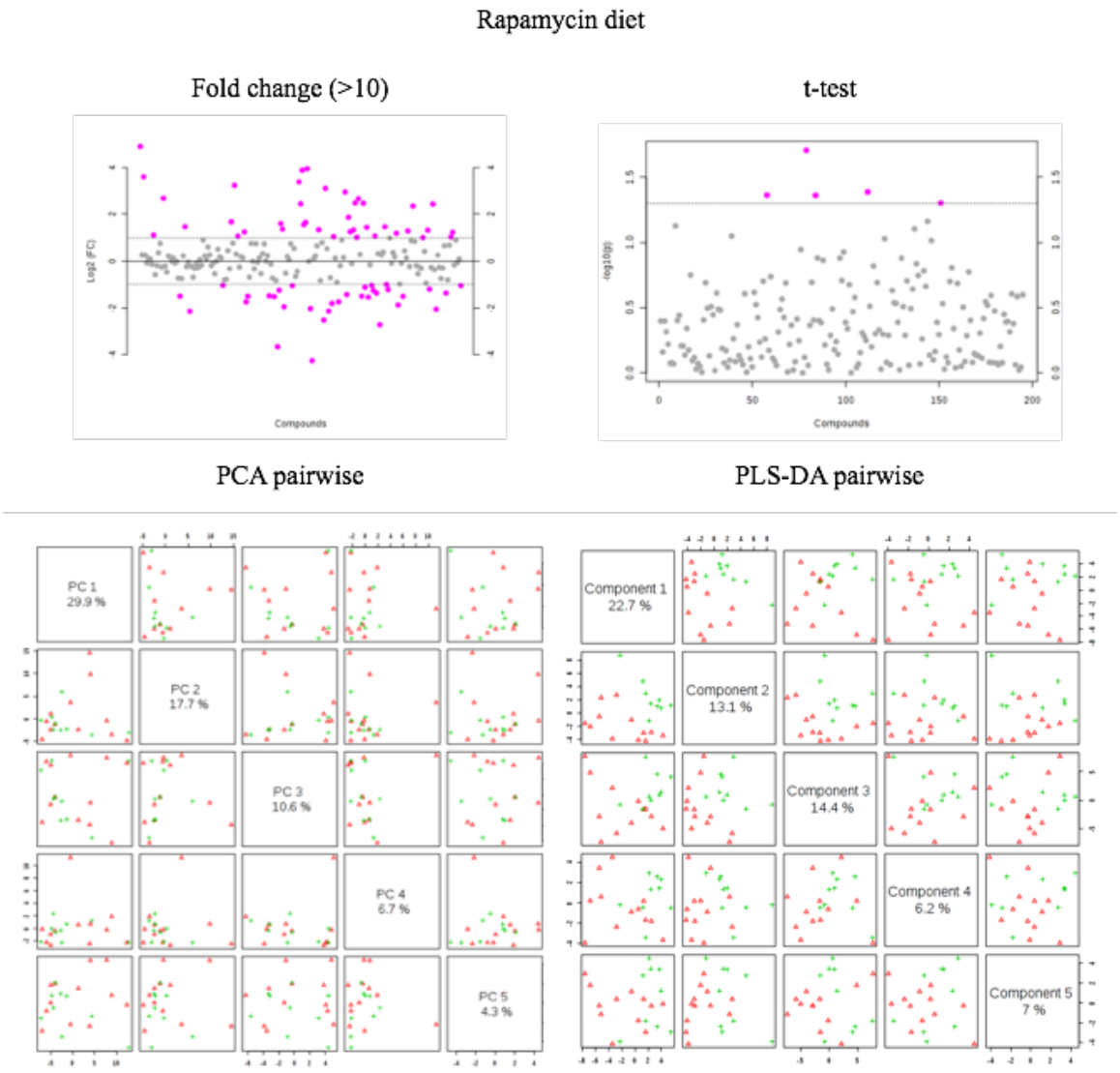

Rapamycin diet

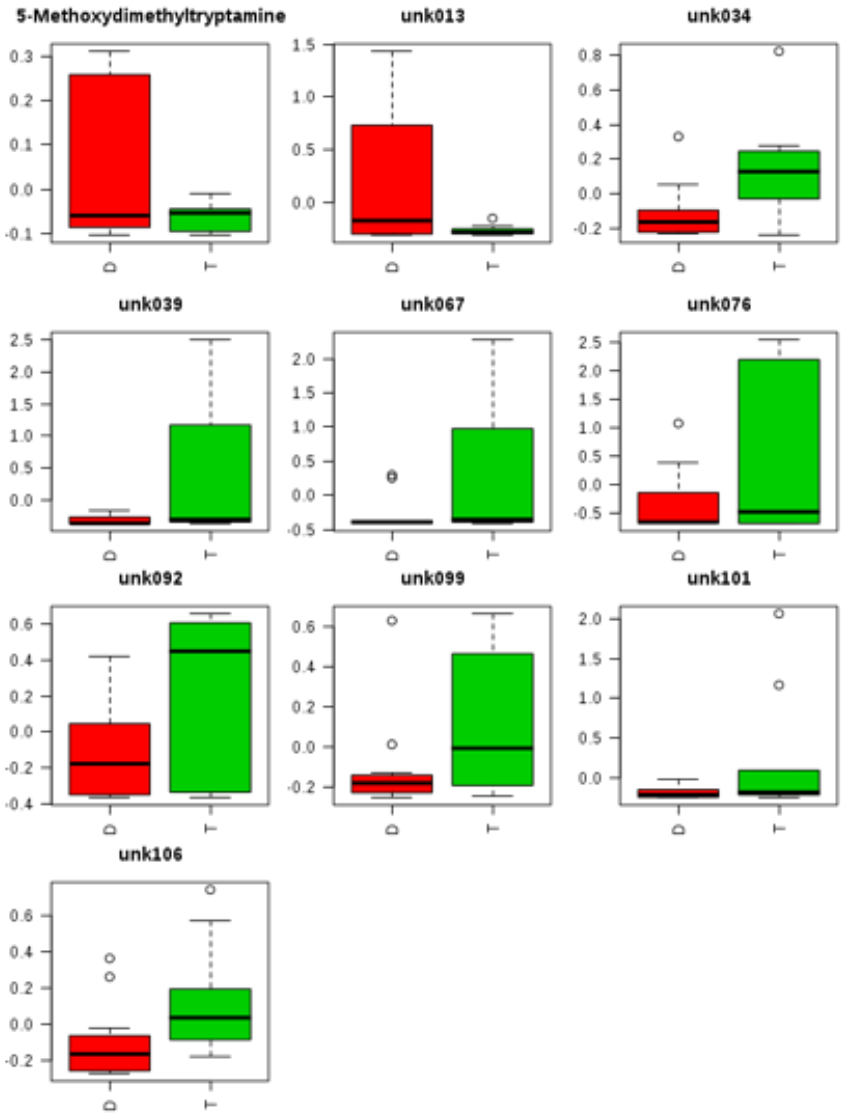

Comparison of control diet and microencapsulated rapamycin diet fed to disomic mice.

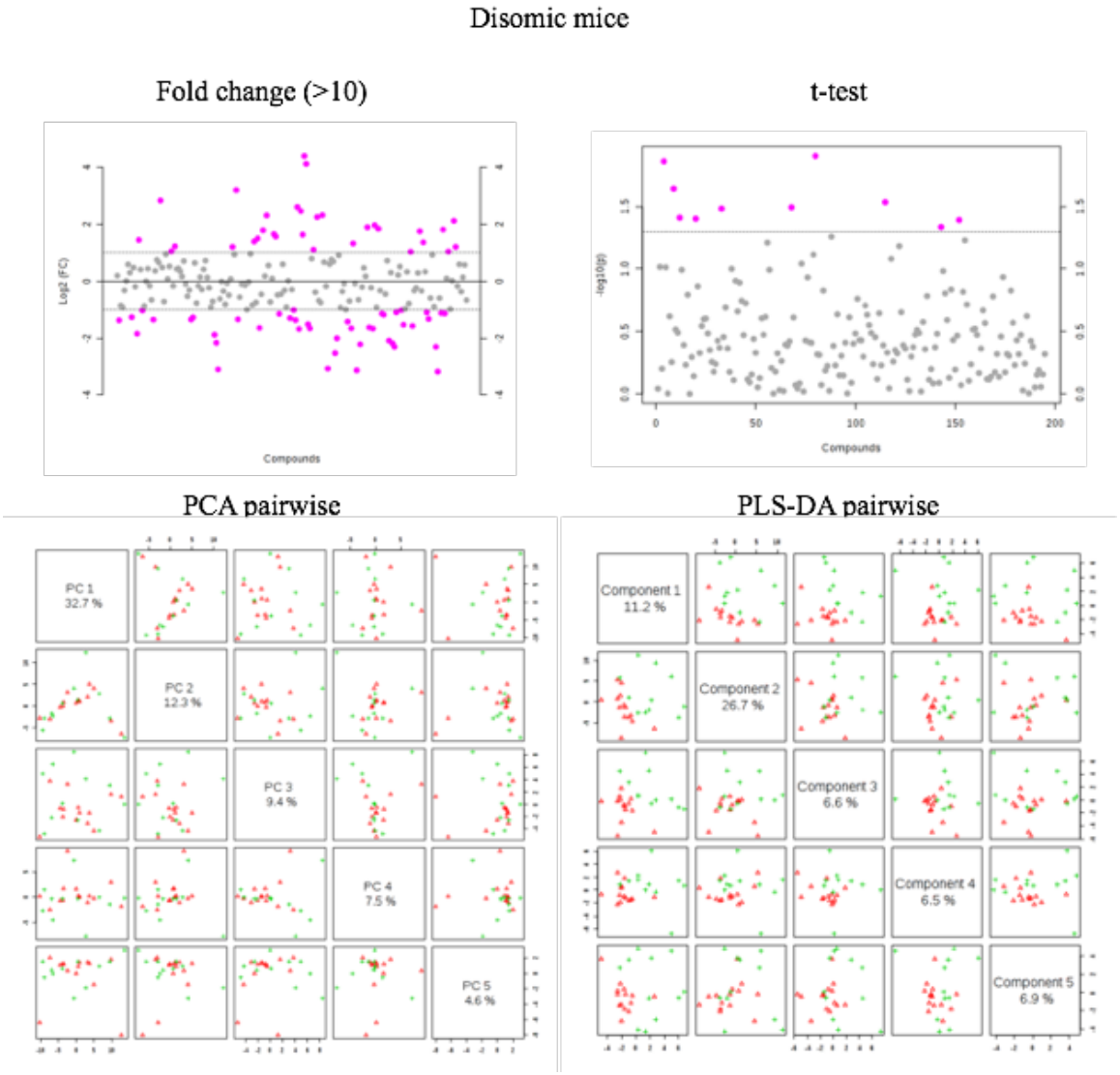

Disomic mice

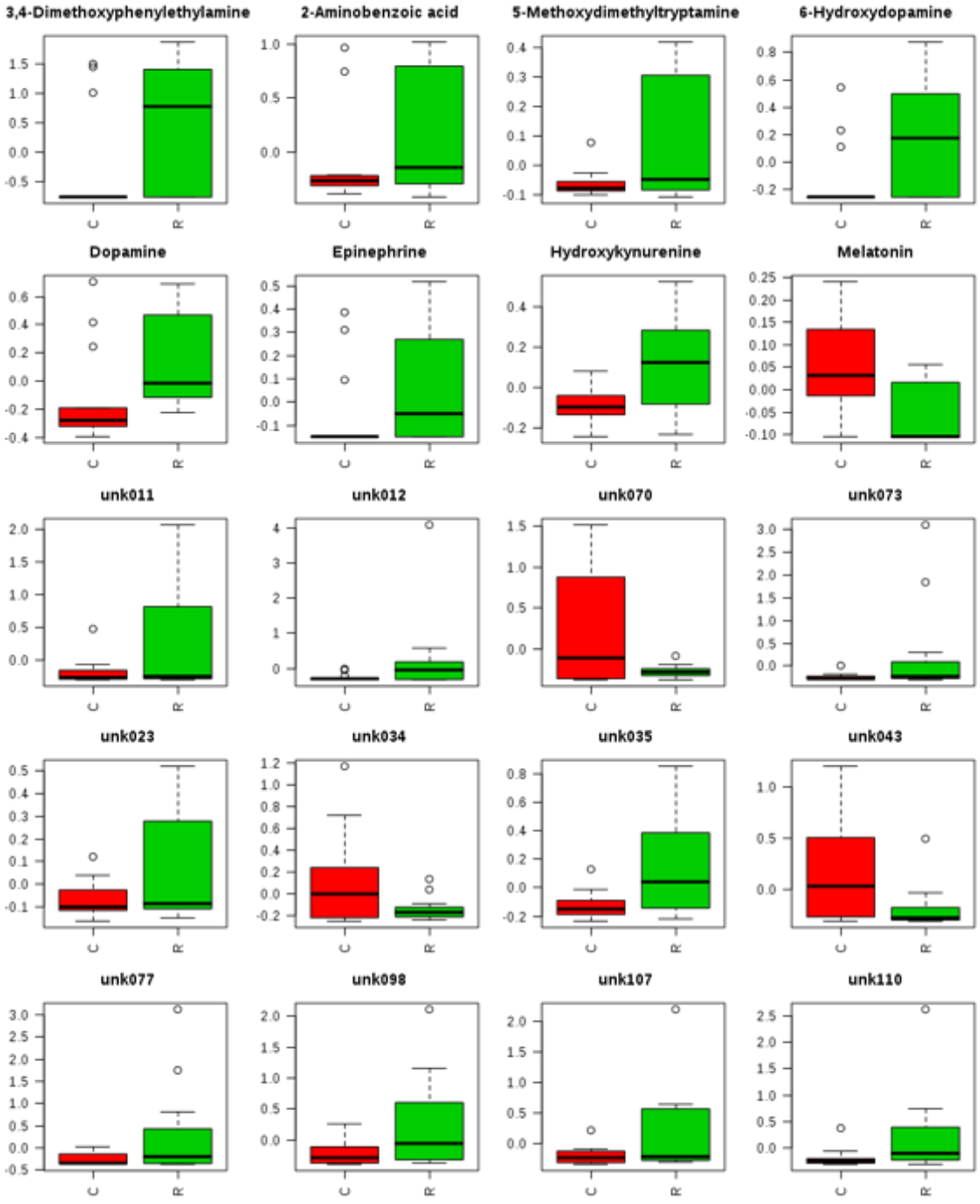

Comparison of control diet and microencapsulated rapamycin diet fed to trisomic mice.

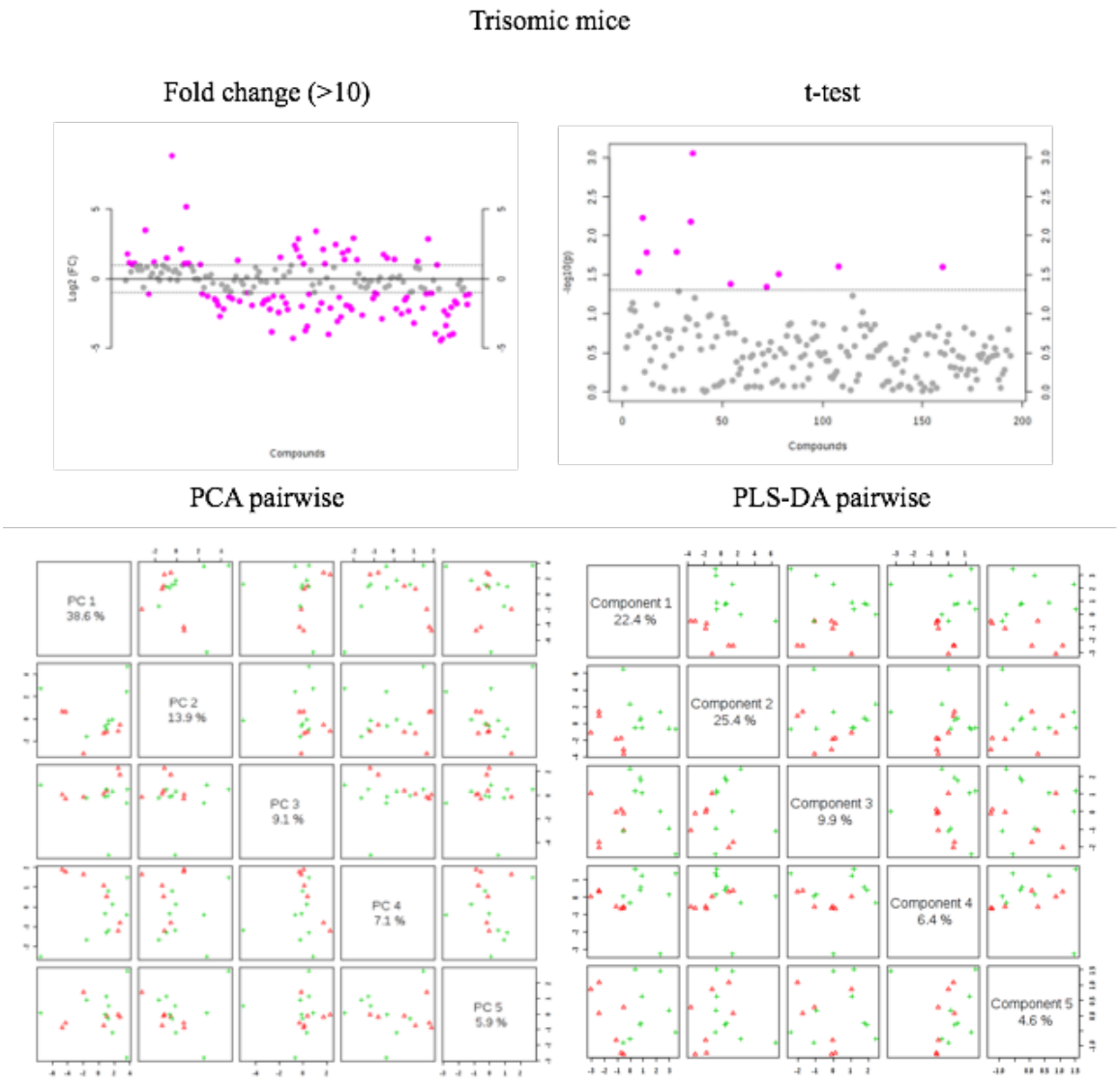

Trisomic mice

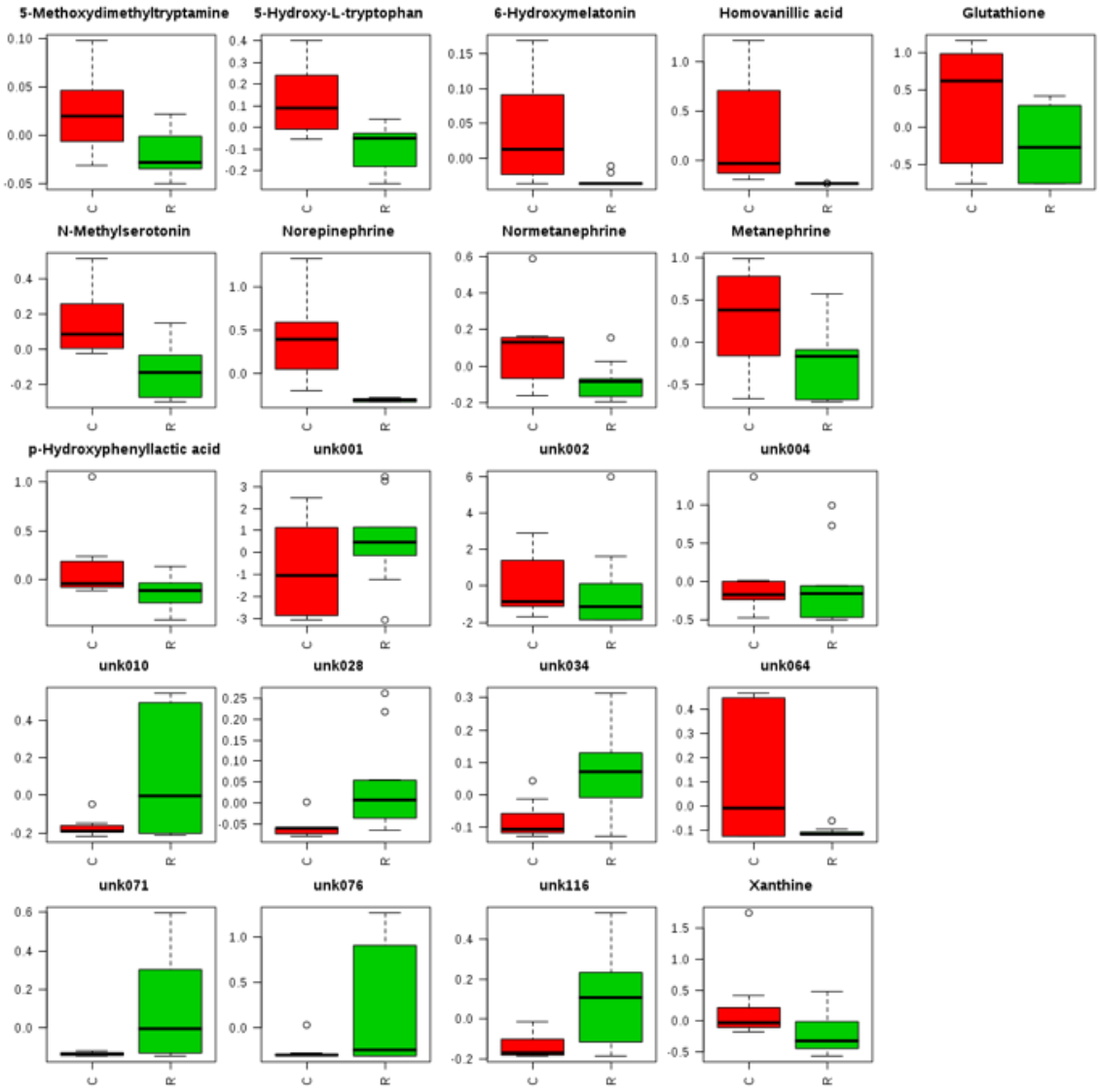

References

Chapter One –

Introduction to Aging, Down syndrome and metabolomics

Alers, S. et al., 2012. Role of AMPK-mTOR-Ulk1/2 in the regulation of autophagy: cross talk, shortcuts, and feedbacks. *Molecular and Cellular Biology*, 32(1), pp.2–11.

Ameur, A. et al., 2011. Ultra-deep sequencing of mouse mitochondrial DNA: mutational patterns and their origins. G. S. Barsh, ed. *PLoS Genetics*, 7(3), p.e1002028.

Anderson, R.M. & Weindruch, R., 2010. Metabolic reprogramming, caloric restriction and aging. *Trends in Endocrinology & Metabolism*, 21(3), pp.134–141.

Anisimov, V.N., Berstein, L.M. & Popovich, I.G., 2011. If started early in life, metformin treatment increases life span and postpones tumors in female SHR mice. *Aging,* 3(2), pp.148-157.

Armanios, M. et al., 2009. Short telomeres are sufficient to cause the degenerative defects associated with aging. *American Journal of Human Genetics*, 85(6), pp.823–832.

Baek, K.-H. et al., 2009. Down's syndrome suppression of tumour growth and the role of the calcineurin inhibitor DSCR1. *Nature*, 459(7250), pp.1126–1130.

Barzilai, N. et al., 2012. The critical role of metabolic pathways in aging. *Diabetes*, 61(6), pp.1315–1322.

Bernardes de Jesus, B. et al., 2012. Telomerase gene therapy in adult and old mice delays aging and increases longevity without increasing cancer. *EMBO molecular medicine*, 4(8), pp.691–704.

Bird, S.S. et al., 2012. Structural characterization of plasma metabolites detected via LC-electrochemical coulometric array using LC-UV fractionation, MS, and NMR. *Analytical Chemistry*, 84(22), pp.9889–9898.

Bjedov, I. et al., 2010. Mechanisms of Life Span Extension by Rapamycin in the Fruit Fly Drosophila melanogaster. *Cell Metabolism*, 11(1), pp.35–46.

Blackburn, E.H., Epel, E.S. & Lin, J., 2015. Human telomere biology: A contributory and interactive factor in aging, disease risks, and protection. *Science*, 350(6265), pp.1193–1198.

Blackburn, E.H., Greider, C.W. & Szostak, J.W., 2006. Telomeres and telomerase: the path from maize, Tetrahymena and yeast to human cancer and aging. *Nature medicine*, 12(10), pp.1133–1138.

Blasco, M.A., 2007. Telomere length, stem cells and aging. *Nature chemical biology*, 3(10), pp.640–649.

Blazek, J.D. et al., 2011. Disruption of bone development and homeostasis by trisomy in Ts65Dn Down syndrome mice. *Bone*, 48(2), pp.275–280.

Bodnar, A.G. et al., 1998. Extension of life-span by introduction of telomerase into normal human cells. *Science*, 279(5349), pp.349–352.

Bureau, U.S.C., 2014. An Aging Nation: The Older Population in the United States. pp.1–28.

Cairney, C.J. et al., 2009. A systems biology approach to Down Syndrome: Identification of Notch/Wnt dysregulation in a model of stem cells aging. *Biochimica et Biophysica Acta. BBA - Molecular Basis of Disease*, 1792(4), pp.353–363.

Calderwood, S.K., Murshid, A. & Prince, T., 2009. The shock of aging: molecular chaperones and the heat shock response in longevity and aging--a mini-review. *Gerontology*, 55(5), pp.550–558.

Chen, Y. et al., 2009. In vivo MRI identifies cholinergic circuitry deficits in a Down syndrome model. *Neurobiology of Aging*, 30(9), pp.1453–1465.

Chicoine, B. & McGuire, D., 1997. Longevity of a woman with Down syndrome: a case study. *Mental retardation*, 35(6), pp.477–479.

Choi, J.H.K. et al., 2009. Age-dependent dysregulation of brain amyloid precursor protein in the Ts65Dn Down syndrome mouse model. *Journal of Neurochemistry*, 110(6), pp.1818–1827.

Colman, R.J. et al., 2009. Caloric Restriction Delays Disease Onset and Mortality in Rhesus Monkeys. *Science*, 325(5937), pp.201–204.

Contestabile, A., Fila, T., Bartesaghi, R., et al., 2009. Cell Cycle Elongation Impairs Proliferation of Cerebellar Granule Cell Precursors in the Ts65Dn Mouse, an Animal Model for Down Syndrome. *Brain Pathology*, 19(2), pp.224–237.

Contestabile, A., Fila, T., Cappellini, A., et al., 2009. Widespread impairment of cell

proliferation in the neonate Ts65Dn mouse, a model for Down syndrome. *Cell Proliferation*, 42(2), pp.171–181.

Coppus, A.M.W. et al., 2008. Survival in Elderly Persons with Down Syndrome. *Journal of the American Geriatrics Society*, 56(12), pp.2311–2316.

Davisson, M.T., Schmidt, C. & Akeson, E.C., 1990. Segmental trisomy of murine chromosome 16: a new model system for studying Down syndrome. *Progress in clinical and biological research*, 360, p.263.

Duchon, A. et al., 2011. Identification of the translocation breakpoints in the Ts65Dn and Ts1Cje mouse lines: relevance for modeling Down syndrome. *Mammalian genome : official journal of the International Mammalian Genome Society*, 22(11-12), pp.674–684.

Duval, N. et al., 2013. Genetic and metabolomic analysis of AdeD and AdeI mutants of de novo purine biosynthesis: Cellular models of de novo purine biosynthesis deficiency disorders. *Molecular genetics and metabolism*, 108(3), pp.178–189.

Edgar, D. et al., 2009. Random Point Mutations with Major Effects on Protein-Coding Genes Are the Driving Force behind Premature Aging in mtDNA Mutator Mice. *Cell Metabolism*, 10(2), pp.131–138.

Finch, C.E., Pike, M.C. & Witten, M., 1990. Slow mortality rate accelerations during aging in some animals approximate that of humans. *Science*, 249(4971), pp.902–905.

Fontana, L., Partridge, L. & Longo, V.D., 2010. Extending Healthy Life Span—From Yeast to Humans. *Science*, 328(5976), pp.321–326.

Galletti, P. et al., 2007. Accumulation of altered aspartyl residues in erythrocyte proteins from patients with Down's syndrome. *FEBS Journal*, 274(20), pp.5263–5277.

Gardiner, K.J., 2010. Molecular basis of pharmacotherapies for cognition in Down syndrome. *Trends in Pharmacological Sciences*, 31(2), pp.66–73.

Granholm, A.-C.E., Sanders, L.A. & Crnic, L.S., 2000. Loss of Cholinergic Phenotype in Basal Forebrain Coincides with Cognitive Decline in a Mouse Model of Down's Syndrome. *Experimental Neurology*, 161(2), pp.647–663.

Gregg, S.Q. et al., 2012. A mouse model of accelerated liver aging caused by a defect in DNA repair. *Hepatology*, 55(2), pp.609–621.

Gruszecka, A. et al., 2015. Telomere shortening in Down syndrome patients--when does it start? *DNA and cell biology*, 34(6), pp.412–417.

Harman, D., 1992. Free radical theory of aging. *Mutation Research/DNAging*, 275(3-6),

pp.257–266.

Harman, D., 1955. Aging: a theory based on free radical and radiation chemistry. *Journal of Gerontology*, pp. 298-300.

Harman, D., 2001. Aging: overview. *Annals of the New York Academy of Sciences*, 928, pp.1–21.

Harrison, D.E. et al., 2009. Rapamycin fed late in life extends lifespan in genetically heterogeneous mice. *Nature*, 460 (7253), pp. 392-395.

Hayflick, L. & Moorhead, P.S., 1961. The serial cultivation of human diploid cell strains. *Experimental Cell Research*, 25(3), pp.585–621.

Hekimi, S., Lapointe, J. & Wen, Y., 2011. Taking a "good" look at free radicals in the aging process. *Trends in Cell Biology*, 21(10), pp.569–576.

Herrera, E. et al., 1999. Disease states associated with telomerase deficiency appear earlier in mice with short telomeres. *The EMBO journal*, 18(11), pp.2950–2960.

Hoeijmakers, J.H.J., 2009. DNA Damage, Aging, and Cancer. *New England Journal of Medicine*, 361(15), pp.1475–1485.

Hunsucker, S.W. et al., 2008. Assessment of post-mortem-induced changes to the mouse brain proteome. *Journal of Neurochemistry*, 105(3), pp.725–737.

Hyde, L.A. & Crnic, L.S., 2001. Age-related deficits in context discrimination learning in Ts65Dn mice that model Down syndrome and Alzheimer's disease. *Behavioral Neuroscience*, 115(6), pp.1239–1246.

Jablonska, B. et al., 2006. The growth capacity of bone marrow CD34 positive cells in culture is drastically reduced in a murine model of Down syndrome. *Comptes Rendus Biologies*, 329(9), pp.726–732.

Jane, I., McKinnon, A. & Flanagan, R.J., 1985. High-performance liquid chromatographic analysis of basic drugs on silica columns using non-aqueous ionic eluents. II. Application of UV, fluorescence and electrochemical oxidation detection. *Journal of chromatography*, 323(2), pp.191–225.

Jenkins, N.L., McColl, G. & Lithgow, G.J., 2004. Fitness cost of extended lifespan in Caenorhabditis elegans. *Proceedings of the Royal Society of London B: Biological Sciences*, 271(1556), pp.2523–2526.

Johnson, S.C., Rabinovitch, P.S. & Kaeberlein, M., 2013. mTOR is a key modulator of ageing and age-related disease. *Nature*, 493(7432), pp.338–345.

Jurecka, A., 2009. Inborn errors of purine and pyrimidine metabolism. *Journal of Inherited Metabolic Disease*, 32(2), pp.247–263.

Jurecka, A. et al., 2008. Clinical, biochemical and molecular findings in seven Polish patients with adenylosuccinate lyase deficiency. *Molecular genetics and metabolism*, 94(4), pp.435–442.

Kaeberlein, M. et al., 2005. Regulation of Yeast Replicative Life Span by TOR and Sch9 in Response to Nutrients. *Science*, 310(5751), pp.1193–1196.

Kemula, W., 1952. *Chromato-polarographic studies*, General consideration and instrumentation. Roczniki ….

Kirkwood, T.B., 1977. Evolution of ageing. *Nature*, 270(5635), pp.301–304.

Kirsammer, G. et al., 2008. Highly penetrant myeloproliferative disease in the Ts65Dn mouse model of Down syndrome. *Blood*, 111(2), pp.767–775.

Kissinger, P.T., 1989. Biomedical applications of liquid chromatography-electrochemistry. *Journal of chromatography*, 488(1), pp.31–52.

Koga, H., Kaushik, S. & Cuervo, A.M., 2011. Protein homeostasis and aging: The importance of exquisite quality control. *Ageing Research Reviews*, 10(2), pp.205–215.

Kristal, B.S., Shurubor, Y.I., Kaddurah-Daouk, R. & Matson, W.R., 2007a. High-performance liquid chromatography separations coupled with coulometric electrode array detectors: a unique approach to metabolomics. *Methods in molecular biology (Clifton, N.J.)*, 358(Chapter 10), pp.159–174.

Lack, D. & S, F.R., 1954. The Natural Regulation of Animal Numbers. *The Natural Regulation of Animal Numbers*.

Linnane, A.W. et al., 1989. Mitochondrial DNA mutations as an important contributor to ageing and degenerative diseases. *Lancet (London, England)*, 1(8639), pp.642–645.

Lomoio, S., Scherini, E. & Necchi, D., 2009. -Amyloid overload does not directly correlate with SAPK/JNK activation and tau protein phosphorylation in the cerebellar cortex of Ts65Dn mice. *Brain Research*, 1297(C), pp.198–206.

Lott, I.T., 2012. Neurological phenotypes for Down syndrome across the life span. *Progress in brain research*, 197, pp.101–121.

Lott, I.T. & Head, E., 2005. Alzheimer disease and Down syndrome: factors in pathogenesis. *Neurobiology of Aging*, 26(3), pp.383–389.

López-Otín, C. et al., 2013. The Hallmarks of Aging. *Cell*, 153(6), pp.1194–1217.

Matson, W.R. et al., 1984. n-ElectrodeThree-DimensionalLiquidChromatographywith Electrochemical Detectionfor Determinationof Neurotransmitters. *Clinical Chemistry*, 30(9), pp.1477–1488.

McClintock, S.A., Purdy, W.C. & Young, S.N., 1985. Evaluation of high-performance liquid chromatography with a dual working-electrode electrochemical detector for the determination of catecholamines in human cerebrospinal fluid. *Analytica Chimica Acta*, 166, pp.171–177.

Medawar, P.B., 1952. An unsolved problem of biology. Lecture to University College of London. pp. 1-24.

Morrow, G. et al., 2004. Overexpression of the small mitochondrial Hsp22 extends Drosophila life span and increases resistance to oxidative stress. *FASEB journal : official publication of the Federation of American Societies for Experimental Biology*, 18(3), pp.598–599.

Moskalev, A.A. et al., 2013. The role of DNA damage and repair in aging through the prism of Koch-like criteria. *Ageing Research Reviews*, 12(2), pp.661–684.

Musch, G., De Smet, M. & Massart, D.L., 1985. Expert system for pharmaceutical analysis. I. Selection of the detection system in high-performance liquid chromatographic analysis: UV versus amperometric detection. *Journal of chromatography*, 348(1), pp.97–110.

Nakamura, E. & Tanaka, S., 1998. Biological ages of adult men and women with Down's syndrome and its changes with aging. *Mechanisms of Ageing and Development*, 105(1), pp.89–103.

Necchi, D., Lomoio, S. & Scherini, E., 2008. Axonal abnormalities in cerebellar Purkinje cells of the Ts65Dn mouse. *Brain Research*, 1238(C), pp.181–188.

Onken, B. & Driscoll, M., 2010. Metformin Induces a Dietary Restriction–Like State and the Oxidative Stress Response to Extend C. elegans Healthspan via AMPK, LKB1, and SKN-1 A. C. Hart, ed. *PLoS ONE*, 5(1), p.e8758.

Park, C.B. & Larsson, N.-G., 2011. Mitochondrial DNA mutations in disease and aging. *The Journal of Cell Biology*, 193(5), pp.809–818.

Patterson, D. & Cabelof, D.C., 2012. Down syndrome as a model of DNA polymerase beta haploinsufficiency and accelerated aging. *Mechanisms of Ageing and Development*, 133(4), pp.133–137.

Payne, B.A.I. et al., 2011. Mitochondrial aging is accelerated by anti-retroviral therapy

through the clonal expansion of mtDNA mutations. *Nature Genetics*, 43(8), pp.806–810.

Pérez, V.I. et al., 2009. The overexpression of major antioxidant enzymes does not extend the lifespan of mice. *Aging Cell*, 8(1), pp.73–75.

Powers, E.T. et al., 2009. Biological and Chemical Approaches to Diseases of Proteostasis Deficiency. *Annual Review of Biochemistry*, 78(1), pp.959–991.

Radzik, D.M. & Lunte, S.M., 2006. Application of Liquid Chromatography/Electrochemistry in Pharmaceutical and Biochemical Analysis: A Critical Review. *Critical Reviews in Analytical Chemistry*, 20(5), pp.317–358.

Reeves, R.H. et al., 1995. A mouse model for Down syndrome exhibits learning and behaviour deficits. *Nature Genetics*, 11(2), pp.177–184.

Reinholdt, L.G. et al., 2011. Molecular characterization of the translocation breakpoints in the Down syndrome mouse model Ts65Dn. *Mammalian genome : official journal of the International Mammalian Genome Society*, 22(11-12), pp.685–691.

Riggin, R.M. & Kissinger, P.T., 1977. Determination of catecholamines in urine by reverse-phase liquid chromatography with electrochemical detection. *Analytical Chemistry*, 49(13), pp.2109–2111.

Rubinsztein, D.C., Mariño, G. & Kroemer, G., 2011. Autophagy and Aging. *Cell*, 146(5), pp.682–695.

Salehi, A. et al., 2006. Increased App Expression in a Mouse Model of Down's Syndrome Disrupts NGF Transport and Causes Cholinergic Neuron Degeneration. *Neuron*, 51(1), pp.29–42.

Sanders, N.C., Williams, D.K. & Wenger, G.R., 2009. Does the learning deficit observed under an incremental repeated acquisition schedule of reinforcement in Ts65Dn mice, a model for Down syndrome, change as they age? *Behavioural Brain Research*, 203(1), pp.137–142.

Sempere, Á. et al., 2010. Study of inborn errors of metabolism in urine from patients with unexplained mental retardation. *Journal of Inherited Metabolic Disease*, 33(1), pp.1–7.

Shaw, F.H. et al., 1999. Toward Reconciling Inferences Concerning Genetic Variation in Senescence in Drosophila melanogaster. *Genetics*, 152(2), pp.553–566.

Smith, E.M., 2005. The Tuberous Sclerosis Protein TSC2 Is Not Required for the Regulation of the Mammalian Target of Rapamycin by Amino Acids and Certain Cellular Stresses. *Journal of Biological Chemistry*, 280(19), pp.18717–18727.

Sturgeon, X. & Gardiner, K.J., 2011. Transcript catalogs of human chromosome 21 and orthologous chimpanzee and mouse regions. *Mammalian genome : official journal of the International Mammalian Genome Society*, 22(5-6), pp.261–271.

Swindell, W.R. et al., 2009. Endocrine regulation of heat shock protein mRNA levels in long-lived dwarf mice. *Mechanisms of Ageing and Development*, 130(6), pp.393–400.

Tomás-Loba, A. et al., 2008. Telomerase reverse transcriptase delays aging in cancer-resistant mice. *Cell*, 135(4), pp.609–622.

Trifunovic, A. et al., 2004. Premature ageing in mice expressing defective mitochondrial DNA polymerase. *Nature*, 429(6990), pp.417–423.

Vacano, G.N., Duval, N. & Patterson, D., 2012. The use of mouse models for understanding the biology of down syndrome and aging. *Current Gerontology and Geriatrics Research*, 2012, p.717315.

Van Remmen, H. et al., 2003. Life-long reduction in MnSOD activity results in increased DNA damage and higher incidence of cancer but does not accelerate aging. *Physiological Genomics*, 16(1), pp.29–37.

Vliet, L.K. et al., 2011. Molecular characterization of the AdeI mutant of Chinese hamster ovary cells: a cellular model of adenylosuccinate lyase deficiency. *Molecular genetics and metabolism*, 102(1), pp.61–68.

Wilkinson, J.E. et al., 2012. Rapamycin slows aging in mice. *Aging Cell*, 11(4), pp.675–682.

Williams, A.D., Mjaatvedt, C.H. & Moore, C.S., 2008. Characterization of the cardiac phenotype in neonatal Ts65Dn mice. *Developmental dynamics : an official publication of the American Association of Anatomists*, 237(2), pp.426–435.

Williams, G.C., 2001. Pleiotropy, natural selection, and the evolution of senescence. *Science's SAGE KE*, 2001(1), p.13.

Wishart, D.S., 2010. *Bioinformatics Methods in Clinical Research: Computational approaches to metabolomics* R. Matthiesen, ed., Totowa, NJ: Humana Press.

Wolfender, J.-L., 2009. HPLC in Natural Product Analysis: The Detection Issue. *Planta Medica*, 75(07), pp.719–734.

Zigman, W.B. & Lott, I.T., 2007. Alzheimer's disease in Down syndrome: Neurobiology and risk. *Mental Retardation and Developmental Disabilities Research Reviews*, 13(3), pp.237–246.

Aoyagi, T. et al., 2015. Cardiac mTOR rescues the detrimental effects of diet-induced obesity in the heart after ischemia-reperfusion. *American journal of physiology. Heart and circulatory physiology*, 308(12), pp.H1530–9.

Bacopoulos, N.C. et al., 1979. Antipsychotic drug action in schizophrenic patients: effect on cortical dopamine metabolism after long-term treatment. *Science*, 205(4413), pp.1405–1407.

Bogdanov, M. et al., 2008. Metabolomic profiling to develop blood biomarkers for Parkinson's disease. *Brain*, 131(2), pp.389–396.

Bohár, Z. et al., 2015. Changing the face of kynurenines and neurotoxicity: therapeutic considerations. *International journal of molecular sciences*, 16(5), pp.9772–9793.

Brattström, L., Englund, E. & Brun, A., 1987. Does Down syndrome support homocysteine theory of arteriosclerosis? *Lancet (London, England)*, 1(8529), pp.391–392.

Cairney, C.J. et al., 2009. Biochimica et Biophysica Acta. *BBA - Molecular Basis of Disease*, 1792(4), pp.353–363.

Chen, Yiquan & Guillemin, G.J., 2009. Kynurenine pathway metabolites in humans: disease and healthy States. *International journal of tryptophan research : IJTR*, 2, pp.1–19.

Chen, Yuanxin et al., 2009. In vivo MRI identifies cholinergic circuitry deficits in a Down syndrome model. *Neurobiology of Aging*, 30(9), pp.1453–1465.

Chicoine, B. & McGuire, D., 1997. Longevity of a woman with Down syndrome: a case study. *Mental retardation*, 35(6), pp.477–479.

Choi, J.H.K. et al., 2009. Age-dependent dysregulation of brain amyloid precursor protein in the Ts65Dn Down syndrome mouse model. *Journal of Neurochemistry*, 110(6), pp.1818–1827.

Contestabile, A., Fila, T., Bartesaghi, R., et al., 2009. Cell Cycle Elongation Impairs Proliferation of Cerebellar Granule Cell Precursors in the Ts65Dn Mouse, an Animal Model for Down Syndrome. *Brain Pathology*, 19(2), pp.224–237.

Contestabile, A., Fila, T., Cappellini, A., et al., 2009. Widespread impairment of cell proliferation in the neonate Ts65Dn mouse, a model for Down syndrome. *Cell Proliferation*, 42(2), pp.171–181.

Coppus, A.M.W. et al., 2008. Survival in Elderly Persons with Down Syndrome. *Journal of the American Geriatrics Society*, 56(12), pp.2311–2316.

Costa, A.C.S. & Grybko, M.J., 2005. Deficits in hippocampal CA1 LTP induced by TBS but not HFS in the Ts65Dn mouse: A model of Down syndrome. *Neuroscience Letters*, 382(3), pp.317–322.

Dal-Cim, T. et al., 2016. Neuroprotection Promoted by Guanosine Depends on Glutamine Synthetase and Glutamate Transporters Activity in Hippocampal Slices Subjected to Oxygen/Glucose Deprivation. *Neurotoxicity research*, 29(4), pp.460–468.

Das, I. et al., 2013. Hedgehog agonist therapy corrects structural and cognitive deficits in a Down syndrome mouse model. *Science Translational Medicine*, 5(201), pp.201ra120–201ra120.

Davisson, M.T., Schmidt, C. & Akeson, E.C., 1990. Segmental trisomy of murine chromosome 16: a new model system for studying Down syndrome. *Progress in clinical and biological research*, 360, p.263.

Fang, Y. & Bartke, A., 2013. Prolonged rapamycin treatment led to beneficial metabolic switch. *Aging*, 5(5), pp.328–329.

Fang, Y. et al., 2001. Phosphatidic Acid-Mediated Mitogenic Activation of mTOR Signaling. *Science*, 294(5548), pp.1942–1945.

Flynn, J.M. et al., 2013. Late life rapamycin treatment reverses age-related heart dysfunction. *Aging Cell*, pp.n/a–n/a.

Galletti, P. et al., 2007. Accumulation of altered aspartyl residues in erythrocyte proteins from patients with Down's syndrome. *FEBS Journal*, 274(20), pp.5263–5277.

Granholm, A.-C.E., Sanders, L.A. & Crnic, L.S., 2000. Loss of Cholinergic Phenotype in Basal Forebrain Coincides with Cognitive Decline in a Mouse Model of Down's Syndrome. *Experimental Neurology*, 161(2), pp.647–663.

Halloran, J. et al., 2012. Chronic inhibition of mammalian target of rapamycin by rapamycin modulates cognitive and non-cognitive components of behavior throughout lifespan in mice. *NSC*, 223(C), pp.102–113.

Hansen, M. et al., 2007. Lifespan extension by conditions that inhibit translation in Caenorhabditis elegans. *Aging Cell*, 6(1), pp.95–110.

Harrison, D.E. et al., 2009. Rapamycin fed late in life extends lifespan in genetically heterogeneous mice. *Nature*.

Holtzman, D.M. et al., 1996. Developmental abnormalities and age-related neurodegeneration in a mouse model of Down syndrome. *Proceedings of the National Academy of Sciences*, 93(23), pp.13333–13338.

Hunsucker, S.W. et al., 2008. Assessment of post-mortem-induced changes to the mouse brain proteome. *Journal of Neurochemistry*, 105(3), pp.725–737.

Hyde, L.A. & Crnic, L.S., 2001. Age-related deficits in context discrimination learning in Ts65Dn mice that model Down syndrome and Alzheimer's disease. *Behavioral Neuroscience*, 115(6), pp.1239–1246.

Insausti, A.M. et al., 1998. Hippocampal volume and neuronal number in Ts65Dn mice: a murine model of down syndrome. *Neuroscience Letters*, 253(3), pp.175–178.

Jablonska, B. et al., 2006. The growth capacity of bone marrow CD34 positive cells in culture is drastically reduced in a murine model of Down syndrome. *Comptes Rendus Biologies*, 329(9), pp.726–732.

Jacinto, E. et al., 2004. Mammalian TOR complex 2 controls the actin cytoskeleton and is rapamycin insensitive. *Nature Cell Biology*, 6(11), pp.1122–1128.

Johnson, S.C., Rabinovitch, P.S. & Kaeberlein, M., 2013. mTOR is a key modulator of ageing and age-related disease. *Nature*, 493(7432), pp.338–345.

Jurecka, A., 2009. Inborn errors of purine and pyrimidine metabolism. *Journal of Inherited Metabolic Disease*, 32(2), pp.247–263.

Kaeberlein, M. et al., 2005. Increased Life Span due to Calorie Restriction in Respiratory-Deficient Yeast. *PLoS Genetics*, 1(5), p.e69.

Kapahi, P. et al., 2004. Regulation of Lifespan in Drosophila by Modulation of Genes in the TOR Signaling Pathway. *Current Biology*, 14(10), pp.885–890.

Kay, A.D. et al., 1987. Cerebrospinal fluid monoaminergic metabolites are elevated in adults with Down's syndrome. *Annals of neurology*, 21(4), pp.408–411.

Kennedy, B.K., Steffen, K.K. & Kaeberlein, M., 2007. Ruminations on dietary restriction and aging. *Cellular and Molecular Life Sciences*, 64(11), pp.1323–1328.

Kirsammer, G. et al., 2008. Highly penetrant myeloproliferative disease in the Ts65Dn mouse model of Down syndrome. *Blood*, 111(2), pp.767–775.

Krebs, M. et al., 2007. The Mammalian target of rapamycin pathway regulates nutrient-

sensitive glucose uptake in man. *Diabetes*, 56(6), pp.1600–1607.

Lamming, D.W. et al., 2013. Young and old genetically heterogeneous HET3 mice on a rapamycin diet are glucose intolerant but insulin sensitive. *Aging Cell*, 12(4), pp.712–718.

LeWitt, P.A. et al., 1992. Markers of dopamine metabolism in Parkinson's disease. *Neurology*, 42(11), pp.2111–2111.

Liu, M. et al., 2002. On the application of 4-hydroxybenzoic acid as a trapping agent to study hydroxyl radical generation during cerebral ischemia and reperfusion. *Molecular and Cellular Biochemistry*, 234-235(1-2), pp.379–385.

Lockrow, J. et al., 2009. Cholinergic degeneration and memory loss delayed by vitamin E in a Down syndrome mouse model. *Experimental Neurology*, 216(2), pp.278–289.

Loeffler, D.A. et al., 1995. Markers of dopamine depletion and compensatory response in striatum and cerebrospinal fluid. *Journal of neural transmission. Parkinson's disease and dementia section*, 9(1), pp.45–53.

Loewith, R. et al., 2002. Two TOR complexes, only one of which is rapamycin sensitive, have distinct roles in cell growth control. *Molecular Cell*, 10(3), pp.457–468.

Lomoio, S., Scherini, E. & Necchi, D., 2009. -Amyloid overload does not directly correlate with SAPK/JNK activation and tau protein phosphorylation in the cerebellar cortex of Ts65Dn mice. *Brain Research*, 1297(C), pp.198–206.

Lott, I.T. & Head, E., 2005. Alzheimer disease and Down syndrome: factors in pathogenesis. *Neurobiology of Aging*, 26(3), pp.383–389.

Maddison, D.C. & Giorgini, F., 2015. The kynurenine pathway and neurodegenerative disease. *Seminars in cell & developmental biology*, 40, pp.134–141.

Maiese, K., 2015. Targeting molecules to medicine with mTOR, autophagy, and neurodegenerative disorders. *British journal of clinical pharmacology*, pp.n/a–n/a.

Majumder, S. et al., 2011. Inducing Autophagy by Rapamycin Before, but Not After, the Formation of Plaques and Tangles Ameliorates Cognitive Deficits M. G. Tansey, ed. *PLoS ONE*, 6(9), p.e25416.

Majumder, S. et al., 2012. Lifelong rapamycin administration ameliorates age-dependent cognitive deficits by reducing IL-1β and enhancing NMDA signaling. *Aging Cell*, 11(2), pp.326–335.

Malagelada, C. et al., 2010. Rapamycin Protects against Neuron Death in In Vitro andIn Vivo Models of Parkinson's Disease. *The Journal of Neuroscience*, 30(3), pp.1166–

1175.

Mann, D.M.A., 1988. The pathological association between down syndrome and Alzheimer disease. *Mechanisms of Ageing and Development*, 43(2), pp.99–136.

Mann, D.M.A., Yates, P.O. & Marcyniuk, B., 1985. Some morphometric observations on the cerebral cortex and hippocampus in presenile Alzheimer"s disease, senile dementia of Alzheimer type and Down"s syndrome in middle age. *Journal of the neurological sciences*, 69(3), pp.139–159.

Maroun, L.E., 1980. Interferon action and chromosome 21 trisomy. *Journal of theoretical biology*, 86(3), pp.603–606.

Masoro, E.J., 2005. Overview of caloric restriction and ageing. *Mechanisms of Ageing and Development*, 126(9), pp.913–922.

Miller, R.A. & Nadon, N.L., 2000. Principles of Animal Use for Gerontological Research. *The Journals of Gerontology Series A: Biological Sciences and Medical Sciences*, 55(3), pp.B117–B123.

Miller, R.A. et al., 2011. Rapamycin, But Not Resveratrol or Simvastatin, Extends Life Span of Genetically Heterogeneous Mice. *The Journals of Gerontology Series A: Biological Sciences and Medical Sciences*, 66A(2), pp.191–201.

Moore, D.R. et al., 2011. Resistance exercise enhances mTOR and MAPK signalling in human muscle over that seen at rest after bolus protein ingestion. *Acta physiologica (Oxford, England)*, 201(3), pp.365–372.

Murdoch, J.C. et al., 1977. Down's syndrome: an atheroma-free model? *British medical journal*, 2(6081), pp.226–228.

Nadon, N.L. et al., 2008. Design of aging intervention studies: the NIA interventions testing program. *Age*, 30(4), pp.187–199.

Nakamura, E. & Tanaka, S., 1998. Biological ages of adult men and women with Down's syndrome and its changes with aging. *Mechanisms of Ageing and Development*, 105(1), pp.89–103.

Necchi, D., Lomoio, S. & Scherini, E., 2008. Axonal abnormalities in cerebellar Purkinje cells of the Ts65Dn mouse. *Brain Research*, 1238(C), pp.181–188.

Patterson, D. & Cabelof, D.C., 2012. Down syndrome as a model of DNA polymerase beta haploinsufficiency and accelerated aging. *Mechanisms of Ageing and Development*, 133(4), pp.133–137.

Perluigi, M. et al., 2014. Neuropathological role of PI3K/Akt/mTOR axis in Down

syndrome brain. *Biochimica et biophysica acta*, 1842(7), pp.1144–1153.

Ramos, F.J. et al., 2012. Rapamycin Reverses Elevated mTORC1 Signaling in Lamin A/C-Deficient Mice, Rescues Cardiac and Skeletal Muscle Function, and Extends Survival. *Science Translational Medicine*, 4(144), pp.144ra103–144ra103.

Reeves, R.H. et al., 1995. A mouse model for Down syndrome exhibits learning and behaviour deficits. *Nature Genetics*, 11(2), pp.177–184.

Ross, C. et al., 2015. Metabolic consequences of long-term rapamycin exposure on common marmoset monkeys (Callithrix jacchus). *Aging*, 7(11), pp.964–973.

Rozen, S. et al., 2005. Metabolomic analysis and signatures in motor neuron disease. *Metabolomics*, 1(2), pp.101–108.

Rueda, N. et al., 2005. Cell proliferation is reduced in the dentate gyrus of aged but not young Ts65Dn mice, a model of Down syndrome. *Neuroscience Letters*, 380(1-2), pp.197–201.

Salehi, A. et al., 2006. Increased App Expression in a Mouse Model of Down's Syndrome Disrupts NGF Transport and Causes Cholinergic Neuron Degeneration. *Neuron*, 51(1), pp.29–42.

Sanders, N.C., Williams, D.K. & Wenger, G.R., 2009. Does the learning deficit observed under an incremental repeated acquisition schedule of reinforcement in Ts65Dn mice, a model for Down syndrome, change as they age? *Behavioural Brain Research*, 203(1), pp.137–142.

Santini, E. et al., 2009. Inhibition of mTOR Signaling in Parkinson's Disease Prevents l-DOPA–Induced Dyskinesia. *Sci. Signal.*, 2(80), pp.ra36–ra36.

Satgé, D. & Vekemans, M., 2011. Down syndrome patients are less likely to develop some (but not all) malignant solid tumours. *Clinical genetics*, 79(3), pp.289–290.

Schapiro, M.B. et al., 1987. Cerebrospinal fluid monoamines in Down's syndrome adults at different ages. *Journal of mental deficiency research*, 31 (Pt 3), pp.259–269.

Schindler, C.E. et al., 2014. Chronic rapamycin treatment causes diabetes in male mice. *AJP: Regulatory, Integrative and Comparative Physiology*, 307(4), pp.R434–R443.

Shi, H. et al., 2002. Characterization of diet-dependent metabolic serotypes: Primary validation of male and female serotypes in independent cohorts of rats. *The Journal of nutrition*, 132(5), pp.1039–1046.

Shioi, T., 2003. Rapamycin Attenuates Load-Induced Cardiac Hypertrophy in Mice. *Circulation*, 107(12), pp.1664–1670.

Spilman, P. et al., 2010. Inhibition of mTOR by Rapamycin Abolishes Cognitive Deficits and Reduces Amyloid-β Levels in a Mouse Model of Alzheimer's Disease P. F. Ferrari, ed. *PLoS ONE*, 5(4), p.e9979.

Stack, E.C. et al., 2008. Therapeutic attenuation of mitochondrial dysfunction and oxidative stress in neurotoxin models of Parkinson's disease. *Biochimica et Biophysica Acta (BBA) - Molecular Basis of Disease*, 1782(3), pp.151–162.

Sundaram, G. et al., 2014. Quinolinic acid toxicity on oligodendroglial cells: relevance for multiple sclerosis and therapeutic strategies. *Journal of neuroinflammation*, 11(1), p.204.

Tain, L.S. et al., 2009. Rapamycin activation of 4E-BP prevents parkinsonian dopaminergic neuron loss. *Nature Neuroscience*, 12(9), pp.1129–1135.

Tramutola, A. et al., 2016. Increased Mammalian Target of Rapamycin Signaling Contributes to the Accumulation of Protein Oxidative Damage in a Mouse Model of Down's Syndrome. *Neuro-degenerative diseases*, 16(1-2), pp.62–68.

Usowicz, M.M. & Garden, C.L.P., 2012. Increased excitability and altered action potential waveform in cerebellar granule neurons of the Ts65Dn mouse model of Down syndrome. *Brain Research*, 1465, pp.10–17.

Weindruch, R. et al., 1986. The retardation of aging in mice by dietary restriction: longevity, cancer, immunity and lifetime energy intake. *The Journal of nutrition*, 116(4), pp.641–654.

Wevers, R.A. et al., 1999. 1H-NMR spectroscopy of body fluids: inborn errors of purine and pyrimidine metabolism. *Clinical Chemistry*, 45(4), pp.539–548.

Wilkinson, J.E. et al., 2012. Rapamycin slows aging in mice. *Aging Cell*, 11(4), pp.675–682.

Wishart, D.S., 2010. *Bioinformatics Methods in Clinical Research: Computational approaches to metabolomics* R. Matthiesen, ed., Totowa, NJ: Humana Press.

Wolfender, J.-L., 2009. HPLC in Natural Product Analysis: The Detection Issue. *Planta Medica*, 75(07), pp.719–734.

Yang, A. & Reeves, R.H., 2011. Increased survival following tumorigenesis in Ts65Dn mice that model Down syndrome. *Cancer research*, 71(10), pp.3573–3581.

Ylä-Herttuala, S. et al., 1989. Down's syndrome and atherosclerosis. *Atherosclerosis*, 76(2-3), pp.269–272.

Zigman, W.B. & Lott, I.T., 2007. Alzheimer's disease in Down syndrome: Neurobiology

and risk. *Mental Retardation and Developmental Disabilities Research Reviews*, 13(3), pp.237–246.

Zuo, H. et al., 2016. Plasma Biomarkers of Inflammation, the Kynurenine Pathway, and Risks of All-Cause, Cancer, and Cardiovascular Disease Mortality: The Hordaland Health Study. *American journal of epidemiology*, 183(4), pp.249–258.

Altschul, S.F. et al., 1990. Basic Local Alignment Search Tool. *Journal of Molecular Biology*, 215, pp.403–410.

An, S. et al., 2008. Reversible Compartmentalization of de Novo Purine Biosynthetic Complexes in Living Cells. *Science*, 320(5872), pp.103–106.

Baresova, V. et al., 2012. Mutations of ATIC and ADSL affect purinosome assembly in cultured skin fibroblasts from patients with AICA-ribosiduria and ADSL deficiency. *Human Molecular Genetics*, 21(7), pp.1534–1543.

Barnes, T.S. et al., 2001. Purification of, Generation of Monoclonal Antibodies to, and Mapping of Phosphoribosyl N-Formylglycinamide Amidotransferase. *Biochemical Journal*, 33, pp.1850–1860.

Becker, J. et al., 2011. Unraveling the Chinese hamster ovary cell line transcriptome by next-generation sequencing. *Journal of Biotechnology*, 156(3), pp.227–235.

Benoıt Pinson et al., 2009. Metabolic intermediates selectively stimulate transcription factor interaction and modulate phosphate and purine pathways. *Genes & Development*, 23(12), pp.1399–1407.

Brodsky, G. et al., 1997. The human GARS-AIRS-GART gene encodes two proteins which are differentially expressed during human brain development and temporally overexpressed in cerebellum of individuals with Down syndrome. *Human Molecular Genetics*, 6, pp.2043–2050.

Dehouck, Y. et al., 2011. PoPMuSiC 2.1: a web server for the estimation of protein stability changes upon mutation and sequence optimality. *BMC Bioinformatics*, 12(1), p.151.

Deng, Y. et al., 2012. Mapping protein-protein proximity in the purinosome. *Journal of Biological Chemistry*.

Firestine, S.M. et al., 2009. Identification of inhibitors of N5-carboxyaminoimidazole ribonucleotide synthetase by high-throughput screening. *Bioorganic & Medicinal Chemistry*, 17(9), pp.3317–3323.

Jackson, M. et al., 1999. Persistence and Protective Efficacy of a Mycobacterium tuberculosis Auxotroph Vaccine. *Infection and Immunity*, 67, pp.2867–2873.

Jurecka, A., 2009. Inborn errors of purine and pyrimidine metabolism. *Journal of Inherited Metabolic Disease*, 32(2), pp.247–263.

Jurecka, A. et al., 2008. Clinical, biochemical and molecular findings in seven Polish patients with adenylosuccinate lyase deficiency. *Molecular genetics and metabolism*, 94(4), pp.435–442.

Knox, A.J. et al., 2008. Mutations in the Chinese hamster ovary cell GART gene of de novo purine synthesis. *Gene*, 429(1-2), pp.23–30.

Li, S.-X. et al., 2007. Octameric Structure of the Human Bifunctional Enzyme PAICS in Purine Biosynthesis. *Journal of Molecular Biology*, 366(5), pp.1603–1614.

Matson, W.R. et al., 1984. n-ElectrodeThree-DimensionalLiquidChromatographywith Electrochemical Detectionfor Determinationof Neurotransmitters. *Clinical Chemistry*, 30(9), pp.1477–1488.

Meyer, E. et al., 1992. Purification and Characterization of the purE, purK, and purC Gene Products: Identification of a Previously Unrecognized Energy Requirement in the Purine Biosynthetic Pathway. *Biochemical Journal*, 31(21), pp.5022–5032.

Narkar, V.A. et al., 2008. AMPK and PPARδ Agonists Are Exercise Mimetics. *Cell*, 134(3), pp.405–415.

Ng, A. et al., 2009. Zebrafish mutations in gart and paics identify crucial roles for de novo purine synthesis in vertebrate pigmentation and ocular development. *Development*, 136(15), pp.2601–2611.

Oates, D.C., Vannais, D. & Patterson, D., 1980. A Mutant of CHO-K1 Cells Deficient in Two Nonsequential Steps of de Novo Purine Biosynthesis. *Cell*, 20, pp.797–805.

Patterson, D., 1975. Biochemical Genetics of Chinese Hamster Cell Mutants with Deviant Purine Metabolism: Biochemical Analysis of Eight Mutants. *Somatic Cell Genetics*, 1, pp.91–110.

Patterson, D. et al., 1999. Human phosphoribosylformylglycineamide amidotransferase (FGARAT): regional mapping, complete coding sequence, isolation of a functional genomic clone, and DNA sequence analysis. *Gene*, 239, pp.381–391.

Rattan, R. et al., 2005. 5-Aminoimidazole-4-carboxamide-1. *Journal of Biological Chemistry*, 280, pp.39582–39593.

Sempere, Á. et al., 2010. Study of inborn errors of metabolism in urine from patients with

unexplained mental retardation. *Journal of Inherited Metabolic Disease*, 33(1), pp.1–7.

Sun, W. et al., 2004. Identification of differentially expressed genes in human lung squamous cell carcinoma using suppression subtractive hybridization. *Cancer Letters*, 212(1), pp.83–93.

Swain, J.L. et al., 1984. Disruption of the Purine Nucleotide Cycle by Inhibition of Adenylosuccinate Lyase Produces Skeletal Muscle Dysfunction. *Journal of Clinical Investigation*, 74, pp.1422–1427.

Taha, T.S. & Deits, T.L., 1993. Detection of Glycinamide Ribonucleotide by HPLC with Pulsed Amperometry: Application to the Assay for Glutamine:5-Phosphoribosyl-1-pyrophosphate Amidotransferase. *Analytical Biochemistry*, 213, pp.323–328.

Tang, Y.-C. et al., 2011. Identification of Aneuploidy-Selective Antiproliferation Compounds. *Cell*, 144(4), pp.499–512.

Tu, A.S. & Patterson, D., 1977. Biochemical Genetics of Chinese Hamster Cell Mutants with Deviant Purine Metabolism. VI. Enzymatic Studies of Two Mutants Unable to Convert Inosinic Acid to Adenylic Acid. *Biochemical Genetics*, 15, pp.195–210.

Vliet, L.K. et al., 2011. Molecular characterization of the AdeI mutant of Chinese hamster ovary cells: a cellular model of adenylosuccinate lyase deficiency. *Molecular genetics and metabolism*, 102(1), pp.61–68.

Yves Dehouck et al., 2009. Fast and accurate predictions of protein stability changes upon mutations using statistical potentials and neural networks: PoPMuSiC-2.0. *Bioinformatics*, 25(19), pp.2537–2543.

Zaza, G. et al., 2004. Acute lymphoblastic leukemia with TEL-AML1 fusion has lower expression of genes involved in purine metabolism and lower de novo purine synthesis. *Blood*, 104(5), pp.1435–1441.

Zikanova, M. et al., 2010. Biochemical and structural analysis of 14 mutant adsl enzyme complexes and correlation to phenotypic heterogeneity of adenylosuccinate lyase deficiency. *Human Mutation*, 31(4), pp.445–455.